Dissertation

submitted to the

Combined Faculties for the Natural Sciences and for Mathematics

of the Ruperto-Carola University of Heidelberg, Germany

for the degree of

Doctor of Natural Sciences

presented by

Patrick Aderhold, Diplom Biologe

Born in: Frankfurt a.M.

Oral-examination:

On the Structure and Function of the COPI coat protein complex Coatomer

Referees: Prof. Dr. Felix Wieland

Prof. Dr. Irmgard Sinning

I Table of content

II Abstract

In eukaryotes newly synthesized proteins and membranes in the early secretory pathway are transported by COPII and COPI vesicles. The key componets for the formation of COPI vesicles are the small GTPase Arf1 and the Coatomer complex. Coatomer is recruited to the donor mebrane by GTP-loaded Arf. On the membrane, coatomer polymerizes and deforms the membrane into a coated bud, which can then pinch of to form a free COPI vesicle. Prior to fusion of a vesicle with its target membrane, the coat is removed from the carrier by hydrolysis of GTP in Arf1.

In this work I investigated the structure of the coatomer complex and its interaction with the small GTPase Arf1.

To this end I decided to use coatomer and Arf derieved from the thermophilic ascomycete *Chaetomium thermophilum*, as proteins from this organism have proven more suitable for structural investigations as proteins from mesophilic organisms. We were able to produce coatomer from *Chaetomium thermophilum* and showed that it produces COPI vesicles. Also we prepared coatomer variants lacking the ε-COP subunit and the C-terminal μ-homology domain of δ-COP. ε-COP and the μ-homolgy domain of δ-COP have been implicated in forming contacts between coatomer triads on COPI-vesicles to stabilize the coat on the membrane. Surprisingly both coatomer variants retained the ability to produce vesicles.

The structure of the coatomer complex was only partially solved at the atomic level. In this work we were able to solve the structure of a βδ-subcomplex of coatomer. The structural information of this complex closes the largest gap in our knowledge of atomic coatomer structure. The structure shows a close homology to γζ-COP. The N-terminal part of γ-COP and β-COP both form curved α-solenoid folds, whereas ζ-COP and the N-terminal part of δ-COP form longin-like folds. Our structure reveals that an extended linker region of δ-COP passes below the α-solenoid of β-COP. The passage of the linker is close to an assumed binding site of the small GTPase Arf1 on β-COP, implicating a potential function of the linker in Arf-binding.

Two major binding sites on coatomer for Arf are implicated in the initial recruitment of the coat complex. One site is situated on γ-COP and the other on β-COP. In addition, the δ-COP

subunit had been reported to bind Arf. We show here that the affinity of βδ-subcomplexes to bind Arf is increased by incorporation of the first two α-helices of the linker region of δ-COP. This data revealed that β-COP and δ-COP bind to the same Arf molecule.

II Abstract (german version)

Die Schlüsselkomponenten für die Bildung von COPI Vesikeln sind die kleine GTPase Arf und der heptamere Coatomer Komplex. Arf in seiner GTP-geladenen Form rekrutiert Coatomer an die Membran. Auf der Membran polymerisiert Coatomer und deformiert diese bis zur Bildung einer Vesikelknospe. Diese muß sich von der Membran abschnüren, um ein freies COPI Vesikel zu bilden. Vor der Fusion des Vesikels mit seiner Zielmembran wird die Proteinhülle des Vesikels durch GTP-Hydrolyse in Arf abgelöst.

In dieser Arbeit wurde die Struktur des Coatomer Komplex sowie seine Interaktionen mit der kleinen GTPase Arf1 untersucht.

Dazu entschied ich mich, Coatomer und Arf aus dem thermophilen Askomyceten *Chaetomium thermophilum* zu verwenden, da gezeigt wurde, dass Proteine dieses Organismus für strukturelle Untersuchungen besser geeignet sind, als Proteine aus mesophilen Organismen. Coatomer aus *Chaetomium thermophilum* wurde hergestellt. Die Funktionalität des hergestellten Coatomers wurde durch seine Fähigkeit, Vesikel zu bilden, nachgewiesen. Zusätzlich wurden Coatomer Varianten erzeugt, denen entweder die ε-COP Untereinheit oder die C-terminale μ-Homologie Domäne der δ-COP Untereinheit fehlten. ε-COP und die μ-Homologie Domäne von δ-COP sollen für die Ausbildung von Kontakten zwischen Coatomer Triaden auf dem COPI Vesikel verantwortlich sein und auf diese Weise die Proteinhülle auf dem Vesikel stabilisieren. Es konnte jedoch gezeigt werden, dass beide Varianten des Coatomer Komplexes noch Vesikel bilden konnten.

Die hochauflösende atomare Struktur des Coatomer Komplexes war nur teilweise bekannt. In dieser Arbeit konnte die Struktur eines βδ-Subkomplexes gelöst warden. Die strukturelle Information dieses Komplexes schließt die größte, in der atomaren Struktur des Coatomer Komplexes noch vorhandene Lücke. Die gelöste Struktur zeigte eine große Ähnlichkeit zu γζ-COP. Die N-terminalen Teile von γ-COP und β-COP bilden geschwungene α-Solenoid

Strukturen aus. ζ-COP und der N-terminale Teil von δ-COP bilden eine longin-artige Stuktur. Durch die hohe Auflösung zeigte sich, dass der lange Linker-Bereich von δ-COP unterhalb des α-Solenoids von β-COP hindurchläuft. Der Linker-Bereich tritt in dem Bereich unter dem α-Solenoid von β-COP hindurch, an dem die Bindungsstelle für die kleine GTPase Arf vermutet wird. Dies impliziert eine potentielle Funktion des Linkers in der Bindung und Stabilisierung von Arf.

Es gibt zwei Bindungsstellen im Coatomer Komplex für Arf, die für die initiale Rekrutierung von Coatomer zuständig sind. Eine Bindungsstelle befindet sich auf γ-COP, die andere auf β-COP. Es wurde aufgrund biochemischer Ergebnisse berichtet, dass δ-COP Arf binden kann. In meiner Arbeit konnte ich zeigen, dass die Bindungsaffinität von βδ-Subcomplexen für Arf ansteigt, wenn die ersten beiden α-Helices der Liker-Region von δ-COP vorhanden sind. Daraus können wir schließen, dass β-COP und δ-COP an ein und dasselbe Arf-Molekül binden.

1 Introduction

1.1 The secretory pathway

Compartmentalization is a descriptive feature of eukaryotic cells. It enables the cell to separate cellular functions to individual compartments. In order to fulfill these cellular functions, the individual compartments possess a specific protein and lipid-composition. The compartments are no static bodies, but do continuously exchange proteins and lipids in a directed and regulated manner. The exchange between compartments is, in most cases, conducted using coated transport vesicles as cargo carriers, which bud from one membrane and fuse with their respective target membrane.

The secretory pathway starts at the site of cargo synthesis and includes the compartment of the endoplasmic reticulum (ER), followed by the ER exit sites (ERES), the ER-to-Golgi intermediate compartment (ERGIC), the Golgi complex and the trans-Golgi network (TGN). Most newly synthesized proteins, which are transported by the secretory pathway, are characterized by an N-terminal hydrophobic signal sequence, which is recognized by the cytosolic signal recognition particle SRP, as soon as the nascent amino acid chain leaves the ribosome. The translation process is stalled and the SRP binds to the ER-localized SRP-receptor. Thereby the ribosome makes contact with the ER-Translocase, a transmembrane-channel protein. Upon GTP hydrolysis SRP and SRP-receptor dissociate. The translation process continues and the synthesized protein is transported co-translationally in the ER. Soluble secretory proteins are transported to the ER-lumen, whereas transmembrane proteins are inserted into the ER-membrane, depending on their signal sequences. Within the ER, most proteins undergo modifications like N-glycosylation. Also, the ER is a compartment with quality control function. Missfolded or unfolded proteins are retained in the ER until they have achieved their correct folded state. The folding process is supported by the action of chaperons. Proteins that fail to achieve their correct folded state can be recognized by either the UPR-system (unfolded protein response) or the ERAD-System (ER associated degradation). The proteins recognized are exported from the ER by translocators to the cytosol. Within the cytosol these misfolded proteins are marked by ubiquitinylation for degradation by the proteasome.

Properly folded proteins are transported from the ER by COPII-vesicles to the ERGIC. COPII vesicles are one of three major classes of carriers that operate in the secretory pathway. The others are COPI and clathrin-coated vesicles. COPII vesicles are composed of the small GTPase Sar1, the heterodimeric Sec23/24 complex and the heterotetrameric Sec13/31 complex. The ERGIC is regarded as a separate compartment, defined by the presence of specific marker proteins like ERGIC-53. It is an interface between the anterograde transport of secretory proteins to the Golgi and the retrograde transport of ER resident proteins back to ER. Within the ERGIC compartment, proteins can be detected from both COPII vesicles, that mediate anterograde transport and from COPI vesicles, that mediate retrograde transport back to the ER. In this respect the ERGIC can be regarded as the first compartment discriminating between retrograde and anterograde transport directions. It is still unknown, if the ERGIC is formed by homofusion of COPII vesicles or by heterofusion of vesicles with an existing compartment.

Protein sorting is done in the Golgi-apparatus. This compartment is composed of stacks of membrane segments, termed *cisternae.* The Golgi-apparatus can be divided into sub-compartments. It starts with the ER-facing cis-Golgi network (CGN), where secretory and membrane proteins arrive carried by COPII vesicles. Cargo is further transported via the cis-Golgi cisternae, the medial cisternae, the trans-golgi cisternae, finally to the trans-Golgi network (TGN). The respective sub-compartments have specific protein- and lipid-compositions and specific sets of enzymes. Thereby the extensive posttranslational modification of proteins, like glycosylation, can be locally regulated. The mechanism of transport between the different Golgi sub-compartments is still not fully understood. At present three different models are existing, the cisternal maturation model, the vesicular transport model and the cisternal progenitor model.

In the cisternal maturation model it is assumed that Golgi cisternae are formed *de novo* on the cis-Golgi side by homotypic fusion of COPII vesicles and ERGIC-clusters (Bannykh and Balch, 1997) (Mironov et al., 2003). The cisternae are regarded as transient carriers, which gradually mature into TGN cisternae and finally disintegrate into secretory vesicles. Golgi resident proteins are recycled by COPI vesicles from older cisternae back to younger cisternae (Glick and Malhotra, 1998) (Rabouille and Klumperman, 2005). The distinct

biochemically composition of the cisternae could be explained by different recycling efficiencies for the various Golgi-proteins (Glick et al., 1997) (Weiss and Nilsson, 2000).

The vesicular transport model describes the Golgi as a set of stable cisternae, each containing a unique set of Golgi proteins including glycosylation enzymes (Kleene and Berger, 1993; Rabouille et al., 1995) (Nilsson et al., 2009). These stable compartments work in tandem to process secretory cargo (Farquhar and Palade, 1981) (Rothman, 1981). This cargo will arrive at the cis-Golgi transported by COPII vesicles and will move during its processing from one compartment to the next shuttled by COPI vesicles on its way to the TGN (Rothman and Wieland, 1996). COPI vesicles are proposed to operate bidirectional. Anterograde COPI vesicles are shuttling forward secretory cargo and retrograde COPI vesicles are recycling Golgi resident proteins (Orci et al., 2000) (Pelham and Rothman, 2000).

In the cisternal progenitor model the Golgi is described as a set of stable compartments that can be segregated into domains (Griffiths, 2000) (Mironov et al., 2005), which are defined by Rab GTPases via a Rab conversion process (Pfeffer, 2010). A domain in the cis-Golgi would undergo Rab conversion and acquire a medial character. This would than result in a transient homotypic fusion with a medial cisternae in an adjacent stack. Secretory cargo can move through the resulting connection. Similar fusion events in later compartments would allow the cargo to pass the entire stack. The transfer of the Rab domains is assumed to operate in conjunction with the COPI transport (Glick and Luini, 2011).

1.2 Vesicular transport

Secretory proteins are transported by vesicles. All known vesicles are composed of a membrane-structure with a diameter of 50 to 100 nm, which is enveloped by a protein coat. This protein coat differs between the different types of vesicles and is actually defining the vesicle type. Figure 1 shows the secretory pathway and the function and place of action of the different types of protein-coated vesicles.

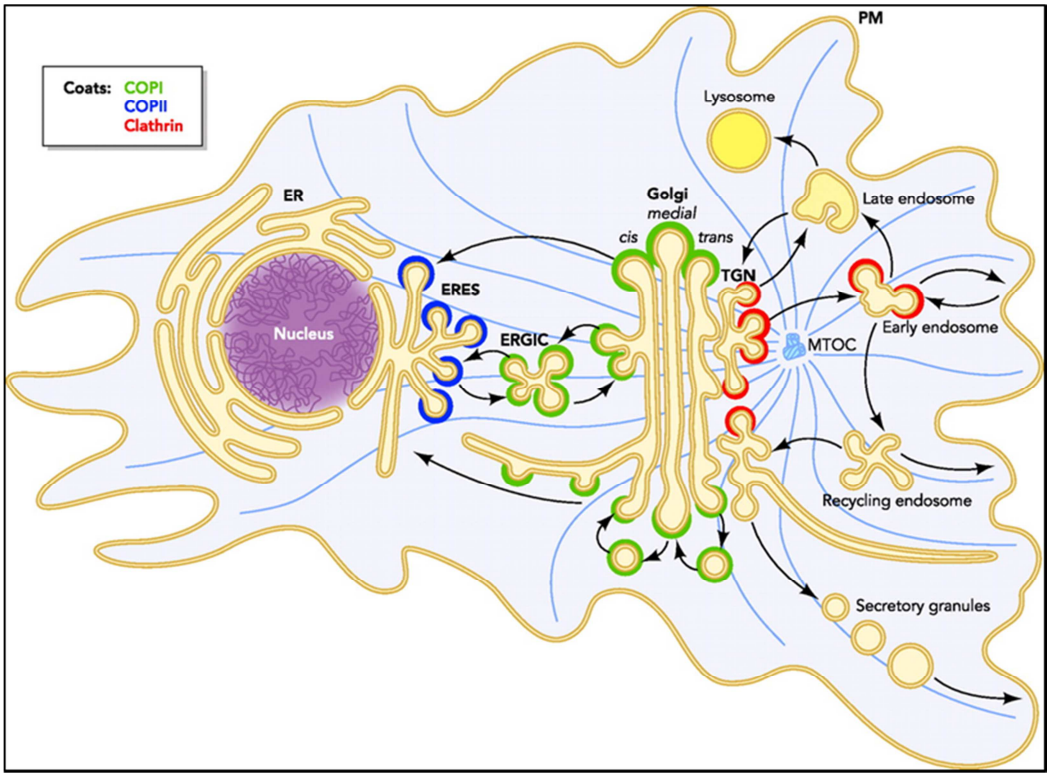

Figure 1: Secretory pathway taken from (Szul and Sztul, 2011). For details see text.

The biogenesis of protein-coated vesicles is regulated by small GTP-binding Proteins of the Ras-superfamiliy. These proteins occur in an active, GTP-bound, state and an inactive, GDP-bound, state and can thereby act as molecular switches. Vesicles are formed by the polymerization of the respective coat-proteins, which enforces curvature on the donor membrane. This leads to the formation of a coated bud. The polymerization continues until the vesicle is formed, which pinches of the membrane. The vesicle is transported to the target membrane. Before fusion with this target membrane, the proteins coat is shed. The fusion of vesicles with the target membrane is mediated by SNARE-proteins (*soluble NSF* (*N-ethylmaleimide sensitive factor*) *attachment protein receptors*) (Rothman and Warren, 1994). In this process the fusion of the two membranes is facilitated by the formation of a 4-helix bundle composed of 4 α-helices of the SNARE-proteins. One α-helix is contributed by the vesicular-SNARE-protein (v-SNARE) and the other 3 α-helices are contributed by the cognate SNARE-proteins of the target membrane (t-SNARE) (Rothman and Warren, 1994) (Söllner et al., 1993). Furthermore the mebrane fusion process is regulated by proteins of the Rab-family and by tether-proteins like the Golgins.

Up to now three different vesicular transport systems have been biochemically described to operate in the secretory patway: the COPII-, the COPI- and the Clathrin-coated-vesicles.

1.2.1 COPII vesicles

COPII vesicles operate in the early secretory pathway in anterograde transport from the ER to the ERGIC or the CGN (Barlowe et al., 1994). Cargo sorting and exit from the ER of soluble proteins occurs via the ER exit sites (ERES). ERES are morphologically defined as smooth projections from the ER, which are coated with COPII coat components. The COPII coat binds and concentrates secretory cargo for the transport by COPII vesicles. It is composed of the small GTPase Sar1, the heterodimeric Sec23/Sec24 complex and the hetero-tetrameric Sec13/Sec31 complex. Sar1 has, like all GTPases, a low intrinsic GDP-to-GTP exchange. At the ER membrane Sar1 is activated by the Guaninnucleotide exchange factor (GEF) Sec12 (Barlowe and Schekman, 1993), which catalyzes the exchange from GDP to GTP. Sec12 is an ER localized membrane protein, which restricts the Sar1 activation to the ER. The exchange to GTP triggers a conformational change, which exposes the N-terminal 23 aminoacids long amphipathic helix of Sar1. This helix anchors Sar1 to the membrane (Barlowe et al., 1993). Activated Sar1 recruits the heterodimeric Sec23/Sec24 complex, by binding directly to Sec23 (Matsuoka et al., 1998). The sorting of cargo in COPII vesicles is mediated by the Sec24 subunit. There are four different isoforms of Sec24 (Sec24a-d), which have been shown to bind different cargoes. Sec24 isoforms a and b bind cargo motifs DXE and LXXL/ME, and Sec24 isoforms c and d bind the IXM motif (Fiedler et al., 1996). Soluble cargo proteins can be exported from the ER by binding to cargo receptors of the ERGIC-53 family, the p24 family and the Erv family, which facilitate their sorting into COPII vesicles (Belden and Barlowe, 2001). The surface activity of Sar1, as well as the binding of Sec23/Sec24 leads to membrane deformation, which is than stabilized by Sec13/Sec31. This results in the formation of COPII vesicle bud (Lee et al., 2005). The Sec23/24 complex recruits the hetero-tetrameric Sec13/Sec31 complex, which forms the outer coat shell. Sec31 interacts directly with Sec23 and Sar1. Polymerization of Sec13/Sec31 leads to formation and to the scission of COPII vesicles. Dissociation of the protein coat, which enables the fusion of the vesicle with the target membrane, is triggered by GTP-hydrolysis, stimulated by Sec23, which is the

GTPase activating protein (GAP) for Sar1. Binding of the outer Sec13/Sec31 coat is prerequisit for full GAP-activity of Sec23 (Antonny et al., 2001).

1.2.1.1 Structure of the COPII coat

As described above, the COPII coat is composed of an outer (Sec13/Sec31) and an inner (Sec23/Sec24) coat layer. The crystal structure of the Sec23Sec24-Sar1 prebudding complex shows that the complex has a bow-tie shape and is elongated in directions parallel to the membrane, with a size of ~ 150 Å in the long direction (Stagg et al., 2006). The complex has a concave inner surface, which is more positively charged than the outer surface and matches the size of a 60 nm vesicle. The Sar1 amino terminus, which is believed to embed residues into the bilayer, is oriented towards the membrane. The folds of Sec23 and Sec24 are closely related and organized into five distinct domains: a β-barrel, a zinc-finger, an α/β vWA or trunk domain, an all helical region and carboxy terminal, gelsolin-like domain. The interface between Sec23 and Sec24 involves residues from strand b14 and loop b4-b15 of Sec24. These residues are not highly conserved, since they engage mainly in main-chain hydrogen bonds with the respective strand in Sec23 creating an inter-subunit β-sheet, which connects the trunk domains. Sar1 interacts extensively with Sec23. Of the 24 residues contacting Sar1 12 are highly conserved in Sec23. The 12 residues cluster in three regions from which patch 1, formed by the aM-aN loop of the helical domain, seems to be most important for recognizing Sar1-GTP (Stagg et al., 2006).

The Sec13Sec31 complex forms a heterotetramer, which adopts the shape of a 28 nm long rod, formed by a central α-soleniod dimer, capped on each side by two β-propeller (WD40-) domains (Fath et al., 2007). The carboxy terminal part of Sec31, which consists of an α-solenoid, that is flexibly linked to the amino terminal part by a proline-rich region, is missing in the structure. Interestingly the Sec31 β-propeller, which consists of seven WD40 repeats, is positioned at either end of the heterotetrameric complex. In this way the Sec13 β-propeller separates the β-propeller and the α-solenoid of Sec31. The Sec31 polypeptide passes directly through Sec13 contributing a seventh blade to the six blades of the Sec13 β-propeller (Fath et al., 2007).

The Sec13Sec31 complex can self-assemble in the absence of the inner coat to form so called empty cages. Cryo-EM studies of these empty cages revealed that they adopt two-fold, three-fold and four-fold symmetry consistent with a cuboctahedron, with a cage diameter of ~ 600 Å (Stagg et al., 2006), (Noble et al., 2013). A COPII coat structure prepared from in vitro reconstitution of the Sec23Sec24 and the Sec31Sec13 complex adopted the form of an icosidodecahedron with a diameter of ~ 1000 Å (Stagg et al., 2008). This structure showed a two layered coat, an inner layer formed by Sec23Sec24 and an outer layer formed by Sec13Sec31. The vertex of the outer coat layer is formed by the convergence of four Sec31 β-propeller domains, a proximal and a distal pair, at the dyad symmetry axis. The ends of the Sec13Sec31 heterotetramer containing the Sec31 β-propellers that are closer to the vertex are termed plus ends. The ends further away from the vertex are termed minus ends. This makes five contact interfaces involving proximal-proximal contacts (cI) and proximal-distal contacts (cII and cIII) (Fath et al., 2007). Contact cI occurs between the β-propeller domains of Sec31 at the plus end of two heteroteramers. Contacts cII and cIII occur between the β-propeller domain of a plus end Sec31 and the β-propeller domain of a neighboring minus end Sec31 in the clockwise and counterclockwise directions. A fourth contact cIV occurs between the β-propeller domain of a minus end Sec31 and the β-propeller domain of a plus end Sec13 in the counterclockwise direction (Stagg et al., 2008). The crystal structure of Sec13Sec31, fitted into the cryo EM map, shows an angle of 50° between axis of the Sec13 β-propeller and the axis of the Sec31 β-propeller (Fath et al., 2007). The adaptability of the COPII coat to accommodate cargoes of different size is most likely based on variability of the angles formed between the heterotetramers at the coat vertex (Stagg et al., 2008), (Zanetti et al., 2013). The angles are defined as angles α and β between adjacent edges lying clockwise from a plus or a minus element (Stagg et al., 2008). In the cuboctahedron and the icosidodecahedron assemblies the α angle is fixed to 60°, whereas the β angle is variable (Stagg et al., 2008). To accommodate for larger cargos like procollagen, it seems that both angles α and β need to be flexible, as was shown in the cryo EM structure of COPII coated membrane tubes (Zanetti et al., 2013). The key for the COPII coat adaptability is very like defined by three properties, the variability of α and β angles, the flexibility of the central hinge region of the Sec13Sec31 heterotetramer and the asymmetry of the Sec13Sec31 rods,

which allow to make plus or minus contacts at both ends, as well as plus contacts at one end and minus contacts at the other end (Zanetti et al., 2013).

The icosidodecahedron structure shows an inner coat layer, which shows a four lobed structure with two-fold symmetry directly under the COPII coat vertex. Four Sec23Sec24 dimers of the crystal structure can be fitted into these densities. Sec23Sec24 seems to occupy two different positions relative to Sec13Sec31. One Sec23Sec24 extends along the Sec13Sec31 edge, whereas the other Sec23Sec24 extends out into the middle of the triangular face (Stagg et al., 2008). Assigning of Sec23 to cryo EM densities aided by a Sec13Sec31-Sec23 structure leads to positioning of Sec24 in a way that the cargo binding domain of Sec24 faces the large open square of the cage, a position which is ideal to interact with cargo molecules (Bhattacharya et al., 2012). The cryo EM structure of coated membrane tubes revealed that the inner coat also adopts a regular lattice, forming a helical array on the tube. Formation of the lattice is mediated by two interfaces. The first larger interface involves Sar1, the gelsolin like domain and the carboxy terminal domain of Sec23 from one heterotrimer (Sec23Sec24-Sar1), which are interacting with the Zn-finger and part of the β-barrel domain of an adjacent heterotrimer. The smaller interaction occurs between the Zn-finger domain of Sec24 of one heterotrimer and the gelsolin like domain and the carboxy terminal domain of Sec24 in the neighboring heterotrimer (Zanetti et al., 2013). There are two membrane interacting regions. The first is formed by a small part of Sec23 together with Sar1, which enables Sar1 to insert its amino terminal amphipatic helix into the membrane. The second is formed by a large basic surface in Sec24, which include the Zn-finger, the β-barrel and α-helical domains. Relative positions of the coat layers are not fixed but roughly aligned in spacing and orientation. The inner coat “rows” are aligned to the left handed rods in the outer coat. Four inner coat heterotrimers are spanning one rod in the outer coat. The columns of the inner coat are aligned to the right handed rods in the outer coat, and two heterotrimers in the inner coat are spanning one rod in the outer coat. Most likely the unstructured carboxy terminal part of Sec31, which is presumed to connect the two coat layers, constrains the coat layers relative to one another but does not fix their position. This flexibility would allow the coat to adapt to different membrane curvatures (Zanetti et al., 2013).

1.2.2 Clathrin coated vesicles

Clathrin coated vesicles (CCV) operate in the late secretory pathway. They mediate the transport between TGN, lysosomes, endosomes and the plasma membrane as well as the process of endocytosis. The clathrin triskelion, composed of three heavy (190 kDa) and three light (25 kDa) chains forms the outer shell and the scaffold of clathrin-coated vesicles (Kirchhausen, 2000). Polymerization of the clathrin triskelion leads to the formation of a stable cage-like structure (Kirchhausen, 2000). This structure can also be formed without the adaptor proteins, which form the inner coat (Crowther and Pearse, 1981). Recruitment and recognition of cargo is mediated by the adaptor protein complexes (AP). The AP complexes have a heterotetrameric architecture composed of two large (110-130 kDa), one medium (50 kDa) and one small (15-20 kDa) subunit. The adaptor protein complexes bind at the same time transmembrane components, phospholipids and clathrin, thereby mediating a link between the innermost cargo proteins and the outer clathrin shell (Owen et al., 2004). There are five different AP complexes, which are involved in different transport processes. AP1 containing clathrin vesicles mediate the transport from the TGN to endosomes. AP3 containing CCVs mediate the transport to lysosomes (Spang, 2008). Clathrin coated vesicles containing AP4 seem to be involved in basolateral transport in epithelia cells (Simmen et al., 2002). Arf1 is the small GTPase necessary for the formation of clathrin coated vesicles containing adaptor complexes AP1, AP3 and AP4 (Spang, 2008). Clathrin coated vesicles containing AP2 mediate the endocytosis at the plasma membrane (Boehm and Bonifacino, 2001). The small GTPase Arf6 is required for formation of clathrin coated vesicles containing AP2. AP5 is clathrin independend and does not bind YxxΦ signals. Its presumed place of action are late endosomes and lysosomes (Hirst et al., 2011).

1.2.2.1 Structure of the clathrin coats

The clathrin coat is composed of two layers. The outermost layer is formed by an array of clathrin triskelia. The inner coat layer is formed by the adaptor protein complexes, which link the incorporated cargos to the outer coat layer.

Each clathrin triskelion is composed of three clathrin heavy chains (CHC) and three clathrin light chains (CLC) and has an approximately three-fold rotational symmetry. Purified clathrin can assemble spontaneously to form cages or, in the presence of adaptor proteins, coats. Crystal structure data showed that the clathrin heavy chain is composed of an N-terminal seven bladed β-propeller domain, which is connected to an α-helical part (ter Haar et al., 1998). The α-helical part is composed of a coil of short α-helices. Individual helix-turn-helix-loop or helix hairpin units form the canonical repeat and stack along an axis to form an elongated right-handed superhelix coil of α-helices, which make up a single extended domain (Ybe et al., 1999). A clathrin heavy cahin repeat motif (CHCR) was identified, with seven complete CHCR found in one triskelion leg (Ybe et al., 1999).

Clathrin coats occur in different sizes and shapes. The coat lattice is formed by open hexagonal and pentagonal faces. The smallest clathrin coats formed are referred to as “mini-coat”, “hexagonal barrel” and “soccer ball”. The hexagonal barrel and the soccer ball coats are most likely the smallest polyhedrons able to accommodate a transport vesicle (Fotin et al., 2004). The architecture of a clathrin triskelion can be subdivided into six domains. The vertex of the clathrin triskelion, the triskelion hub, is made up by three proximal legs of CHC. These legs are held together by the helical tripod trimerization domain, which is formed by the carboxy terminal 100 residues of each clathrin heavy chain. This domain is situated directly beneath the point where the three proximal legs meet (Fotin et al., 2004). The proximal leg segment comprises CHCR7 and CHCR6 and is followed in the amino terminal direction by the knee domain made up by the carboxy terminal part of CHCR5. The knee domain in turn is followed by the distal leg domain composed of the amino terminal part of CHCR5, CHCR4 and CHCR3. The distal leg domain leads to the ankle domain, which is composed of CHCR2, CHCR1 and CHCR0. This domain is finally followed by the amino terminal located terminal domain, which is formed by the β-propeller (Edeling et al., 2006). The individual clathrin triskelia intertwine to form the clathrin coat. Travelling to the center

of the cage from the vertex of one clathrin triskelion, first the helical tripod trimerization domain is encountered, which is situated directly under the point where the three proximal legs of one triskelion meet. Below this there is a triangular structure, which is formed by three distal leg segments. These distal leg segments each originate from a separate neighboring clathrin triskelion. Travelling further to the center, three ankle segments are encountered, each from three further triskelia and below these three terminal domains. The terminal domains originate again in three separate triskelia, which are not connected to the triskelia of the distal leg segments and the ankle segments above them. Also the terminal domains curve towards each other, which almost forms an enclosure beneath the distal and trimerization domains (Fotin et al., 2004).

The function of the clathrin light chain (CLC) is still debated in the field. A cryo EM difference structure of the clathrin coat with and without the light chain showed a density, that corresponds to a single α-helix of 71 residues running along the outer edge of the clathrin cage (Fotin et al., 2004). Two contact sites where predicted: CHC-K1326-CLC-W108 and CHC-K1514-CLC-W130, which both corresponded with the cryo EM fit (Fotin et al., 2006), (Fotin et al., 2004). Crystal structures from the complete CLC bound to the CHC hub showed a regulatory function of CLC on clathrin assembly. The ankle regions of the solved structure showed either a straight ankle or a bend ankle conformation. The straight ankle conformations are associated with extended CLC, whereas the bend ankle conformation is associated with a more compact structure of the CLC (Wilbur et al., 2010). In the more compact structure the resolved CLC density is present at the trimerization domain and spans half of the proximal leg segment. The CLC amino terminal part is bending away from the CHC ankle region, which seems to be important for regulating clathrin assembly. In the bend ankle conformation the CHC structure is compatible with the assembled clathrin cage allowing hexagonal or pentagonal angles. If the CLC is bound the ankle is straight and clathrin assembly is inhibited (Wilbur et al., 2010).

Travelling further to the center of the clathrin coat the layer below the clathrin terminal domains is made up by the adaptor protein complexes (APs). The adaptor protein complexes (AP1-AP4) are heterotetrameric complexes with two large (100 -130 kDa) and two small subunits. The two large subunits are termed β1-β4 and γ, α, δ and ε in AP1-AP4. The small subunits are termed μ1-4 and σ1-4 for AP1-AP4. The large subunits are composed of two

domains, the amino terminal trunk domain, which makes up two thirds of the large subunit, and the carboxy terminal appendage domain. Both domains are connected by a flexible linker region. Proteolysis studies indicate that the APs are composed of a central brick like core that is connected to two globular appendages by flexible linkers (Zaremba and Keen, 1985), (Schröder and Ungewickell, 1991). Recently the core structures of AP1 and AP2 have been solved (Collins et al., 2002), (Kelly et al., 2008), (Jackson et al., 2010), (Ren et al., 2012). The trunk domains of the large subunits α and β2 are solenoids of stacked α-helices. The amino terminal part of μ2 (μ2 1-135) and σ2 adopt a login domain like fold. These four subunits are arranged into a bowl, in which the elongated carboxy terminal domain of μ2 is situated. AP2 has two positively charged sites, one on α and one on μ2, which allow binding of PtdIns4,5P_2. The site on α is presumed to be important for initial binding of AP2 to PtdIns4,5P_2 and cargo containing membranes (Gaidarov et al., 1996), (Höning et al., 2005). Cargo binding motifs haven been localized on σ2 (di-leucine based [ED]xxxL[LI] motif) and on the carboxy terminal part of μ2 (tyrosine based YxxΦ motif) (Chaudhuri et al., 2009), (Kelly et al., 2008), (Ohno et al., 1995), (Owen and Evans, 1998). Structural data show that upon cargo binding the AP complexes undergo a conformational change from a closed state to on open state (Collins et al., 2002), (Kelly et al., 2008), (Jackson et al., 2010), (Ren et al., 2012). For AP2 in the locked, cargo motif free conformation, both cargo motif binding sites are blocked by the β2 subunit. β2Tyr6 and β2Phe7 block the [ED]xxxL[LI] site and β2Glu364-β2Val406 block the YxxΦ site. In an [ED]xxxL[LI] site bound structure the amino terminal part of β2 is displaced, which allows binding to the [ED]xxxL[LI] motif. However the YxxΦ site remains blocked. In both the locked conformation and the [ED]xxxL[LI] motif bound state, the YxxΦ site is located on the orthogonal face compared to PtdIns4,5P_2 binding sites on α and the [ED]xxxL[LI] site (Kelly et al., 2008). It requires a large conformational change to allow binding of YxxΦ cargo embedded in a PtdIns4,5P_2 containing membrane.

A released structure with both cargo binding sites occupied describes the open confirmation of AP2 (Jackson et al., 2010). Upon transition from the closed state to the open state the AP2 bowl collapses inwards. In the process the carboxy terminal part of the μ subunit is expelled. The collapse is facilitated by rotations about four hinge points, from which two are located in α and two are located in β2. In this way each large subunit is composed of three rigid groups. The buried surface area changes from 10040 Å in closed state to 9700 Å in the open

state. This indicates that the closed conformation is presumably the more stable one and predominates in solution. The interfaces between the subunits α and σ2, α and β2 and β2 and the amino terminal part of μ2 remain largely unaffected by the conformational change upon state transition. The major conformational changes occur in the carboxy terminal part of μ2 and the amino terminal part of β2. The carboxy terminal part of μ2 undergoes a 129° screw rotation about its long axis with a translation of 39 Å relative to it amino terminal part. The subunit contacts made by C-μ2 are changed completely. All contacts with α and σ2 are lost upon the conformational change. The conformational relocation of C-μ2 results in the co-planar arrangement of the binding sites of PtdIns4,5P_2 and the cargo binding sites for YxxΦ and [ED]xxxL[LI] motifs on the surface of AP2. This enables contact to various signals on the plasma membrane. Three additional regions with positive electrostatic potential could be identified. The first is composed of basic residues in the amino terminal part of β2 (Lys5, Lys12, Lys26, Lys27, Lys29 and Lys36). Mutations in these residues inhibited recruitment of the AP2 to PtdIns4,5P_2 containing membranes (Höning et al., 2005), (Jackson et al., 2010). The second (Lys330, Lys334, Lys350, Lys352, Lys354, Lys356, Lys367, Lys368, Lys373) and third (Lys167, Arg169, Arg170, Lys421) regions are located on C-μ2. Mutations in these regions only slightly reduced recruitment of AP2 (Jackson et al., 2010), (Collins et al., 2002), (Gaidarov et al., 1996), (Rohde et al., 2002). Therefore AP2 recruitment most probably occurs mainly through the α and β2 PtdIns4,5P_2 binding sites. Upon recruitment to the membrane the binding of AP2 can be further stabilized through binding of YxxΦ and [ED]xxxL[LI] cargo motifs.

For AP1 it was shown, that the small GTPase Arf1 can unlock the AP1 complex and activate cargo binding (Ren et al., 2012). The AP1 core also occurs in a closed (Heldwein et al., 2004) and an open confirmation (Ren et al., 2012). In contrast to AP2 phosphoinositides alone are insufficient to recruit AP1. The key factor for recruitment of AP1 to the TGN is the small GTPase ADP ribosylation factor 1 (Arf1) (Seaman et al., 1996), (Stamnes and Rothman, 1993), although high levels of cargo signals can override this requirement (Lee et al., 2008). The structure, which was solved in the presence of Arf1-GTP but in the absence of cargo tails and phosphoinositides, could be superimposed to the open AP2 structure (Jackson et al., 2012). In the AP1 structure Arf1 bridges two AP1 cores. In this way Arf1 is binding to two separate regions in AP1. In the larger interface (~720 Å) the switch I and switch II regions of Arf1 are

buried against helices a1, a3 and a5 of β1. The contacts on β1 are centered on Gln59, Ile85 and Asn89. The contacts on Arf1 include residues Ile46, Ile49, Gly50, Phe51, Asn52 and Val53 of switch I, Trp66, Lys73, Ile74, Leu77, His80, Tyr81 and Gln83 of switch II and Tyr35 of a1. The binding site on β1 is compatible with a predicted Arf1 binding site in the helices a4 and a6 of the beta subunit of COPI (Yu et al., 2012), which correspond to the helices a3 and a6 in b1 of AP1. In the smaller interface (~690 Å) the carboxy terminal a4, b6 and a5 on the back side of Arf1, which is the opposite face of the switch I and switch II regions, are buried against the helices a12-a16 of the γ subunit. On the back side of Arf1 a cluster of large hydrophobic residues is participating in this interface (Trp153, Tyr154 and Trp172). At the periphery Ala136, Ala137 and Gln176 are also involved in contacts with γ. The residues involved on the γ subunit could not be identified due to the low resolution of the structure (Ren et al., 2012). Mutational analysis of the predicted interfaces showed that only mutation of the β1 biding side (β1I85D/V88D) completely abolished binding to Arf1-GTP. Mutation of the γ binding site (γL102E) reduced binding to 10% of wildtype levels. In this way the γ binding site seems functional but its affinity for Arf1 is lower compared to the β1 binding site. Biochemical analysis suggested that the γ recruitment site of AP1 is not much involved in AP1 activation. The occupancy of this site seems to be incompatible with membrane binding of the dimeric AP1 assembly. It was proposed that AP1 binds in the closed confirmation to two copies of Arf1 via the two recruitment sites. After binding the present cargo would shift the equilibrium to the open state, which would be stabilized by establishing the Arf1 back side contact. The γ recruitment site would have to dissociate to allow membrane binding in the cargo bound confirmation (Ren et al., 2012).

1.2.3 COPI vesicles

COPI vesicles operate in the early secretory pathway in the retrograde transport from the Golgi back to the ER and in intra-Golgi transport. COPI vesicles can form at the ERGIC from anterograde carriers and at Golgi cisternae.

Components of COPI vesicles

1.2.3.1 The coatomer complex

The coat protein complex of COPI vesicles coatomer, with a molecular weight of ~ 600 kDa, is composed of seven subunits α (138 kDa), β (107 kDa), β´ (102 kDa), γ (100 kDa), δ (57 kDa), ε (34 kDa), and ζ (22 kDa). It can be reversibly dissociated into a trimeric (αβ´ε) and a tetrameric (βγδζ) subcomplex using elevated salt concentrations (Lowe and Kreis, 1995). Under physiological conditions the complex seems to remain fully assembled during its complete life-cycle within the cell. For the γ-COP and ζ-COP subunits two different isoforms (γ_1, γ_2, ζ_1 and ζ_2) could be identified in higher eukaryotes (Blagitko et al., 1999), which enables the formation of four different isotypic COPI-vesicles. γ_1-COP and γ_2-COP have a sequence identity of 80% at amino acid level. ζ_1-COP and ζ_2-COP have a sequence identity of 61%. The discrepancy in sequence identity is mainly due to the N-terminal part, which is 30 amino acids longer in ζ_2-COP (Wegmann et al., 2004).

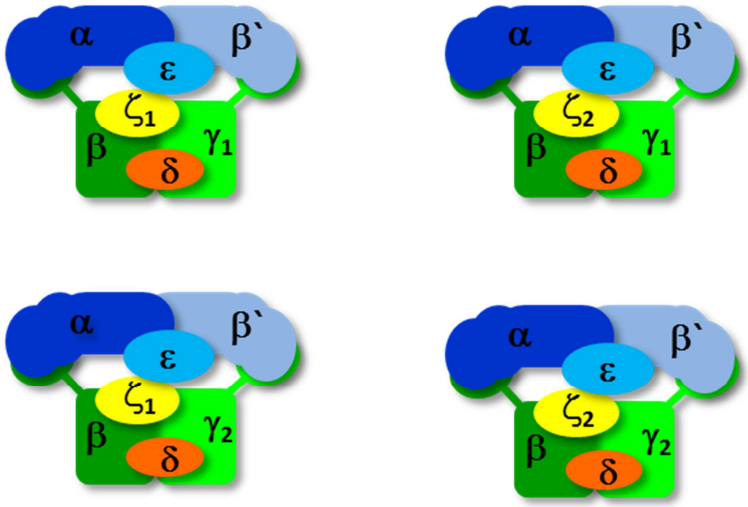

Figure 2: Isoforms of the coatomer complex

The different isotypes (figure 2) of coatomer are not evenly distributed within the cell. In vivo analysis of coatomer isoform distribution showed that $\gamma_1\zeta_1$ is the most abundant isoform with 55%, followed by the $\gamma_2\zeta_1$ isoform with 25% and the $\gamma_1\zeta_2$ isoform with 15% (Moelleken et al., 2007). The $\gamma_2\zeta_2$ isoform is the least abundant form of coatomer making up

only 5% of the total coatomer population. Also the different coatomer isoforms show a distinct subcellular localization. The majority (~ 70%) of the γ_1-containing coatomer is localized to the cis-Golgi, whereas the majority (~60%) of the γ_2-containing coatomer is localized to the trans-Golgi. Coatomer containing ζ_2-COP is predominantly (~80%) localized to the cis-Golgi (Moelleken et al., 2007). For ζ_1-COP up to now no specific subcellular localization could be shown due to the lack of ζ_1-specfic antibodies. The differential localization of the coatomer isoforms raises the question, if the different isoforms are involved in different transport vectors, or if they transport different cargoes. This question is still under investigation and up to now no conclusive answer could be presented.

1.2.3.2 p24 family proteins

p24 proteins are typeI-transmembrane proteins. In mammals six different p24 proteins could be identified p23, p24, p25, p26, p27 and tp24. They are a component of COPI and COPII vesicles (Sohn et al., 1996), (Stamnes et al., 1995) and are circulating within the early secretory pathway (Nickel et al., 1997) with distinct localizations for the specific members. The architecture of the p24 proteins is composed of a large amino teminal luminal domain with a conserved coiled-coil region, a transmembrane domain and a short cytosolic C-terminal domain with a di-phenylalanin and a di-basic motif (KKxx, KKx_n or KRx_n with n>3). The amino terminal domain is presumed to mediate the oligomerisation of the proteins via its coiled-coil domain (Emery et al., 2000), (Füllekrug et al., 1999). The binding of p24 to coatomer is dependent on both C-terminal motifs. Mutation of either the KKxx or the FF residues reduces the binding significantly and mutation in both motifs abolishes the interaction entirely (Béthune et al., 2006b), (Cosson and Letourneur, 1997), (Reinhardt et al., 1999), (Sohn et al., 1996). The interaction of coatomer with the dimeric cytoplasmic domain of p23 induces a conformational change and leads to aggregation of the complex in vitro (Reinhardt et al., 1999). All members of the p24 family bind as dimers to two independent sites in the appendage and the trunk domain of the coatomer subunit γ. Dimers of p23 induce a conformational change in the trunk domain of γ-COP (Béthune et al., 2006b), which is transduced to the α-COP subunit (Langer et al., 2007). The dimeric form of p24 proteins

also bind to Arf1 and in this way are important for the initiation of the COPI vesicle biogenesis (Gommel et al., 2001).

1.2.3.3 ADP ribosylation factor 1 (Arf1)

Arf1 is the small Guanin nucleotid binding protein (GNBP) essential for the biogenesis of COPI vesicles (Serafini et al., 1991). Arf proteins are part of the Ras protein superfamily. This superfamily includes the Ras-, Rho-, Arf-, Rab-, Ran-, Rit-, Rad-, and Rag-family of proteins (Boguski and McCormick, 1993). All of them share the same function to serve as molecular switches, which means that the proteins can adopt two different conformations. They cycle between an active, GTP- bound, and an inactive, GDP-bound, conformation (Vetter and Wittinghofer, 2001), (Wittinghofer et al., 1993).

The Arf proteins are highly conserved. All of them share the same feature of an amino terminal located amphiphilic α-helix, which is posttranslationally myristoylated (Antonny et al., 1997). The six Arf proteins are subdivided into three classes based on their sequence identity. Class 1 contains the Arf proteins 1-3, class 2 contains Arf4 and Arf5 and class 3 contains Arf6 (Donaldson and Jackson, 2011). Class 1 Arf proteins in *homo sapiens* have a size of 181 amino acids and share a high sequence identity with only seven amino acids different between Arf1-3. They are involved in the activation of lipid modifying enzymes like the activation of phospholipase D and play a role in vesicular transport (Honda et al., 2005). In class 2 Arf5 is assumed to be involved in the transport within the Golgi to the TGN (Claude et al., 1999). Arf4 like Arf1 is localized to the cis-Golgi and can assume the function of Arf1 upon its knockdown (Volpicelli-Daley et al., 2005). The class 3 Arf protein Arf6 has a size of 175 amino acids and is thus a bit shorter than the other Arf proteins. Arf6 localizes primarily to the plasma membrane. It functions as a small GNBP-regulator (Guanin nucleotide binding protein) for AP2 clathrin coated vesicles in the process of endocytosis and as a regulator for actin polymerization by recruitment of rho family proteins (Honda et al., 2005). Arf6 is also involved in the transport from the plasma membrane to the endosomes.

The structure of Arf

A descriptive structural feature of small GNBPs is the G domain, which has the ability to bind and hydrolyze guanine nucleotides dependent on the presence of stabilizing magnesium ions. The G domain is composed of six β-strands and five α-helices, which contain five conserved stretches, termed G1-5. The conformational changes, which occur during the switch from the active to the inactive state, mainly take place within three conserved regions.

The first region is the G1 motif, also termed P-loop, which contain the consensus sequence GxxxGSK/T. This sequence interacts with the α and β phosphate groups and coordinates the magnesium ion localized in the active center. The second region is the G2 motif, also termed switch I, with a conserved T residue. The third region is the G3 motif, also termed switch II, with the consensus sequence DxxG.

Up to now it has not been possible to solve the structure of full length Arf1, which is hampered by the insolubility of GTP bound Arf1. The structure of GDP bound full length Arf1 (Amor et al., 1994) shows differences to the structure of GDP bound full length Ras (Goldberg, 1998). In GDP bound Arf the amino acids 41-47 form an additional seventh β-strand (Amor et al., 1994), which is not present in other GNBPs of the Ras superfamily (Amor et al., 1994), (Goldberg, 1998). A structure of a soluble form of Arf1 (NΔ17Arf1), with the non-hydrolysable GTP analog GMP-PNP, shows great similarity to GTP bound Ras (Goldberg, 1998).

In Arf1 and in Ras, in the GTP bound form, the γ phosphate of GTP is coordinated by switch I and switch II. The coordination occurs mainly via hydrogen bonds between the conserved threonine in switch I (Thr48 in Arf1, Thr34 in Ras) and the conserved glycin in switch II (Gly70 in Arf1, Gly60 in Ras) (Vetter and Wittinghofer, 2001), (Goldberg, 1998). A highly conserved glutamin (Gln71 in Arf1, Gln61 in Ras) together with a conserved aspartate (Asp67 in Arf1, Asp57 in Ras) is coordinating the water molecule, which is acting as the attacking nucleophile during the hydrolysis (Vetter and Wittinghofer, 2001), (Goldberg, 1998). The nucleotide exchange causes only minimal structural changes within the p-loop, which coordinates the α and β phosphate groups.

Compared to other proteins of the Ras family, the Arf proteins show an additional conformational change. This rearrangement is attributed to the interswitch region, which is 3 to 5 amino acids shorter in Arf proteins compared to other members of the Ras superfamily. The interswitch region is composed of b2, a loop and b3. In the GDP bound state the conserved W78 keeps the interswitch region and switch II in a conformation that prevents the coordination of GTP by Gly70 and Asp67 (Pasqualato et al., 2002). In this way the amino terminal helix can fold back over the protein core, which leads to the formation of a hydrophobic pocket for the myristoyl anchor (Pasqualato et al., 2002), (Goldberg, 1998). In this state the amino acids Tyr58, Asn60, Ile61 and Phe63 of loop 3 presumably interact with the amino terminal helix (Amor et al., 1994).

The conformational change upon exchange to GTP causes the interswitch region to be raised by 7-8 Å (Goldberg, 1998), which also affects switch I and switch II regions (Pasqualato et al., 2002). This requires the amino terminal, myristoylated α-helix to be exposed. The solvent exposure of the amino terminal helix with its myristoyl anchor is energetically unfavorable. Therefor exchange to GTP can take place only at membrane localized Arf.

The position of the amino terminal a helix upon membrane binding is still under debate. A NMR structure of Arf1-GTP on bicells showed that the myristoyl anchor is not inserted in the membrane, but folds back partially and is lying parallel to the amino terminal helix on the membrane (Liu et al., 2010). This model is not able to explain the membrane surface activity of Arf1 (Beck et al., 2009). The model might be hampered by the high curvature of the bicells, which is not present in cellular membranes. The lipids in the outer layer of bicells are packed less densly then in cellular membranes, which might be compensated by the association of the myristoyl anchor.

Dimerization of Arf1

Another question is, if Arf1 is dimerising during COPI vesicle biogenesis and how Arf1 dimers are accommodated in the forming COPI vesicle coat. Through the use of thiol specific crosslinkers it could be shown that Arf1 can form dimers on the membrane (Beck et al., 2011). The distance between crosslinked intermolecular cysteins was shown to be 16 Å. A

model was generated, in which the N- and C-termini of the Arf1 proteins are facing to the membrane. Based on the model different amino acids in the presumed dimer interface were mutated to alanine. The variant Y35A was shown to be unable to form dimers. A further characterization showed that Arf1Y35A can bind to membranes in the presence of coatomer, but is unable to form free COPI vesicles (Beck et al., 2009). Cryo-EM studies of COPI vesicle formation with the Arf1Y35A mutant showed scission arrested vesicles (Beck et al., 2011). It is assumed that Arf1 dimers might play a role in the scission process.

1.2.3.4 ArfGAPs

ArfGAP proteins are characterized by a conserved GAP domain of ~ 70 amino acids that contains a zinc finger motif and an invariant arginine residue (Cukierman et al., 1995), (Donaldson and Jackson, 2011), (Goldberg, 1999). In *homo sapiens* up to now 31 ArfGAPs could be identified, which are subdivided into 9 groups. From this pool only the ArfGAPs 1-3 are localized to the Golgi (Donaldson and Jackson, 2011). ArfGAPs are recruited to COPI vesicles by directly binding to Arf, to cytoplasmic tails of cargo proteins and to coatomer. ArfGAP1 contains two ALPS motifs (ArfGAP1 lipid packaging sensor), which are unstructured in solution. These motifs can recognize and bind curved membranes. During this binding they form amphiphilic α-helices (Bigay et al., 2005). ArfGAP1 can also bind to the C-terminal part of δ-COP (Rawet et al., 2010). ArfGAPs stimulate GTP hydrolysis of Arf1 and are therefore essential for the uncoating process. The activity of ArfGAP1 is proportionally higher at curved membranes than at flat membranes (Bigay et al., 2005). ArfGAP2 and ArfGAP3 do not directly interact with membranes. They are recruited indirectly by binding to the γ-appendage domain of coatomer (Frigerio et al., 2007), (Owen et al., 2004), (Pevzner et al., 2012). In the presence of coatomer the activity of ArfGAP2 and ArfGAP3 is significantly higher than the activity of ArfGAP1 (Weimer et al., 2008). ArfGAP proteins are also important for the incorporation of cargo into COPI vesicles (Malsam et al., 1999), (Nickel et al., 1998).

1.2.3.5 Arf-GEFs

At present 15 different Arf-Guanin nucleotide exchange factors are described in mammals. They all share the 200 amino acid catalytic Sec7 domain (Jackson and Casanova, 2000). Some of these GEFs, like the cytohesin ARNO, contain a PH domain in an autoinhibited conformation (DiNitto et al., 2007). This autoinhibition is abolished upon interaction of the PH domain with the membrane lipids $PI(4,5)P_2$ or $PI(3,4,5)P_3$ and at the same time with activated Arf6 or Arl4. After inhibition is relieved membrane bound ARNO can catalyze nucleotide exchange on Arf6-GDP or Arf1-GDP (Stalder et al., 2011). The GEF protein involved in COPI vesicle biogenesis is GBF1. GBF1 is most probably localized to the cis-Golgi by its interaction with Rab1 (Zhao et al., 2002), (Monetta et al., 2007). There it enables nucleotide exchange and activation of Arf1. GBF1 has also been reported to interact with Arf4 (Szul et al., 2005).

1.3 Biogenesis of COPI vesicles

The biogenesis of COPI (figure 3) vesicles can be divided into five partially interdependent steps: coat recruitment, uptake of cargo, budding, membrane separation (scission) and uncoating.

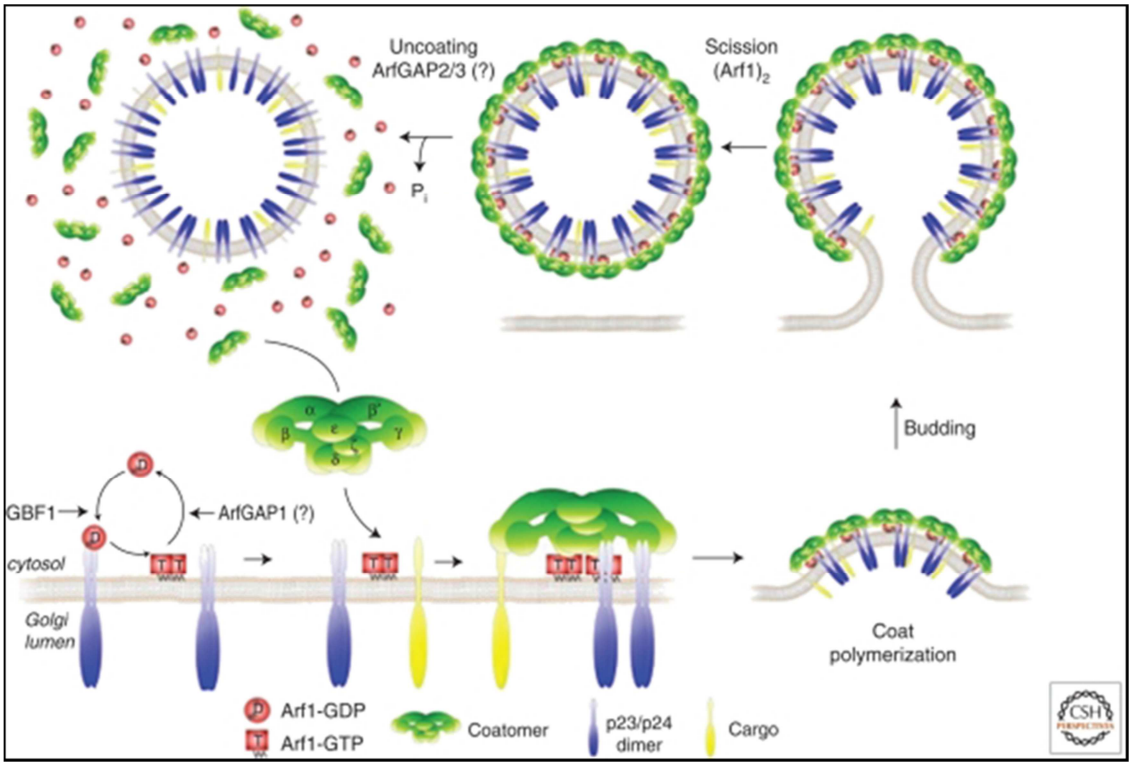

Figure 3: COPI vesicle biogenesis (Popoff et al., 2011). For details see text.

The formation of COPI vesicles is initiated by the recruitment of the small Ras-like GTPAse Arf1. Like all GTPases Arf1 cycles between an active GTP-bound and an inactive GDP-bound form. It contains Golgi-localization signals within its sequence. Arf1-GDP binds to Golgi-membranes via cytosolic domains of dimeric complexes of p24 family proteins (Gommel et al., 2001), (Majoul et al., 2001), or by interaction with the v-SNARE protein membrin (Honda et al., 2005). Arf1 is activated on Golgi membranes by nucleotide exchange to GTP catalyzed by the Guanin-nucleotide exchange factor GBF1, a member of the Sec7 superfamily (Claude et al., 1999), (Spang et al., 2001), (Kawamoto et al., 2002), (Zhao et al., 2002). The catalytic domain of GBF1 is a Sec7 domain containing a conserved glutamic residue exposed at the tip of a hydrophobic loop between helices six and seven (Beraud-Dufour et al., 1998). The exchange of the nucleotide is mediated by electrostatic competition of the conserved glutamic side chain with the β-phosphate of the nucleotide. Exchange from GDP to GTP triggers a conformational change in Arf1, which leads to the exposure of its amino-terminal amphipathic and myristolated helix. This exposure causes the insertion of the helix into the lipid bilayer and anchors Arf1 to the membrane (Franco et al., 1996), (Antonny et al., 1997). After binding of Arf1 to the membrane the coatomer complex can be recruited by Arf1 and

p24-dimers *en bloc*, in contrast to the clathrin/AP and the COPII system where two separate coat layers are recruited successively. Upon its recruitment coatomer forms multiple interfaces with Arf1-GTP. Arf1-GTP interacts with coatomer subunits β´-COP, β-COP, δ-COP, the trunk domain of γ-COP (Zhao et al., 1997), (Zhao et al., 1999), (Sun et al., 2007) and with ε-COP (Eugster et al., 2000). Coatomer also binds to p24-dimers at two independent binding sites within γ-COP, which interact with conserved $FFXXBB(X)_n$ binding motifs of the p24 proteins (Béthune et al., 2006a). This interaction triggers a conformational change of the coatomer complex (Reinhardt et al., 1999), which most probably initiates its polymerization (Langer et al., 2008). The formation of a vesicle bud requires membrane deformation, which is accomplished by two processes. In the first process the small GTPase Arf1 is interacting with its amino termial amphipatic helix with the membrane and is inserting its myristoyl-anchor into the membrane upon its activation. This leads to changes in the structure of the membrane, which is also described as membrane surface activity (Beck et al., 2009). In the second process polymerization of coatomer enforces tension on the membrane, which is most probably resolved by bending of the membrane and the formation of a vesicle-bud (Dodonova et al., 2015). The fourth step in the COPI vesicle biogenesis is membrane scission, the separation of the newly formed vesicle from its donor membrane. For this step dimerization of Arf1 is required (Beck et al., 2009).

In order that vesicles formed can fuse with their respective target membrane, the protein coat has to be shed. The uncoating step is initiated by the GTP-hydrolysis of Arf1, which is stimulated by the ArfGAP proteins (Cukierman et al., 1995). In vitro experiments, in which purified ArfGAPs were added to COPI-vesicles, have shown that no other factors are required for this process (Reinhardt et al., 2003). In the last step the coat free COPI vesicle can fuse with its target membrane. The fusion process is mediated by SNARE-proteins.

1.4 The structure of the COPI coat

In contrast to the COPII and the clathrin coat the COPI coat is formed by the heptameric coatomer complex, which is recruited *en bloc* to the membrane. The coatomer complex fulfills the functions of both recruitment/binding of cargo and scaffold formation for the budding vesicle. Coatomer can be divided in a trimeric (αβ´ε) and a tetrameric (γβδζ)

subcomplex under high salt conditions (Pavel et al., 1998) (Lowe and Kreis, 1995). Structurally the tetrameric subcomplex is related to the cargo binding adaptor protein complexes, and that the trimeric subcomplex is similar to the scaffold forming clathrin complex. Recently crystal structures for several subcomplexes of coatomer have been described but a complete high resolution structure is still missing. Also only low resolution single particle EM-structures of complete cytosolic coatomer are available up to now (Yip and Walz, 2011).

A single particle EM structure of soluble coatomer showed that the complex is composed of two major domains. The first domain is roughly globular and is connected to the midsection of the second more extended domain. Both domains can adopt multiple conformations. Especially the extended domain seems to be highly flexible, with multiple orientations for the terminal regions. The carboxy terminal ends of δ-COP and γ-COP could be assigned to the lower part of the globular domain by tagging with GFP. GFP fused to the C-terminus of δ-COP and γ-COP was visible as additional density in the EM structure. GFP fused to the C-terminus of α-COP, β´-COP and ε-COP failed to show additional densities (Yip and Walz, 2011).

The first high resolution structural insights into the coatomer complex were derived from crystal structures of the γ-COP appendage domain (Hoffman et al., 2003), (Watson et al., 2004). Secondary structure predictions and proteolytic digestion analysis had indicated that the large subunits of the tetrameric subcomplex were composed of an amino terminal trunk domain and a carboxy terminal appendage domain, which was connected to the trunk domain by a flexible linker region, similar to the adaptor protein complexes. The γ-COP appendage domain is itself composed of two subdomains. The amino terminal domain has an immunoglobulin-like fold, which contains two β-strands packing against each other to form a β-sandwich. The immunoglobulin-like fold is preceded by a single α-helix. The second subdomain is composed of a central antiparallel, five-stranded β-sheet, that is flanked by three α-helices. The first of these helices (a1) is packing against the upper face of the β-sheet, thereby creating a cleft between this helix and the solvent-exposed parts of the β-sheet surface. The α-helices a2 and a3 are packing against the lower face of the β-sheet. They are part of the hydrophobic interface between the two subdomains. The structure of

the γ-COP appendage domain shows a high overall structural similarity to the appendage domains of α and β of the AP2 complex. In AP2 the carboxy terminal subdomain of the appendages is referred to as the platform domain, which serves as a binding platform for a variety of proteins involved in CCV formation. The platform domain and the immunoglobulin-like domain of γ-COP and of the appendages of αAP2 and βAP2 can be superimposed quite well. There are some unique differences, which occur in the γ-COP appendage. The α-helix preceding the immunglobulin-like domain is unique in the γ-COP appendage. Also γ-COP has a unique insertion between strand b8 and b9. This insertion forms an extended loop, which folds across the bottom of the immunoglobulin-like domain. The largest difference between the three appendages is the relative orientation between the two subdomains. This orientation is governed by the interface between the two subdomains, which is not flexible. Differences in the relative orientations can be attributed to the respective interface between the subdomains. The γ-COP appendage as well as the AP2 appendages contains a conserved F/W motif, which is present in the helix a1 of the platform domain. γ-COP residues Phe772 and Trp776 form a solvent-exposed hydrophobic patch, which is located in a shallow cleft on the platform surface. This cleft is formed by the helix a1 and the face of the β-sheet. The aromatic residues are flanked by a cluster of basic residues Arg843 Arg845 and Arg859. For AP2 the F/W motif is known to be implicated in the binding of proteins, which are bound by the platform domain (Owen et al., 1999), (Owen et al., 2000), (Traub et al., 1999). In γ-COP it has been shown that the F/W motif is involved in binding of ARFGAP2, since a W776S mutant of the γ-COP appendage showed no ARFGAP2 binding compared to the wildtype (Watson et al., 2004).

Further insight into the coatomer structure was derived from a solution NMR-structure of ζ-COP, the smallest subunit (~20kDa) of coatomer (Yu et al., 2009). The overall fold of ζ-COP is very similar to AP1-σ1 and AP2-σ2. The structure is composed of an amino terminal tail, a five stranded antiparallel β-sheet, a two stranded antiparallel β-sheet and five α-helices. The center of the structure is formed by the five stranded antiparallel β-sheet, which is sandwiched by helix a1 on one side and helices a2 and a4 on the other side. Helices a2 and a4 are linked by the smaller helix a3. Modelling and mutagenesis studies proposed an interface for ζ-COP and γ-COP based on hydrophobic patches (Yu et al., 2009).

A structure of a truncated αβ´-COP subcomplex, reported in 2010 showed that β´-COP has an arrangement of two amino terminal β-propeller domains followed by an α-solenoid (Lee and Goldberg, 2010). This α-solenoid of β´-COP binds in antiparallel manner to an α-solenoid of the α-COP subunit. Three copies of this αβ´-COP subcomplex converged through their amino terminal β-propeller domains of β´-COP to form a triskelion. Each triskelion leg extends approximately 175 Å around its curved path and 120 Å radially from the triskelion center. It was proposed that this triskelion structure constitutes the vertex of the COPI cage (Lee and Goldberg, 2010). This domain organization in β´-COP is similar to the one in the Sec13Sec31 complex of the COPII cage. The β-propeller domains of β´-COP are composed of seven blades like the ones in Sec13Sec31. Both β-propeller domains interact through a small interface, in which loops from blades 1, 2 and 7 of the carboxy terminal propeller interact with residues on loops 5, 6 and 7 of the amino terminal propeller. This interface might indicate some flexibility between the two β-propellers. Compared to the COPII system the axes of the β-propellers are oriented differently. The axes of the two β-propellers in β´-COP are positioned almost parallel and displaced 25 Å from each other. The curvature of the triskelion is created by an angle of ~ 90° between the axis of the carboxy terminal β-propeller and the following α-solenoid domain. This α-solenoid domain is an almost straight rod of ~90 Å and is composed of sixteen α-helices. The curvature in the α-solenoid region arises from the 40° angled interaction of the β´-COP α-solenoid with the α-solenoid of α-COP. This antiparallel interaction of the two α-solenoid domains is similar to the homdimerization of Sec31 through its α-solenoid domains (Fath et al., 2007). It was proposed that the COPI triskelion is a design intermediate between the COPII system and the clathrin system. The domain organization and vertex contacts are similar to COPII, and the triskelion with curved legs radiating from a three-fold center is similar to clathrin. In the proposed COPI vertex three αβ´-COP complexes are oriented around a three-fold rotational axis and all three amino-terminal β-propellers interact in the same way. A structure of a complex of the carboxy terminal part of α-COP with ε-COP does not share any overlapping elements with the αβ´-COP subcomplex. Both subcomplexes are most likely connected by a highly acidic linker region of α-COP (~80 residues), which seems to be unstructured according to proteolysis experiments (Lee and Goldberg, 2010), (Hsia and Hoelz, 2010). ε-COP adopts a fold of a characteristic TPR-protein superhelix based on its tetratricopeptide

repeats. The superhelix coils in a right-handed fashion around one end of the rod-shaped α-COP molecule. The carboxy terminal 20 residues of ε-COP form a final α-helix that makes additional contacts with α-COP. ε-COP envelops about one third of the α-COP rod. The α-COP carboxy terminal domain has a mixed structure, which is composed of five elements. The amino terminal region is mostly α-helical and is continued by a β-hairpin finger, which is encircled by ε-COP. This region is continued by a three helix bundle, which is followed by short α-solenoid and three orthogonal oriented β-hairpins at the carboxy terminus. The αε-COP subcomplex adopts the overall fold of a compact rod of ~115 Å with a diameter of ~35 Å.

The recruitment of coatomer and the initiation of coat formation was further elucidated by a structure of a truncated γζ-COP subcomplex bound to Arf1-GMPPNP (Yu et al., 2012). In the structure the α-solenoid of γ-COP adopts the fold of a curved right handed superhelix, composed of 15 α-helices. The α-solenoid binds as an arc around the ζ-COP subunit. The structure of ζ-COP closely resembles the longin fold of σ-adaptin in the AP2 complex. Arf1 makes no contacts with ζ-COP, but ζ-COP is most likely required to stabilize γ-COP to allow its interaction with Arf1. The interface of Arf1 and γ-COP is formed by hydrophobic side chains of residues, which are mainly supplied by helices a4 and a6 of γ-COP and the switch I and switch II regions of Arf1. In the interface only two hydrogen-bonds are formed. Lys75 of γ-COP makes contact with the carbonyl oxygen atom of His80 in Arf1, possibly interacting with the helix dipole of the switch II α-helix. The other hydrogen bond is formed by side chain groups of Thr74 of γ-COP and Tyr81 of Arf1. The central core of the interface is formed by a cluster of hydrophobic side chains, which belong to residues Phe51, Leu77 and Tyr81 in Arf1 and Phe71, Thr74 and Ile104 in γ-COP. Mutation of the interface residues abolished binding of Arf1-GTP to γζ-COP in pull-down assays. Based on the identified interface of Arf1-γζ-COP and sequence homology binding site residues for Arf1 in β-COP were proposed. The chosen residues Leu59, Ile99 and Leu100 were mutated and tested in pull-down assays. All three mutations nearly abolished binding of βδ-COP to Arf1-GTP (Yu et al., 2012). Mutational analysis of a tetrameric complex (γζβδ) in the pull-down assay showed that individual mutation of β-COP and γ-COP only reduced the binding of the tetrameric complex to Arf1-GTP. Combined mutation of β-COP and γ-COP on the other side abolished the interaction. Since the trimeric subcomplex (αβ´ε) does not bind to Arf1, coatomer seems to contain two

binding sites for Arf1, which are located in γ-COP and β-COP. However interactions of Arf1 are also reported with β´-COP, δ-COP and ε-COP.

The amino terminal β-propeller domains of α-COP and β´-COP haven been implicated in recognition and binding of dilysine cargo motifs (Letourneur et al., 1994), (Lowe and Kreis, 1995), (Fiedler et al., 1996), (Schröder-Köhne et al., 1998), (Eugster et al., 2004). Crystal structures haven been described for the α-COP and β´-COP amino terminal β-propeller domains bound to KKxx, KxKxx, KxHxx and RKxx cargo peptides (Ma and Goldberg, 2013). The β-propeller domains of both subunits bind to dilysine motifs via a conserved surface region, which is located near to the central pore of the propellers (Jackson et al., 2012), (Ma and Goldberg, 2013). Three primary interactions between the retrieval motif and the propellers could be identified. The carboxy terminal end of a KxKxx peptide binds to a basic patch formed by the residues Arg15, Lys17 and Arg59 in β´-COP. The two lysine side chains interact with two acidic patches. The acidic patch 1 involves β´-COP residue Asp206, which binds to the -3 lysine side chain. Acidic patch 2 is formed by β´-COP residues Asp98 and Asp117, which bind to lysine -5 of the peptide. Secondary contacts are formed by the backbone carbonyl oxygen atoms of residues -4, -3 and -2, which interact with the charged side chains of Arg59 and Arg101 in β´-COP. The KxKxx binding to α-COP and β´-COP β-propellers is in close correspondence. The binding sites in the propellers are closely conserved, with only two residues differing. The differing residues are conserved alterations. Tyr33 of β´-COP changes to His31 in α-COP and Phe142 of β´-COP changes to Tyr139 in α-COP.

Interestingly KxKxx and KKxx motifs adopt different binding modes. KKxx motifs adopt a helical conformation in the binding site. The terminal carboxylated group is bound in the same way to the basic patch for both peptide classes. Also the interaction of the backbone carbonyl oxygen atoms with the side chains occurs in a similar fashion. However the lysine side chains of KKxx are recognized by acidic patches 1 and 2, but bind in a reversed fashion compared to the KxKxx peptide. KxHxx peptide adopts a binding mode that is highly similar to the one of KxKxx peptides. A minor positional shift of the histidine residue enables its side chain e2 nitrogen to make contact with Asp206 of β´-COP in acidic patch 1.

The RKxx motif does not mimick the KKxx mode of binding. Instead the RKxx motif adopts a binding mode similar to the one of KxKxx peptides from the position -4 to the C-terminus. The arginine side chain adopts a unique binding postion, which is outside the dilysine binding site. The arginine residue is extended to form contacts via the guanidinium group and the backbone carbonyl oxygen of β´-COP residue Arg185. In α-COP this particular carbonyl oxygen is not available for this contact, because the carbonyl group of Arg213 points way from the binding site. This reveals an incompatibility of α-COP with this binding motif. The orientation of the carbonyl group of Arg185 in β´-COP is enforced by a salt bridge between residues Glu184 and Arg163. This pairing is highly conserved in β´-COP. This feature however is lacking in α-COP, since the Glu184 position is changed to a conserved aspartic acid in α-COP.

Overall a dilysine-type motif adopts one of three possible binding modes, which is depended on the combination of the two basic residues KxK, KK and RK. All binding modes have a strict requirement for a basic residue at the -3 position of the motif. The recognition of this residue controls the distance to the acidic patches 1 and 2 on α-COP and β´-COP. α-COP and β´-COP do not discriminate between KKxx and KxKxx motifs. Differences in the binding site architecture allow only α-COP to bind to dilysine motifs with a β-branched residue at -2 position. Also only β´-COP is able to bind to RKxx signals (Ma and Goldberg, 2013).

Recently the structure of the carboxy terminal domain of δ-COP, the delta μ-homology domain (MHD) was solved (Lahav et al., 2015). The structure shows potential dimers in the crystallographic unit cell. The δ-MHD is composed of two subdomains. Subdomain 1 is formed by residues 267-375 and residues 472-505. It includes the N-terminus and a β-sandwich, which is composed of a five-stranded β-sheet associated with a two-stranded β-sheet. A short α-helix closes one side of the sandwich. The second subdomain includes residues 376-471 and is formed by a β-sandwich made up of two four-stranded β-sheets. Overall the structure is similar to the carboxy terminal part of μ2-AP2. The main difference between the structures is the position of the residues that link both subdomains, which form unstructured loops (Lahav et al., 2015). Comparison of the subdomains showed that subdomain 1 of δ-MHD is more similar to the closed form of the μ2-AP2-MHD than its open state. Subdomain 2 of δ-MHD is more similar to the open form of μ2-AP2-MHD than to its

closed state. A remarkable difference between δ-MHD and μ2-AP2-MHD is the relative electrostatic potential of the surfaces. The μ2-AP2-MHD is predominantly positively charged whereas the δ-MHD instead has an almost completely negatively charged surface.

Important insights into the COPI coat architecture could be derived from cryo EM structures of the COPI coat assembled on vesicles (Faini et al., 2012). Owing the inherent flexibility of coatomer and heterogeneity of vesicles, the structure of the coated vesicle was produced using subtomogram averaging to identify the repetitive unit of the COPI coat. This was done for two sets of vesicles produced in separate reactions, which both converged on the same structure. The structure obtained shows a three-fold symmetrical arrangement of leaf-shaped densities, which are surrounding a central platform. Three leaves form one triad, with a diameter of approximately 32 nm. This triad makes contact the membrane below each leaf and below the central platform. One leaf has approximately the same mass as one coatomer-Arf1 complex (Faini et al., 2012). Interestingly, fitting of crystal structures in the cryo EM map showed that both the AP2 core and the αβ´-COP triskelion could not be fitted as rigid bodies into the cryo EM map. This indicates that the triskelion does not represent the structural form of αβ´-COP in the assembled coat or that the triskelion arms might be oriented in a way different from the crystal structure.

Another interesting and important feature of the structure is that the triads make different connections between each other in the COPI coat. The corners and edges of the triads are arranged around local three fold symmetry axes in a triangular lattice. Also on all vesicles there are positions where the corners of two triads come together, either singly or paired, rather than the corners of three triads. This is essentially required for the assembly of a curved lattice since a triangular lattice would be flat. An increase of the three corner interaction over the two corner interaction, or of the of the paired two corner interaction over the single two corner interaction, increases the diameter of the resulting coat lattice and allows a variability of vesicle sizes. The coats also contained gaps within the triangular lattice, which is likely to represent a budding scar. In total triads make contacts via the corners of three triads, via edges of three triads, via single two corner interactions and via paired two corner interactions. Structure comparison between the triad contacts showed that the central platform and the cores of the leaves are conserved, whereas parts of the leaf that form corners and edges of the triad adopt different conformations. Depending on

its position in the coat lattice coatomer seems to be able to form homotrimeric or dimeric interactions. So in contrast to the COPII and clathrin coats, where multiple identical subunits make the same set of interactions with the same number of interaction partners, assembled coatomer can adopt different conformations to make interactions with a different number of neighboring coatomer complexes (Faini et al., 2012). Most likely COPI vesicles are able to adapt to different cargo size by regulating the frequencies of different triad patterns in the COPI coat during its assembly.

A higher resolution cryo EM structure of COPI coated vesicles enabled fitting of the existing crystal structures as well as fitting of homology models for structural parts that are still not available as crystal structures (Dodonova et al., 2015). Interestingly this structure revealed that αβ´-COP does not assemble into a triskelion in the membrane bound COPI coat as previously proposed (Lee and Goldberg, 2010). Instead the α-solenoids of α-COP and β´-COP form an arch over the γζβδ-COP subcomplex. The amino terminal β-propeller domains of α-COP and β´-COP are oriented towards the membrane in a way that their KxKxx motifs are positioned optimally towards the membrane for cargo binding. α-COP and β´-COP do not form a cage as COPII or clathrin coats do. Instead they are linked via βγδζ-COP subcomplexes forming an interconnected assembly. The adaptor-like βγδζ-COP subcomplex seems to adopt a more extended conformation than the closed and the open conformation of the clathrin adaptors. This conformation is referred to as “hyper-open”. In the hyper open form also the α-solenoids of γ-COP and β-COP form an arch, which is situated below the arch formed by α-COP and β´-COP and is connected to the membrane via the interactions of their trunk domains witch Arf1. The coatomer triads are interconnected by flexible domains. Interactions are formed by the MHD domains of δ-COP and between ε-COP and the carboxy terminal domain of α-COP. ε-COP also forms homodimeric interfaces interconnecting triads.

1.5 Structural comparison of the COPI, COPII and the clathrin coat

The adaptor protein complexes of the clathrin coat and the adaptor-like subcomplex of COPI (γζβδ-COP) have a distant sequence homology and an overall structural similarity. Sequence comparisons between γ-COP and β-COP and between δ-COP and ζ-COP have suggested that the adaptor-like subcomplex might have originated from the duplication of an ancestral protodimer of a large and a small subunit (Schledzewski et al., 1999). The adaptor of the COPII system, Sec23Sec24, showed no sequence homology or structural similarity, when compared to the clathrin and COPI system, which might suggest a different origin. A comparison of the outer scaffold or cage forming complexes revealed no significant sequence homology. However in all three systems the cage forming complexes or subcomplexes share a similar arrangement of protein domains used as building blocks. In all coats the outer layer is formed by one or two β-propeller domains followed by elongated α-solenoids (Field et al., 2011). This arrangement seems to be particularly favorable, as β-propeller domains are often used in mediating interactions with protein motifs. This makes them suited to act in cargo recruitment (ter Haar et al., 1998), (Eugster et al., 2004). α-solenoid domains have an intrinsic local flexibility, which enables them to arrange either in straight rods or in a bent conformation. This feature makes them ideal for building up cages or scaffolds. The arrangement of β-propeller domains and α-solenoids is a feature, which also occurs in components of nuclear pore complexes. These respective components interact with curved regions of the nuclear membrane. Such similarities hint to a general mechanism, by which protein complexes interact with curved membranes.

Although all three coat system show similarities in protein domain organization, the cage building complexes or subcomplexes form very different coats upon polymerization. In the case of clathrin and COPII the same building blocks are used to make the same contacts with the same interaction valence. The different sizes of the vesicles are accommodated by flexibility in the clathrin triskelion legs or by variation of the interaction angle between different rods in COPII. In COPI triangular arrangements are forming patterns of two or three. In this regard the same protein can form either dimeric or trimeric interactions. The different arrangements adopt different curvatures. Smaller vesicles have a higher abundance of dimeric contacts, which increases the curvature (Dodonova et al., 2015).

1.6 *Chaetomium thermophilum*

Chaetomium themophilum is a thermophilic filamentous fungus of the phylum Ascomycota and belongs to the family of Chaetomiaceae. It grows on dung, soil and rotting plants and has a temperature tolerance of up to 60 °C. The fungus contributes to the breakdown of cellulose. *Chaetomium thermophilum* was first described in 1948 (La Touche, 1948). In recent years proteins from *Chaetomium thermophilum* haven been successfully employed in structural studies (Amlacher et al., 2011), (Leidig et al., 2013). Proteins of thermophilic organism are more suitable for structural studies, since they are more stably folded and contain less flexible domains. Analysis of xylanases enzymes from *Chaetomium thermophilum* indicated thermostability at up to 60 °C (Hakulinen et al., 2003).

2 Results

In this thesis recombinant *Chaetomium thermophilum* coatomer and coatomer subcomplexes should be prepared, which subsequently should be used in structural studies on coatomer using protein crystallization, negative stain electron microscopy and in fuctional studies by biochemnical methods. The goal was to obtain a better understanding of the molecular architecture of coatomer and the process of coat formation on COPI vesicles. For expression of recombinant coatomer complexes the Baculovirus expression system (Berger et al., 2004) was employed. The steps of cloning, expression and purification of *Chaetomium thermophilum* coatomer and coatomer subcomplexes as well as structural analysis, crystallization and negative stain electron microscopy are described in the following section.

2.1 Cloning of *Chaetomium* Coatomer and coatomer subcomplexes

The first step in the preparation of *Chaetomium thermophilum* coatomer was the amplification of the seven coatomer subunits by PCR from *Chaetomium thermophilum* cDNA. The *Chaetomium thermophilum* cDNA was obtained from the workgroup of Prof. Dr. Ed C. Hurt at the BZH. All seven coatomer subunits were amplified using the thermostable *Phusion* polymerase (NEB, New England USA), which produced blunt-end products. The primer oligonucleotides used to amplify the subunits introduced specific restriction sites, which allowed the subsequent cloning of the subunits into the pFBDM vector of the Baculovirus expression system.

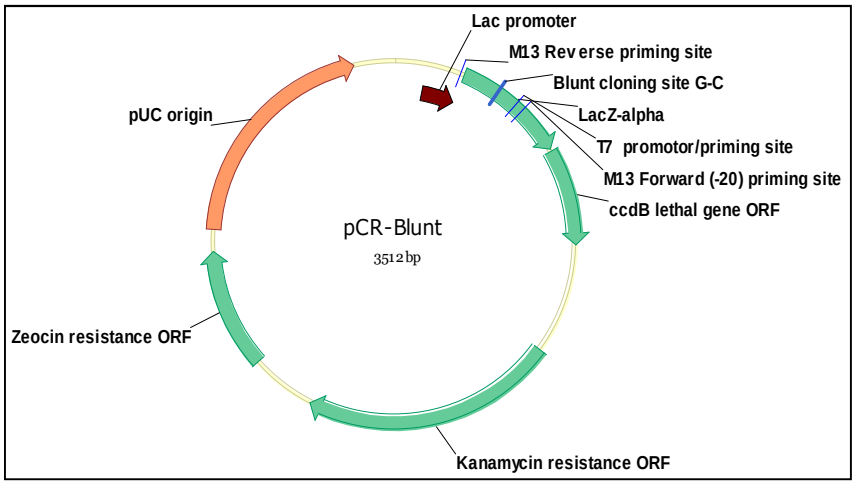

Figure 4: Vector map pCR-Blunt.

2.1.1 Cloning strategy

After amplification all subunits were ligated into the pCR-Blunt vector (figure 4) for sequencing using the *Zero Blunt PCR Cloning Kit* (Invitrogen, Karlsruhe). Sequencing of the ligated subunits was performed using the supplied M13 forward and M13 reverse primer oligonucleotides and with specific sequencing primers designed for the respective subunits.

NotI-α-COP-*XbaI*	3654 bps
NotI-HOST-α-COP-*XbaI*	3789 bps
NheI-β´-COP-*XmaI*	2502 bps
NotI-HOST-β-COP-*XbaI*	3015 bps
NotI-HOST-γ-COP-*XbaI*	2889 bps
NotI-γ-COP-*XbaI*	2754 bps
NheI-δ-COP-*XmaI*	1542 bps
NotI-ε-COP-*XbaI*	891 bps
NheI-ζ-COP-*XhoI*	594 bps

Figure 5: Cloning strategy of *Chaetomium thermophilum* coatomer. For details see text.

In order to enable an affinity purification of *Chaetomium thermophilum* coatomer and coatomer subcomplexes we to fused a TEV-cleavable tandem affinity Tag composed of a

HIS_6-Tag and a OneStrep-Tag, followed by a TEV cleavage site (figure 6) to the 5´-end of selected subunits (figure 5). The tandem Tag was ordered as complementary oligonucleotides, annealed and cloned into the pMA-vector using restriction sites *XbaI* and *NcoI* producing the pMA-HOST2t vector. Utilizing this vector, the tandem Tag could be fused to the 5´-end of the cDNA of a subunit by ligating the cDNA into the pMA-HOST2t vector (figure 6) using the restrictions sites *ClaI* and *XbaI*. After this cloning step the subunit with the fused affinity Tag at its 5´-end could be excised from the pMA-HOST2t vector using restrictions sites *XbaI* and *NotI*. The tagged subunit could then be cloned into the pFBDM transfer vector.

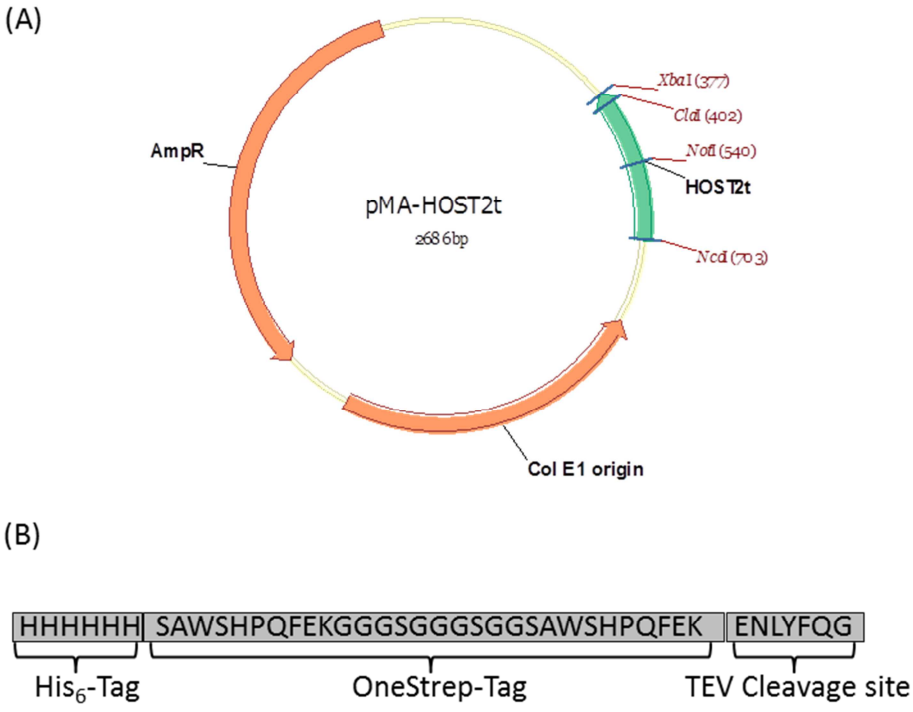

Figure 6: (A): Vector map pMA-HOST2t, (B): HOST-tandem affinity-TAG composition.

To produce an expression construct for *Chaetomium thermophilum* coatomer all seven subunits of coatomer were combined in one pFBDM transfer vector (figure 8) using the multiplication module. To introduce single subunits, a modified pFBDM transfer vector pFBDM1 (figure 7) was used, which contained only one multiple cloning site.

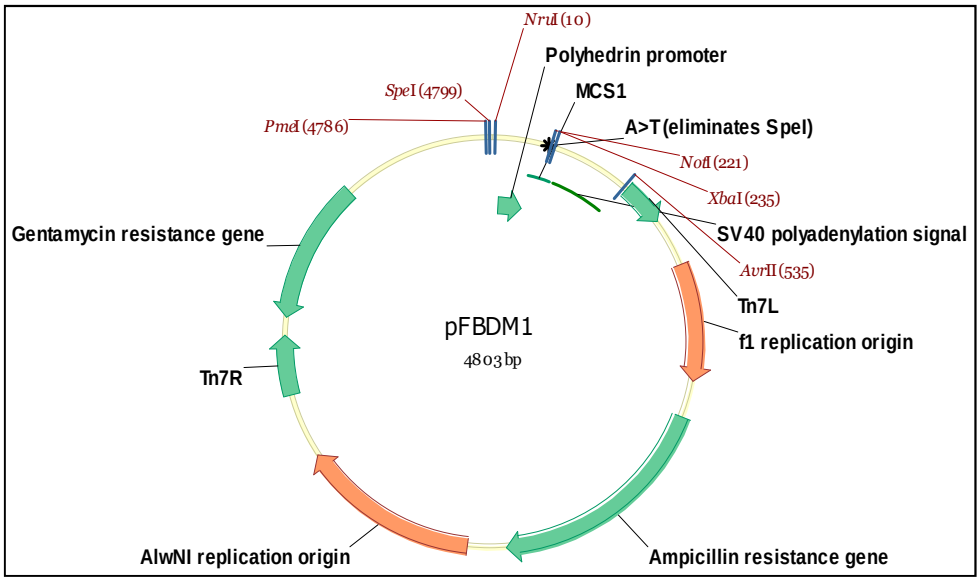

Figure 7: Vector map pFBDM1.

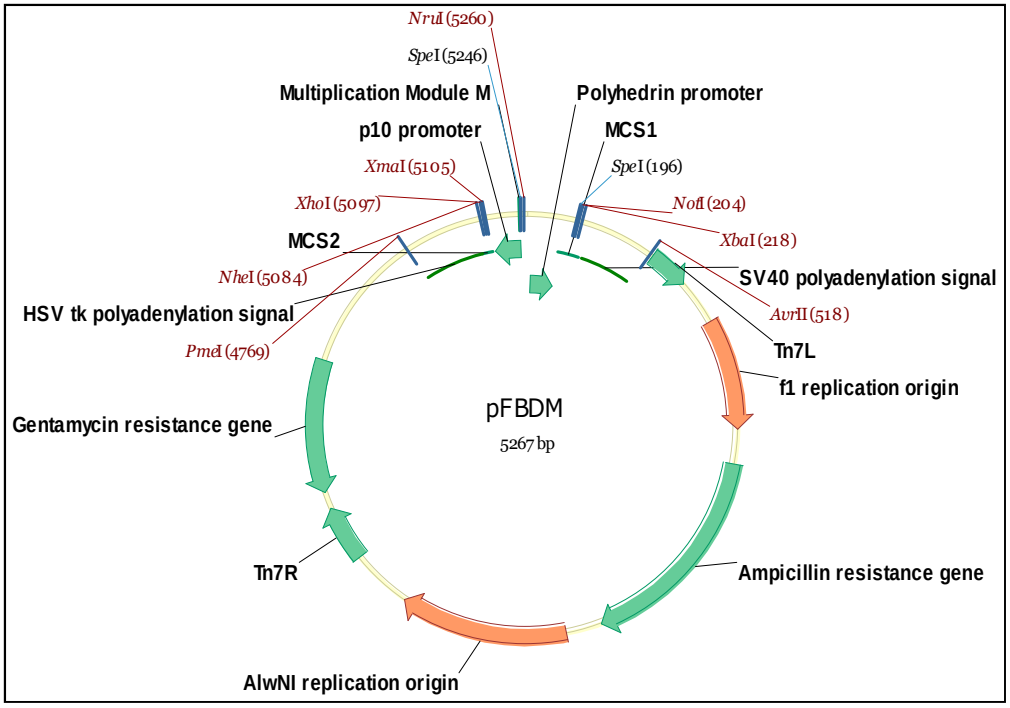

Figure 8: Vector map pFBDM.

In order to allow subcomplexes of coatomer to be expressed and purified as well, the cDNA of the subunits α-COP, β-COP and γ-COP were cloned in the pMA-HOST2t vector to fuse the tandem affinity Tag to the 5´-end of the subunits cDNA. To prepare the transfer vector with

all seven subunits first a trimeric transfer vector with the subunits α-COP, β´-COP and ε-COP and a tetrameric transfer vector witch the subunits β-COP, γ-COP, δ-COP and ζ-COP were cloned. The trimeric transfer vector was cloned in two different variants, a variant without affinity tag pFBDM-αβ´ε and a variant with affinity tag pFBDM-HOST-αβ´ε. Both forms were prepared by first cloning the subunits β´-COP and ε-COP in the pFBDM vector using both multiple cloning sites. The α subunit with or without the affinity tag was then cloned into the resulting pFBDM-β´ε vector using the multiplication module (figure 9).

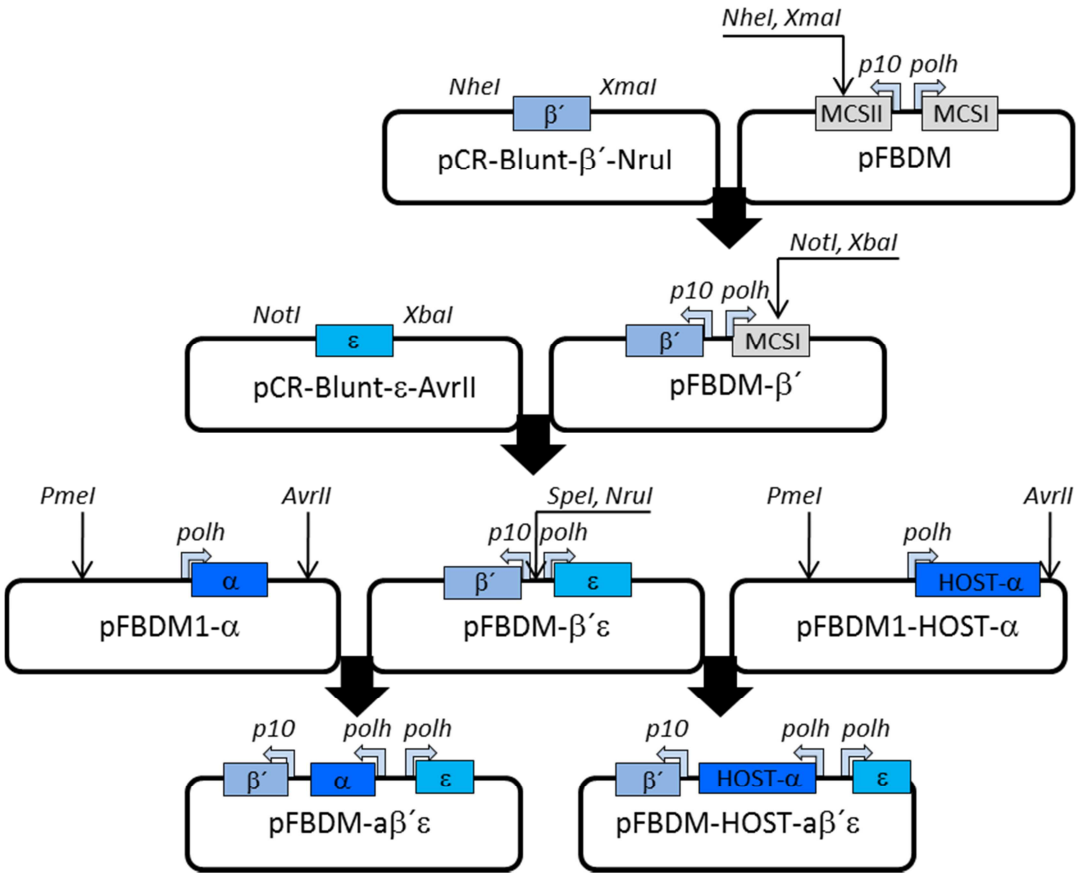

Figure 9: Cloning strategy of *Chaetomium thermophilum* coatomer trimer.

The tetrameric transfer vector pFBDM-HOST-βγδζ was prepared by combining two dimeric transfer vectors. The tagged subunit HOST-β-COP and δ-COP were cloned in one pFBDM vector using both multiple cloning sites producing pFBDM-HOSTβδ (figure 10).

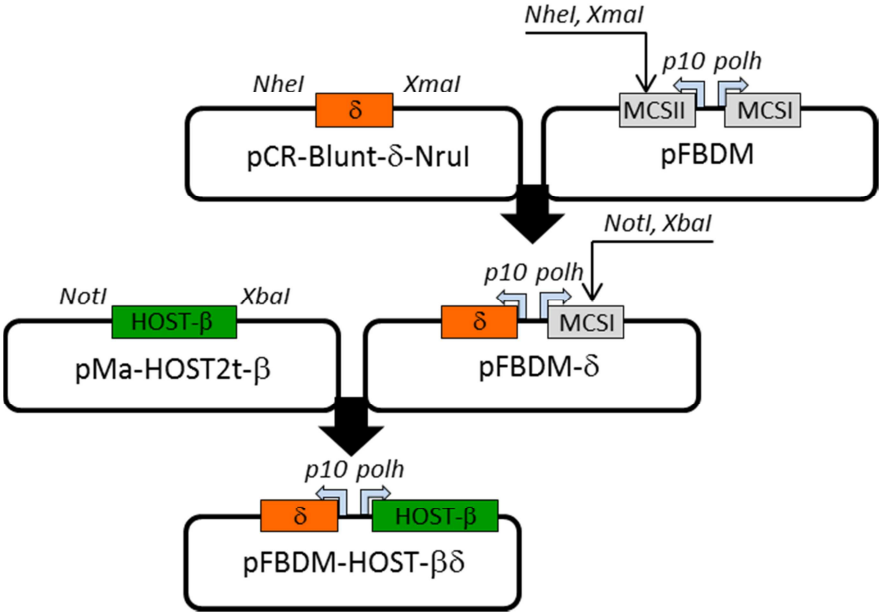

Figure 10: Cloning strategy of *Chaetomium thermophilum* coatomer βδ dimer.

The subunit γ-COP was cloned as a tagged and as an untagged variant together with the subunit ζ-COP in one pFBDM vector producing pFBDM-HOST-γζ and pFBDM-γζ. The variants of the dimeric transfer vectors with affinity tags could be used to express dimeric subcomplexes (figure 11).

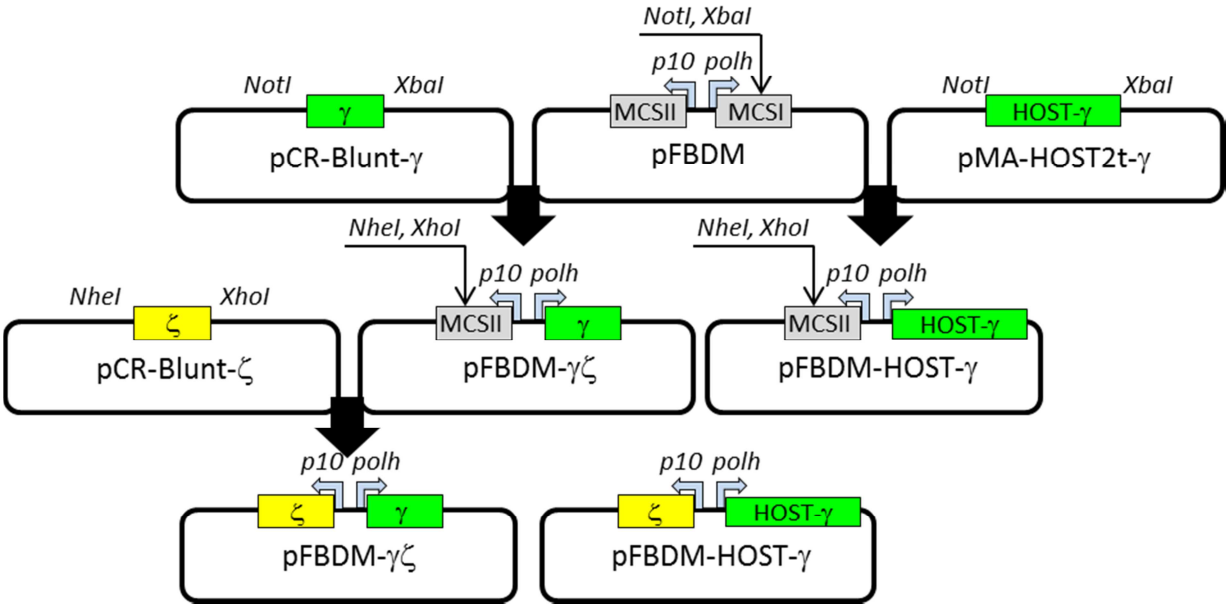

Figure 11: Cloning strategy of *Chaetomium thermophilum* coatomer γζ dimer.

To prepare the tetrameric transfer vector, the expression cassette of γ-COP and ζ-COP was cut out of pFBDM-γζ and cloned into the pFBDM-HOST-βδ vector using the multiplication module (figure 12).

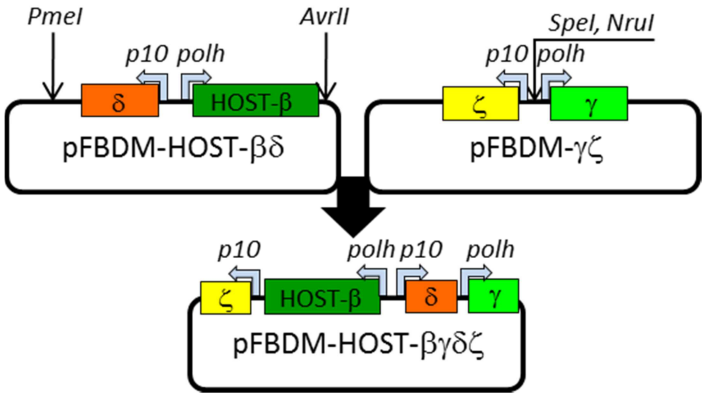

Figure 12: Cloning strategy of *Chaetomium thermophilum* coatomer tetramer.

The final heptameric transfer vector was created by combining the trimeric and tetrameric transfer vectors. The expression cassette of α-COP, β´-COP and ε-COP were cut out from pFBDM-αβ´ε and cloned into pFBDM-HOST-βγδζ using the multiplication module (figure 13).

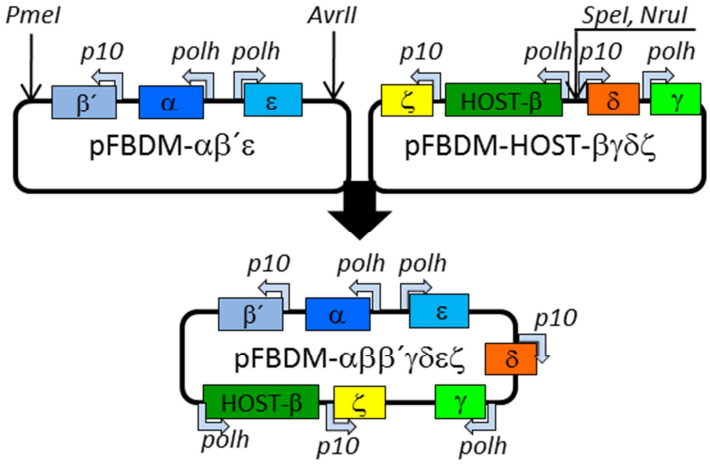

Figure 13: Cloning strategy of *Chaetomium thermophilum* coatomer heptamer.

All of the described constructs were cloned and sequenced. The resulting plasmids were used to express *Chaetomium thermophilum* coatomer and coatomer subcomplexes using the Baculo-virus expression system.

2.2 Expression of *Chaetomium thermophilum* coatomer and coatomer subcomplexes

The plasmids pFBDM-HOST-βδ, pFBDM-HOST-γζ and pFBDM-HOST-βδγζ were transformed into *E. coli* DH10b MultiBac cells by electroporation. The resulting recombinant BACMID DNAs were isolated and transfected in SF9 insect cells as described in the methods sections for the Baculo virus system to produce the recombinant Baculo virus, which was used to infect Sf9 insect cells to express the coatomer subcomplexes.

The dimeric subcomplexes of *Chaetomium thermophilum* coatomer βδ-COP and γζ-COP were expressed with the HOST tandem affinity TAG fused to the N-terminus of the β-COP and the γ-COP subunit. The efficiency of the produced recombinant virus was controlled by SDS-PAGE. Expression of the subcomplexes was performed in 500 ml scale cultures, which were infected with 1.5 ml to 3 ml of the recombinant Baculovirus. After infection the expression was continued for 3 days (figure 14).

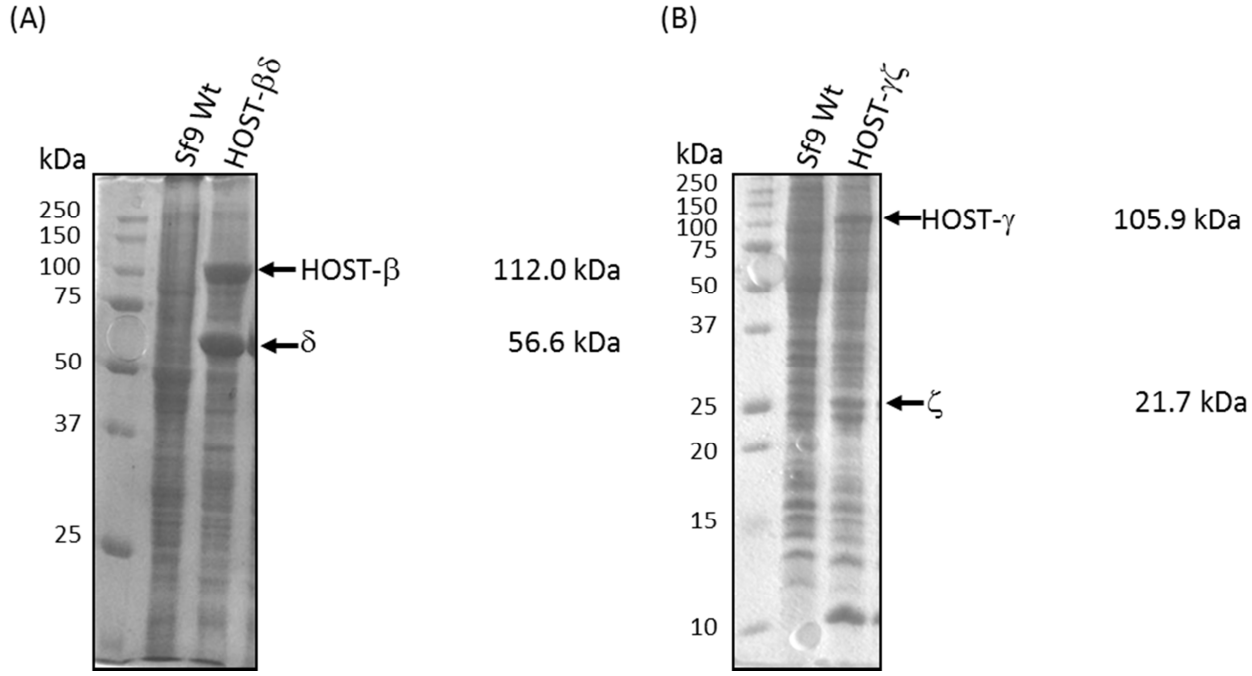

Figure 14: Expression control of the dimeric subcomplexes βδ and γζ

(A): 12 % SDS-PAGE (βδ) stained with Coomassie. 1 ml cells suspension of the expression culture and of wildtype Sf9 cells (negative control) was pelleted and resuspended in 150 µl H_2O and 50 µl 4 x SDS sample buffer. 2 µl of each sample was loaded on the gel.

(B): 15 % SDS-PAGE (γζ) stained with Coomassie. 1 ml cells suspension of the expression culture and of wildtype Sf9 cells (negative control) was pelleted and resuspended in 150 µl H_2O and 50 µl 4 x SDS sample buffer. 2 µl of each sample was loaded on the gel.

The tetrameric subcomplex of *Chaetomium thermophilum* coatomer βγδζ-COP was expressed with the HOST tandem affinity TAG fused to the N-terminus of the β-COP. The efficiency of the expression was controlled by SDS-PAGE. Expression of the subcomplexes was performed in 500 ml scale cultures, which were infected with 1.5 ml to 3 ml of the recombinant Baculovirus. After infection the expression was continued for 3 days (figure 15).

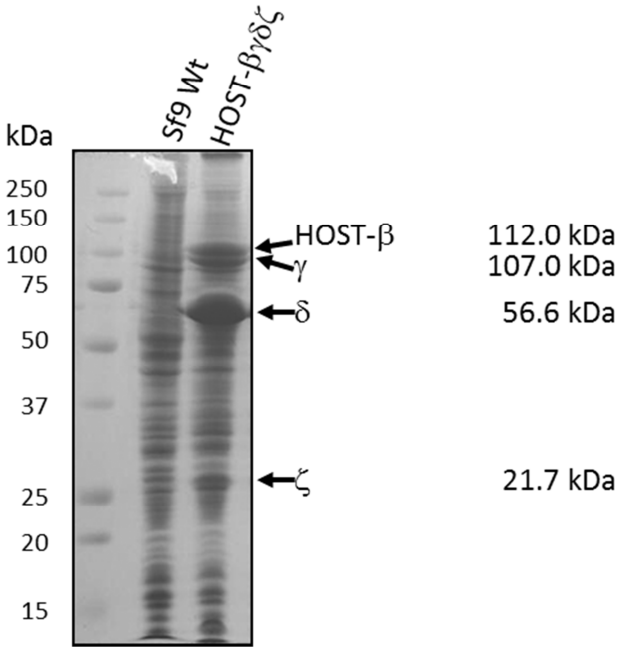

Figure 15: Expression control of the tetrameric subcomplex βγδζ

12 % SDS-PAGE stained with Coomassie. 1 ml cells suspension of the expression culture and of wildtype Sf9 cells (negative control) was pelleted and resuspended in 150 µl H_2O and 50 µl 4 x SDS sample buffer. 2 µl of each sample was loaded on the gel.

2.3 Expression of *Chaetomium thermophilum* coatomer and coatomer subcomplexes using separate Baculo viruses

The trimeric subcomplex αβ´ε could not be expressed in a reasonable way using the obtained pFBDM-HOST-αβ´ε construct for virus preparation. To bypass this problem the trimeric subcomplex was expressed by preparing two separate recombinant Baculoviruses for HOST-α-COP and for β´ε-COP using the constructs pFBDM-β´ε and pFBDM-HOST-α (figure 16).

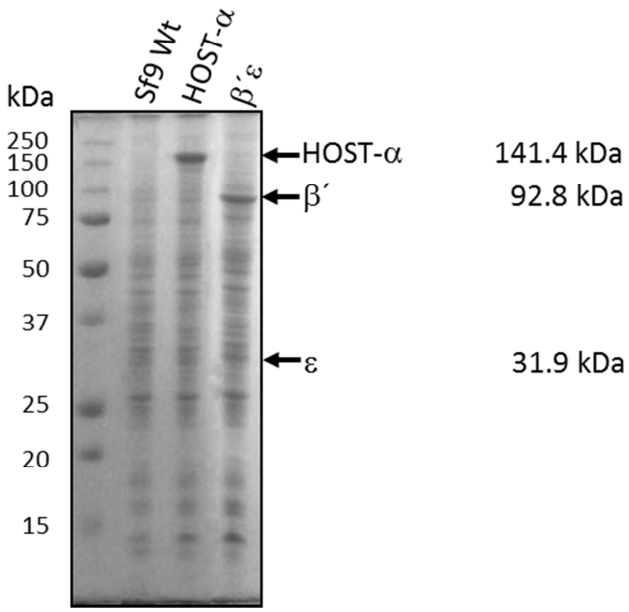

Figure 16: Virus preparation HOST-α-COP and β´ε-COP

15 % SDS-PAGE stained with Coomassie. 1 ml cells suspension of the virus culture and of wildtype Sf9 cells (negative control) was pelleted and resuspended in 150 µl H_2O and 50 µl 4 x SDS sample buffer. 2 µl of each sample was loaded on the gel.

The obtained recombinant viruses were used to co-infect SF9 insect cell cultures to express the trimeric subcomplex (figure 17). As two separated viruses were used in the expression, the volume of each virus had to be adjusted in the co-infection to obtain a stoichiometric expression of all subunits. The expression was performed in 500 ml scale infected with 2ml virus of HOST-α-COP and 2 ml virus of β´ε-COP.

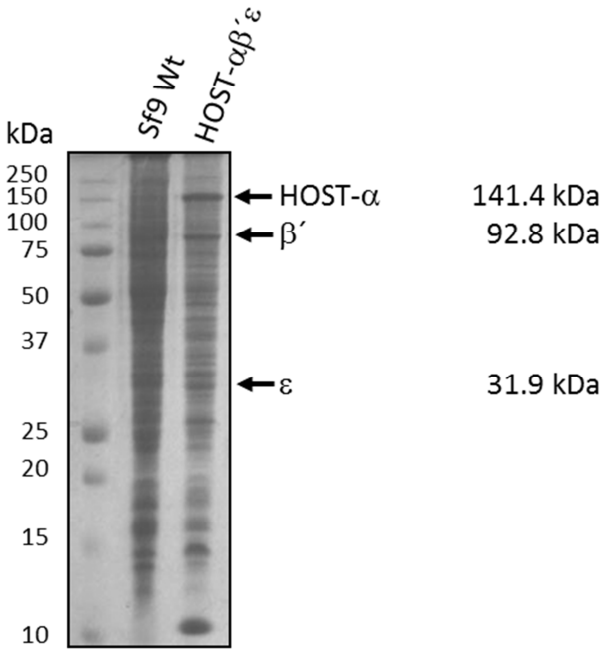

Figure 17: Expression control of the trimeric subcomplex αβ´ε

15 % SDS-PAGE stained with Coomassie. 1 ml cells suspension of the virus culture and of wildtype Sf9 cells (negative control) was pelleted and resuspended in 150 µl H_2O and 50 µl 4 x SDS sample buffer. 2 µl of each sample was loaded on the gel.

The virus containing supernatant of the αβ´ε expression was used to prepare BIIC stocks, which contained the complete virus for the expression of the trimeric subcomplex.

The heptameric *Chaetomium thermophilum* coatomer was expressed using the pFBDM-HOST-αββ´γδεζ construct. Virus prepared from this construct (figure 18) enabled expression of all seven coatomer subunits and was used to infect SF9 insect cell expression cultures. The expression was performed in 500 ml scale infected with 6 ml virus. After infection the expression was continued for 3 days.

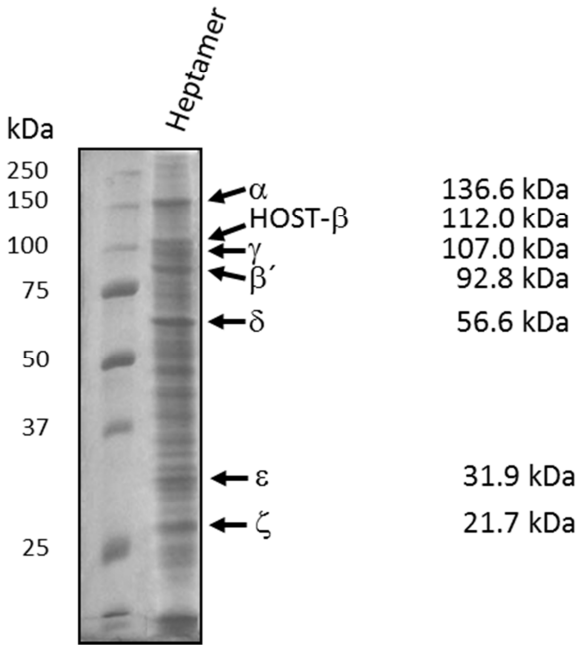

Figure 18: Expression control of the coatomer heptamer

15 % SDS-PAGE stained with Coomassie. 1 ml cells suspension of the virus culture and of wildtype Sf9 cells (negative control) was pelleted and resuspended in 150 µl H_2O and 50 µl 4 x SDS sample buffer. 2 µl of each sample was loaded on the gel.

The virus was used to prepare BIIC stocks, which contained the complete virus for the expression of heptameric *Chaetomium thermophilum* coatomer.

2.4 Purification of *Chaetomium thermophilum* coatomer and coatomer subcomplexes

Chaetomium thermophilum coatomer and coatomer subcomplexes were purified by Strep-tactin affinity purification using the incorporated HOST-tandem affinity TAG followed by size exclusion chromatography. The strep-tactin affinity purification of *Chaetomium thermophilum* coatomer complex is depicted in figure 19. After affinity purification the coatomer complex is already quite pure containing only minor contaminations.

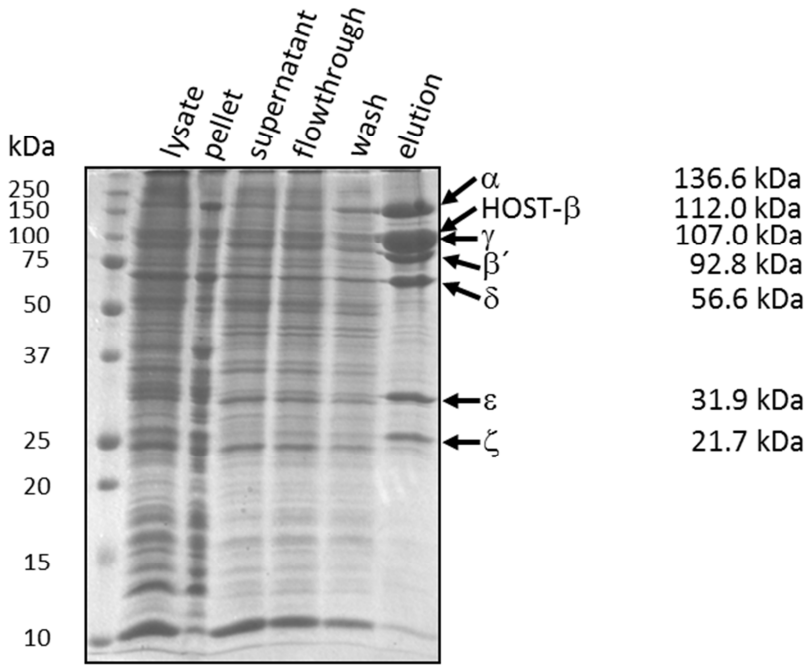

Figure 19: Strep-tactin purification of the coatomer heptamer

15 % SDS-PAGE stained with Coomassie. 2 µl of lysate, pellet, supernatant and flowthrough fractions mixed with 5 µl 4 x SDS sample buffer and 10 µl of wash and elution fractions mixed with 3.5 µl of 4x SDS sample buffer was loaded on the gel.

Further purification was achieved by size exclusion chromatography. The profil of coatomer on a Superose 6 10/300 GL column is depicted in figure 20. Coatomer eluted at the expected size of 552.4 kDa and showed a symmetric peak. Fractions of the Peak were analysed by SDS-PAGE. As depicted in the Coomassie stained gel in figure 20, the complex is pure after the size exclusion chromatography with no residual visible contaminations.

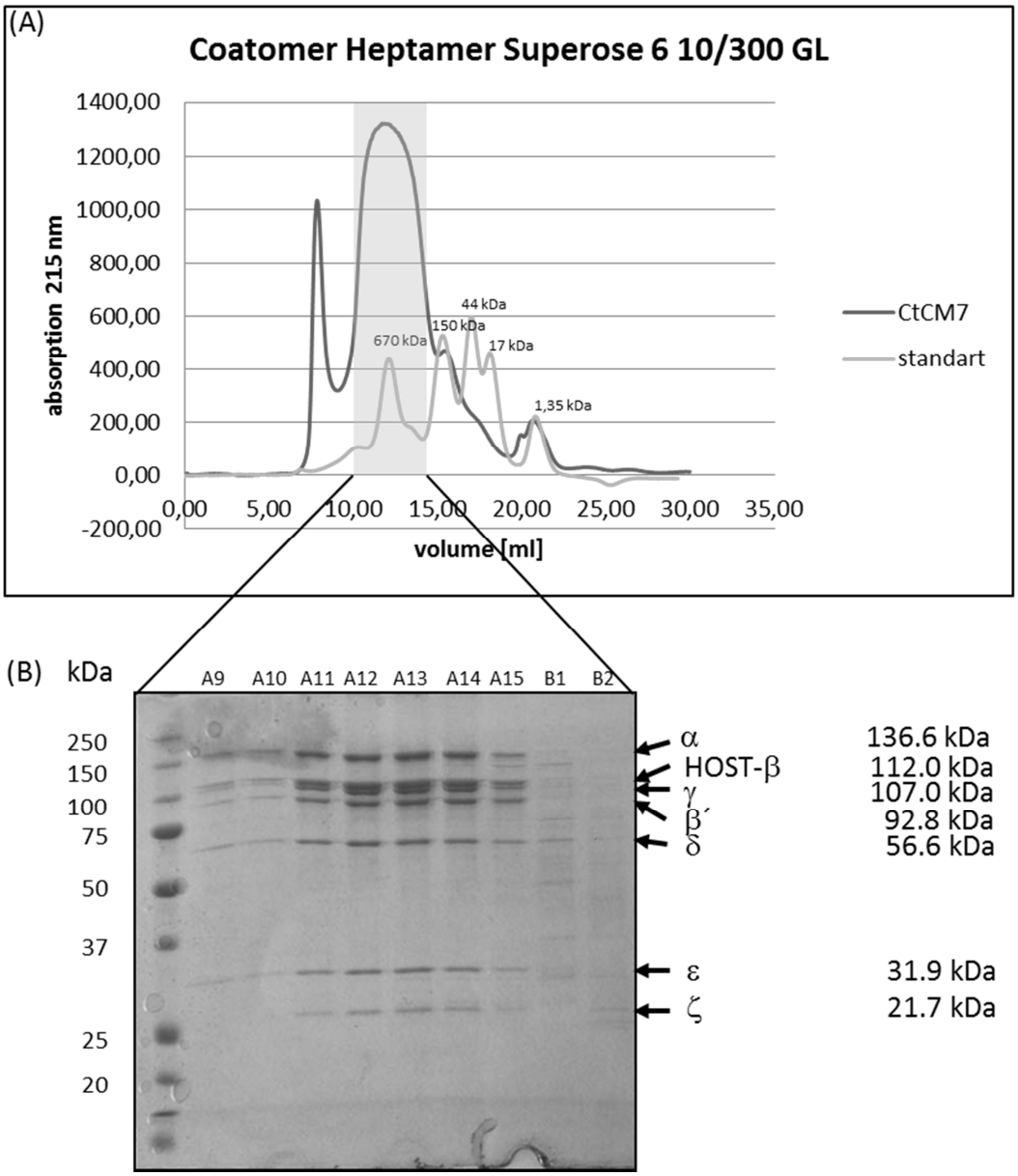

Figure 20: Chromatographic profile of the size exclusion chromatography of heptameric coatomer

(A): The elution profile of *Chaetomium thermophilum* coatomer (dark grey) is overlayed with the elution profile of a protein size standard (light grey). The UV absorption at 215 nm is blotted against the elution volume.

(B): 15 % SDS-PAGE stained with Coomassie. 5 µl of each *Chaetomium thermophilum* coatomer Superose 6 10/300 GL elution fraction mixed with 3.5 µl 4 x SDS sample buffer was loaded on the gel.

The peak fractions of coatomer were pooled and used for subsequent experiments. The yield of the purification is in the range of 4 to 5 mg of pure coatomer complex from one 500 ml insect cell expression culture.

The strep-tactin affinity purification of the trimeric (αβ´ε) subcomplex is depicted in figure 21. After the affinity purification the trimeric subcomplex of coatomer contains only minor contaminations.

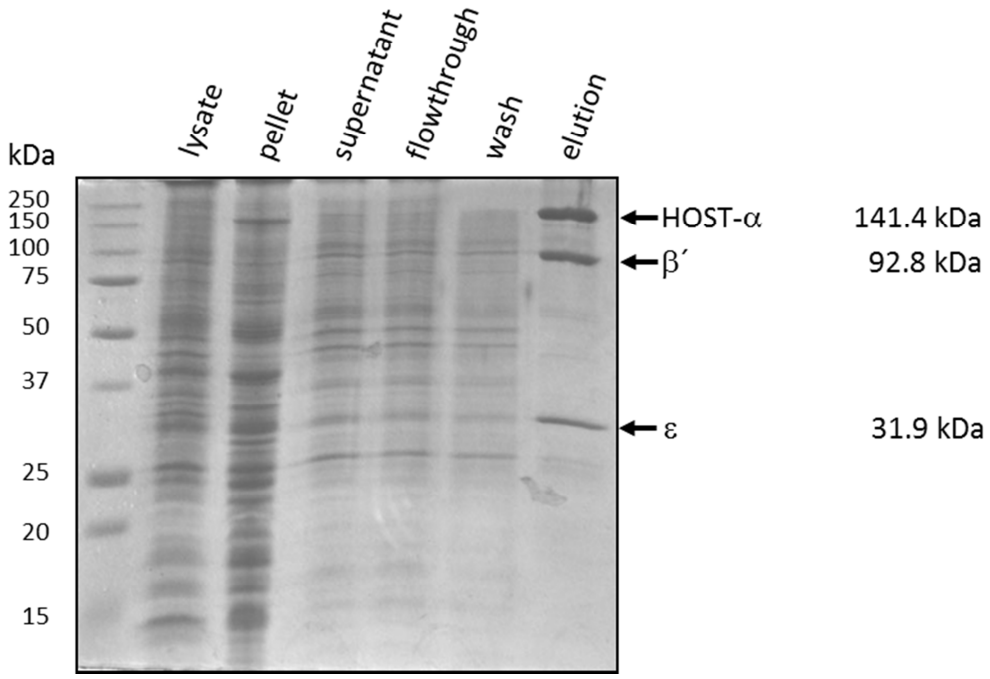

Figure 21: Strep-tactin purification of the trimeric subcomplex

15 % SDS-PAGE stained with Coomassie. 2 µl of lysate, pellet, supernatant and flowthrough fractions mixed with 5 µl 4 x SDS sample buffer and 10 µl of wash and elution fractions mixed with 3.5 µl of 4x SDS sample buffer was loaded on the gel.

The chromatographic profile of the size exclusion chromatography of the trimeric *Chaetomium thermophilum* coatomer subcomplex on a Superose 6 10/300 GL column is depicted in figure 22. The coatomer subcomplex eluted at the expected size of 266.08 kDa and showed a symmetric peak. Fractions of the Peak were analysed by SDS-PAGE. As depicted in figure 22 the subcomplex seems completely pure after the size exclusion chromatography with no residual visible contaminations. The subcomplex proved to be

stable after purification with no degradation even after incubation at room temperature for one week.

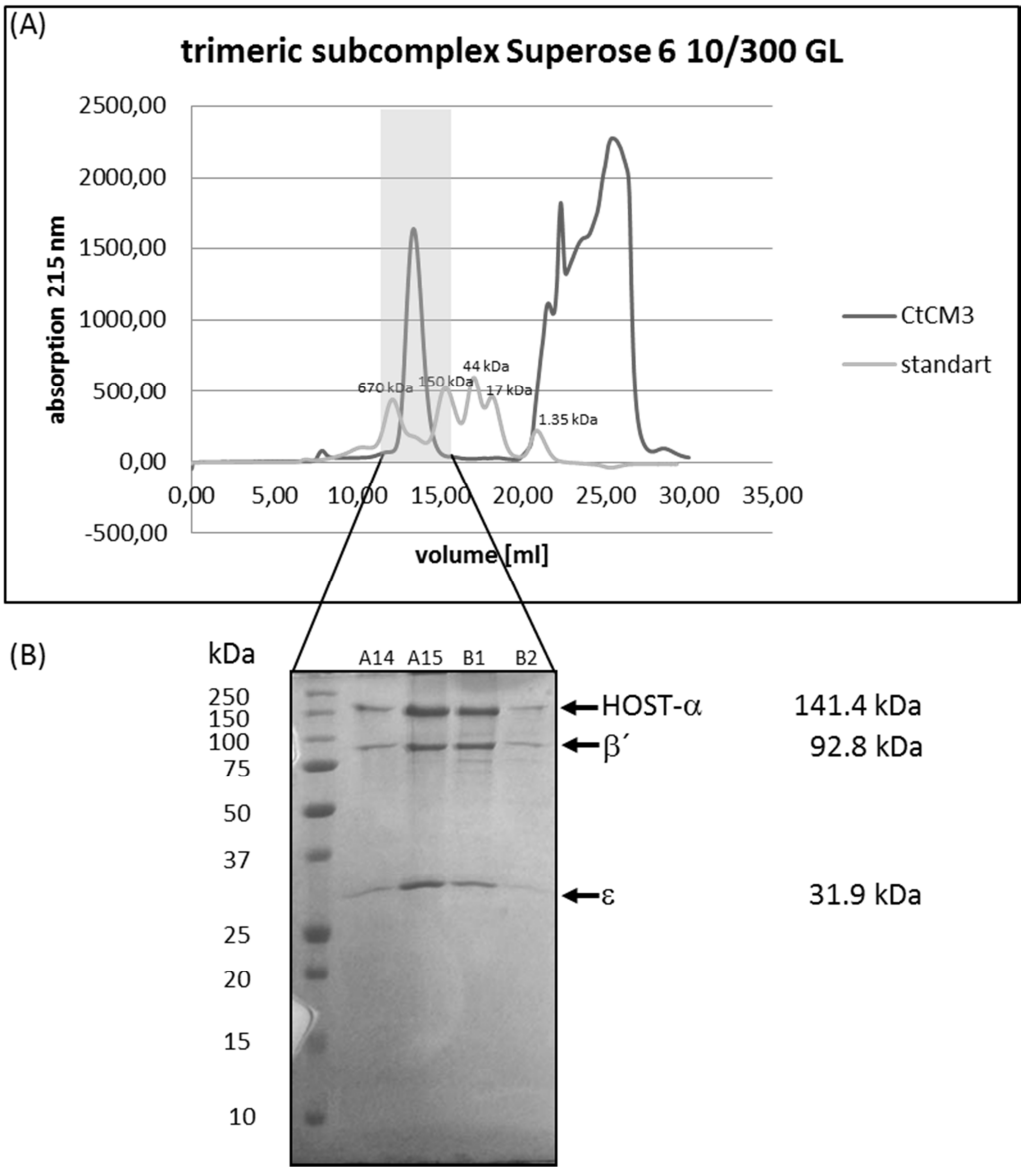

Figure 22: Chromatographic profile of the size exclusion chromatography of the trimeric subcomplex

(A): The elution profile of the trimeric coatomer subcomplex (dark grey) is overlayed with the elution profile of a protein size standard (light grey). The UV absorption at 215 nm is blotted against the elution volume in ml.

(B): 15 % SDS-PAGE stained with Coomassie. 5 µl of each *Chaetomium thermophilum* coatomer trimer Superose 6 10/300 GL elution fraction mixed with 3.5 µl 4 x SDS sample buffer was loaded on the gel.

The strep-tactin affinity purification of the tetrameric (βγδζ) subcomplex is depicted in figure 23. After affinity purification, the tetrameric subcomplex contains still visible contaminations. The tetrameric subcomplex is not as stable as the trimeric subcomplex and shows some degradation of the larger subunits β-COP and γ-COP.

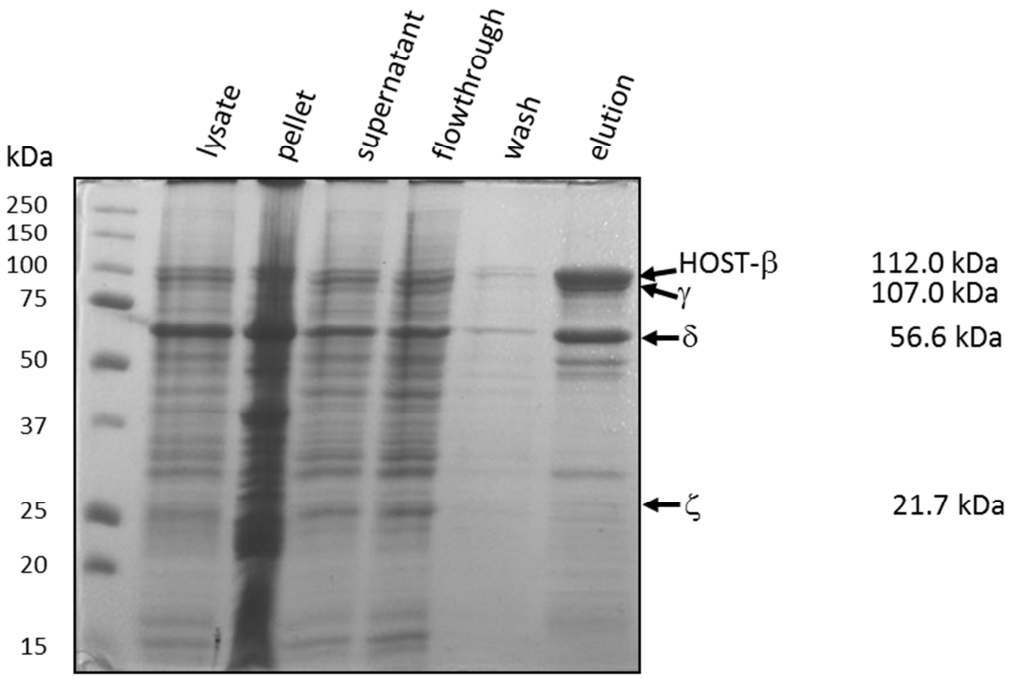

Figure 23: Strep-tactin purification of the tetrameric subcomplex

15 % SDS-PAGE stained with Coomassie. 2 µl of lysate, pellet, supernatant and flowthrough fractions mixed with 5 µl 4 x SDS sample buffer and 10 µl of wash and elution fractions mixed with 3.5 µl of 4x SDS sample buffer was loaded on the gel.

The chromatographic profile after size exclusion chromatography of the tetrameric coatomer subcomplex on a Superose 6 10/300 GL column is depicted in figure 24. The subcomplex eluted at the expected size of 266.58 kDa and showed a symmetric peak. However substantial parts of the loaded protein seemed to have aggregated and migrated in the void volume of the column. Fractions of the peak were analyzed by SDS-PAGE. As depicted in figure 24, the fractions of the symmetric peak of the elution volume expected for the complex showed still some degradation, indicating a reduced stability of this complex compared to the complete coatomer complex.

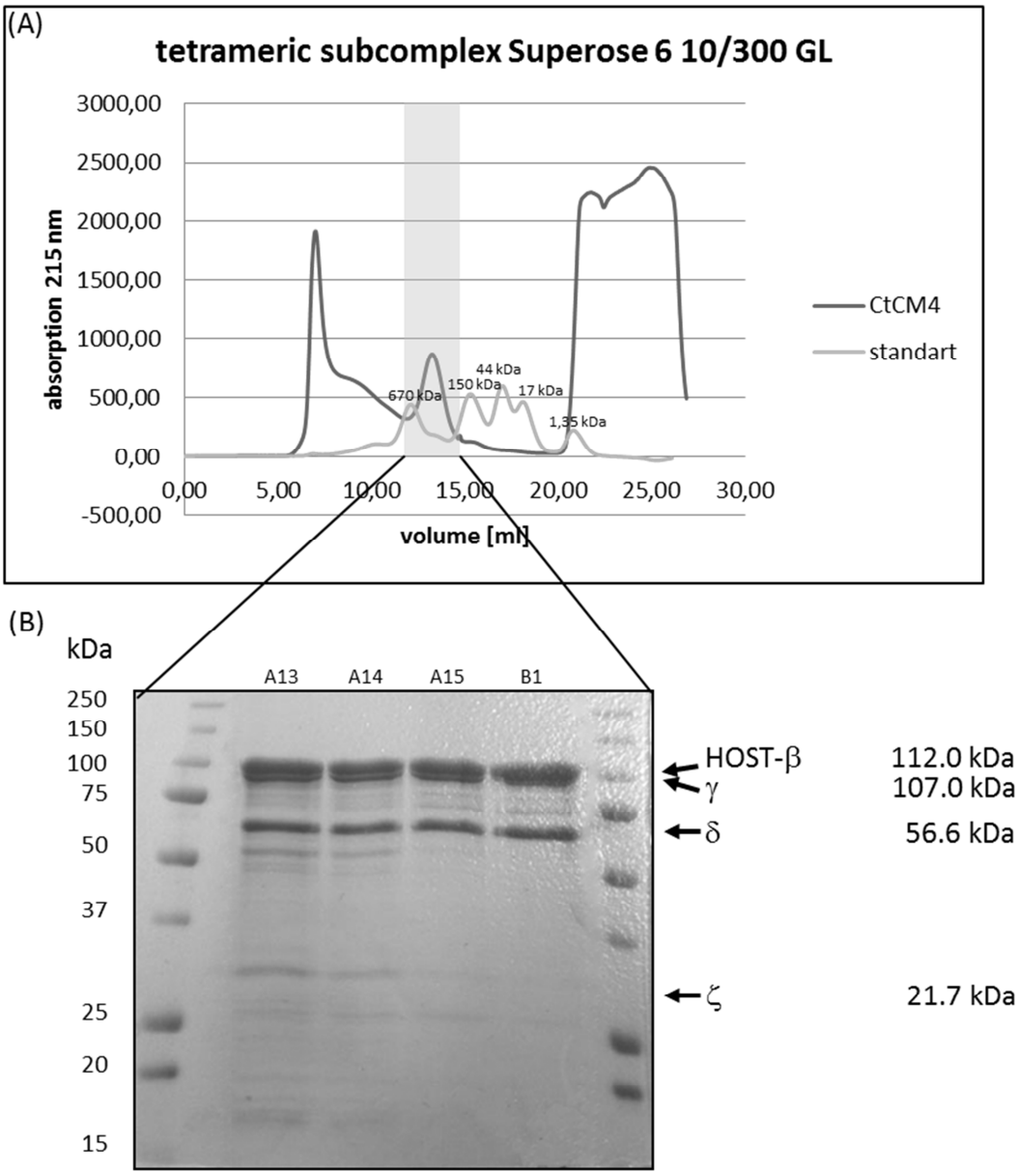

Figure 24: Chromatographic profile of the size exclusion chromatography of the tetrameric subcomplex

(A): The elution profile of the tetrameric coatomer subcomplex (dark grey) is overlayed with the elution profile of a protein size standard (light grey). The UV absorption at 215 nm is blotted against the elution volume in ml.

(B): 15 % SDS-PAGE stained with Coomassie. 5 µl of each coatomer tetramer Superose 6 10/300 GL elution fraction mixed with 3.5 µl 4 x SDS sample buffer was loaded on the gel.

The strep-tactin affinity purification of a dimeric (βδ) subcomplex is depicted in figure 25. After the affinity purification the dimeric subcomplex of coatomer contains still visible contaminations. The dimeric βδ subcomplex is not completely stable and shows some degradation. The subcomplex was subsequently further purified using size exclusion chromatography.

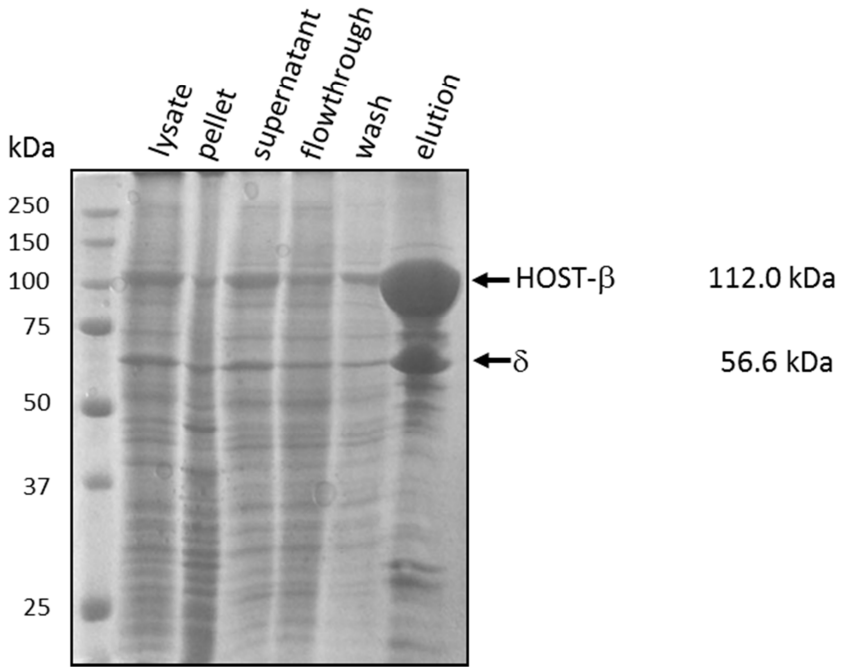

Figure 25: Strep-tactin purification the dimeric subcomplex βδ

15 % SDS-PAGE stained with Coomassie. 2 µl of lysate, pellet, supernatant and flowthrough fractions mixed with 5 µl 4 x SDS sample buffer and 10 µl of wash and elution fractions mixed with 3.5 µl of 4x SDS sample buffer was loaded on the gel.

The corresponding profile after chromatography of the dimeric βδ subcomplex on a Superose 6 10/300 GL column is depicted in figure 26. The subcomplex eluted at the expected size of 168.6 kDa and showed a symmetric peak with a small shoulder. Fractions of the peak were analyzed by SDS-PAGE. As depicted in figure 26, the fractions of the peak of the expected elution volume showed still some degradation, indicating a reduced stability of this complex compared to the complete coatomer complex.

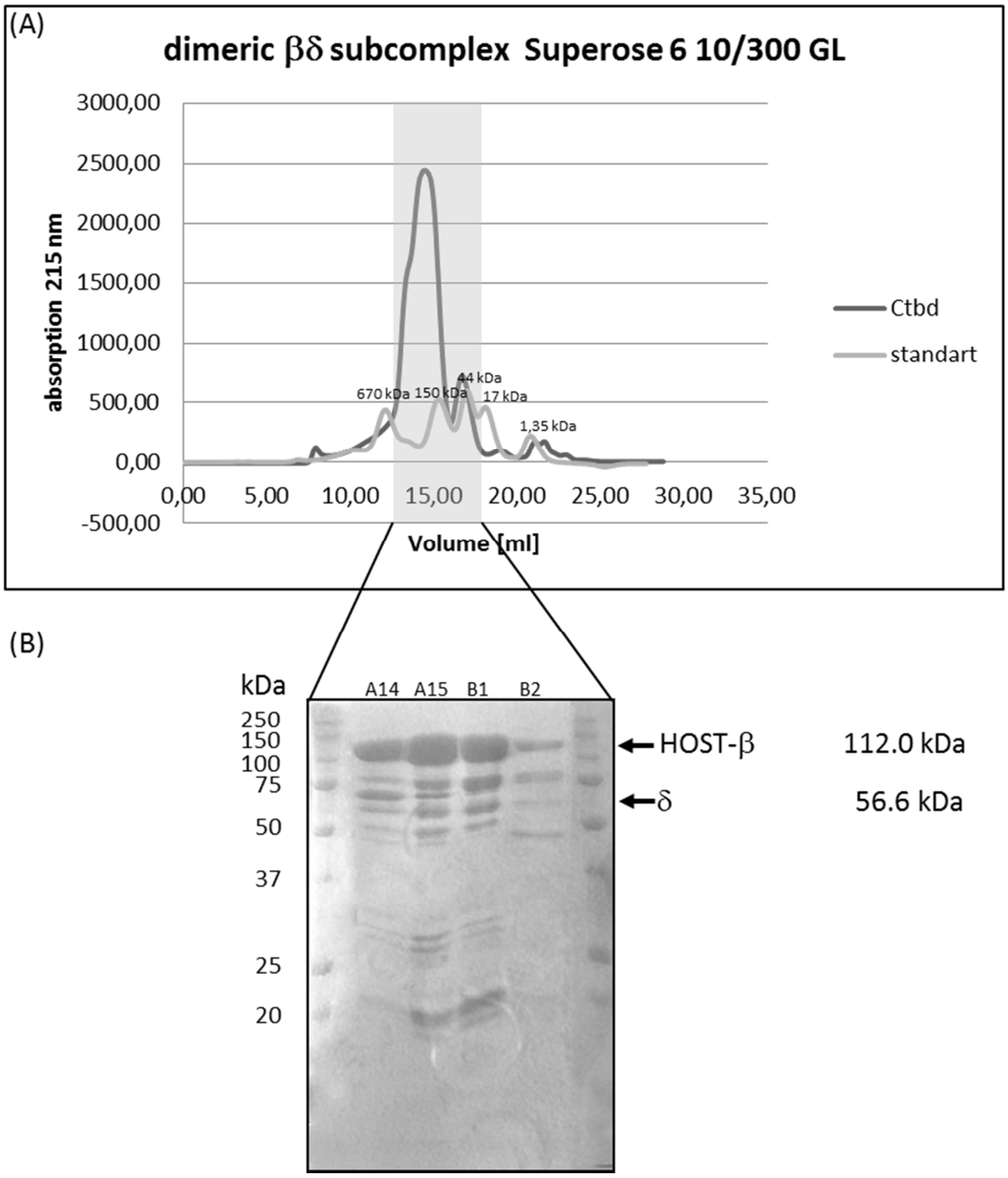

Figure 26: Chromatographic profile of the size exclusion chromatography of the dimeric βδ subcomplex

(A): The elution profile of the trimeric coatomer subcomplex (dark grey) is overlayed with the elution profile of a protein size standard (light grey). The UV absorption at 215 nm is blotted against the elution volume in ml.

(B): 15 % SDS-PAGE stained with Coomassie. 5 µl of each coatomer dimer Superose 6 10/300 GL elution fraction mixed with 3.5 µl 4 x SDS sample buffer was loaded on the gel.

The strep-tactin affinity purification of a dimeric (γζ) subcomplex is depicted in figure 27. After affinity purification, the dimeric subcomplex contains still visible contaminations and therefor was subjected to further pruification.

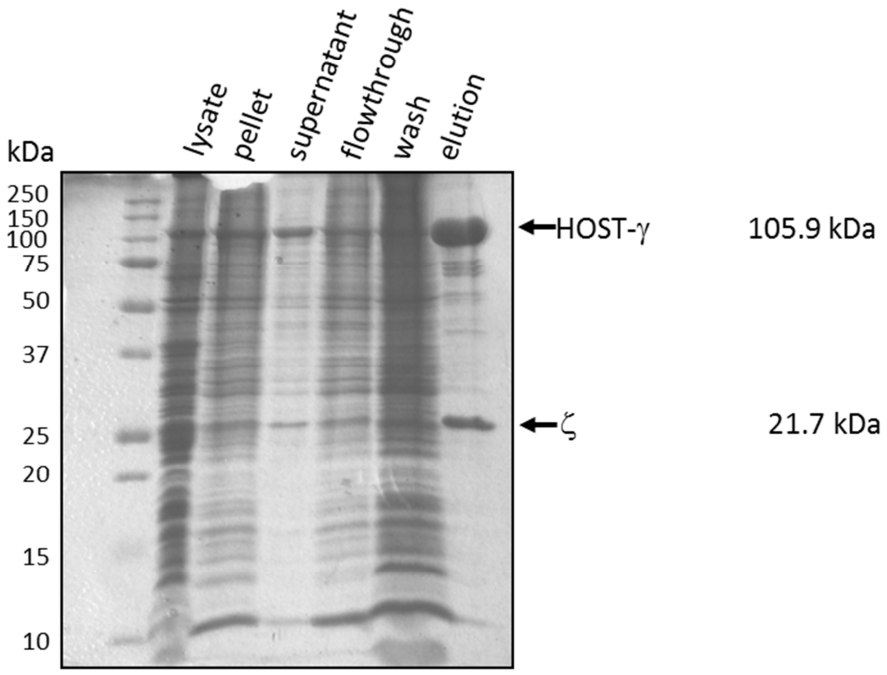

Figure 27: Strep-tactin purification of the dimeric γζ subcomplex

15 % SDS-PAGE stained with Coomassie. 2 µl of lysate, pellet, supernatant and flowthrough fractions mixed with 5 µl 4 x SDS sample buffer and 10 µl of wash and elution fractions mixed with 3.5 µl of 4x SDS sample buffer were loaded on the gel.

The profile of a size exclusion chromatography of the dimeric γζ subcomplex on a Superdex 200 10/300 GL column is depicted in figure 28. The subcomplex eluted at the expected size of 122.65 kDa and showed a symmetric peak. Fractions of the peak were analysed by SDS-PAGE. As depicted in figure 28, the fractions of the peak of the expected elution volume for the complex showed still some degradation, indicating again a reduced stability of this complex compared to the complete coatomer complex.

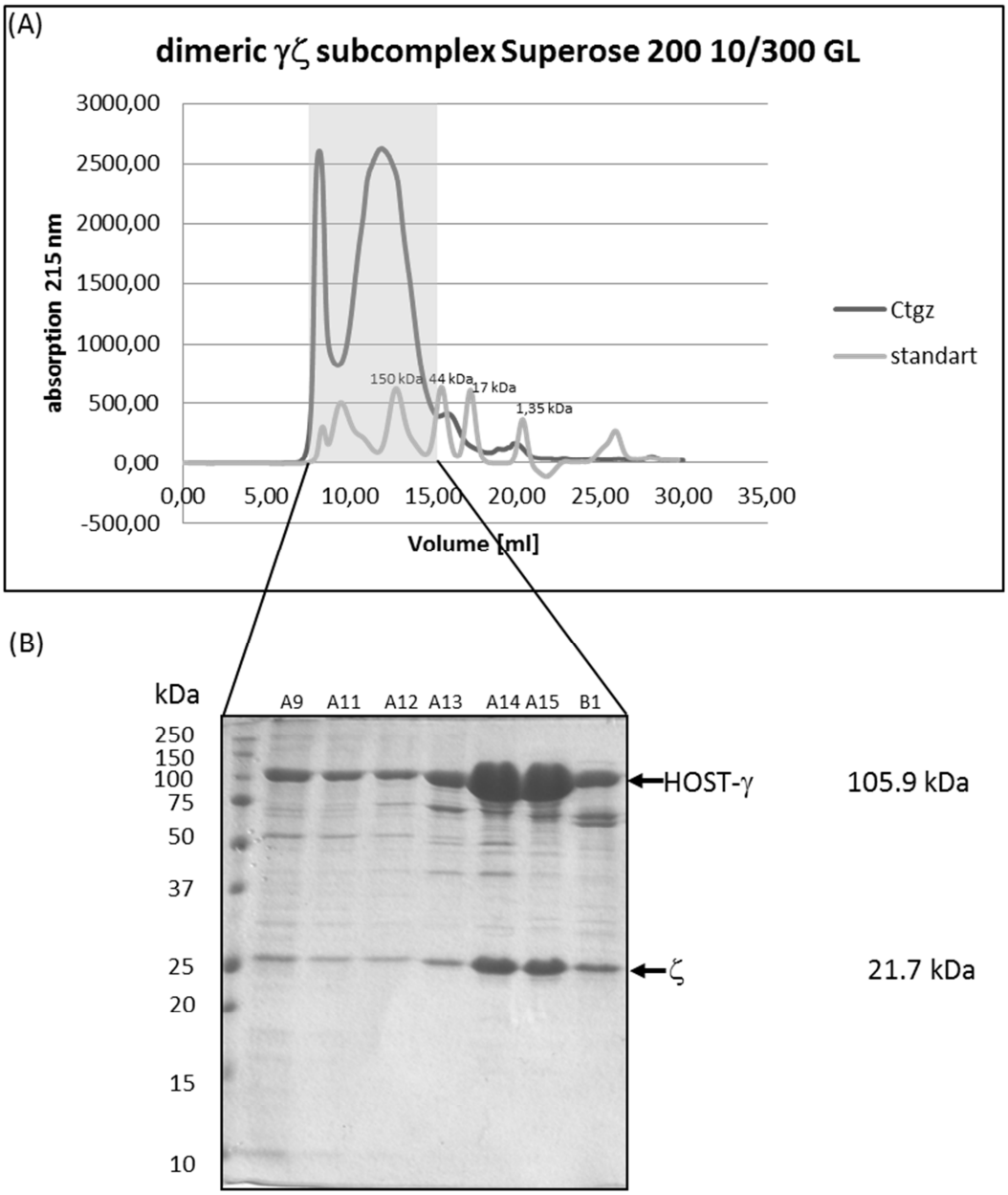

Figure 28: Chromatographic profile of the size exclusion chromatography of the dimeric γζ subcomplex

(A): The elution profile of the dimeric coatomer subcomplex (dark grey) is overlayed with the elution profile of a protein size standard (light grey). The UV absorption at 215 nm is blotted against the elution volume in ml.

(B): 15 % SDS-PAGE stained with Coomassie. 5 µl of each coatomer dimer Superdex 200 10/300 GL elution fraction mixed with 3.5 µl 4 x SDS sample buffer was loaded on the gel.

2.5 Vesicle Formation by *Chaetomium thermophilum* coatomer

To assess the functionality of the prepared *Chaetomium thermophilum* coatomer complex, its ability to make vesicles from unilamellar golgi-like liposomes containing 30 nmol p23 lipopeptide and 1 mol % PIP2 was tested. For the vesicle formation recombinant expressed Arf from *Chaetomium thermophilum* was used. As depicted in figure 29 *Chaetomium coatomer* was able to make vesicles in a GTPγS and Arf dependend manner. The vesicles showed the expected size for COPI vesicles in the range of 70 to 80 nm as depicted in figure 29.

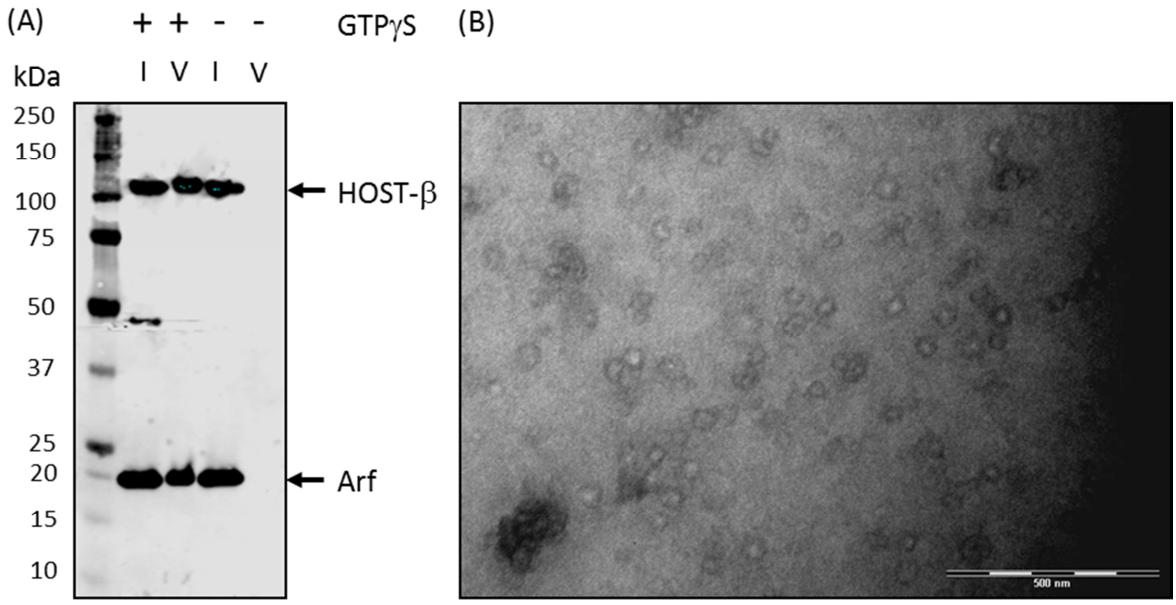

Figure 29: (A): Western-Blot Vesicle formation with *Chaetomium thermophilum* coatomer from golgi-like liposomes. 2 % of the input fraction and 50 % of the vesicle fractions were loaded on the gel. Detection was performed with Anti-HIS antibody and Anti-CtArf antibody. (B): negative stain EM picture of the vesicle fraction (stained with 3% w/v uranyl acetate).

2.6 Limited Proteolysis of *Chaetomium coatomer* and coatomer subcomplexes

To determine, which domains of *Chaetomium thermophilum* coatomer are most stable and therefor most suitable for crystallization the coatomer subcomplexes, β686δ-COP, γζ-COP and αβ´ε-COP as well the complete heptameric coatomer were analyzed by limited proteolysis. The subcomplexes and complete coatomer were incubated with serial dilutions of the protease subtilisin. The molar ratios of complex to subtilisin covered a range from 1 to

1 up to 1 to 0.001. The resulting fragments were separated by SDS-PAGE and analyzed by mass spectrometry.

The fragments separated by SDS-PAGE of coatomer after treatment with subtilisin are depicted in figure 30.

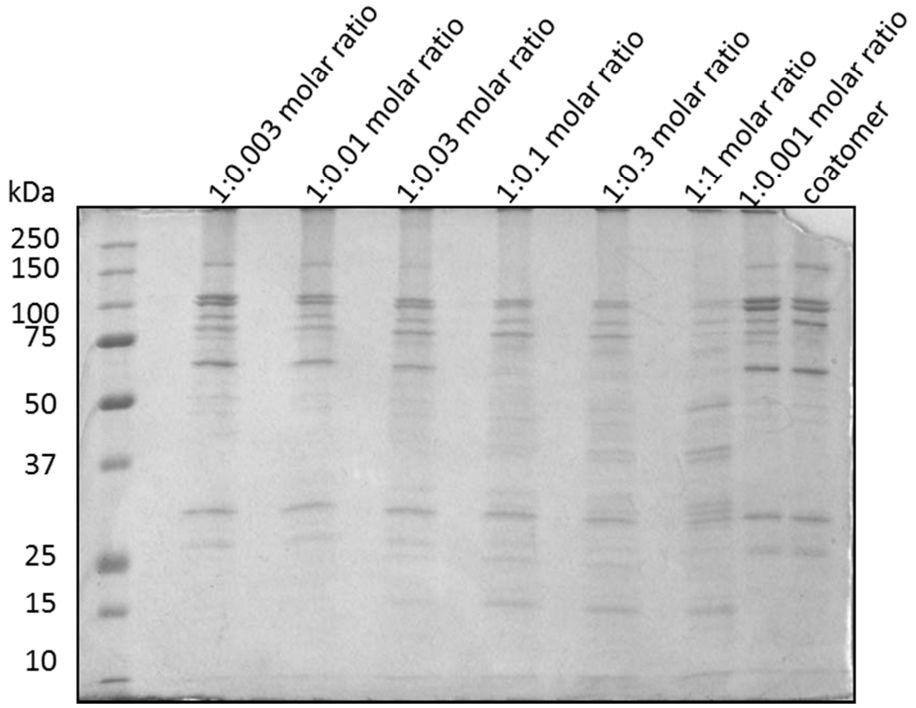

Figure 30: Limited Proteolysis of heptameric coatomer

15 % SDS-PAGE stained with Coomassie. 10 µl of subtilisin treated subcomplex of the respective ration mixed with 3.5 µl 4 x SDS sample buffer was loaded on the gel.

The fragment pattern produced proved to be too complex for reasonable mass spec analysis. Also, since insoluble fragments were not of interest, it was decided to analyze the complex with two specific coatomer-subtilisin ratios (1:0.3 and 1:0.1), which would be separated by size exclusion chromatography to obtain the remaining soluble complex, which could then be analyzed by mass spectrometry.

The fragments separated by SDS-PAGE of coatomer after treatment with subtilisin are depicted in figure 31.

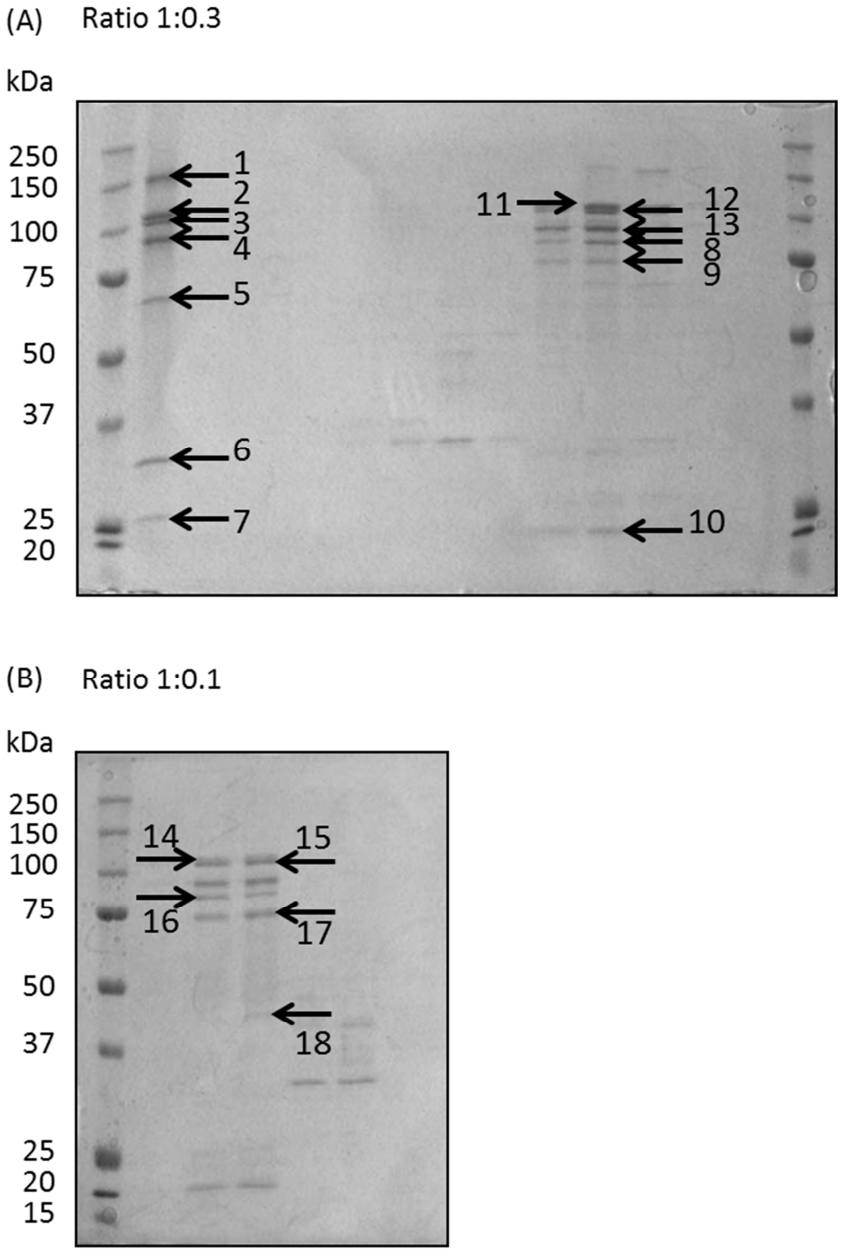

Figure 31: Limited Proteolysis of heptameric coatomer ratios 1:0.3 and 1:0.1

(A): 15 % SDS-PAGE stained with Coomassie. 10 µl of subtilisin treated complex of the ration 1:0.3 mixed with 3.5 µl 4 x SDS sample buffer was loaded on the gel.

(B): 15 % SDS-PAGE stained with Coomassie. 10 µl of subtilisin treated complex of the ration 1:0.1 mixed with 3.5 µl 4 x SDS sample buffer was loaded on the gel.

The bands numbered in figure 31 were subjected to proteolytic digestion and mass spectrometry, and borders for subtilisin truncation where identified by comparison of peptide peak intensities. The identified stable truncation fragments are depicted in figure 32.

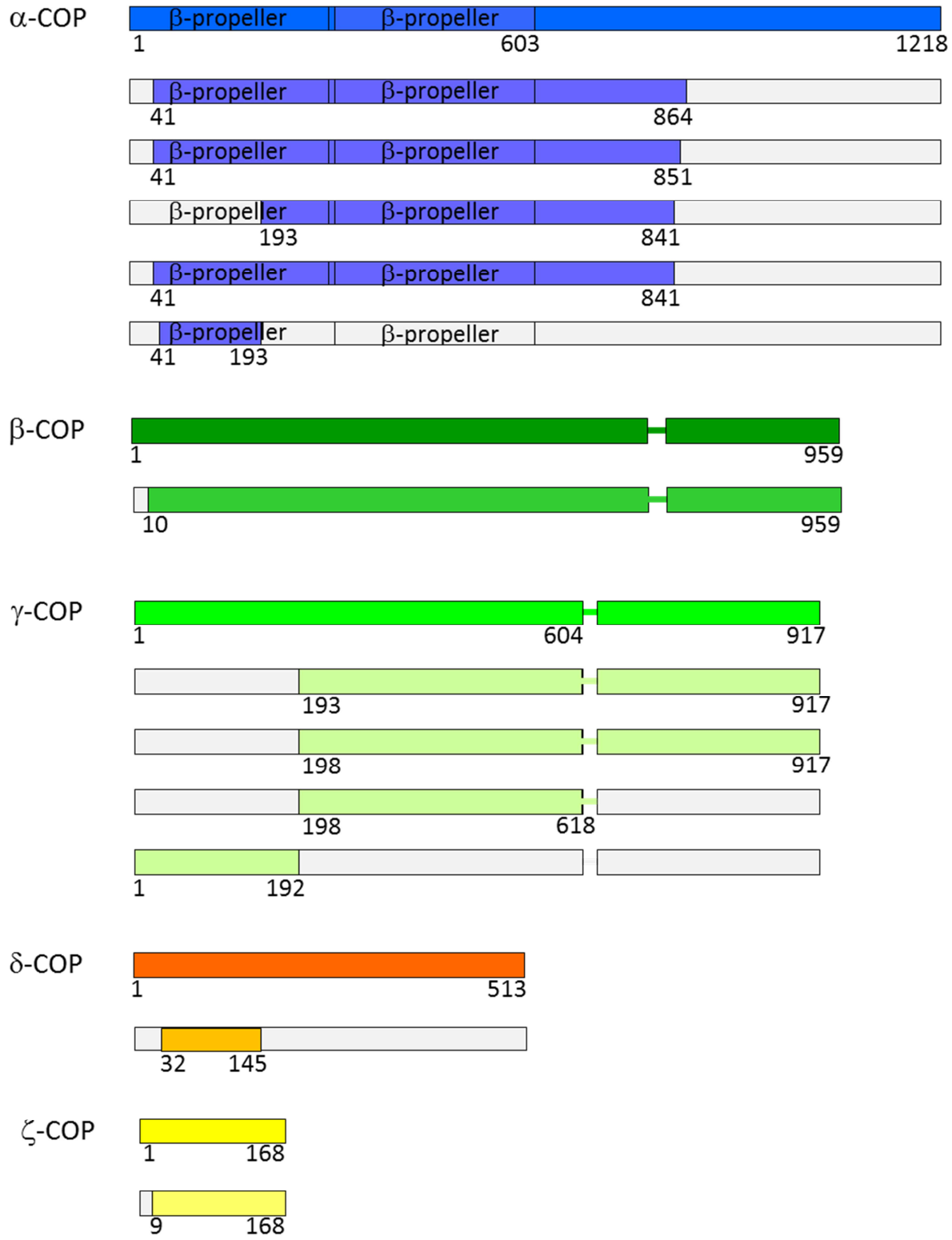

Figure 32: Stable core fragments resulting from limited Proteolysis of heptameric coatomer.

Depicted are the identified stable fragments of the respective subunits compared to full length proteins. Numbers refer to amino acid residue position.

In order to obtain a more detailed view on stable subcomplexes and domains of coatomer also the trimeric and dimeric subcomplexes were analyzed by limited proteolysis.

The fragments of the subtilisin treated coatomer subcomplex αβ´ε, separated by SDS-PAGE, which were analyzed by mass spectrometry, are depicted in figure 33 as indicated by numbered arrows.

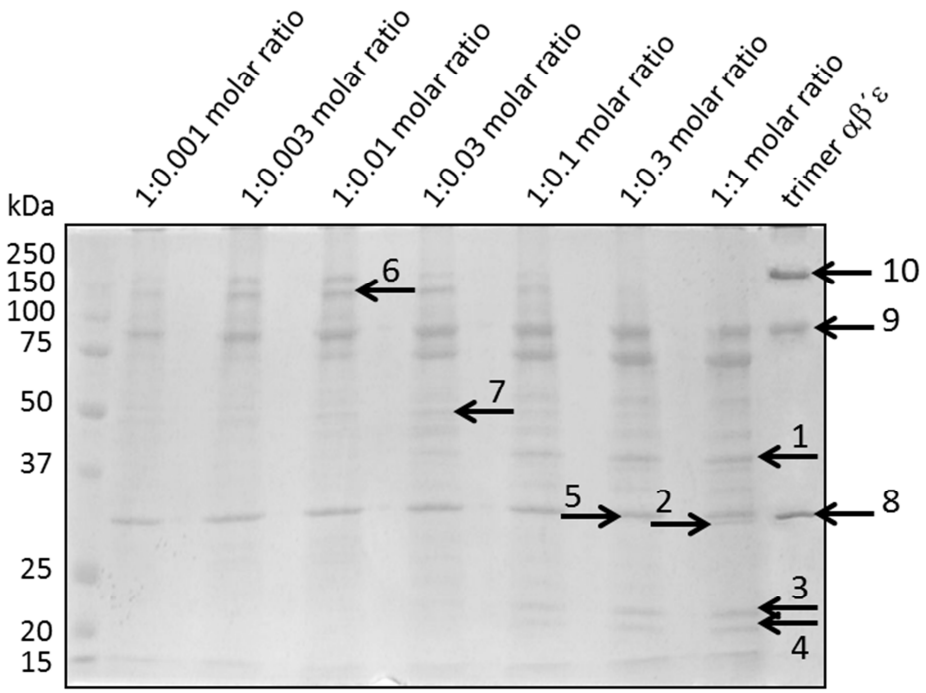

Figure 33: Limited Proteolysis of the trimeric subcomplex αβ´ε

15 % SDS-PAGE stained with Coomassie. 10 µl of subtilisin treated subcomplex of the respective ration mixed with 3.5 µl 4 x SDS sample buffer was loaded on the gel.

Borders for subtilisin truncation where identified by comparison of peptide peak intensities. The identified stable truncation fragments are depicted in figure 34.

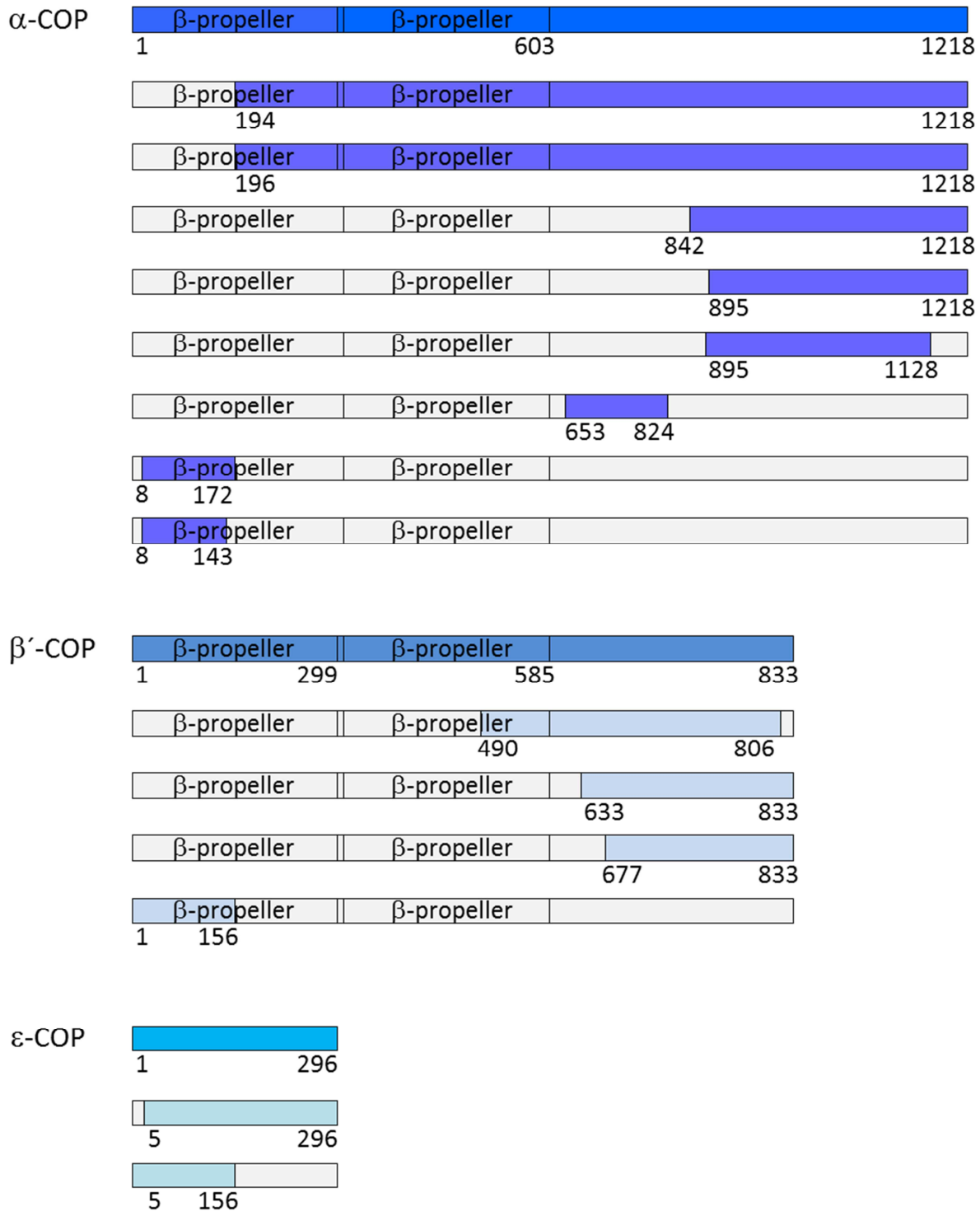

Figure 34: Identified stable core fragments resulting from limited Proteolysis of the trimeric subcomplex αβ´ε

Depicted are the identified stable fragments of the α-COP, β´-COP and ε-COP subunits compared to full length proteins. Numbers refer to amino acid residue positions.

Fragments of the subtilisin treated coatomer subcomplex β686δ, separated by SDS-PAGE, which were analyzed by mass spec are depicted in figure 35, as indicated by numbered arrows.

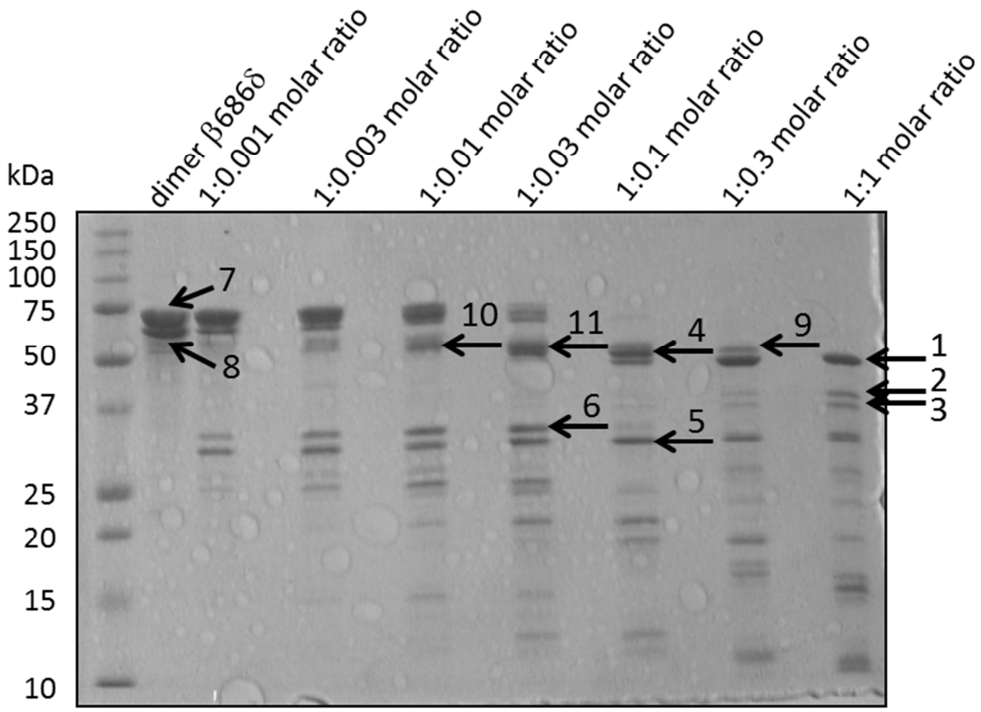

Figure 35: Limited Proteolysis of the dimeric β686δ subcomplex

15 % SDS-PAGE stained with Coomassie. 10 µl of subtilisin treated subcomplex of the respective ration mixed with 3.5 µl 4 x SDS sample buffer was loaded on the gel.

Borders for subtilisin truncation where identified in the mass spectrometric records by comparison of peptide peak intensities. The identified stable truncation fragments are depicted in figure 36.

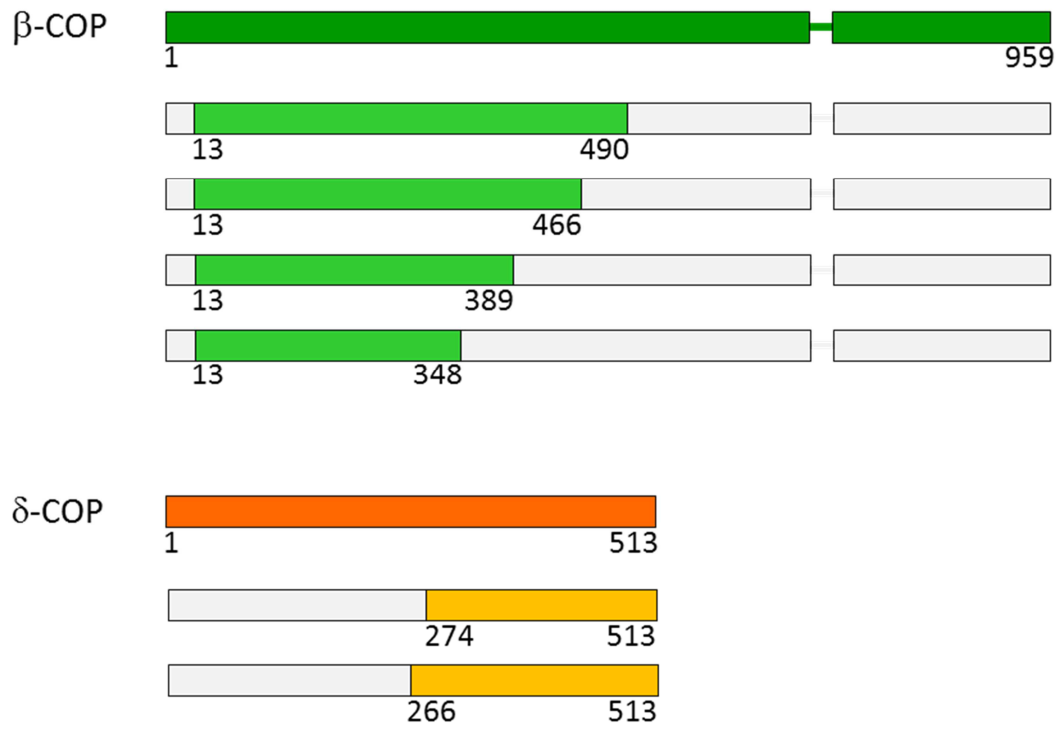

Figure 36: Identified stable core fragments resulting from limited Proteolysis of the dimeric subcomplex β686δ

Depicted are the identified stable fragments of the Ctβ and Ctδ subunits compared to full length proteins.

Fragments of the subtilisin treated coatomer subcomplex γζ, separated by SDS-PAGE that were analyzed by mass spectrometry are depicted in figure 37.

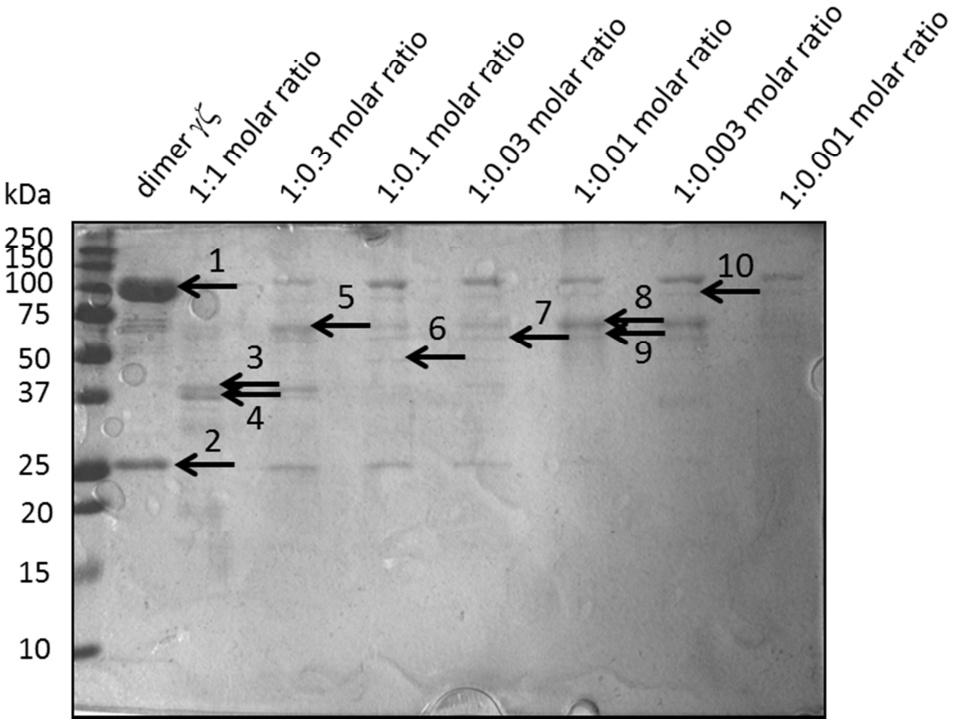

Figure 37: Limited Proteolysis of the dimeric subcomplex γζ

15 % SDS-PAGE stained with Coomassie. 10 µl of subtilisin treated subcomplex of the respective ration mixed with 3.5 µl 4 x SDS sample buffer was loaded on the gel.

Borders for subtilisin truncation where again identified by comparison of peptide peak intensities. Identified stable truncation fragments are depicted in figure 38.

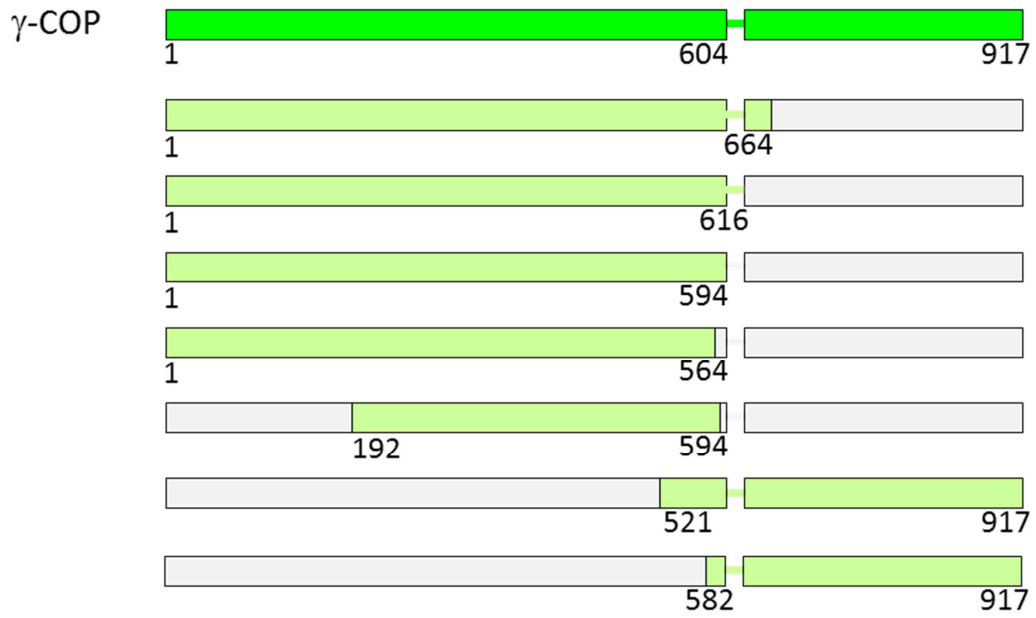

Figure 38: Identified stable core fragments resulting from limited Proteolysis of the dimeric subcomplex γζ

Depicted are the identified stable fragments of the Ctγ subunit compared to the full length protein.

2.7 Design of crystallization constructs

Based on the data obtained from the limited proteolysis and on structural data from related vesicle coats, new subcomplexes for structural analysis by protein crystallography were designed (table 1). These constructs were made to investigate the structure of distinct domains of coatomer that were proposed to be involved in Arf-binding, in cargo- and machinery-binding and in coatomer-coatomer interactions.

complex	subunit composition	domains
α825β´793	α1-825, β´1-793	N-terminal β-propeller domains and following α-solenoid stretch of α-COP and β´-COP
α825Mβ´793	α1-825-F185KM189KN195KM199KF200K,	N-terminal β-propeller domains and following α-solenoid stretch of α-COP and

	β´1-793	β´-COP
α603	α1-603	2 N-terminal β-propeller domains of α-COP
β´585	β´1-585	2 N-terminal β-Propeller domains of β´-COP
β´299	β´1-299	N-terminal β-propeller domain of β´-COP
CM4β608γ586	β1-608, γ1-586, δ, ζ	Tetramer without appendage domains and linker of β-COP and γ-COP
CM4β686γ666	β1-686, γ1-666, δ, ζ	Tetramer without appendage domains of β-COP and γ-COP
β19-391δ	β19-391, Ctδ	N-terminal α-solenoid with Arf binding site of β-COP, full-length δ-COP
β19-407δ	β19-407, Ctδ	N-terminal α-solenoid with Arf binding site of β-COP, full-length δ-COP
β19-391δ1-243	β19-391, Ctδ1-243	N-terminal α-solenoid with Arf binding site of β-COP, longin-domain and linker part of δ-COP
β19-391δ1-175	β19-391, Ctδ1-175	N-terminal α-solenoid with Arf binding site of β-COP, longin-domain and linker part of δ-COP
β19-391δ1-137	β19-391, Ctδ1-137	N-terminal α-solenoid with Arf binding site of β-COP, longin-domain of δ-COP
β19-391δ1-124	β19-391, Ctδ1-124	N-terminal α-solenoid with Arf binding site of β-COP, longin-domain of δ-COP
β683-960	β683-960	appendage domain of β-COP
γ648-918	γ648-918	appendage domain of γ-COP

δ124	δ1-124	Longin domain of δ-COP
δ137	δ1-137	Longin domain of δ-COP
β608δ	β1-608, Ctδ	β-COP without appendage domain and linker, full-length δ-COP
β686δ	β1-686, Ctδ	β-COP without appendage domain, full-length δ-COP
CM4γ586	β, γ1-586, δ, ζ	Tetramer without appendage domain and linker of γ-COP
CM4γ586δ243	β, γ1-586, δ1-243, ζ	Tetramer without appendage domain and linker of γ-COP and without μ-homology domain of δ-COP

Table 1: crystallization constructs

Listed are *Chaetomium coatomer* subcomplexes, designed for crystallization.

Crystallization of some of the designed and produced subcomplexes (table 2) was not followed up because the complexes turned out to be unsuitable for crystallization trials.

complex	**Expression system**	**Result**
α603	Baculovirus (SF9 cells)	Insoluble
CM4β608γ586	Baculovirus (SF9 cells)	Complex assembly compromised
β683-960	Baculovirus (SF9 cells)	Insoluble
δ124	*E. coli* BL21 DE3	Insoluble
δ137	*E. coli* BL21 DE3	Insoluble
CM4γ586	Baculovirus (SF9 cells)	Complex assembly compromised

CM4γ586δ243	Baculovirus (SF9 cells)	Complex assembly compromised
β19-407δ	Baculovirus (SF9 cells)	too much degradation
β608δ	Baculovirus (SF9 cells)	Complex assembly compromised

Table 2: Unsuitable crystallization constructs

Listed are *Chaetomium coatomer* subcomplexes that proved unsuitable for crystallization.

2.8 Expression and purification of crystallization constructs

Expression of the *Chaetomium* coatomer subcomplexes for crystallization was done in Sf9 insect cells. The Purification was performed as for the other complexes using strep-tactin affinity chromatography and size exclusion chromatography.

Purifications of subcomplexes not resulting in succesfull crystallization or preparation of single particle EM structures are shown in Appendix I.

The chromatographic profile of the size exclusion chromatography of the dimeric subcomplex α825β´793 on a Superose 6 10/300 GL column is depicted in figure 39. The proteins eluted at the expected size of 186.8 kDa and showed a symmetric peak. Fractions of the peak were analyzed by SDS-PAGE. As depicted in figure 39 the subcomplex shows high purity after size exclusion chromatography with no residual visble contaminations.

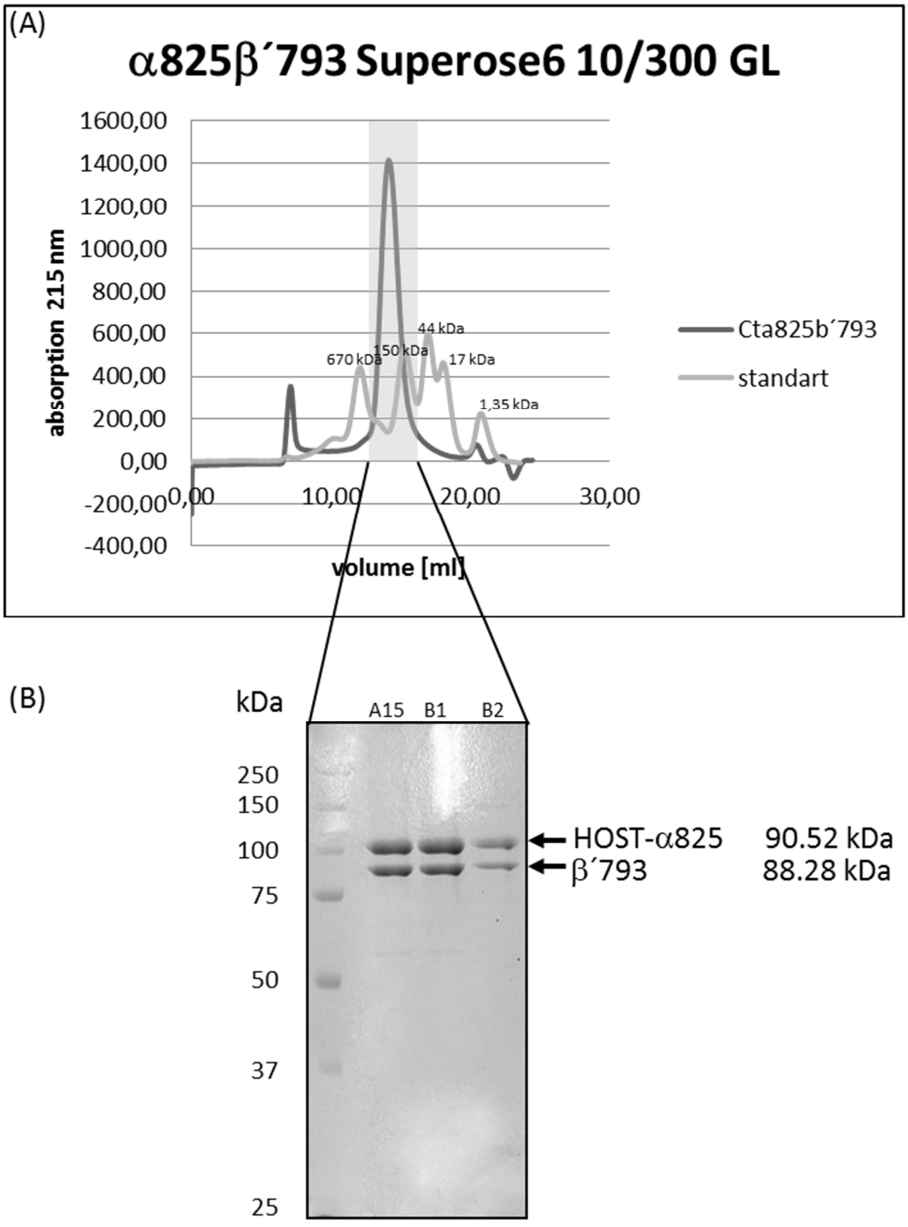

Figure 39: Chromatographic profile of the size exclusion chromatography of the dimeric subcomplex α825β´793

(A): The elution profile of the dimeric subcomplex (dark grey) is overlayed with the elution profile of a protein size standard (light grey). The UV absorption at 215 nm is blotted against the elution volume in ml.

(B): 12 % SDS-PAGE stained with Coomassie. 5 µl of each coatomer dimer Superose 6 10/300 GL elution fraction mixed with 3.5 µl 4 x SDS sample buffer was loaded on the gel.

Size exclusion chromatography of the truncated βδ subcomplex β19-391δ on a Superdex 200 10/300 GL column is depicted in figure 40. The proteins eluted at the expected size of 104 kDa and showed a symmetric peak. Fractions of the peak were analyzed by SDS-PAGE. As depicted in figure 40 the subcomplex shows good purity. A small shoulder in the peak

contained only Ctβ19-391 indicating a not completely stoichiometric expression of the subunits. The free β19-391 could be separated from the complex.

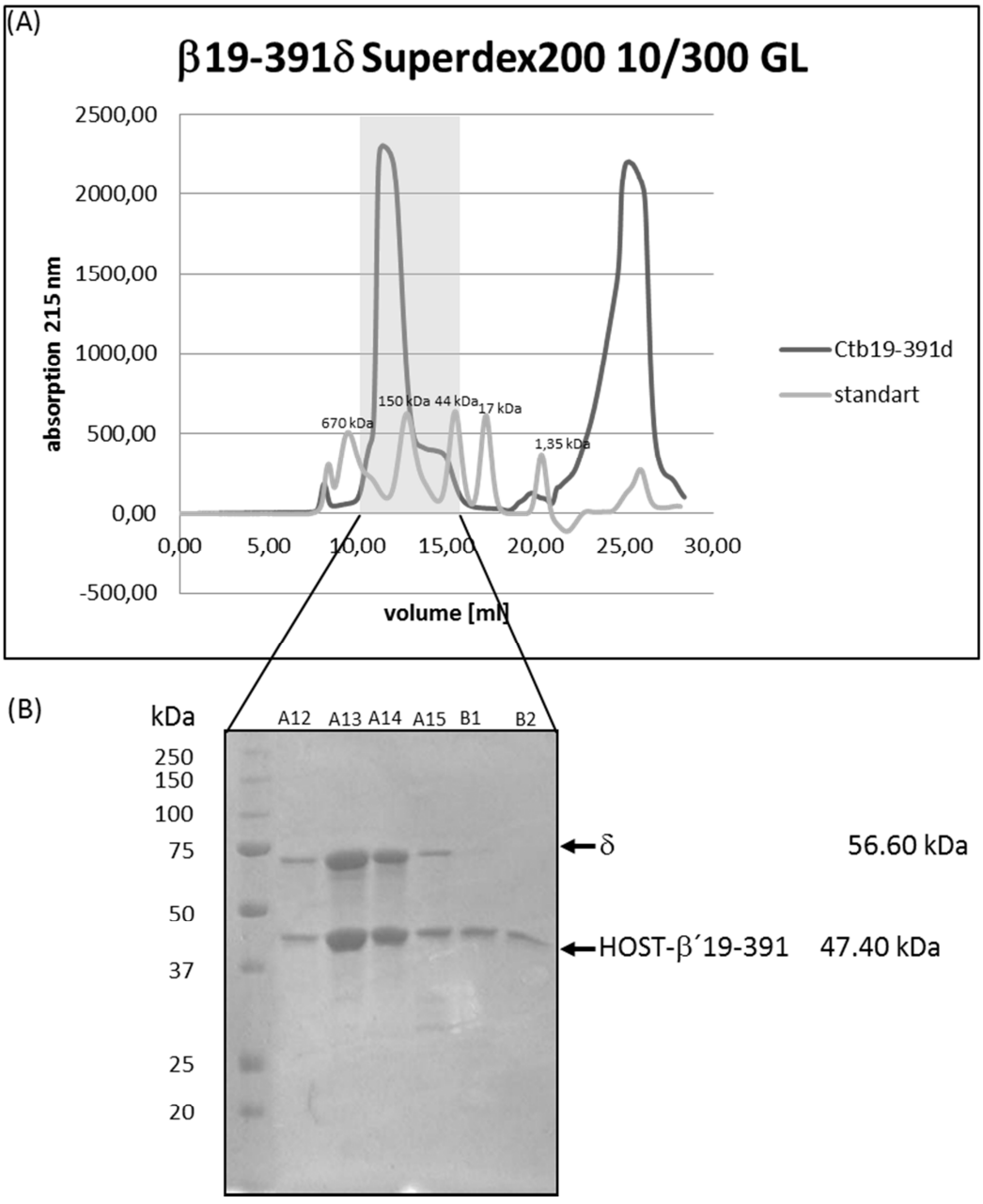

Figure 40: Chromatographic profile of the size exclusion chromatography of the dimeric subcomplex β19-391δ

(A): The elution profile of the truncated coatomer βδ-subcomplex (dark grey) is overlayed with the elution profile of a protein size standard (light grey). The UV absorption at 215 nm is blotted against the elution volume in ml.

(B): 15 % SDS-PAGE stained with Coomassie. 5 µl of each coatomer dimer Superose 6 10/300 GL elution fraction mixed with 3.5 µl 4 x SDS sample buffer was loaded on the gel.

The chromatographic profile of the size exclusion chromatography of the truncated coatomer βδ subcomplex β19-391δ1-175 on a Superose 6 10/300 GL column is depicted in figure 41. The coatomer subcomplex eluted at the expected size of 67.64 kDa and showed a symmetric peak. Fractions of the peak were analyzed by SDS-PAGE, as depicted in figure 41.

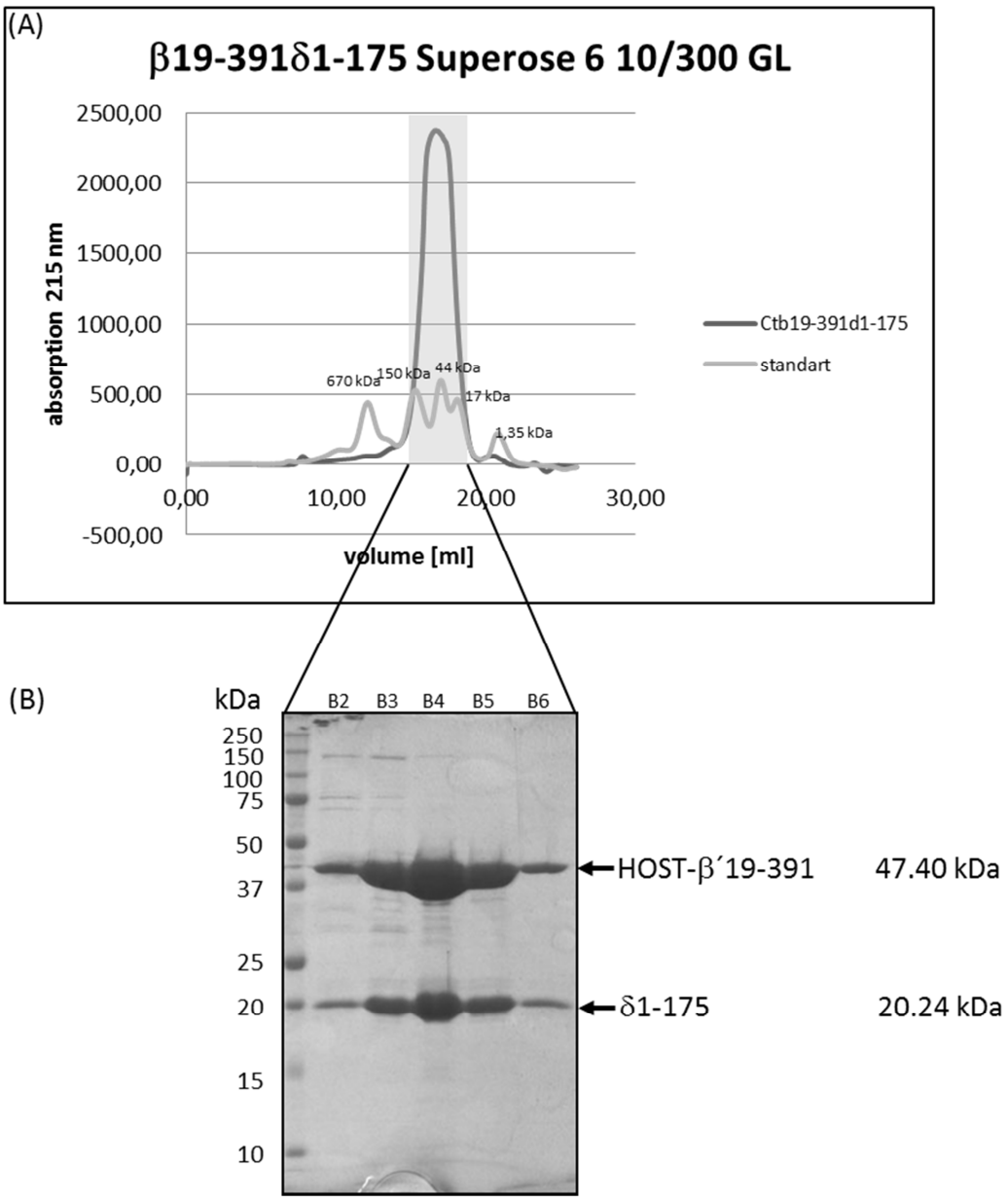

Figure 41: Chromatographic profile of the size exclusion chromatography of the dimeric subcomplex β19-391δ1-175

(A): The elution profile of the truncated coatomer βδ-subcomplex (dark grey) is overlayed with the elution profile of a protein size standard (light grey). The UV absorption at 215 nm is blotted against the elution volume in ml.

(B): 15 % SDS-PAGE stained with Coomassie. 5 µl of each coatomer dimer Superose 6 10/300 GL elution fraction mixed with 3.5 µl 4 x SDS sample buffer was loaded on the gel.

The chromatographic profile of the size exclusion chromatography of the truncated coatomer βδ subcomplex β19-391δ1-137 on a Superose 6 10/300 GL column is depicted in figure 42. The coatomer subcomplex eluted at the expected size of 63.01 kDa and showed a symmetric peak. Fractions of the peak were analyzed by SDS-PAGE, as depicted in figure 42.

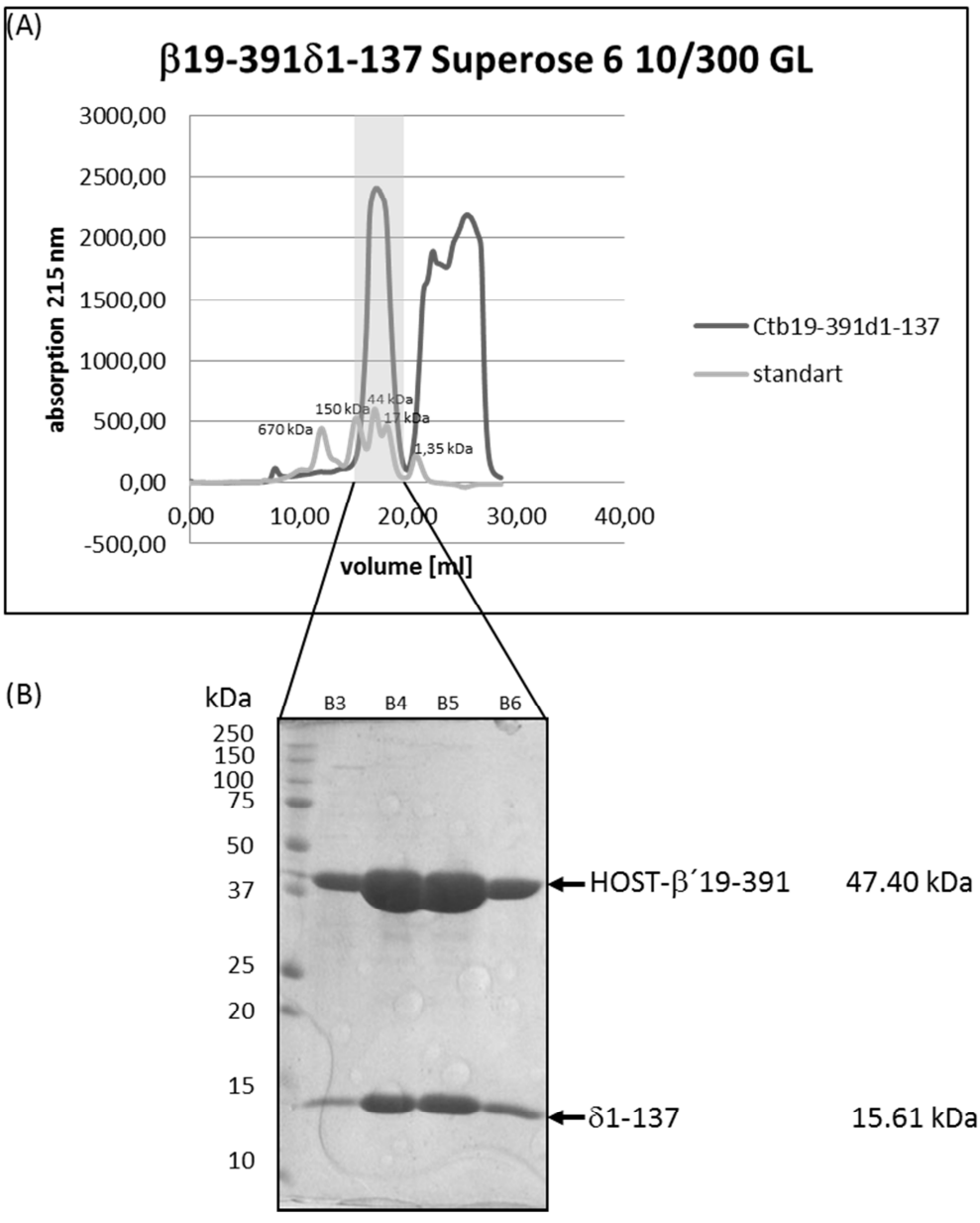

Figure 42: Chromatographic profile of the size exclusion chromatography of the dimeric subcomplex β19-391δ1-137

(A): The elution profile of the truncated coatomer βδ-subcomplex (dark grey) is overlayed with the elution profile of a protein size standard (light grey). The UV absorption at 215 nm is blotted against the elution volume in ml.

(B): 15 % SDS-PAGE stained with Coomassie. 5 µl of each coatomer dimer Superose 6 10/300 GL elution fraction mixed with 3.5 µl 4 x SDS sample buffer was loaded on the gel.

2.9 Expression and purification of a soluble form of *Chaetomium thermophilum* Arf

For structurall studies of the interaction of the small GTPase Arf with coatomer and coatomer subcomplexes a soluble form of Arf of *Chaetomium thermophilum* was prepared.

```
                    1                                                  50
ARF1 human      (1) ---MGNIFANLFKGLFGKKEMRILMVGLDAAGKTTILYKLKLGEIVTTIP
    CtArf1      (1) MGLAGSKLFSFLSLLMKQKEMRILMVGLDAAGKTTILYKLKLGEVVTTIP
 Consensus      (1)     G         L   KEMRILMVGLDAAGKTTILYKLKLGEIVTTIP
                    51                                                 100
ARF1 human     (48) TIGFNVETVEYKNISFTVWDVGGQDKIRPLWRHYFQNTQGLIFVVDSNDR
    CtArf1     (51) TIGFNVETVEYRNIQFTVWDVGGQDKIRPLWRHYFQNTQGIIFVVDSNDR
 Consensus     (51) TIGFNVETVEYKNI FTVWDVGGQDKIRPLWRHYFQNTQGIIFVVDSNDR
                   101                                                 150
ARF1 human     (98) ERVNEAREELMRMLAEDELRDAVLLVFANKQDLPNAMNAAEITDKLGLHS
    CtArf1    (101) DRVPEAREELQRMLNEDELRDALLLVFANKQDLPNAMTVAEITDKLGLHS
 Consensus    (101) DRV EAREEL RML EDELRDALLLVFANKQDLPNAM  AEITDKLGLHS
                   151                                184
ARF1 human    (148) LRHRNWYIQATCATSGDGLYEGLDWLSNQLRNQK
    CtArf1    (151) LRQRKWYIQSTCATTGDGLFEGLDWLAQEIKKSS
 Consensus    (151) LR R WYIQATCATSGDGLFEGLDWLAN IK
```

Figure 43: Alignment *of Chaetomium thermophilum* Arf and human Arf1

The N-terminal amphipathic helix of Arf is depicted in bold

Upon GTP-binding and activation, Arf undergoes a conformational change, which leads to exposure of its previously buried amphipatic and myristoylated N-terminal α-helix. The exposed helix anchors Arf to the membrane and strongly reduces the solubility of the GTP-loaded protein. Therefore for experiments on Arf, which are conducted in solution, truncated forms of Arf lacking the N-terminal helix are used.

For mammalian Arfs the N-terminal 17 amino acids are removed (Paris et al., 1997). As depicted in figure 43, compared to human Arf1 *Chaetomium thermophilum* Arf has a 3 amino acids longer N-terminal part. In analogy to the NΔ17 constructs for mammalian Arf

the N-terminal 20 amino acids of *Chaetomium thermophilum* were omitted in the construct designed as depicted in figure 44.

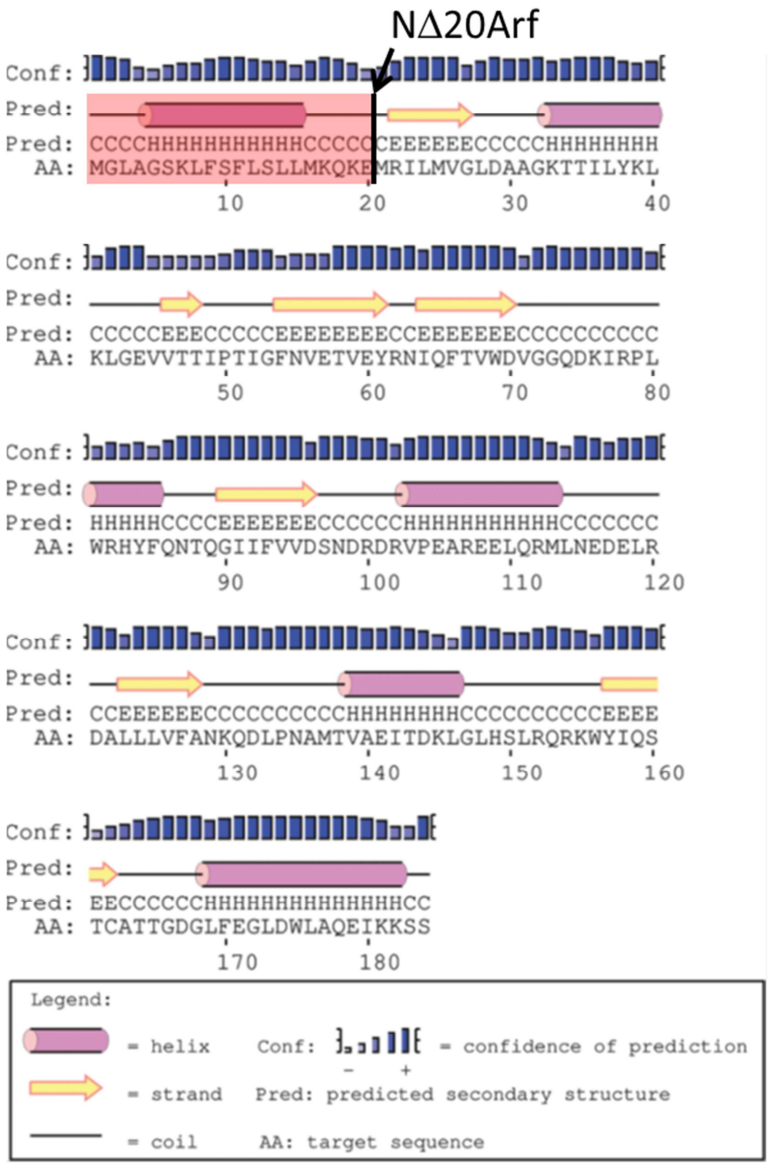

Figure 44: Secondary structure prediction of *Chaetomium thermophilum* Arf

The deleted N-terminal 20 amino acids of Arf are depicted in red. Secondary structure prediction was performed using the PSIPRED-Server of the Department of Computer Science of the UCL (University College London).

NΔ20Arf was cloned in a pETM11-vector fusing an HIS_6-TAG and a TEV-Cleavage site to the N-terminus. The small GTPase was expressed in *E. coli BL21* cells for 4 hrs. The expression and the Ni-NTA affinity purification of NΔ20Arf are depicted in figure 45.

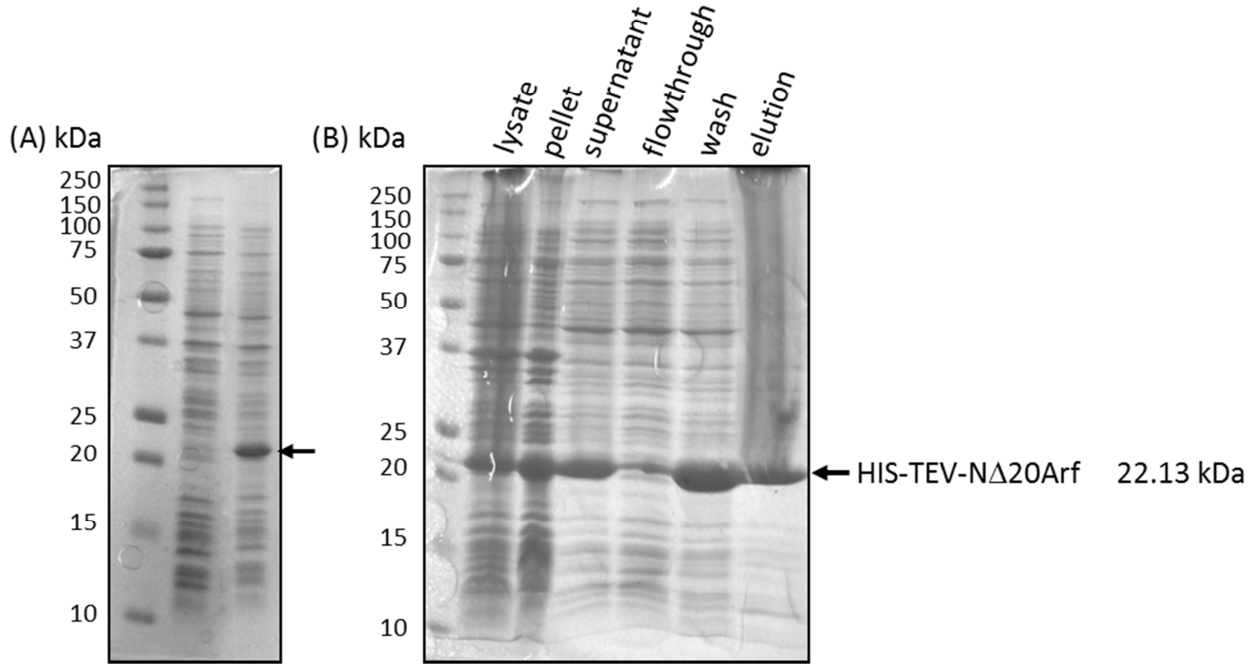

Figure 45: Expression and Ni-NTA affinity purification of NΔ20Arf

(A): 15 % SDS-PAGE stained with Coomassie. 2 µl of uninduced and 4 hrs expression cultur mixed with 5 µl 4 x SDS sample buffer was loaded on the gel.

(B): 15 % SDS-PAGE stained with Coomassie. 2 µl of lysate, pellet, supernatant and flowthrough fractions mixed with 5 µl 4 x SDS sample buffer and 10 µl of wash and elution fractions mixed with 3.5 µl of 4x SDS sample buffer was loaded on the gel.

The chromatographic profile of a size exclusion chromatography of *Chaetomium thermophilum* NΔ20Arf on a Superdex 75 16/60 GL column is depicted in figure 46. NΔ20Arf eluted at the expected apparent size of 22.13 kDa and showed a symmetric peak. Fractions of the peak were analyzed by SDS-PAGE.

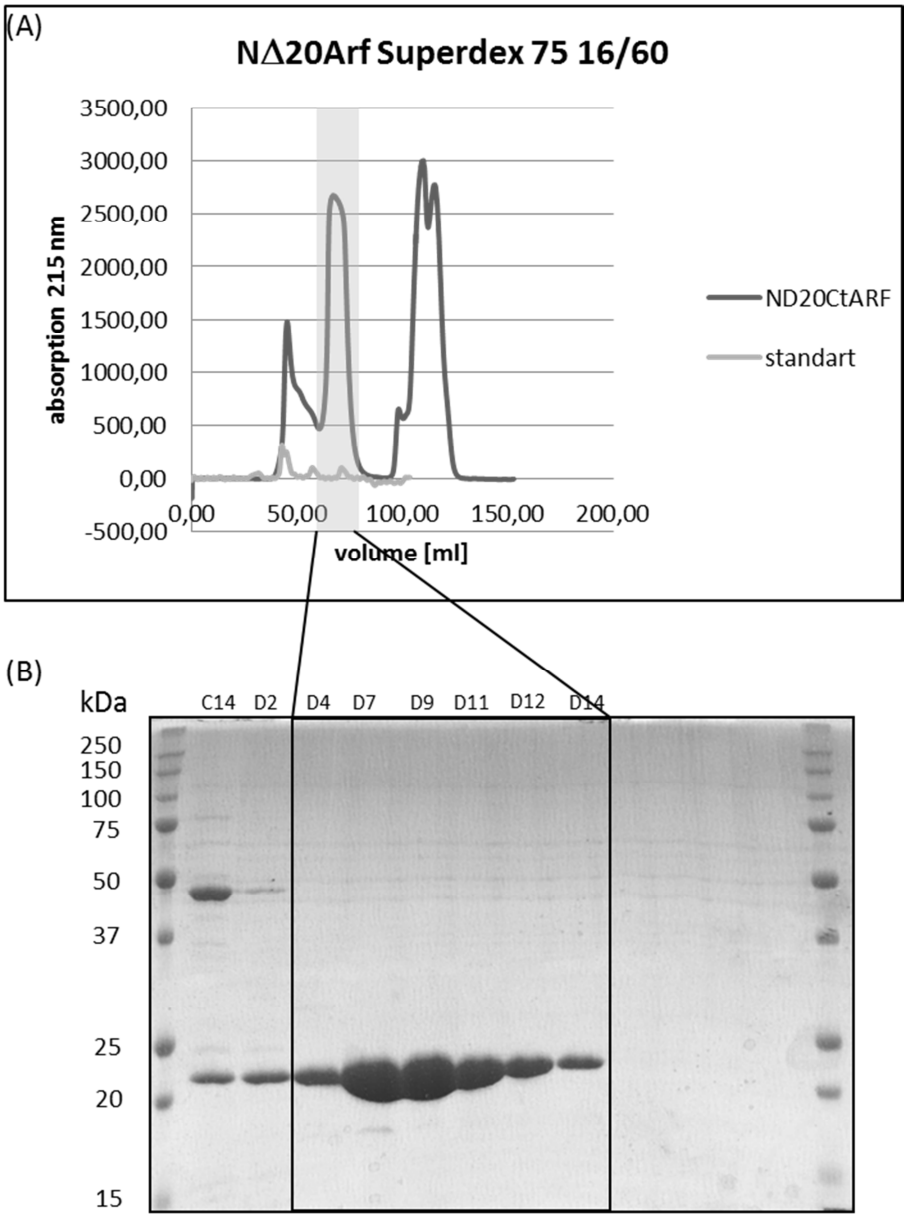

Figure 46: Chromatographic profile of NΔ20Arf

A): The elution profile of *Chaetomium thermophilum* NΔ20Arf (dark grey) is overlayed with the elution profile of a protein size standard (light grey). The UV absorption at 215 nm is blotted against the elution volume in ml.

(B): 15 % SDS-PAGE stained with Coomassie. 5 µl of each *Chaetomium thermophilum* NΔ20Arf Superdex 75 16/60 GL elution fraction mixed with 3.5 µl 4 x SDS sample buffer was loaded on the gel.

Also two mutant variants of NΔ20Arf NΔ20ArfQ74L and NΔ20ArfT34N were a prepared, which are locked in the active (GTP-loaded) or inactive (GDP-loaded) conformation. These mutants behaved like the wildtype during expression and purification.

2.10 Preparation of *Chaetomium thermophilum* coatomer complexes lacking ε-COP and the C-terminal part of δ-COP

In the cryo-EM structure of COPI vesicles published in 2012 (Faini et al., 2012) it was shown that the linkage between different coatomer triads were made up by contacts involving either the ε-COP subunit or the C-terminal part of the δ-COP subunit, the δ-COP μ-homology domain. To address a function of these domains in connecting triads of coatomer on the vesicle, coatomer variants lacking these domains were prepared. These coatomer variants were expressed in insect cells using separated viruses (βδγζ, α and β´ for the hexameric coatomer variant αββ´γδζ and βδ243, γζ, αβ´ε for the coatomer variant lacking the μ-homology domain of δ-COP αββ´γδ243εζ). αββ´γδζ and αββ´γδ243εζ were purified using strept-tactin affinity chromatography and size exclusion chromatography. As depicted in figure 47 and figure 48 αββ´γδζ and αββ´γδ243εζ formed complexes and eluted at the expected apparent molecular mass. The stability of the complexes is slightly reduced compared to native heptameric coatomer.

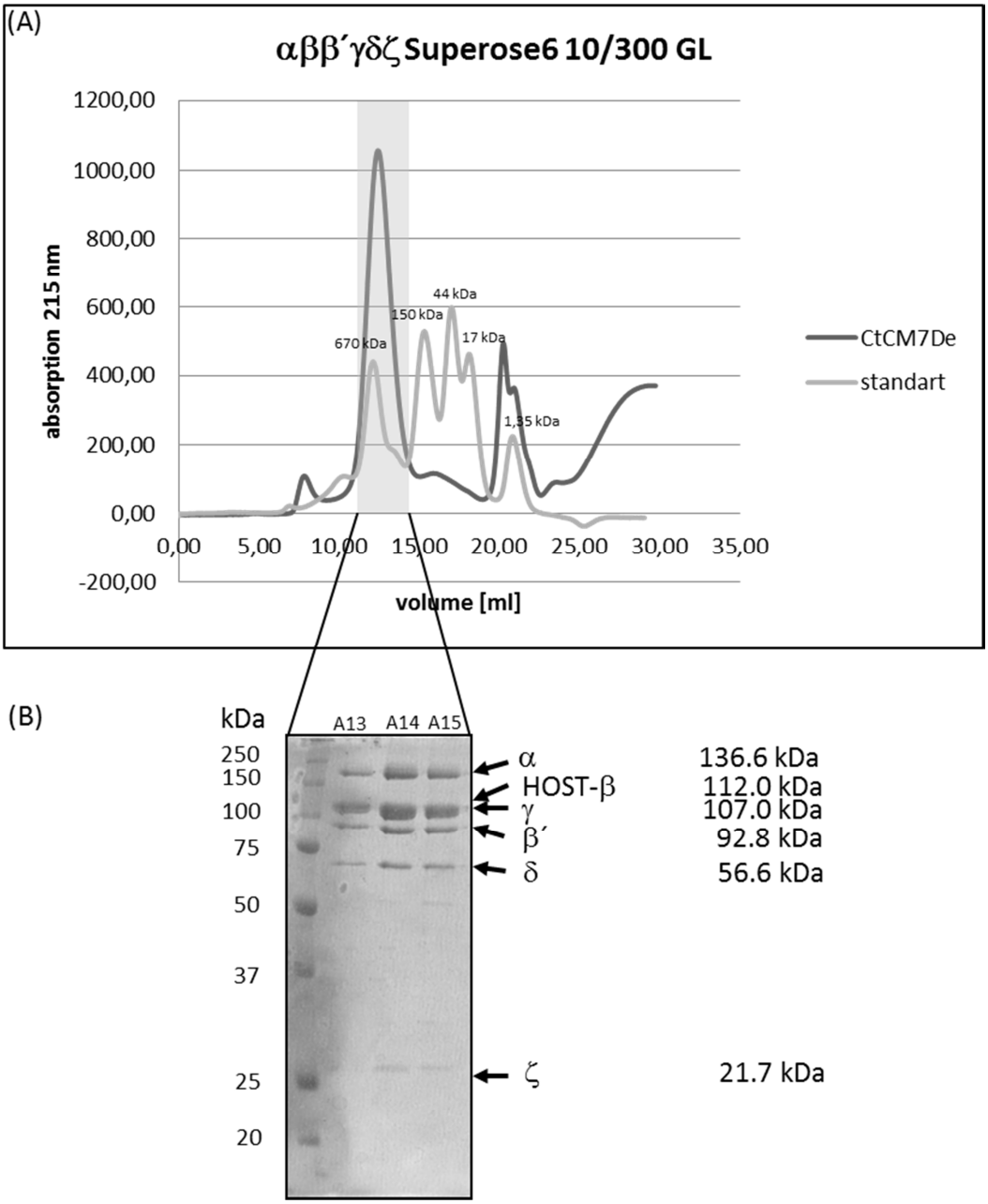

Figure 47: Chromatographic profile of the size exclusion chromatography of the hexameric subcomplex aββ´γδζ

(A): The elution profile of the αββ´γδζ coatomer (dark grey) is overlayed with the elution profile of a protein size standard (light grey). The UV absorption at 215 nm is blotted against the elution volume in ml.

(B): 15 % SDS-PAGE stained with Coomassie. 5 µl of each αββ´γδζ coatomer Superose 6 10/300 GL elution fraction mixed with 3.5 µl 4 x SDS sample buffer was loaded on the gel.

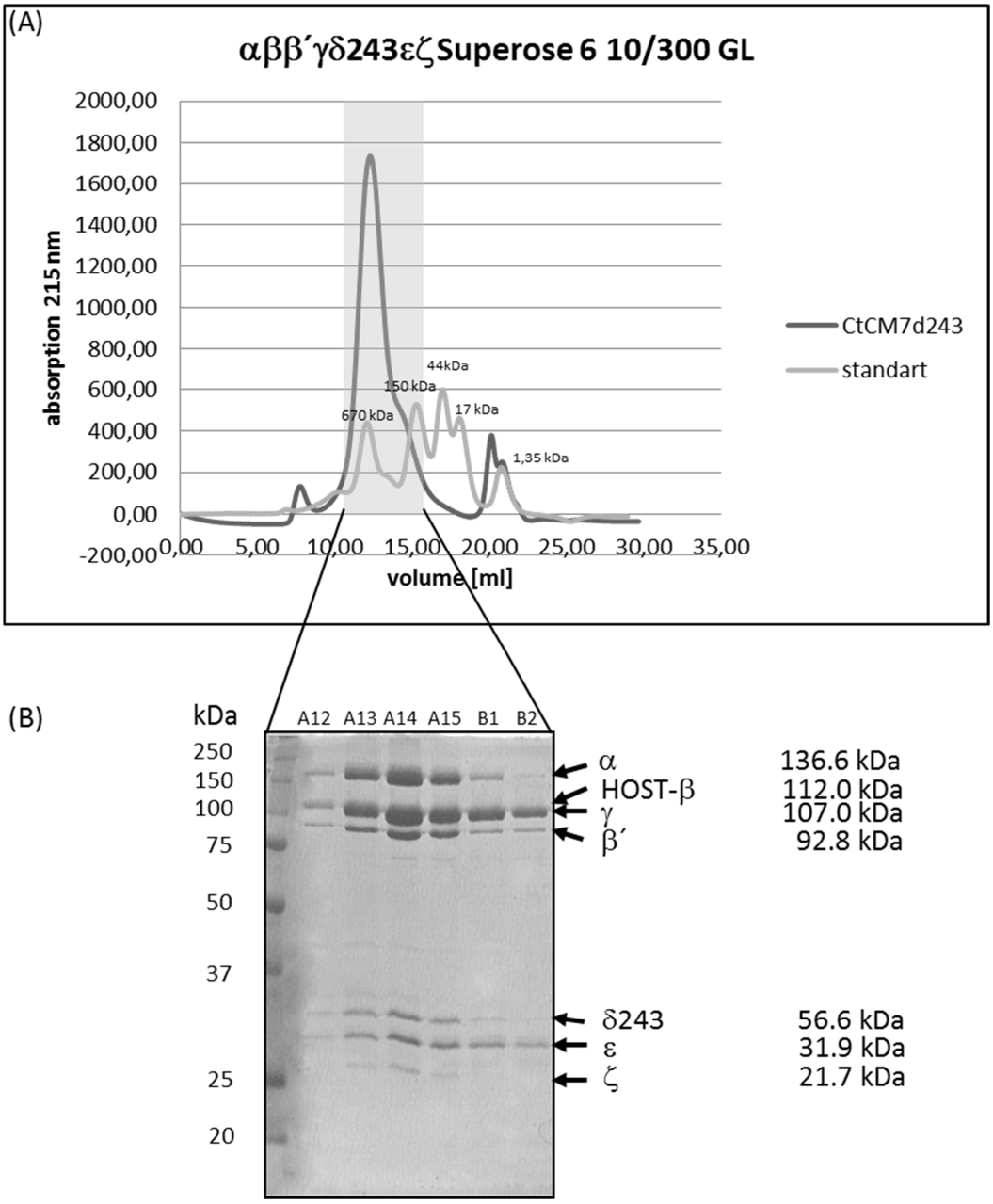

Figure 48: Chromatographic profile of the size exclusion chromatography of the truncated coatomer complex aββ´γδ243εζ

(A): The elution profile of the *Chaetomium thermophilum* αββ´γδ243εζ coatomer (dark grey) is overlayed with the elution profile of a protein size standard (light grey). The UV absorption at 215 nm is blotted against the elution volume in ml.

(B): 15 % SDS-PAGE stained with Coomassie. 5 µl of each αββ´γδ243εζ coatomer Superose 6 10/300 GL elution fraction mixed with 3.5 µl 4 x SDS sample buffer was loaded on the gel.

To test their functionality the ability of both complexes to make vesicles from unilamellar golgi-like liposomes was tested, as described in Materials and Methods. As depicted in figures 49 and 50, both complexes were able to make vesicles.

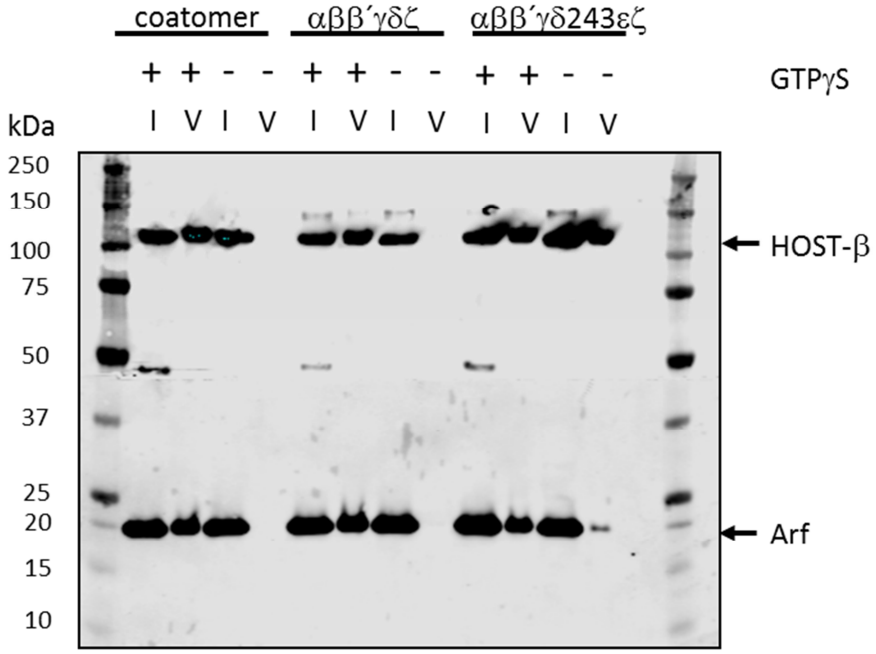

Figure 49: Western-Blot of vesicle formation with coatomer variants lacking ε-COP or the μ-homology domain of δ-COP from golgi-like liposomes. 2 % of the input fraction and 50 % of the vesicle fractions were loaded on the gel. Detection was performed with Anti-HIS antibody and Anti-CtArf antibody.

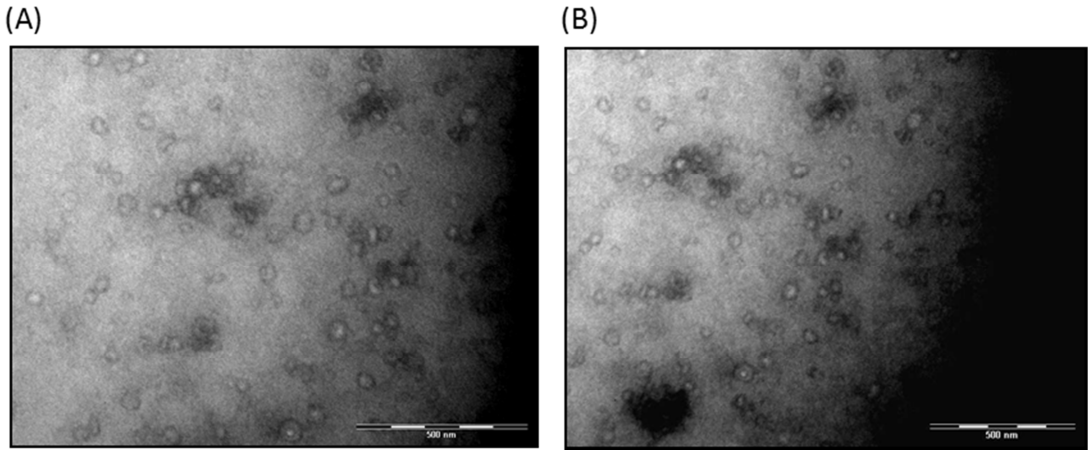

Figure 50: (A): negative stain EM picture of the vesicle fraction obtained with αββ´γδζ coatomer (stained with 3% w/v uranyl acetate). (B): negative stain EM picture of the vesicle fraction obtained with αββ´γδ243εζ coatomer (stained with 3% w/v uranyl acetate)

The vesicles showed the expected size of 70 to 80 nm for COPI vesicles as depicted in figure 50. No difference to COP-vesicles made with complete *Chaetomium thermophilum* coatomer was observed in negative stain electron microscopy.

2.11 Crystallization of *Chaetomium coatomer* subcomplexes

The purified *Chaetomium coatomer* subcomplexes were subjected to crystallization screens. All crystallization experiments were done in the crystallization facility of the BZH (Heidelberg). As initial screens, JCSG 1-4 screens were used for all complexes. Complex α825β´793, complete mouse coatomer CM7$\gamma_1\zeta_1$ and the truncated β686γ66δζ subcomplex did not yield any crystals in all tested conditions. The crystallization screens of all tested subcomplexes are listed in table 3.

Complex	concentration	Temp.	Crystals	Screen
α825β´793	10 mg/ml, 5 mg/ml	4°C	-	JCSG 1-4
α825β´793	12 mg/ml	4°C	-	JCSG 1-4
CM7$\gamma_1\zeta_1$	20 mg/ml, 10 mg/ml	4°C	-	JCSG 1-4
β686γ666δζ	17 mg/ml, 10 mg/ml	4°C	-	JCSG 1-4
β19-391δ	5 mg/ml, 13 mg/ml	4°C, 18°C	+	JCSG 1-4
β19-391δ	5,23 mg/ml	18°C	-	JCSG 1-4
β19-391δ	5 mg/ml, 13 mg/ml	4°C, 18°C	-	finescreen PEG 8000, imidazol
β19-391δ	5 mg/ml, 13 mg/ml	18°C	+	finescreen 16072014
β19-391δ	5 mg/ml, 13 mg/ml	18°C	+	finescreen 23072014
β19-391δ	13 mg/ml	18°C	-	Optimizer
β19-391δ	13 mg/ml	18°C	-	ADDit
β19-391δ	13 mg/ml, 5 mg/ml	18°C	+	PEGs
β19-391δ1-137	16 mg/ml, 8 mg/ml	18°C	+	JCSG 1-4
β19-391δ1-137	16 mg/ml, 8 mg/ml	18°C	+	ClassicsLite

β19-391δ1-137	16 mg/ml, 8 mg/ml	18°C	+	Cryos
β19-391δ1-137	16 mg/ml, 8 mg/ml	18°C	+	MemGold
β19-391δ1-137	16 mg/ml, 8 mg/ml	18°C	-	Cations
β19-391δ1-137	16 mg/ml, 8 mg/ml	18°C	+	Anions
β19-391δ1-137	16 mg/ml, 8 mg/ml	18°C	+	finescreen 151014 PEG4000
β19-391δ1-137	16 mg/ml, 8 mg/ml	18°C	+	finescreen 16104 divers
β19-391δ1-137	16 mg/ml, 8 mg/ml	18°C	+	PEGs
β19-391δ1-137	16 mg/ml, 8 mg/ml	18°C	+	finescreen 151014 pAD5
β19-391δ1-137	16 mg/ml, 8 mg/ml	18°C	-	finescreen 151014 pAD5, magic triangle
β19-391δ1-137	16 mg/ml, 8 mg/ml	18°C	-	finescreen 151014 pAD5, K_2PtCl_4
β19-391δ1-137	16 mg/ml, 8 mg/ml	18°C	-	finescreen 151014 pAD5, $Hg(OAc)_2$
α825Mβ´793	13 mg/ml, 8 mg/ml	18°C	-	JCSG 1-4
β19-391δ1-137 SeMet Baculo	13 mg/ml, 8 mg/ml	18°C	-	finescreen 8181G10
β19-391δ1-137 SeMet Baculo	13 mg/ml, 8 mg/ml	18°C	+	finescreen 270315
β19-391δ1-137 SeMet Baculo	16 mg/ml, 8 mg/ml	18°C	+	finescreen 220415 SeMet
β19-391δ1-137 SeMet Bacteria	13 mg/ml, 9 mg/ml	18°C	+	JCSG 1-4
β19-391δ1-137 SeMet Bacteria	13 mg/ml, 9 mg/ml	18°C	-	finescreen 220415 SeMet

β19-391δ1-137 SeMet Bacteria	13 mg/ml, 9 mg/ml	18°C	-	finescreen 270315
β19-391δ1-137 SeMet Bacteria	13 mg/ml, 9 mg/ml	18°C	-	PEGs
β19-391δ1-137 SeMet Bacteria	13 mg/ml, 9 mg/ml	18°C	-	Cryos
β19-391δ1-137 SeMet Bacteria	13 mg/ml, 8 mg/ml	18°C	-	finescreen pad-semet 140715
β19-391δ1-137 SeMet Bacteria	13 mg/ml, 8 mg/ml	18°C	+	finescreen 9165_E11.2_refine
β19-391δ1-137 SeMet Bacteria	13 mg/ml, 8 mg/ml	18°C	-	JCSG+
β19-391δ1-137 SeMet Bacteria	13 mg/ml, 8 mg/ml	18°C	-	Index
OSTβ19-391-HTδ1-137 SeMet Bacteria	8 mg/ml	18°C	-	PEGs
HTβ19-391-HTδ1-137 SeMet Bacteria	13 mg/ml, 8 mg/ml	18°C	-	JCSG 1-4
HTβ19-391-HTδ1-137 SeMet Bacteria	13 mg/ml, 8 mg/ml	18°C	-	PEGs
HTβ19-391-HTδ1-137 SeMet Bacteria	13 mg/ml, 8 mg/ml	18°C	-	JCSG+
β19-391δ SeMet Bacteria	20 mg/ml, 13 mg/ml	18°C	-	JCSG 1-4
β19-391δ SeMet Bacteria	20 mg/ml, 13 mg/ml	18°C	-	JCSG+
β19-391δ SeMet	20 mg/ml, 13 mg/ml	18°C	-	ClassicsLite

Bacteria				
β19-391δ SeMet Bacteria	20 mg/ml, 13 mg/ml	18°C	-	PEGs
β19-391δ SeMet Bacteria	20 mg/ml, 13 mg/ml	18°C	-	Mem-Gold
β19-391δ SeMet Bacteria	20 mg/ml, 13 mg/ml	18°C	-	MemStart + MemSys
β19-391δ SeMet Bacteria	20 mg/ml, 13 mg/ml	18°C	-	Cryos
β19-391δ1-175 SeMet Baculo	13 mg/ml	18°C	+	JCSG 1-4
β19-391δ1-175 SeMet Baculo	13 mg/ml	18°C	+	JCSG+

Table 3: Crystals screens of *Chaetomium thermophilum* coatomer subcomplexes

The complex β19-391δ was tested at a concentration of 5 mg/ml and 13 mg/ml at 4°C and 18°C in the initial JCSG 1-4 screens. Crystals (figure 51) grew after 13 days at several PEG related conditions, which are listed in table 4. For refinement of the crystallization conditions additional Optimizer-, ADDit- and PEG-screens as well as three specifically designed finescreens were tested. The crystals were isolated by Dr. Andrea Gumiero (BZH, Heidelberg) and shock-frozen in liquid nitrogen. Measurement of the crystals was performed at the synchrotron in Grenoble France. The measured crystals diffracted up to a resolution of 2.7 Å and had the space group of C2221.

screen	condition
JCSG 1	0.2 M lithium nitrate, 20 % w/v PEG 3350
JCSG 1	0.2 M sodium thiocyanate, 20 % w/v PEG 3350
JCSG 1	0.2 M magnesium formiate, 20 % w/v PEG 3350
JCSG 1	0.2 M magnesium chloride, 20 % w/v PEG 3350
JCSG 2	0.1 M Tris pH 7, 20 % w/v PEG 1000
JCSG 2	0.1 M HEPES pH 7, 10 % w/v PEG 6000
JCSG 2	0.2 M potassium sulfate, 20 % w/v PEG 3350

Table 4: Initial crystallization conditions of β19-391δ

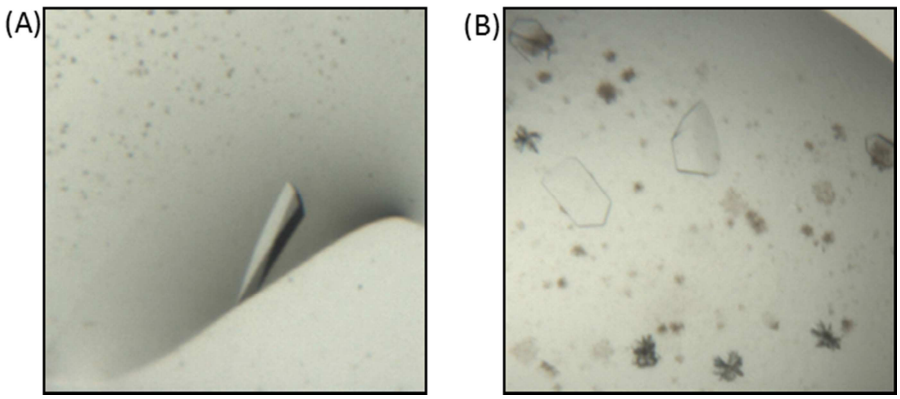

Figure 51: Crystals of the dimeric subcomplex β19-391δ

Depicted crystals grew at the conditions: (A) 0.1 M sodium acetate pH 4,6, 40 % v/v PEG 200; (B) 0.2 M calcium chloride, 15 % w/v PEG 3350.

In parallel to the crystal measurement some of the less suitable crystals were dissolved and analyzed using SDS-PAGE.

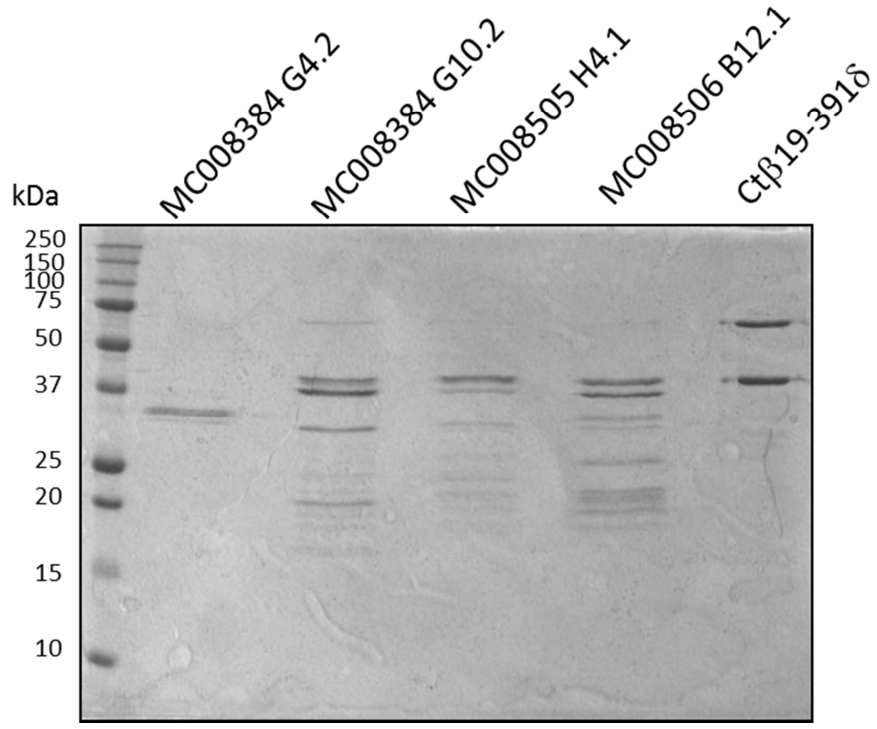

Figure 52: Dissolved crystals of the dimeric subcomplex β19-391δ

15 % SDS-PAGE stained with Coomassie. Dissolved crystals of the conditions 0.2 M Calcium acetate, 20 % w/v PEG 3350; 0.2 M potassium sulfate, 20% w/v PEG 3350; 0.3 M magnesium sulfate, 20% w/v PEG 3350; 0.1 M Tris, 0.2 M $MgCl_2$, 16% w/v PEG 8000, pH 7.0 were loaded on the gel.

As depicted in figure 52, the SDS-Page showed that the crystals had not incorporated the full-length δ-subunit, which was partially degraded in the crystal. From the measured crystals several datasets were obtained from which the best had a resolution of 2.7 Å. The datasets were processed by Dr. Jürgen Kopp (BZH, Heidelberg), but the structure could not be solved using molecular replacement. Because of the degradation modified constructs with truncated parts of the δ-subunit were tested in crystal screens.

The complex β19-391δ1-137 was tested at a concentration of 8 mg/ml and 16 mg/ml at 18°C in the initial JCSG 1-4 screens. First Crystals (figure 53) grew already after 21 hours again at several PEG-containing conditions (table 5). For refinement of the crystallization conditions additional ClassicsLite, Cryos, MemGold, Cations, Anions and PEG-screens as well as three specifically designed finescreens were tested. The crystals were isolated by Dr. Andrea

Gumiero (BZH, Heidelberg) and shock-frozen in liquid nitrogen. Measurement of the crystals was performed at the synchrotron in Grenoble, France. The measured crystals diffracted up to a resolution of 2.4 Å and had the space group of C2221.

screen	condition
JCSG 1	0.2 M potassium citrate, 25 % w/v PEG 3350
JCSG 1	0.2 M sodium chloride, 10 % w/v PEG 8000, 0.1 M sodium potassium phosphate pH 6.2
JCSG 1	0.2 M MES pH 6.0, 0.2 calcium acetate, 20 % w/v PEG 8000
JCSG 1	0.2 M ammonium sulfate, 20 % w/v PEG 3350
JCSG 1	0.2 M magnesium formate, 20 % w/v PEG 3350
JCSG 1	0.2 M magnesium chloride, 20 % w/v PEG 3350
JCSG 1	0.1 M sodium citrate, 20 % w/v PEG 3350
JCSG 1	0.18 M tri ammonium citrate pH 7.0, 20 % w/v PEG 3350
JCSG 1	0.2 M magnesium acetate, 20 % w/v PEG 3350
JCSG 1	0.2 M di-sodium tartrate, 20 % w/v PEG 3350
JCSG 1	0.2 M calcium acetate, 20 % w/v PEG 3350
JCSG 1	0.2 M sodium potassium tartrate, 20 % w/v PEG 3350
JCSG 1	0.2 M calcium acetate, 0.1 M Tris pH 7.0, 20 % w/v PEG 3000
JCSG 1	0.2 M potassium thiocyanate, 20 % w/v PEG 3350
JCSG 1	0.2 M di-ammonium tartrate, 20 % w/v PEG 3350
JCSG 2	0.18 M tri-ammonium citrate pH 7.0, 20 % w/v PEG 3350
JCSG2	0.085 M HEPES pH 7.5, 8.5 % v/v 2-propanol, 0.17 w/v PEG 4000,

	15 % v/v glycerol
JCSG 2	0.1 M Tris pH 7.0, 20 % w/v PEG 1000
JCSG 2	0.2 M lithium sulfate, 20 % w/v PEG 3350
JCSG 2	0.1 M sodium potassium phosphate pH 6.2, 0.2 M sodium chloride, 20 % w/v PEG 1000
JCSG 2	0.2 M potassium sulfate, 20 % w/v PEG 3350
JCSG 2	1 M lithium chloride, 0.1 M MES pH 6.0, 20 % w/v PEG 6000
JCSG 3	0.2 M di-sodium hydrogen phosphate, 20 % w/v PEG 3350
JCSG 3	0.1 M sodium chloride, 0.1 M HEPES pH 7.5, 1,6 M ammonium sulfate
JCSG 3	1 M lithium chloride, 20 % w/v PEG 6000, 0.1 M HEPES pH 7.0
JCSG 3	0.16 M magnesium acetate, 16 % w/v PEG 8000, 0.08 M sodium cacodylate pH 6.5, 20 % w/v glycerol
JCSG 3	0.2 M calcium chloride, 20 % w/v PEG 3350
JCSG 3	0.17 M ammonium acetate, 25.5 % w/v PEG 4000, 0.085 M sodium citrate pH 5.6, 15 % v/v glycerol
JCSG 3	0.2 M calcium chloride, 20 % w/v PEG 3350
JCSG 4	0.1 M lithium chloride, 0.1 M HEPES pH 7.0

Table 5: Crystallization conditions of the dimeric subcomplex β19-391δ1-137

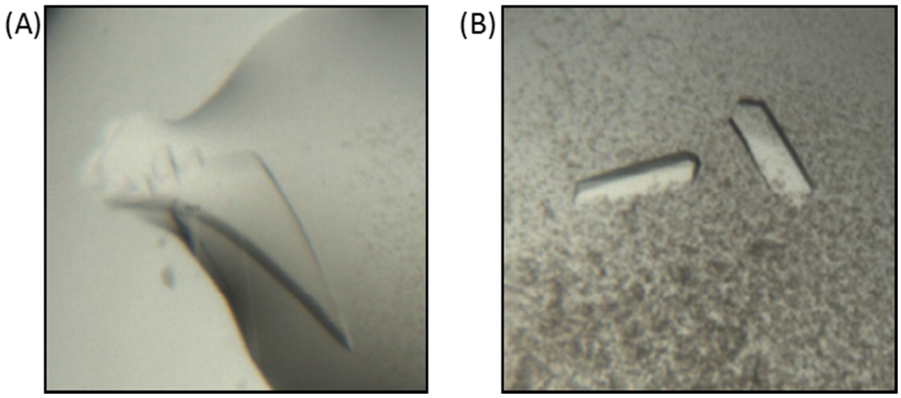

Figure 53: Crystals of the dimeric subcomplex β19-391δ1-137

Depicted crystals grew at the conditions: (A) 0.2 M ammonium sulfate, 0.1 M sodium cacodylate pH 6,5, 15 % w/v PEG 8000; (B) 0.16 M magnesium acetate, 0.08 M sodium cacodylate pH 6.5, 16 % w/v PEG 8000, 20 % v/v glycerol

Also for β19-391δ1-137 some of the less suitable crystals were dissolved and analyzed using SDS-PAGE.

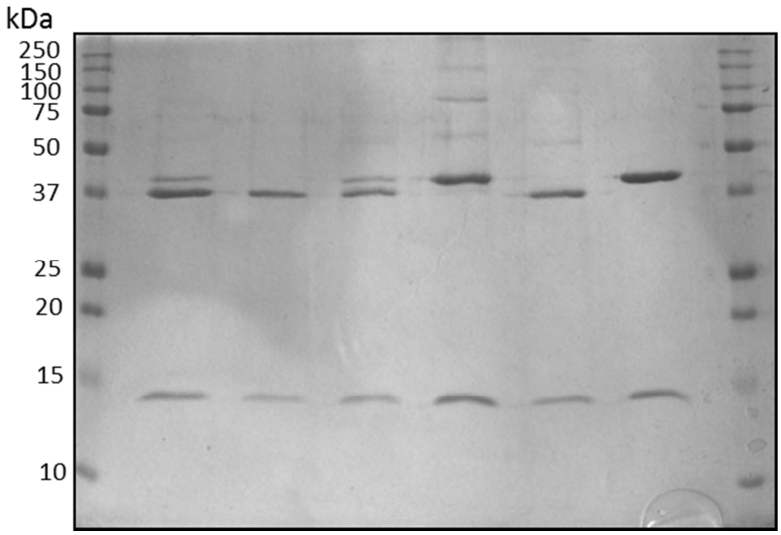

Figure 54: Dissolved crystals of the dimeric subcomplex β19-391δ1-137

15 % SDS-PAGE stained with Coomassie. Dissolved crystals of the conditions 0.2 M Na_2HPO_4, 20 % w/v PEG 3350; 0.1 M Sodium-cacodylate, 14.5 % w/v PEG 4000, 0.4 M Ammoniumacetate pH 5.6; 4M ammoniumsulfate, 40 % w/v PEG 8000 1M sodium-cacodylate pH 6.5 were loaded on the gel.

As depicted in figure 54, SDS-Page showed that the crystals this time had incorporated the full-length δ1-137-subunit. The degradation of Ctβ19-391, which was observed in the SDS-

PAGE, only affected the amino terminal HOST-TAG of Ctβ19-391 as confirmed by mass spectrometry. From the measured crystals several datasets were obtained from which the best had a resolution of 2.4 Å. The datasets were processed by Dr. Jürgen Kopp (BZH Heidelberg), but the structure could not be solved using molecular replacement with all search models available. Because of this, soaking of crystals with heavy metals, as well as seleno-methionine labelling to obtain additional phase information was tried. Crystallization with incorporation of heavy metals did not yield any crystals. Therefore this approach was discontinued.

2.12 Seleno-methionine labelling of Ctβ19-391δ1-137 in bacteria

Seleno-methionine labelling of β19-391δ1-137 was first performed in a bacterial expression system, as a more efficient labelling can be achieved in bacteria compared to the Baculo-virus expression system. Therefor both truncated subunits were cloned in the bi-cistronic expression vector pET-DUET (Novagen) and expressed *in E.coli* BL21 DE3 cells. The expression was successful. Fusion of an affinity TAG to only one of the subunits resulted in a not stoichiometric expression of both subunits. To overcome this, two different constructs were designed, one with a HIS_6-TAG fused to the N-terminus of both subunits and one with a OneStrep-Tag fused to the N-terminus of β19-391 and a HIS_6-TAG fused to the N-terminus of δ1-137. The complex was purified by Ni-NTA / Strep-Tactin affinity purification and size-exclusion chromatography as depicted in figure 55.

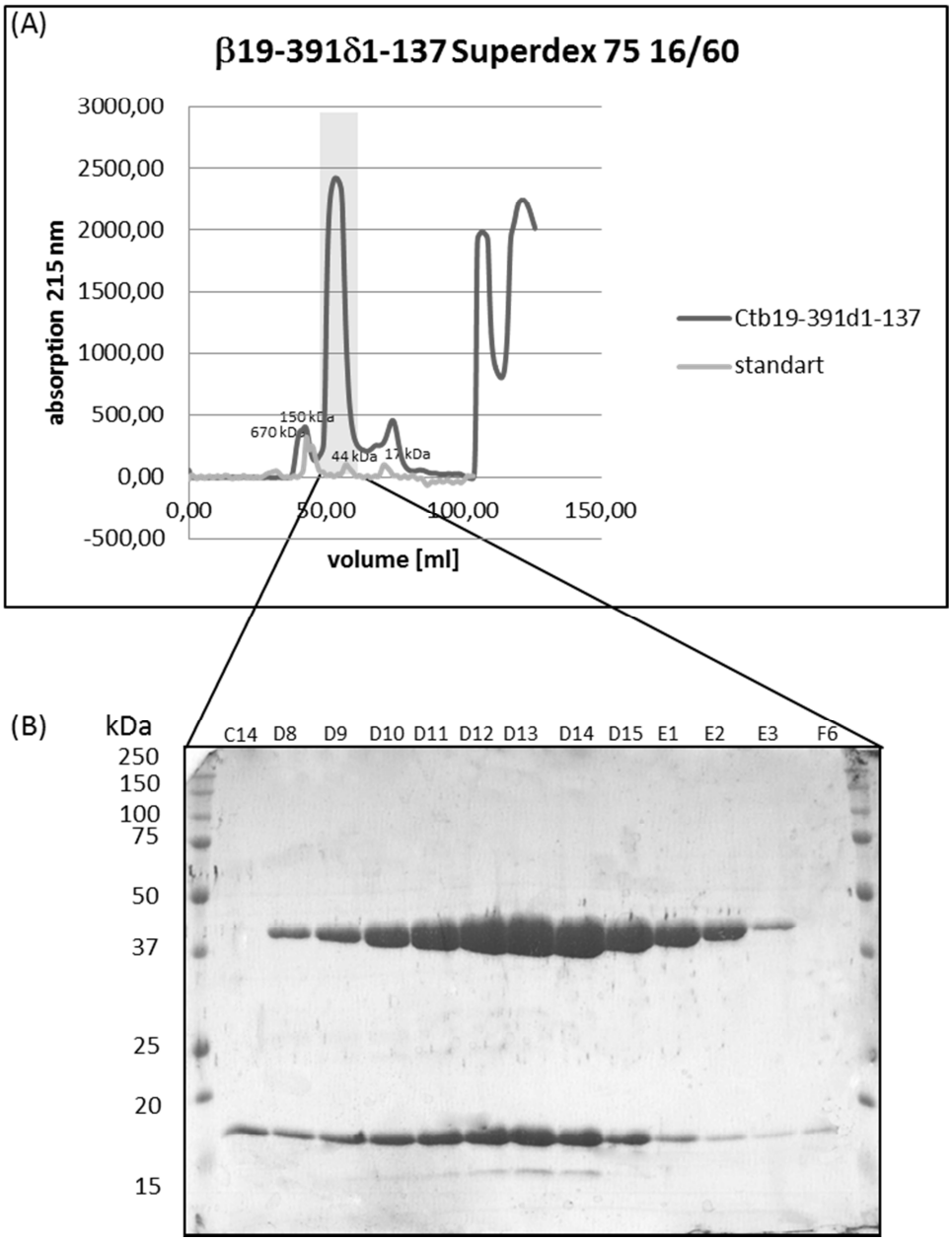

Figure 55: Chromatographic profile of the size exclusion chromatography of the dimeric subcomplex β19-391δ1-137

(A): The elution profile of the truncated coatomer βδ-subcomplex (dark grey) is overlayed with the elution profile of a protein size standard (light grey). The UV absorption at 215 nm is blotted against the elution volume in ml.

(B): 15 % SDS-PAGE stained with Coomassie. 5 µl of each coatomer dimer Superdex 75 16/60 elution fraction mixed with 3.5 µl 4 x SDS sample buffer was loaded on the gel.

The β19-391δ1-137 complex expressed in *E. coli* labelled with seleno-methionine produced only very few crystals of bad quality in the crystal screens. These crystals were not sufficient

for data acquisition to obtain phase information. Therefore seleno-methionin labelling was continued in the Baculo-virus expression system.

2.13 Seleno-methionine labelling of Ctβ19-391δ1-175 in insect cells

For seleno-methionine labelling in insect cells the complex β19-391δ1-175 was used, since the N-terminal part of the linker region of Ctδ was of particular interest. The seleno-methionine labeled complex behaved as the native complex during expression and purification. Crystals started to grow after 19 hrs at several conditions containing PEG (figure 56).

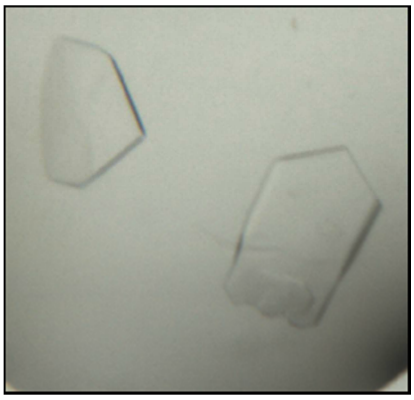

Figure 56: Crystals of Seleno-methionine labeled dimeric subcomplex β19-391δ1-175

Depicted crystals grew: 0.2 M magnesium chloride, 0.1 M Tris pH 7, 10 % w/v PEG 8000

2.14 Structure of β18-389δ2-151

The structure of β18-389δ2-151 was solved by Dr. Jürgen Kopp (BZH, Heidelberg). Analysis of the datasets obtained from seleno-methionine labelled crystals of β19-391δ1-175 revealed signals for 8 out of a total of 9 seleno-methionine sites within the complex. Structure determination showed the orthorhombic space group of C222(1) as determined previously for the native datasets and a resolution of 2.57 Å. Initial building of the structure was done in the seleno-methionine datasets. For later refining of the structure also the native datasets recorded earlier were used. Datasets showed clear electron-density for residues 18-389 of

Ctβ-COP and for residues 2-151 of Ctδ-COP. For the later residues of the Ctδ subunit 152-175, which were incorporated in the protein, no electron density was visible to build the structure. Crystallographic data regarding the structure are listed in table 6.

Crystallographic data Ctβ19-389δ2-151	
Space group	C222(1)
resolution	2.57 Å
R	18.21
R_{free}	22.74

Table 6: Crystallographic data of β18-389δ2-151

The overall structure of β18-389δ2-151 is composed of the curved β18-389 subunit, which adopts a α-solenoid fold consisting of 20 pairwise packed α-helices and the δ2-151 subunit with a longin-like fold. The α-solenoid-fold of β18-389 is forming a right-handed arch around the δ2-151 subunits, which adopts a classic longin α-β-α sandwich-fold consisting of a 5 stranded antiparallel β-sheet and 5 α-helices. Helices 1-4 of δ2-151 are part of the longin-like fold, whereas helix 5 is already part of the linker, which forms the connection to the C-terminal μ-homology domain of δ-COP. Apart from helix 5 the fold of δ2-151 closely resembles the fold of the ζ-COP subunit and the longin fold of the σ-adpatin subunit of AP2 (figure 57).

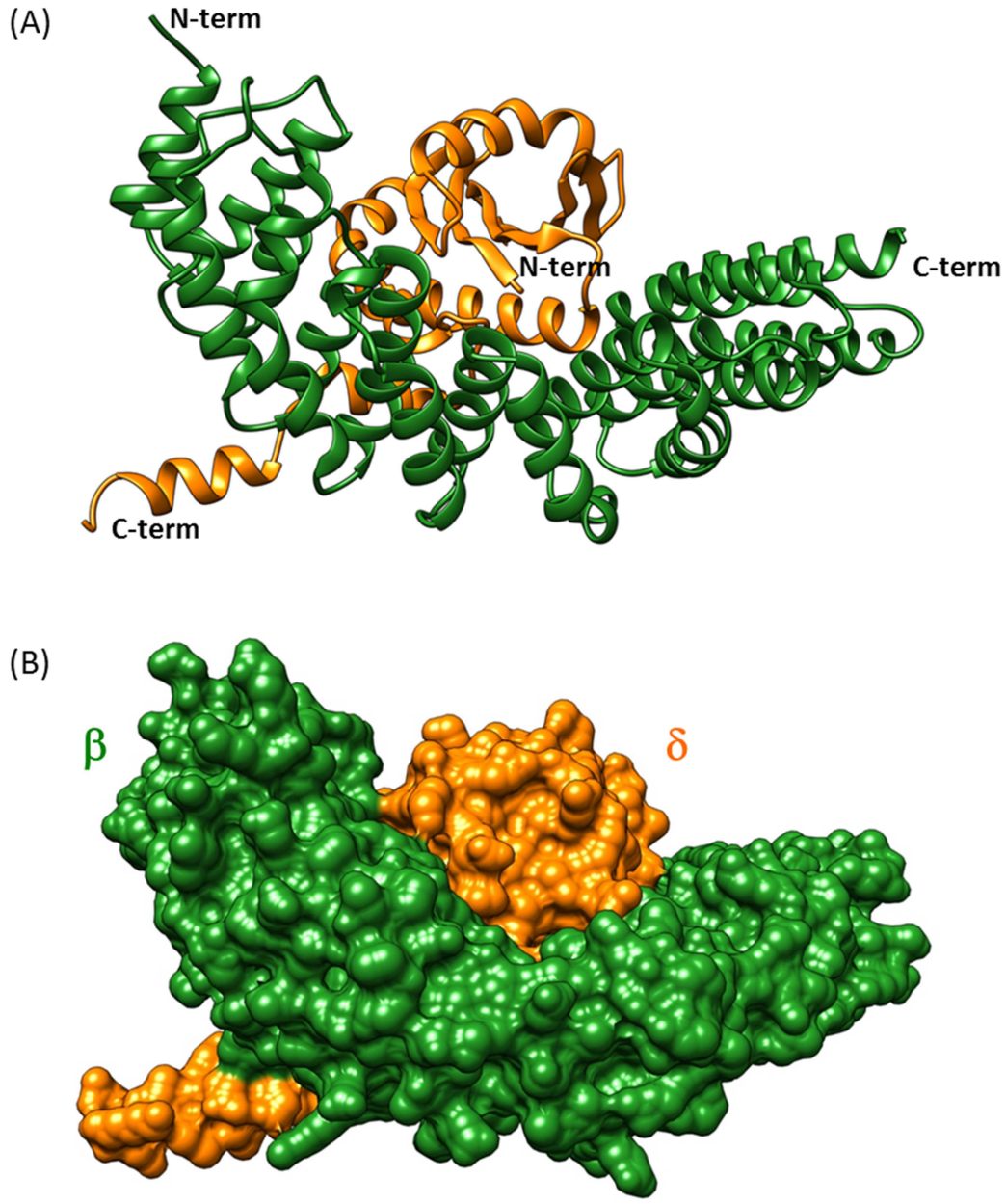

Figure 57: Structure of β18-389δ2-151 (top view)

(A): Structure of β18-389δ2-151 backbone representation; (B): Structure of β18-389δ2-151 surface representation

The dimensions of the complete structure are approximately 86 Å in the longest axis (x-Axis), 56 Å in the second axis (y-axis) and 48 Å the third axis (z-axis). β18-389 alone also extends 86 Å in its longest axis (x-axis), around 20 Å in the second axis (y-axis) and around 32 Å in the third axis (z-axis). Following the curvature of the α-solenoid of β18-389 a distance of 112 Å is covered (figure 58).

The longin-like domain of δ2-151 adopts, as expected, a very compact fold, which has a dimension of around 30 Å in all 3 axis not covering helix 5, which protrudes in the linker.

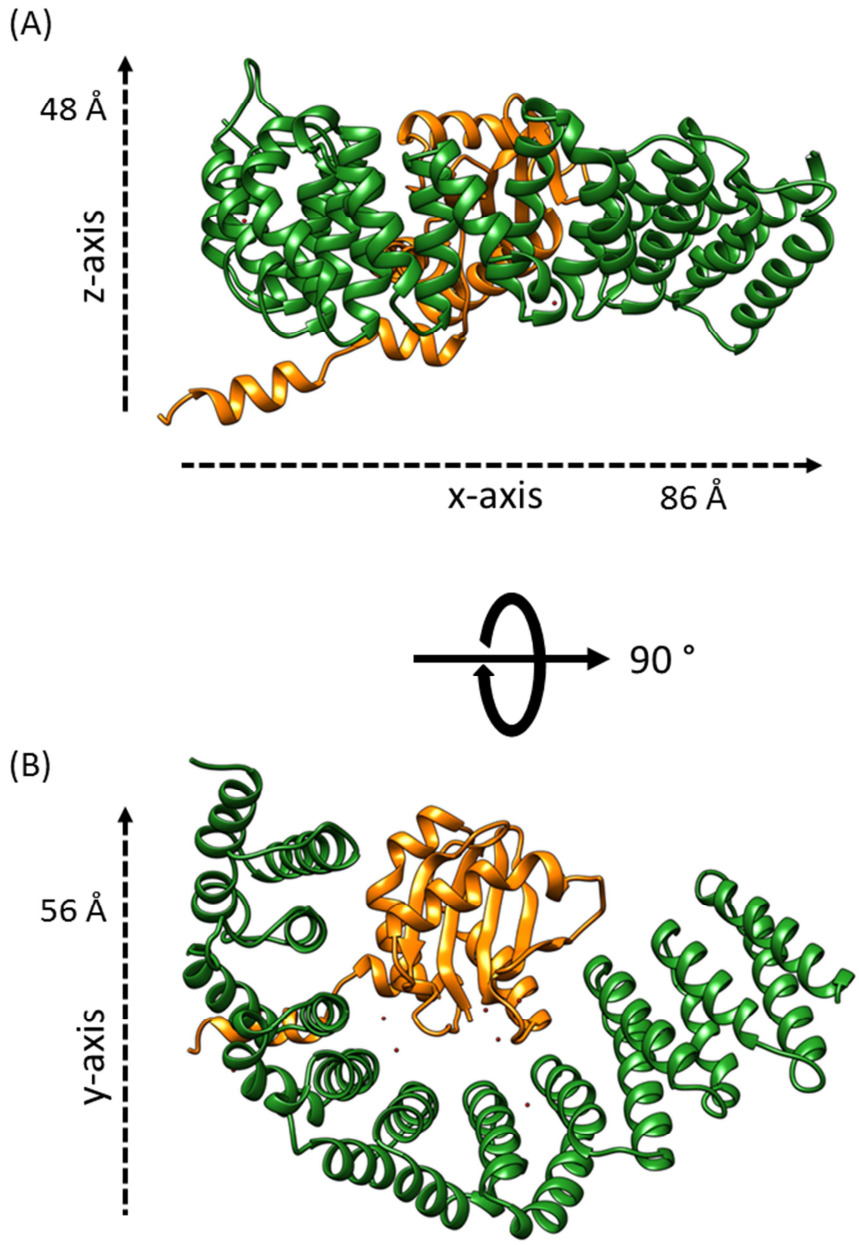

Figure 58: Dimensions of β18-389δ2-151

(A): Dimensions of β18-389δ2-151 side view; (B): Dimensions of β18-389δ2-151 top view

The structure incorporates 7 water molecules. Both subunits are connected by a large interface, which involves hydrophobic and polar interactions. The interacting residues are

part of helices 2, 4, 6, 8, 10, 12, 14 and 16 of β18-389 and helices 2, 3, 4 and 5 of δ2-151. Also the loops connecting helices 3 and 4 and 4 and 5 of δ2-151 are providing residues for the subunit interface as depicted in figure 59.

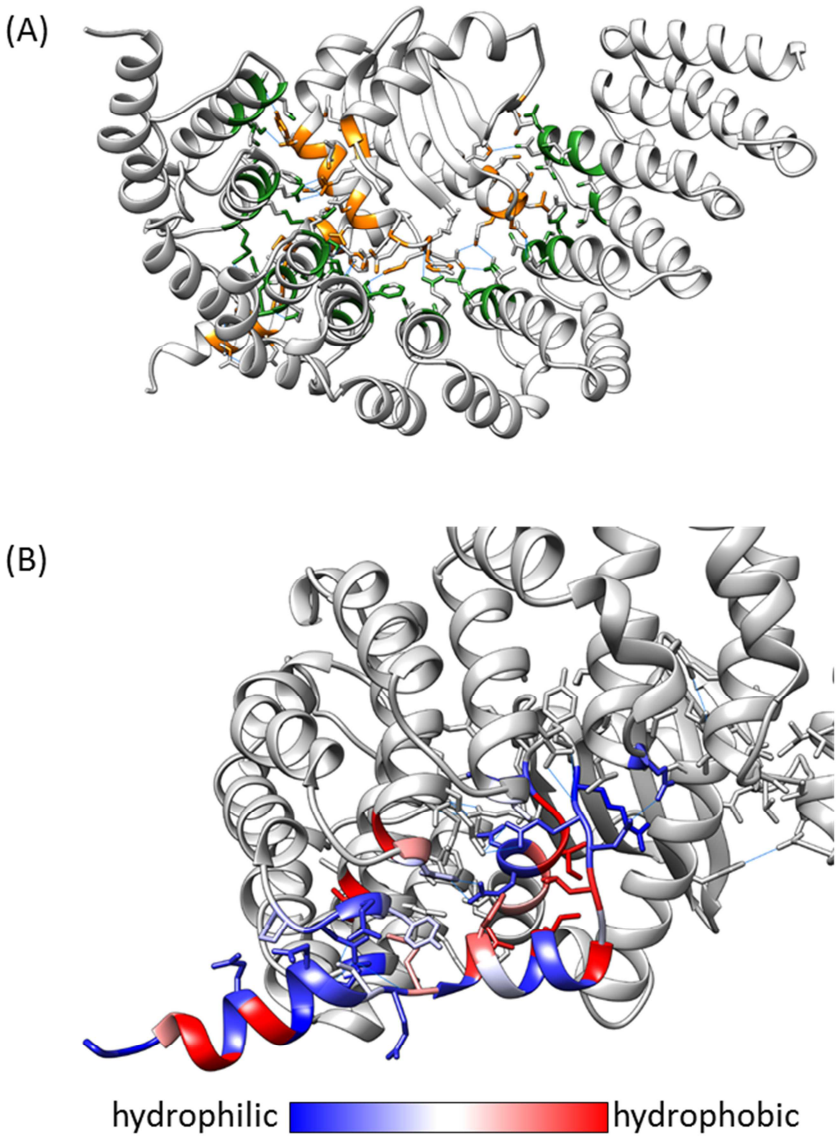

Figure 59: subunit interface of β18-389δ2-151

(A): residue contacts making up the interface of β18-389δ2-151, (B): residue contacts of helices 4 and 5 of δ2-151

The most interesting part of the structure is composed of the helices 4 and 5 of the δ2-151 subunit. As depicted in figure 57 these helices, which are the start of the linker region of δ, show that the linker is passing below the α-solenoid of the β subunit. The contacts, which are made by helix 4 of δ are mostly hydrophobic, whereas the contacts made by helix 5 are mostly hydrophilic, indicating a flexibility in the linker, which is starting at helix 5 (figure 59). However the passing of the linker of δ below the β subunit is already defined by helix 4 of δ, which forms stable hydrophobic interactions. As depicted in figure 60 helix 5 of δ2-151 is stabilized by pairing with helix 5 of another δ2-151 subunit within the crystal, forming parts of the crystal contacts.

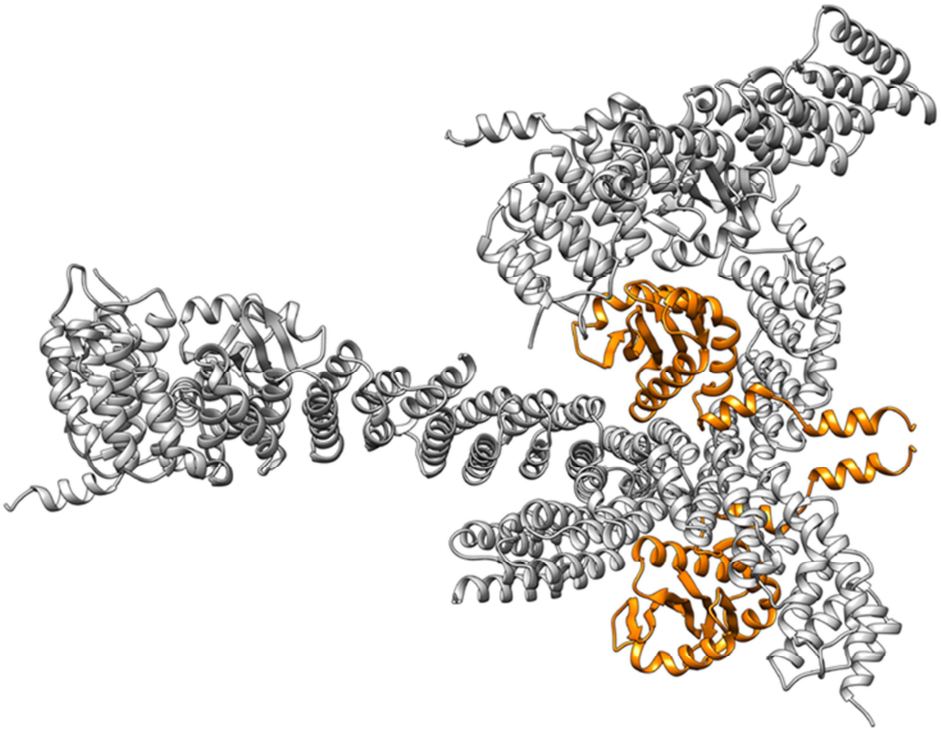

Figure 60: Crystal contacts of β18-389δ2-151

Helix 5 of δ2-151 is passing below the α-solenoid of β-COP near the postulated Arf-binding site on β (Yu et al., 2012). As Arf binding to the amino terminal part of δ-COP has been reported previously (Sun et al., 2007) this makes implications for a potential function of this helix in Arf binding, which was further investigated.

2.15 Co-Crystallization of *Chaetomium coatomer* subcomplexes with NΔ20CtArf

As the small GTPase Arf is reported to bind to several subunits within coatomer *Chaetomium* coatomer subcomplexes were tested in co-crystallization experiments with soluble NΔ20Arf in its GTP loaded state (Table 7).

Complex	concentration	Temp.	Crystals	Screen
β686γ666δζ+ NΔ20ArfGMPPNP	20 mg/ml, 10 mg/ml	4°C	-	JCSG 1-4
β686γ666δζ+ NΔ20ArfGMPPNP	20 mg/ml, 10 mg/ml	4°C	-	ClassicsLite
β686γ666δζ+ NΔ20ArfGMPPNP	20 mg/ml, 10 mg/ml	4°C	-	Cryos
β686γ666δζ+ NΔ20ArfGMPPNP	30 mg/ml, 20 mg/ml	18°C	-	JCSG 1-4
β686δ+ NΔ20ArfQ74LGTP	22 mg/ml, 15 mg/ml	18°C	-	JCSG 1-4
β19-391δ+ NΔ20ArfQ74LGTP	15 mg/ml, 7,5 mg/ml	18°C	-	JCSG 1-4
β19-391δ+ NΔ20ArfQ74LGTP	20 mg/ml, 7,5 mg/ml	18°C	+	JCSG 1-4
β19-391δ+ NΔ20ArfQ74LGTP	20 mg/ml, 7,5 mg/ml	18°C	+	PEGs

β19-391δ+ NΔ20ArfQ74LGTP	20 mg/ml, 7,5 mg/ml	18°C	-	$AmSO_4$
β19-391δ+ NΔ20ArfQ74LGTP	20 mg/ml, 13 mg/ml 7,5 mg/ml	18°C	+	finescreen 190814
β19-391δ+ NΔ20ArfQ74LGTP	20 mg/ml, 13 mg/ml 7,5 mg/ml	18°C	+	PEGs
β19-391δ+ NΔ20ArfQ74LGTP	20 mg/ml, 13 mg/ml, 7,5 mg/ml	18°C	+	Index
β19-391δ1-137+ NΔ20ArfQ74LGTP	15 mg/ml, 10 mg/ml	18°C	-	JCSG 1-4
β19-391δ1-137+ NΔ20ArfQ74LGTP	15 mg/ml, 10 mg/ml	18°C	-	JCSG+
β19-391δ1-137+ NΔ20ArfQ74LGTP	15 mg/ml, 10 mg/ml	18°C	-	PEGs
β19-391δ1-137+ NΔ20ArfQ74LGTP	22 mg/ml, 13 mg/ml	18°C	-	JCSG 1-4
β19-391δ1-137+ NΔ20ArfQ74LGTP	22 mg/ml, 13 mg/ml	18°C	-	JCSG +
β19-391δ1-137+ NΔ20ArfQ74LGTP	30 mg/ml, 25 mg/ml	18°C	+	JCSG 1-4
β19-391δ1-137+ NΔ20ArfQ74LGTP	30 mg/ml, 25 mg/ml	18°C	+	JCSG+

β19-391δ1-137+ NΔ20ArfQ74LGTP	30 mg/ml, 25 mg/ml	18°C	+	PEGs
β19-391δ1-175+ NΔ20ArfQ74LGTP	18 mg/ml, 7 mg/ml	18°C	+	Mem-Gold
β19-391δ1-175+ NΔ20ArfQ74LGTP	18 mg/ml, 7 mg/ml	18°C	+	ClassicsLite
β19-391δ1-175+ NΔ20ArfQ74LGTP	18 mg/ml, 7 mg/ml	18°C	+	PEGs
β19-391δ1-175+ NΔ20ArfQ74LGTP	18 mg/ml, 7 mg/ml	18°C	+	JCSG+
β19-391δ1-175+ NΔ20ArfQ74LGTP	18 mg/ml, 7 mg/ml	18°C	+	MemStart + MemSys
β19-391δ1-175+ NΔ20ArfQ74LGTP	18 mg/ml, 7 mg/ml	18°C	-	Anions
β19-391δ1-175+ NΔ20ArfQ74LGTP	18 mg/ml, 7 mg/ml	18°C	-	Cations

Table 7: Co-crystallizations screens

Crystals were obtained at several conditions in trials to crystallize NΔ20Arf with the subcomplexes β19-391δ, β19-391δ1-137 and β19-391δ1-175. Several crystals were measured and datasets were acquired. However all measured crystals had the same space group of C222(1) as the crystals of the isolated subcomplexes, indicating that NΔ20Arf was not incorporated in the crystal. In the last co-crystallization of β19391δ1-175 with NΔ20Arf

the acquired datasets showed for the first time a signal for Arf. However the electron density was not buildable, indicating only partial incorporation of Arf.

2.16 Site directed UV-Crosslink βδ subcomplexes with ArfY167Bp

To investigate the interaction of Arf with beta/delta COP, an Arf variant incorporating a photolabile amino acid in position 167 was used. It was shown before that position 167 of Arf can crosslink to δ-COP using coatomer. As shown in figure 61, the subcomplex β19-391δ could crosslink to ArfY167Bp on golgi-like liposomes. In SDS-PAGE the apparent size of the crosslink product corresponded to Arf and δ-COP linked covalently (78.3 kDa). The product could be detected with an antibody directed against Arf. No antibodies against δ-COP of *Chaetomium thermohilum* were available but the observed crosslink product migrates with the same apparent mass as does a crosslink product, obtained using the same Arf and complete mouse coatomer. This crosslink product could be detected both with an antibody directed against Arf and an antibody against mose δ-COP. The crosslink product was analysed by mass spectrometry to identify the peptide containing the crosslinking position in δ-COP, but a crosslinked peptide could unfortunately not be found. The complex β19-391δ1-243 did not produce a crosslink product under these conditions.

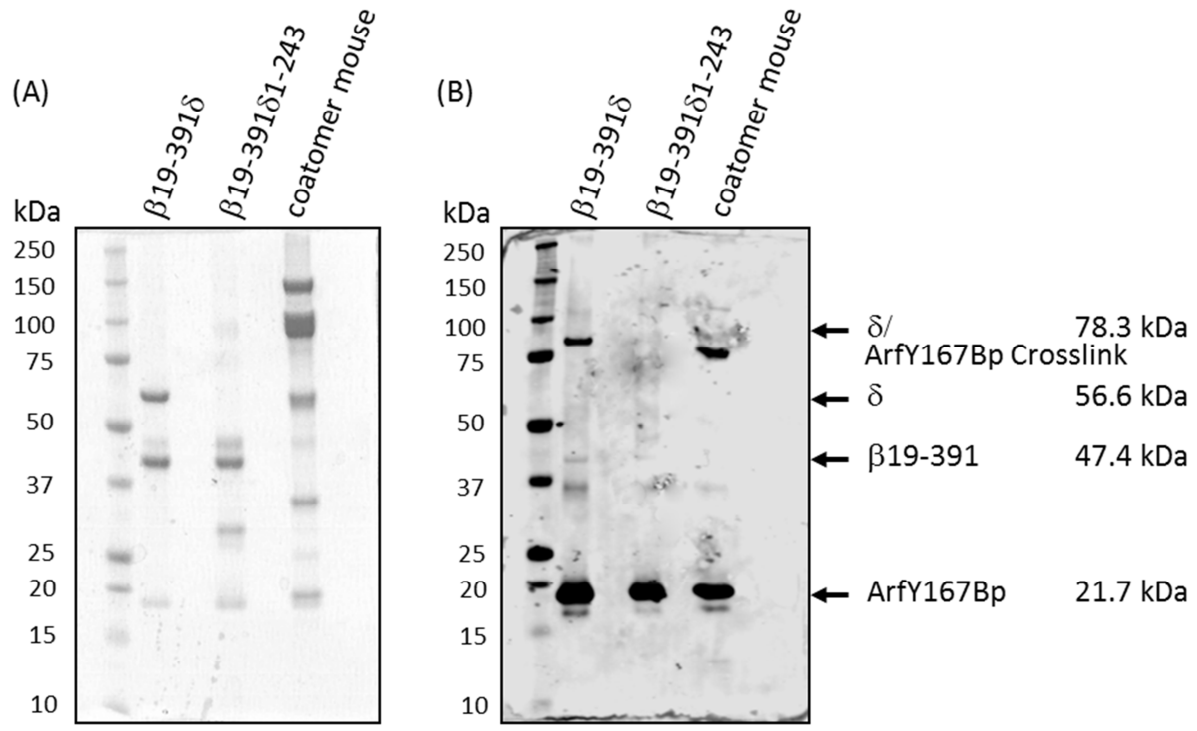

Figure 61: UV-Crosslink βδ-subcomplexes with ArfY167Bp

(A): 4%-12% Bis-Tris Gel stained with colloidal Coomassie 10 µl of the sample mixed with 3.5 µl 4 x sample buffer was loaded on the gel.

(B): Western-Blot Crosslink products detected with Anti-Arf antibody.

2.17 Binding of NΔ20Arf with βδ subcomplexes

To further investigate the binding of Arf to beta/delta COP and especially the binding to δ-COP, pulldown experiments with subcomplexes incorporating different parts of δ-COP and NΔ20Arf in its GTP loaded state were perfomed. As the binding site of Arf to delta-COP was assumed to be in the linker region of δ-COP, subcomplexes incorporating the same part of β-COP (β19-391) and different parts of δ-COP (δ1-137, δ1-175, δ1-243, δ) were used. The subcomplex β19-391δ1-137 does not contain the linker region of δ-COP, whereas the subcomplexes β19-391δ1-175 and δ1-243 comprise the first two, respective the third predicted α-helix of the linker region. Also a subcomplex with full-leght δ (Ctβ19-391δ) and the full-length γζ-subcomplex were investigated.

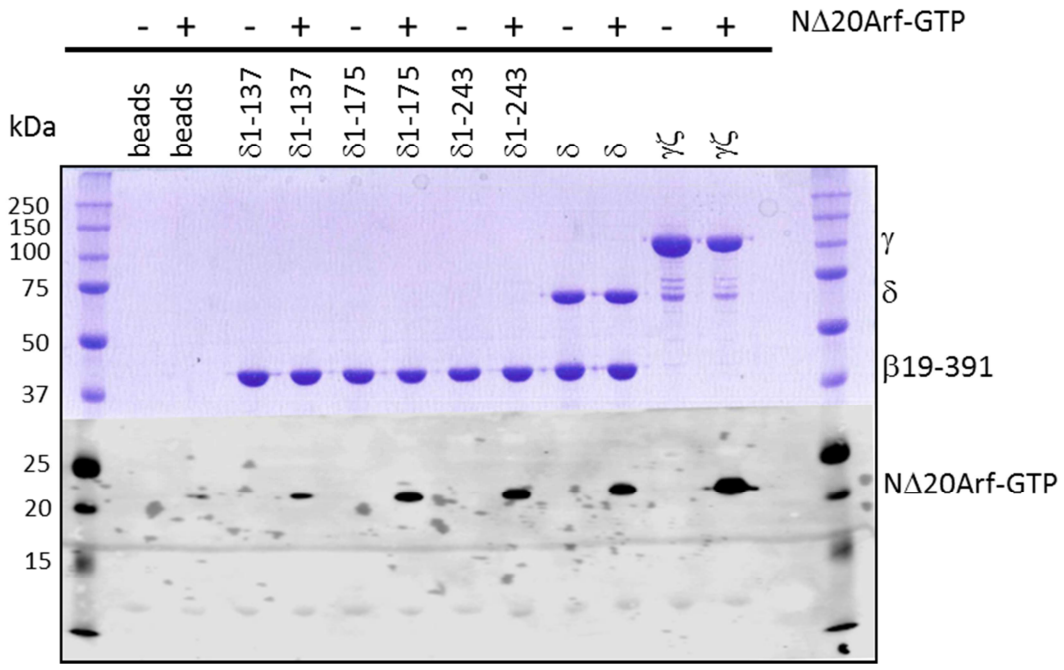

Figure 62: Pulldown NΔ20Arf-GTP with βδ-subcomplexes

Western Blot of 15% SDS-PAGE detected with Anti-CtArf and Anti-HIS_6 antibodies, 18% of the pulldown reaction was loaded on the gel.

As depicted in figure 62, the binding affinity of NΔ20Arf-GTP to beta/delta subcomplexes is increased, as soon as parts of the linker region of δ-COP are incorporated in the subcomplex. The subcomplex incorporating δ1-137 showed only minor binding of NΔ20Arf-GTP, slightly above background level. The subcomplex with δ1-175, which containes the first two helices of the linker region of δ-COP, showed increased binding of NΔ20Arf-GTP. The subcomplexes comprising further parts of δ-COP, namely the third linker helix (δ1-243) and full-length δ-COP, showed additional increase in binding, but binding levels NΔ20Arf-GTP to both of these complexes showed no difference. A comparison to NΔ20Arf-GTP binding of the homolougous γζ subcomplex showed a general weaker binding affinity for beta/delta subcomplexes than for the gamma/zeta subcomplex.

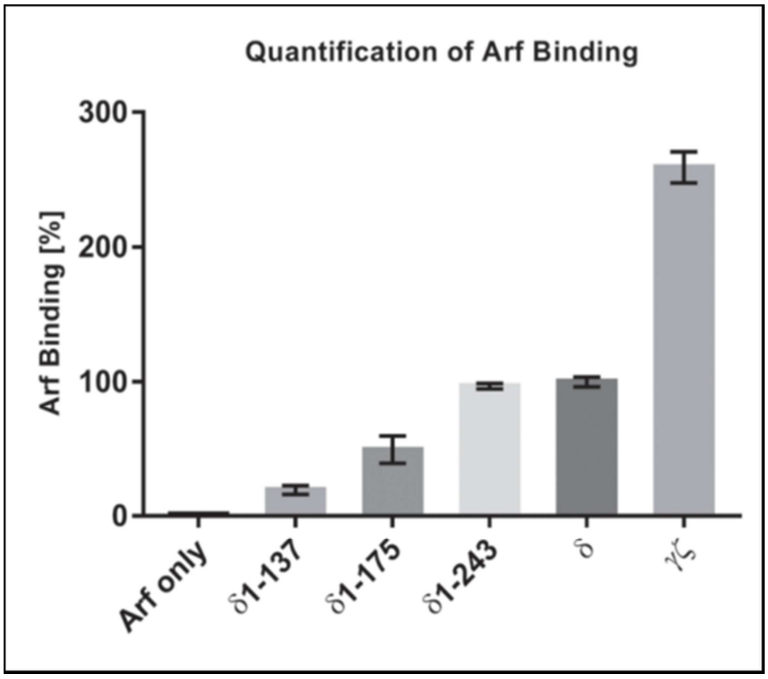

Figure 63: Quantification of Pulldown NΔ20Arf-GTP with βδ-subcomplexes

The quantification was done by pixeling the western blot signals of three replicate pulldown assays using the Imagestudio software of the Licor-system (Li-Cor Biosciences) and normalizing the quantification to Arf binding to the subcomplex incorporating full-length δ-COP (means +/- SEM; n=3).

Quantification of the binding of NΔ20Arf to βδ subcomplex was done by pixeling the western-blot signals. Binding was normalized with Arf binding to β19-391δ set to 100 %. As depicted in figure 63, quantification revealed an Arf binding of 50 % upon incoportaion of the first two α-helices of the δ-COP linker region (δ1-175). Incorporation of the third helix increased the Arf binding to 96 % (δ1-243) compared a βδ subcomplex iwith full-length δ-COP. Comparison of Arf binding of β19-391δ with γζ subcomplex revealed that binding to γζ-COP has a significantly higher affinity (about 250 %).

2.18 Single particle EM structure of α825β´793

Coatomer subcomplexes were also investigated using single particle electron microscopy. Subcomplexe were used in this investigation to more closly analyse the location of coatomer subunits, as up to now only a single particle structure of complete cytosolic coatomer was available (Yip and Walz, 2011). We were able to prepare a single particle EM structure of the

subcomplex α825β´793. Figure 64 shows the class averages, reprojections and surfaces of the subcomplex α825β´793.

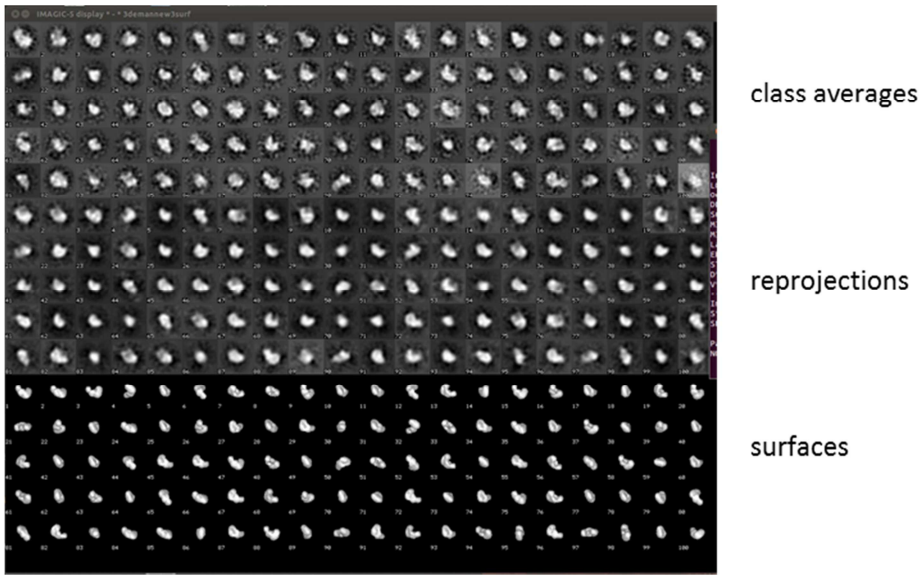

Figure 64: α825β´793 class averages, reprojections, surfaces

The structure was prepared with the help of Dr. Dirk Flemming from the EM-facility at the BZH. α825β´793 shows a curved structure, composed of a roughly oval shaped domain on the right, which is continued by a slightly curved, thinner domain on the left side. The structure has an overall diameter of ~130 Å, which is in good accordance with the known size of coatomer of around 160 Å. If the structure is compared to the single particle structure of the full cytosolic coatomer (EMD-5269), as depicted in figure 65, it shows that the truncated α-COP and β´COP subunits are making up the major part of the central stalk-like domain and the left arm of the coatomer complex. The missing density compared to EMD-5269 is the right arm of the coatomer complex, as well as major parts in the lower stalk-like domain, indicating that these parts are composed of subunits other then α-COP and β´-COP.

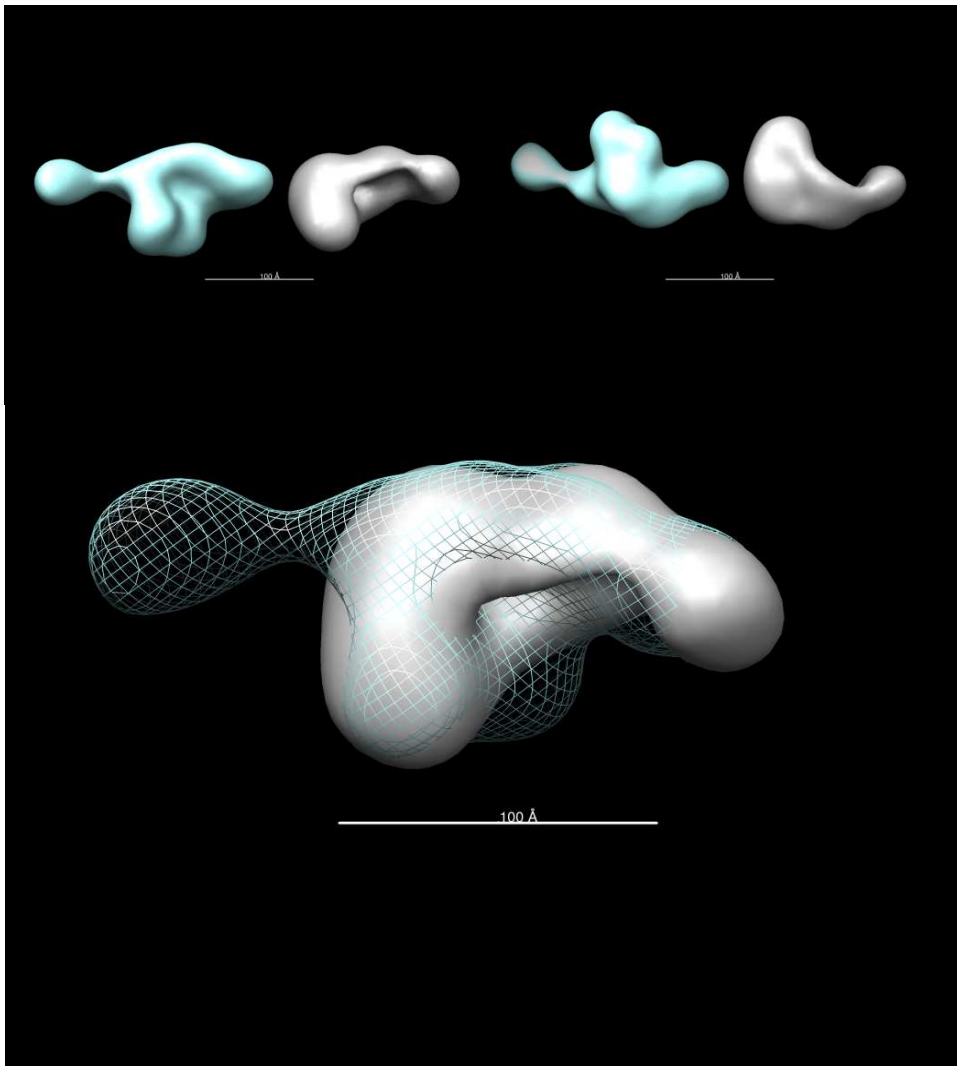

Figure 65: Comparison α825β´793 with EMD-5269

3 Discussion

In this thesis function and architecture of the COPI coat complex coatomer and its interaction with the small GTPase Arf was investigated structurally. To this end, a thermostable form of the coatomer complex and various subcomplexes derived from the organism *Chaetomium thermophilum* were prepared and characterized. Thermostable coatomer and its subcomplexes were analysed by limited proteolysis to identify the most suitable parts for crystallization. Subcomplexes determined this way were subjected to crystallization screens, and a subcomplex of truncated beta/delta COP was successfully crystallized. The structure of the crystallized subcomplex was solved using seleno-methionine labelling and MAD-phasing. Finally the interaction of Arf with this subcomplex was analysed.

3.1 Cloning, expression and purification of *Chaetomium thermophilum* coatomer and coatomer subcomplexes

For structural investigation of protein complexes by X-ray crystallography, negative stain or cryo electron microscopy, the stability of the proteins investigated is a crucial factor. It has been repeatedly reported that proteins, derived from thermophilic organisms, have an enhanced stability, which is due to more compact packaging, reduced flexibility and less pronounced surface loops. Therefore coatomer derived from the thermophilic ascomycete *Chaetomium thermophilum* was chosen as tool in the structural investigation of coatomer. In order to recombinantly express a complex of seven subunits, the Baculo-virus expression system was choosen, which allows the expression of multi-subunit protein complexes from one plasmid. Also the Baculo-virus driven expression in insect cells provides a high yield of the target protein, as well as a better chance for correct protein folding compared to bacterial expression systems. As the crystallization of the complete coatomer complex could prove difficult and in order to investigate the architecture of coatomer more closely, dimeric, tetrameric and trimeric subcomplexes of coatomer were prepared. Since a high purity of the investigated protein is prerequisite for successful crystallization, the coatomer complex and its subcomplexes were designed to be purified by a TEV-cleavable One-Strep-Tag affinity TAG. This TAG achieves a high purity of the target protein after affinity

purification. In this way it was possible in this thesis to produce *Chaetomium thermophilum* coatomer as well as a variety of its subcomplexes. Coatomer from *Chaetomium thermophilum* proved to be remarkably stable even after prolonged incubation at room temperature. Likewise, most of the subcomplexes prepared showed the similar stability. The complexes were produced at high yield in the range of 4 to 5 mg per 500 ml of expression culture, showed a high purity after purification by Strep-Tactin affinity chromatography and size exclusion chromatography, and are soluble at high concentrations, a factor important for the crystallization process. These results allowed to further pursue the project with limited proteolysis analysis of the complexes and crystal screens. The prepared pool of subcomplexes of coatomer, derived from *Chaetomium thermophilum*, provide a valuable tool in future structural investigations of this important heptameric protein complex.

3.2 Limited Proteolysis of *Chaetomium coatomer* and coatomer subcomplexes

Limited proteolysis is an important tool to investigate, which domains und subcomplexes of a protein complex are most stable and in this respect most suited for structural studies. The concept is based on the fact that an unspecific protease is first cleaving those parts of a protein complex that are most easily accessible to the protease. These are in most cases surface localized or flexible parts of the complex investigated. Analysis of coatomer and its subcomplexes by limited proteolysis with subtilisin gave valuable information about several stable subdomains of the various coatomer subunits. This included the N-terminal part of α-COP up to position ~840, which included the two N-terminal β-propeller domains followed by an α-solenoid stretch. This N-terminal part was further vulnerable to proteolysis at positions around 194 and 650. This indicates a flexible loop in the first N-terminal β-propeller of α-COP. The part from 650 to 825 was already known to form an α-solenoid stretch, which forms an interface to β´-COP (Lee and Goldberg, 2010). β´-COP revealed a C-terminal fragment from position 633/677 up to 833. Another fragment from position 490 to 806 indicated another flexible part in the C-terminal β-propeller of β´-COP. ε-COP showed only one fragment from positions 5 to 156. β-COP gave a couple of N-terminal fragments starting at position 13 up to positions 490, 466, 389 and 348, which most likely respresent α-solenoid folds. δ-COP showed C-terminal fragments, which could be attributed to its μ-

homology domain, and an N-terminal fragment from positions 32 to 145, part of its N-terminal longin like domain. The γ-COP subunit showed fragments that included its N-terminal trunk domains and the C-terminal appendage domain. There was an additional position in the N-terminal part at around position 193, exposed to the protease, indicating again a flexible part of the protein. ζ-COP showed no stable subdomain, which was expected because of it compact fold. The information obtained from the limited proteolysis was used together with existing structural data and secondary structure predictions to design constructs for crystallization screens. Most noteable were the data on the N-terminal stable fragments of β-COP. The N-terminal part of this subunit forms a complex with the N-terminal longin like-domain of δ-COP. Also the information on the stable fragments of α-COP and β´-COP, which are forming a dimeric complex, by an interface in their C-terminal α-solenoid regions (Lee and Goldberg, 2010), was used to design a complex for crystall screens.

3.3 Crystallization constructs

The protein subcomplexes for crystallization screens were designed taking into account the information obtained from limited proteolysis as well as published structural data on coatomer (Watson et al., 2004), (Lee and Goldberg, 2010), (Hsia and Hoelz, 2010), (Yu et al., 2012), (Faini et al., 2012), (Ma and Goldberg, 2013), (Dodonova et al., 2015), (Suckling et al., 2015) and the adaptor protein complexes. The subcomplexes designed covered the different functions of coatomer, including Arf- and membrane binding, cargo-binding and scaffold formation. In this respect, various parts of the coatomer complex were investigated. Four subcomplexes were designed to generate trunk-complexes of the tetrameric adaptor related subcomplex, composed of the subunits β-, γ-, δ- and ζ-COP. The four subcomplexes include a trunk complex lacking appendage domains and linker regions of β-COP and γ-COP (CM4β608γ586), a trunk-complex lacking the appendage domains of β-COP and γ-COP, but including the linker regions (CM4β686γ666), and a trunk complex lacking appendage and linker of only γ-COP (CM4γ585), as well as a trunk complex lacking appendage and linker of γ-COP and the μ-homology domain of δ-COP (CM4γ586δ243). Of these four trunk-complexes only the one including the linker region of both large subunits (CM4β686δ666) remained assembled as a complex. All other trunk-complexes fell apart. This indicates a crucial

function of the linker regions of both β-COP and γ-COP in assembly of the tetrameric subcomplex. This is in contrast to the architecture of the adaptor protein complexes, where the linker regions of the large subunits have no function with regard to enabling assembly of the four subunits into a complex, as they can be deleted without affecting complex integrity (Kelly et al., 2008), (Jackson et al., 2010), (Ren et al., 2012).

Two complexes were designed of the appendage domains of β-COP and γ-COP (β683-960, γ648-918), but only the appendage domain of γ-COP proved to be soluble. This may again point to a function of the β-COP appendage that differs from the adaptor protein complexes. This will have to be investigated by future experiments.

Two complexes were designed incorporating the truncated two large subunits of the outer coat α-COP and β´-COP. These complexes were comprised of the two N-terminal β-propeller domains of α-COP and β´-COP and following α-solenoid stretch that forms the interface of both subunits (α825β´-793). The most N-terminal β-propellers of α-COP and β´-COP are reported to be implicated in binding of cargo motifs (Ma and Goldberg, 2013). The limited proteolysis showed that the N-terminal β-propeller is vulnerable to proteolysis at a region of 150 to 190, a presumed loop between blades 4 and 5 of the propeller. As this loop has a hydrophobic character, which could impede crystallization, a second construct was designed, in which 5 residues were mutated to arginine to make this region more hydrophilic (α825-F185K-M189K-N195K-M199K-F200K-β´793). Both subcomplexes were soluble.

To investigate the β-propeller domains of α-COP and β´-COP alone, three complexes were designed. The complexes α1-603 and β´1-585 incorporated the two β-propeller domains of α-COP respective β´-COP. For β´-COP another complex incorporating only the N-terminal β-propeller was designed (β´1-299). Of these three, only the two complexes of β´-COP proved to be soluble and stable. The N-terminal part of α-COP was vulnerable for degradation.

Of particular structural interest were the subunits β-COP and δ-COP as they represented the largest missing piece in the structural picture of the coatomer complex at the level of X-ray resolution. Also both subunits were reported to possess binding sites for the small GTPase Arf. To investigate these interactions, several subcomplexes of β-COP and δ-COP were designed. Two subcomplexes containing full-length δ-COP and truncated β-COP, lacking

either the appendage domain (β686δ) or the appendage domain and the linker region (β608δ), were prepared. Of these complexes only β686δ was stable and soluble. Taking into consideration the information from the limited proteolysis two additional complexes incorporating an N-terminal part of β-COP with the assumed Arf-binding site and full-length δ-COP were prepared (β19-391δ, β19-407δ). Both complexes proved to be soluble, whereas β19-391δ showed greater stability.

These subcomplexes were tested in crystallization screens. Crystals were obtained for the β19-391δ complex. However, SDS-PAGE analysis of the cyrstals revealed that the δ-COP subunit was proteolytically nicked in the linker region that connects the N-terminal longin-like domain and the C-terminal μ-homology domain. As a result only parts of δ-COP were incorporated in the crystal. The extended linker region of δ-COP, comprising 138 amino acids, is particular vulnerable for proteolysis, as was already observed during purification. Therefor four additional subcomplexes were designed with various parts of the linker region (β19-391δ1-124, β19-391δ1-137, β19-391δ1-175, β19-391δ1-243). Interestingly, the linker region of δ-COP contains three predicted α-helixes of unknown function. The complexes β19-391δ1-175 and β19-391δ1-243 were designed to incorporate the first two respective all three of these α-helices, whereas β19-391δ1-137 only contained the longin-like domain of δ-COP. Crystals were obtained for β19-391δ1-137 and for β19-391δ1-175. Seleno-methionine labelling was necessary to solve the structure, which is reasonable, as the complex has a high predcited α-solenoid content, which is difficult to solve using molecular replacement.

3.4 Structure of β18-389δ2-151

The structure of β18-389δ2-151 shows high overall similarity to the structure of γζ-COP published in 2012 (Yu et al., 2012). In both cases the α-solenoid of β-COP (respective γ-COP) forms a curved right-handed superhelical fold, which binds as an arch around δ-COP (respective ζ-COP). β18-389δ2-151 gives a more complete picture, as it contains no strand breaks in the loop regions connecting the different helices in the α-solenoid of β-COP. Although the overall folds of β-COP and γ-COP are quite similar, both structures cannot be overlaid easily as the helix arrangement in the α-solenoid shows substantial differences. This

makes it difficult to make assumptions on an interface of Arf and β-COP based on the γζ-Arf structure. Yu *et al*. proposed 3 residues in β-COP, based on their structure of γζ-Arf, to contribute to a β-COP Arf interface, namely residues Leu59, Ile99 and Leu100. In *Chaetomium thermophilum* these would translate into residues Leu58, Ile98 and Leu99. While Ile98 and Leu99 seem to be able to contribute to an interface with Arf, our structure shows that Leu58 is too far away from the outer surface of the α-solenoid to be part of an actual interface with Arf.

The fold of the N-terminal longin like domains of δ-COP and of ζ-COP is very similar and both structures can be overlaid quite well. The most interesting part of β18-389δ2-151 actually is the C-terminal part of the δ-subunit. Our structure shows that the linker region between the N-terminal longin-like domain and the C-terminal μ-homology domain of delta-COP passes below the α-solenoid of the β-COP subunit, thus providing novel structural information. As can be seen in the crystal contacts, helix 5 of δ2-151 is stabilized by pairing with helix 5 from another copy of δ2-151 in the crystal. Although the orientation of helix 5 of δ2-151 could be due partially to the crystal contacts, the passage of the linker below the β-COP subunit is already defined by helix 4 of δ2-151. The contacts made by helix 4 are mainly hydrophobic and involve residues Ile127, Ile130, Phe133 and Leu134, indicating not much flexibility in this helix. The contacts made by helix 5 on the other hand are more hydrophilic. The start of helix 5 has an amphiphilic character (residues 143 till 148), which would enable it to make contact to the membrane. This is not the case for the rest of the helix although it is not clear if the α-helices in the linker region remain folded all the time, or if they undergo a conformational change upon transition from soluble to membrane bound state of coatomer. It was shown recently in a cryo EM structure of coatomer (Dodonova et al., 2015) that beta/delta COP, unlike gamma/zeta COP, is not close to the membrane, but leaves a grove between parts of the helix and the membrane. This would enable the linker not to remain in immediate contact with the membrane.

Interestingly, the passage of the linker below β-COP is in a region of β-COP that has been proposed to form an interface with the small GTPase Arf (Yu et al., 2012). This points to a function of the linker region of δ-COP in Arf-binding to beta/delta-COP. δ-COP has been reported to bind to Arf (Sun et al., 2007). Based on published data and the findings of this

thesis, we propose a model for how Arf binds to both beta-COP and delta-COP. In this model, β-COP and δ-COP bind to the same Arf molecule, if the linker of δ-COP passed below Arf, as depicted in figure 66.

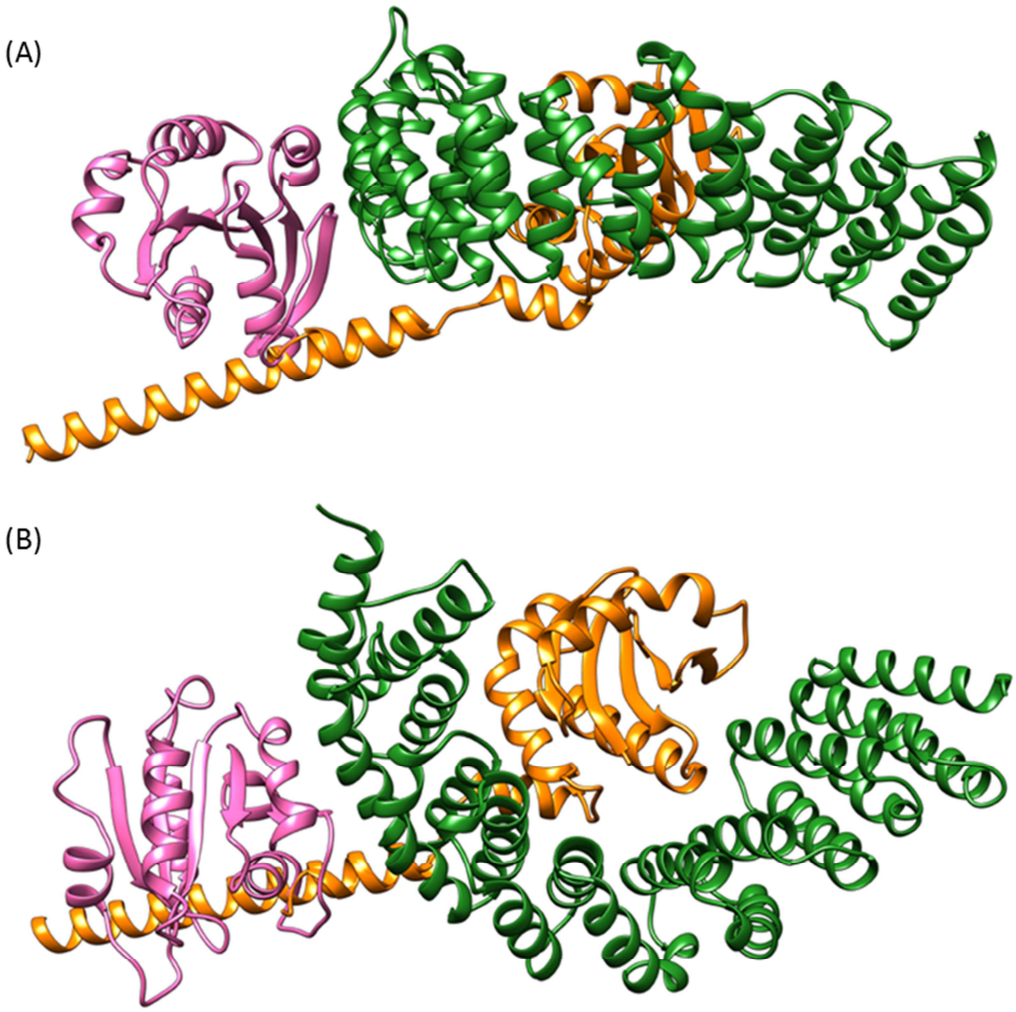

Figure 66: Model Arf-binding to beta/delta-COP

(A): Model side view, (B): Model top view

The model is in accordance with biochemical data of Arf-binding to beta/delta-COP. Arf sites implicated in binding of Arf to beta/delta-COP (Arf residues Ile46 binding to β-COP, Arf residue Tyr167 binding to δ-COP (Sun et al., 2007) and β-COP residues Ile98 and Leu99 binding to Arf) (Yu et al., 2012), fit well with our proposed model, as depicted in figure 67.

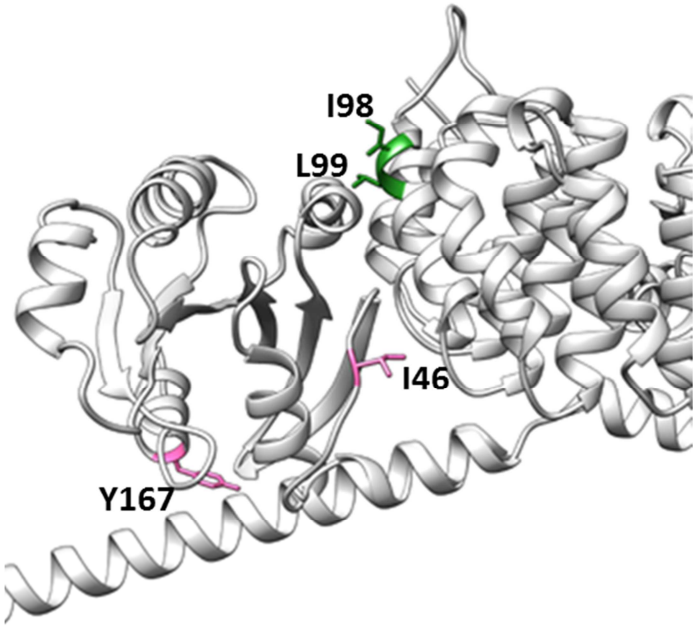

Figure 67: Residues involved in Arf-binding to beta/delta-COP

Fitting of the β18-389δ2-151 structure in the published cryo-EM structure of the COPI coat (Dodonova et al., 2015) revealed that helix 5 of δ-COP is located in a previously unoccupied EM density of the COP-coat. Although the δ-COP linker region is not resolved in the cryo-EM map, the presence of this previously unoccupied density shows that the orientation of helices 4 and 5 also exists in the COPI coat assembled on a membrane, as depicted in figure 68.

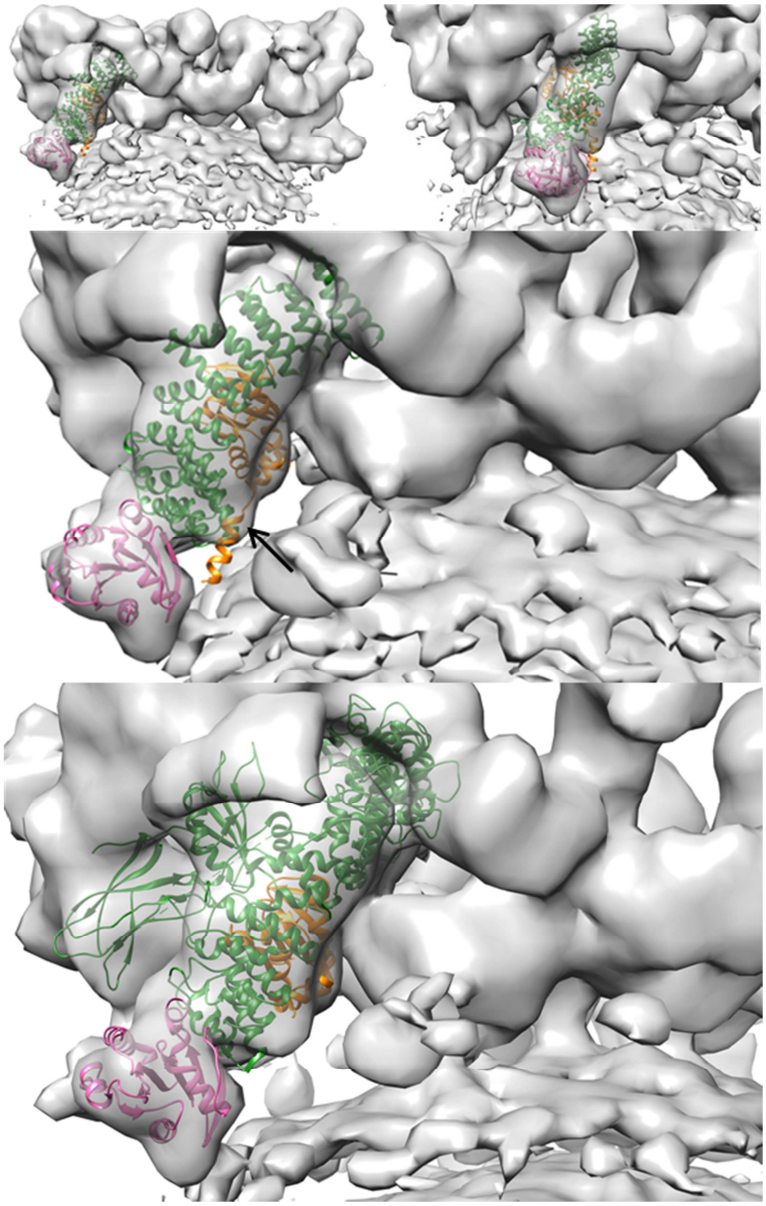

Figure 68: Fitting of β18-389δ2-151 in a Cryo-EM map (EMD-2985). Black arrow depicts previously unoccupied density in EMD-2985 compared to fit of homology model of βδ in PDB 5A1U. Fitting was done using UCSF Chimera package (Version 1.11, University of California, San Francisco).

The position of helix 5 of the δ-COP linker region in the assembled COPI coat and the amphipatic patch in this helix formed by residues Ile143, Ile146 and Ile147 (oriented towards the membrane) raises the possibility of a function of this helix in cargo binding. A possible candidate for this could be the KDEL receptor. Helix 5 of δ-COP was described as essential for the retrieval of the HDEL bearing proteins Kar2 and Pdi1 in *S. cerevisiae (Arakel et al., 2016)*. Mutational analysis in the critical hydrophobic patch of this helix showed the retrieval of these proteins to depend on the presence of residues I143, I146 and I147. Here I have shown

that the δ-COP linker helix is also important for an interaction with Arf, arguing for a potential function of Arf in KDEL binding and release. Arf could stabilize the orientation of δ-COP on the membrane and position it to enable binding to the KDEL receptor. Release of KDEL receptor bound cargo has up to now been attributed mechanistically to pH differences between the the ER and the Golgi (Wilson et al., 1993), which is pH 7.2 +/- 0.2 (ER) and pH 6.4 +/- 0.3 (Golgi) and thus not very pronounced. The data obtained here do not allow neglecting a pH effect. However, the KDEL receptor bears similarities to GPCRs, and Arf binding to the membrane is reverted by GTP hydrolysis during the uncoating process. Consequently, helix 5 of δ-COP would not be stabilized any more by Arf. In analogy to GPCRs, this effect could possibly be transmitted by conformational change of the KDEL receptor to the luminal side of the vesicle, and thus could contribute to cargo release.

Closer investigation of the structure reveals an elongated loop on the upper site of the α-solenoid of β-COP connecting the helices 4 and 5. This loop encompases the residues 84 to 95 of β-COP and represents the longest loop making connections between α-helices in the whole α-solenoid. It has a mostly hydrophilic character. This loop region and also its size is a conserved feature of β-COP from *Saccharomyces cerevisiae* to mammals. The homologous γ-COP does not contain a loop of simililar length connecting helices in its α-solenoid. The positioning of this loop directly on the upper side of the proposed Arf-binding site of β-COP would allow it to make additional contact to the small GTPase. In this respect this loop and the linker helix of δ-COP could act as kind of a clamp, to stabilize the interaction of Arf with the beta/delta subcomplex. The loop would make contact on the upper side of the Arf molecule, and the helix would make contact on its membrane facing side. The function of this region will have to be the subject of future experiments.

3.5 Binding of Arf to δ-COP

The binding affinity of beta/delta subcomplexes for NΔ20Arf GTP is increased after incorporation of the first two α-helices of the linker region of δ-COP into the complex. This confirms a function of this helix in Arf-binding. If the helices are not present in beta/delta subcomplexes, Arf-binding is strongly reduced. Interestingly, binding of NΔ20Arf GTP to beta/delta subcomplexes of coatomer is significantly weaker than binding to the

homologous gamma/zeta subcomplex. This might indicate that the Arf binding site on γ-COP is the primary binding site for the recruitment of coatomer. This is in accordance with Arf binding to AP1 were β1-adaptin was proposed to serve as the primary Arf binding site, as its shows a higher binding affinity for Arf than γ1-adaptin (Ren et al 2012). Based on the structure of β18-389δ2-151 we created a model incorporating Arf bound to both β-COP and the first two helices of the linker region of δ-COP. This model is in accordance with previously obtained data that showed a UV depended crosslink between Arf-residue 167 and δ-COP (Sun et al., 2007) and a bivalent crosslink product, which was obtained with Arf residues 167 and 46, that bind δ-COP and β-COP, respectively (Simone Röhling, unpublished data). The model allowes assigning additional residues of the linker helix of δ-COP as potentially interacting with the small GTPase Arf, as depicted in figure 69.

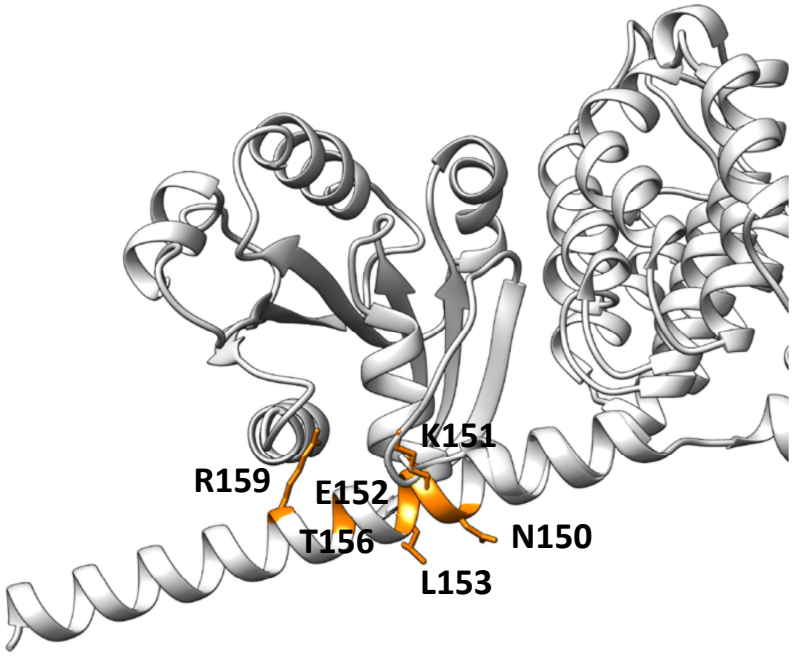

Figure 69: Residues of δ-COP potentially interacting with Arf

These residues include positions Arg159, Thr156, Leu153, Glu152, Lys151 and Asn150 of Ctδ-COP. The potential function of these residues in the formation of a δ-COP-Arf interface will have to be investigated by future work involving mutagenesis studies und pull-down experiments.

3.6 Structure of α825β´793 in the soluble form of coatomer

The structure of α825β´793 allows some additional insight how this subunits are arragend in soluble coatomer. In the structure (EMD-5269) presented by Walz and co-workers in 2011 (Yip and Walz, 2011) the location of γ-COP and δ-COP was assigned to the lower part of the central stalk-like domain. An additional density could be visualized in this region, which was caused by the fusion of GFP to the C-termini of the subunits γ-COP and δ-COP. However, with the same approach no localization of the subunits α-COP, β´-COP and ε-COP was possible, as no additional density could be observed. The comparison of the structure of α825β´793 with EMD-5269 now allows the localization of the subunits α-COP and β´-COP to the central stalk-like domain and to the right arm domain of coatomer. The left arm domain might be formed by the C-terminal part of α-COP, which was not present in the structure of α825β´793. This part is connected to the rest of α-COP by a short felxibel linker and forms an interface with ε-COP, as shown in a crystal structure (Lee and Goldberg, 2010). The localization seems plausibel as it is in close proximity to the space occupied by the remaining part of α-COP, as shown in the structure of α825β´793. Also the left arm and the right arm of coatomer are known to exibit strong flexibility in the structure published by Walz and co-workers. The complete elucidation of the localization and arragenment of each subunit in the soluble coatomer complex will require a higher resolution structure, which will again have to be subject of future work.

4 Material and Methods

4.1 Molecular Biology

4.1.1 General buffers and solutions

Buffer / Solution	composition	
Coomassie staining solution	ethanol	40 % (w/v)
	acetic acid	10 % (w/v)
	Coomassie R250	0.25 % (w/v)
Coomassie destaining solution	ethanol	20 % (w/v)
	acetic acid	5 % (w/v)
DNA sample buffer 5x	tris /HCl	50 mM
	urea	4 M
	glycerol	25 % (w/v)
	bromphenolblue	0.1 % (w/v)
	EDTA	100 mM
SDS-PAGE electrophoresis buffer 1x	tris	25 mM
	glycin	250 mM
	SDS	0.1 % (w/v)
SDS-PAGE sample buffer 4x	tris/HCl pH 6.8	200 mM
	glycerol	40 % (w/v)
	β-mercaptoethanol	12 % (w/v)
	SDS	8 % (w/v)
	bromphenolblue	0.2 % (w/v)
Western-Blot transfer buffer	tris	48 mM
	glycine	39 mM
	SDS	1.3 mM
	methanol	20 % (w/v)
PBS (phosphate buffered saline) 1x	NaCl	137 mM
	Na_2HPO_4	4.3 mM
	KCl	2.7 mM
	KH_2PO_4	1.5 mM
	pH 7,4	
PBS-T	1 x PBS	
	tween 20	0.05 % (v/v)
	pH 7.4	

Table 8: General buffers and solutions

Special buffers and solutions that were used are described in the respective methods section.

4.1.2 Restriction enzymes and DNA-Polymerases

All in this thesis used restriction endonucleases and the respective digestion buffers were purchased from the company New England Biolabs (New England, USA). The *Phusion High fidelity DNA-Polymerase* used in this thesis was also purchased from New England Biolabs.

4.1.3 Primers

All primers and oligonucleotides were ordered from the company Biomers (Ulm).

PCR Primers

Primer name	Sequence 5´- 3´ restrictions sites underlined	amplified subunit
CtaCOP_fw NotI CtaCOP-rv XbaI	ATATGCGGCCGCATGCAGTCCTCTACGGGAAT ATATTCTAGATTAAGCAAACAGCTTCAACC	Ctα-COP
Cta-M_fw ClaI CtaCOP_rv XbaI	GCTACGATCGATCAGTCCTCTACGGGAATGCT ATATTCTAGATTAAGCAAACAGCTTCAACC	CtαCOP-M
Cta-M_fw ClaI Cta825_rv XbaI	GCTACGATCGATCAGTCCTCTACGGGAATGCT ATATATTCTAGATTATGTTGCCTTAGTTGGCCAGT	Ctα825-M
Cta-M_fw SpeI Cta603_rv NotI	ATATATACTAGTCAGTCCTCTACGGGAATGCT ATATATGCGGCCGCTTACTGAAGAATTCGGGGCTTAG	Ctα603-M
Cta-M_fw XmaI Cta603_rv NheI	CCAGTTAACCCGGGATGGGACACCATCATCATCACCACAGC GCATGCGCTAGCTTACTGAAGAATTCGGGGCTTAGC	HOST-Ctα603
Cta650-M_fw ClaI Cta825_rv XbaI	ATCCGATCGATGCTCTCCAGTTCGTGCAAG ATATATTCTAGATTATGTTGCCTTAGTTGGCCAGT	Ctα650-825-M
Cta903-M_fw ClaI CtaCOP_rv XbaI	GAGACCATCGATGCTGCCAGCAGCGAAGCT ATATTCTAGATTAAGCAAACAGCTTCAACC	Ctα903-1218-M
Cta603_fw NdeI Cta603_rv BamHI	ATATCATATGCACCCGCAATTCGAAAAGGGCGGTG ATATGGATCCTTACTGAAGAATTCGGGGCTTAGC	Ctα603
Ctb-M_fw ClaI CtbCOP_rv XbaI	GCTACGATCGATTCGTTCCTCGACAATGCATAC ATATTCTAGATTAAGCAGCCGAACCGATTT	CtβCOP-M
Ctb-M_fw ClaI Ctb608_rv XbaI	GCTACGATCGATTCGTTCCTCGACAATGCATAC AAACTGTCTAGATTAAACACGAATGATGGAGATCATG	Ctβ608-M
Ctb-M_fw ClaI Ctb686_rv XbaI	GCTACGATCGATTCGTTCCTCGACAATGCATAC GGACAGTCTAGATTAAATGGGAACCACGTCGTCAAC	Ctβ686-M
ND18Ctb_fw ClaI Ctb391_rv XbaI	CAACGATCGATACTCCGACCCTCCAGGAGC CGCTTCTAGATTATTAGGAGAACTTGACTGC	Ctβ19-391-M
ND18Ctb_fw ClaI Ctb407_rv XbaI	CAACGATCGATACTCCGACCCTCCAGGAGC GCAGATCTAGATTATTAATCGGCGATGAAGTC	Ctβ19-407-M
ND18Ctb_fw BamHI Ctb391_rv NotI	CAACGGGATCCGACTCCGACCCTCCAGGAGCTG CACGGCGGCCGCTTATTAGGAGAACTTGACTGC	Ctβ19-391-M
ND18Ctb_fw BamHI Ctb407_rv NotI	CAACGGGATCCGACTCCGACCCTCCAGGAGCTG CACGGCGGCCGCTTATTAATCGGCGATGAAGTC	Ctβ19-407-M
Ctb716_fw NdeI Ctb_rv EcoRI	CAGTCATATGTCCGAGGATCTCTCGAGC CGGAGAATTCTTATTAAGCAGCCGAACCGAT	Ctβ716-960
Ctb683_fw NdeI Ctb_rv EcoRI	AGTTCATATGGTGGTTCCCATTCGCCAACTG CGGAGAATTCTTATTAAGCAGCCGAACCGAT	Ctβ683-960
Ctb716-960_fw NotI Ctb716-960_rv XbaI	ATATGCGGCCGCATGTCCGAGGATCTCTCGAGCAAGCTC ATATTCTAGATTAAGCAGCCGAACCGATTTTGTTC	Ctβ716-960
Ctb716_fw XmaI Ctb960_rv NheI	ATATCCCGGGATGTCCGAGGATCTCTCGAGCAAGCTC ATATGCTAGCTTAAGCAGCCGAACCGATTTTGTTC	Ctβ716-960
Ctb716-960_fw NdeI	ATATCATATGTCCGAGGATCTCTCGAGCAAGCTC ATATGGATCCTTAAGCAGCCGAACCGATTTTGTTC	Ctβ716-960

Ctb716-960_rv BamHI		
ND18TEVCtb_fw BamHI Ctb391_rv NotI	CAACGGGATCCGGAAAATCTTTACTTCCAAGGGACTCCGAC CCTCCAGGAGCTG CACGGCGGCCGCTTATTAGGAGAACTTGACTGC	TEVNΔ18Ctβ
CtbpCOP_fw XmaI CtbpCOP_rv NheI	GCATCGCCCGGGATGACTACCTATACACAGCGT GCATCGGCTAGCTTACTCATCCTCACTCCCTT	Ctβ´-COP
CtbpCOP_fw XmaI Ctbp793_rv NheI	GCATCGCCCGGGATGACTACCTATACACAGCGT GCATGCGCTAGCTTACTCACCAGGCACTCCCAGAG	Ctβ´793
Cta603_fw XmaI Ctbp585_rv NheI	CCAGTTAACCCGGGATGGGACACCATCATCATCACCACAGC GAGTGCGCTAGCTTAAGCGAAAGAAGTAACCG	HOST-Ctβ´585
Cta603_fw XmaI Ctbp299_rv NheI	CCAGTTAACCCGGGATGGGACACCATCATCATCACCACAGC GCCGGGCTAGCTTAACCAAGCTTAATAACCACAG	HOST-Ctβ´299
CtgCOP_fw NotI CtgCOP_rv XbaI	ATATGCGGCCGCATGAGCTACGGGAAGAAGGA ATATTCTAGATTACGCAACAGATCCCACCA	CtγCOP
CtgCOP_fw NotI Ctg586_rv XbaI	ATATGCGGCCGCATGAGCTACGGGAAGAAGGACGAG GGTAGATCTAGATTATGATGTGACATACATAACAAG	Ctγ586
CtgCOP_fw NotI Ctg666_rv XbaI	ATATGCGGCCGCATGAGCTACGGGAAGAAGGACGAG GTTGCCTCTAGATTAAAACTCCCTGATCTCCGGGAT	Ctγ666
Ctg_fw ClaI Ctg_rv XbaI	CAGCATCGATAGCTACGGGAAGAAGGACGA ATATTCTAGATTACGCAACAGATCCCACCA	CtγCOP-M
Ctg_fw ClaI Ctg372_rv XbaI	CAGCATCGATAGCTACGGGAAGAAGGACGA ATATTCTAGATTAGGCCTCATTGCCGGTCTTGAG	Ctγ372-M
Ctg_fw ClaI Ctg564_rv XbaI	CAGCATCGATAGCTACGGGAAGAAGGACGA ATATTCTAGATTACCGATTGGCTATATCGTCCTCCTC	Ctγ564-M
Ctg648-918_fw NotI CtgCOP_rv XbaI	ATATGCGGCCGCATGGCTGTGGCGCAGAAGTACGCCCAG ATATTCTAGATTACGCAACAGATCCCACCA	Ctγ648-918
Ctg648-918_fw XmaI Ctg_rv NheI	ATATCCCGGGATGGCTGTGGCGCAGAAGTACGCCCAG ATATGCTAGCTTACGCAACAGATCCCACCA	Ctγ648-918
Ctg648-918_fw NdeI Ctg648-918_rv BamHI	ATATCATATGGCTGTGGCGCAGAAGTACGCCCAG ATATGGATCCTTACGCAACAGATCCCACCACC	Ctγ648-918
CtdCOP_fw XmaI CtdCOP_rv NheI	ATATCCCGGGATGGTTGTGCTCGCTGCGTC ATATGCTAGCCTACTCAATTACGTAGGAATCC	CtδCOP
Ctd_fw NdeI Ctd124_rv BamHI	ATGCTCATATGGTTGTGCTCGCTGCGTCCATC GGTTGGATCCTTAGTTCTCCCGATACCCGAGG	Ctδ124
Ctd_fw NdeI Ctd137_rv BamHI	ATGCTCATATGGTTGTGCTCGCTGCGTCCATC CGCTCGGATCCTTACTCCATCTCCAAGAAGGT	Ctδ137
dCOP_fw NdeI dCOP124_rv BamHI	GGAACATATGGTGCTGTTGGCAGCAGCAGTC GTGCGGATCCTTAATTCTCCCGGTATCCCAG	δCOP124
dCOP_fw NdeI dCOP137_rv BamHI	GGAACATATGGTGCTGTTGGCAGCAGCAGTC TTCTCGGATCCTTAGTCCATTTCTGTAAAGGT	δCOP137
CtdCOP_fw BamHI CtdCOP124_rv EcoRI	ATATGGATCCATGGTTGTGCTCGCTGCGTC GTGCGAATTCTTAGTTCTCCCGATACCCGAGG	Ctδ124
CtdCOP_fw BamHI CtdCOP137_rv EcoRI	ATATGGATCCATGGTTGTGCTCGCTGCGTC TTCTCGAATTCTTACTCCATCTCCAAGAAGGT	Ctδ137

Ctdlongin_fw NdeI TEVCtdlongin_rv AatII	GGGTCATATGGTTGTGCTCGCTGCGTCCATCTGC CCGCGACGTCGCCCTGAAAATAAAGATTCTCGTTCTCCCGA TACCCGAGGTTG	CtδTEV
Ctdlongin_fw NdeI TEVCtd137_rv AatII	GGGTCATATGGTTGTGCTCGCTGCGTCCATCTGC CCGCGACGTCGCCCTGAAAATAAAGATTCTCCTCCATCTCCA AGAAGGTTTTG	Ctδ137TEV
Ctd_fw NdeI Ctd_rv EcoRV	ATGCTCATATGGTTGTGCTCGCTGCGTCCATC CACGGATATCTTACTACTCAATTACGTAGGA	Ctδ
CtdCOP_fw XmaI Ctd243_rv NheI	ATATCCCGGGATGGTTGTGCTCGCTGCGTC ATATGCTAGCTTACTCGCTCTTCACACGTTCAAACATATCC	Ctδ243
CtdCOP_fw XmaI Ctd175_rv NheI	ATATCCCGGGATGGTTGTGCTCGCTGCGTC ATATGCTAGCTTAACGGCTGGCCTCCTTGCGCTGC	Ctδ175
CtdCOP_fw XmaI Ctd137_rv NheI	ATATCCCGGGATGGTTGTGCTCGCTGCGTC ATATGCTAGCTTACTCCATCTCCAAGAAGGTTTTGATCTG	Ctδ137
CtdCOP_fw XmaI Ctd124_rv NheI	ATATCCCGGGATGGTTGTGCTCGCTGCGTC ATATGCTAGCTTAGTTCTCCCGATACCCGAGGTTGAT	Ctδ124
Ctd_fw NdeI Ctd137_rv EcoRV	ATATCATATGGTTGTGCTCGCTGCGTCCATCTG ATATGATATCTTACTCCATCTCCAAGAAGGTTTTGATCTG	Ctδ137
Ctd_fw NdeI Ctd243_rv EcoRV	ATATCATATGGTTGTGCTCGCTGCGTCCATCTG ATATGATATCTTACTCGCTCTTCACACGTTCAAACATATCC	Ctδ243
HIS-TEV-Ctd137_fw NdeI Ctd137_rv EcoRV	ATATCATATGCATCACCATCATCACCACGAAAATCTTTACTTCC AAGGGGTTGTGCTCGCTGCGTCCATCTGC ATATGATATCTTACTCGCTCTTCACACGTTCAAACATATCC	HIS-TEV- Ctδ137
CteCOP_fw NotI CteCOP_rv XbaI	ATATGCGGCCGCATGGATCCCTACTCGGCCGAAGG ATATTCTAGATCATGCCGCGGCCTTGCTAG	CtεCOP
Cte_fw XmaI Cte_rv NheI	ATATCCCGGGATGGATCCCTACTCGGCC ATATCGATCGTCATGCCGCGGCCTTGCT	CtεCOP
CtzCOP_fw XhoI CtzCOP_rv NheI	ATATCTCGAGATGCCCGGACTGTCACTGTA ATATGCTAGCTCACAAACCCTGCCGCAACC	CtζCOP
ND20CtArf_fw NdeI Sf9 opt ND20CtArf_rv EcoRI Sf9 opt	CAAAAACATATGAGAATTTTGATGGTGGGCTTGGACGCC GCGCATGAATTCTTACGACGATTTTTTAATTTCTTGGGC	NΔ20CtARF
TEVND20CtArf_fw EcoRI TEVND20CtArf_rv NotI	CATCCCGAATTCGGAGAATCTTTATTTTCAGGGC GACGGGCGGCCGCTTATTAGTTCGACGATTTTTTAATTTC	TEVNΔ20CtAR F
HISTEVND20CtArf_ fw BglII HISTEVND20CtArf_ rv AatII	GAGAAGATCTATGAAACATCACCATCACCAT CGAGGACGTCTTAGTTCGACGATTTTTTAATTTC	HISTEVNΔ20 CtArf

Table 9: PCR-primer restriction sites are depicted underlined

Mutagenesis Primer

Primer Name	Sequence 5´- 3´ Mutations underlined	Mutation
Ctbp C2124G fw2-NruI Ctbp C2124G rv2-NruI	GTACACCTCCACATCCGA**C**CGCGAAGGTCT AGACCTTCGCG**G**TCGGATGTGGAGGTGTAC	-NruI site
CtbC318G_fw -NruI CtbC318G_rv -NruI	CTCTGCAAGCTTCG**G**GAGCCCGAACTACT AGTAGTTCGGGCTC**C**CGAAGCTTGCAGAG	-NruI site
CtdG1425C_fw -NruI CtdG1425C_rv -NruI	GGTGCGCTTCGC**C**AAGACAACGCCG CGGCGTTGTCTT**G**GCGAAGCGCACC	-NruI site
CtARFQ74L2_fw CtARFQ74L2_rv neu	GGCGGC**CTG**GACAAAATTAGACC CACGTCCCACACCGTAAATTG	Mutation Q74L
CtARFT34N_fw CtARFT34N_rv2	CGCCGGCAAA**AAC**ACGATTTTGTAC GCGTCCAAGCCCACCATCAAA	Mutation T34N
ND20CtARFStopM_fw ND20CtARFStop_rv	AATCGTCGAACTAAT**A**TA**ATAA**GGTACCCTCG TTTTAATTTCTTGGGCCAACCAGTCCAAGC	additional Stop Codon added
Cta_F185KM189K_fw Cta_F185KM189K_rv	ATGTCC**AAG**GAAGACCAG**AAG**GCTCGC GCGAGC**CTT**CTGGTCTTC**CTT**GGACAT	Mutations F185K M189K
Cta_N195KM199K_fw Cta_N195KM199K_rv	AACGCA**AAG**CAAACCGAC**AAG**TTTGGTAACAC GTGTTACCAAA**CTT**GTCGGTTTG**CTT**TGCGTT	Mutations N195K M199K
Cta_F200K_fw new Cta_F200K_rv new	CAAACCGACAAG**AAG**GGTAACACTGATGC GCATCAGTGTTACC**CTT**CTTGTCGGTTTG	Mutation F200K
Cte-NheI_fw new Cte-NheI_rv new	GTACAAGGCT**TC**CAAGGCCGCG CGCGGCCTTG**GA**AGCCTTGTAC	-NheI site

Table 10: Mutagenesis primer exchanged nucleotides are depicted in bold

Sequencing primer

Primer name	Sequence 5´- 3´	subunit
pBak-PAC-FP	TAAAATGATAACCATCTCGC	pFBDM MCSI
pEGFP-C2-RP	TTTAAAGCAAGTAAAACCTC	pFBDM MCSI
S-pFBDMMCS2 (b) f	GTTTTATTCTGTCTTTTTATTG	pFBDM MCSII
S-pFBDMMCS2 (b) r	CAATATATTATAGTTAAATAAG	pFBDM MCSII
S-Cta280 f	ACCCTGAATGGACACTTGGA	Ctα
S-Cta877 f	GCAGTCAATACGTTCAAGCG	Ctα
S-Cta1478 f	AGACGACGGCAGAACTTGCA	Ctα
S-Cta2083 f	GCTCACGGCAACCATAGCAT	Ctα
S-Cta2681 f	CTGTTGACGGAGCTGAGACC	Ctα
S-Cta777 rv	GGCACCCACTGACGTTCTGG	Ctα
S-Cta2788 fw	GCCATGCAACTCCTCAACCG	Ctα
S-Ctb401 f	CTCTTCTTTCTTCTGTGCGC	Ctβ
S-Ctb1050 f	GTGGAAGAGGTTGTTCTGCT	Ctβ
S-Ctb1694 f	ACCTTGCTACCGTGCTCGCA	Ctβ
S-Ctb1637 f	CGAAGACTCTTCGAAACTGTC	Ctβ
S-Ctb1296 f	GTCAAGTTCTCCGAAGTCGC	Ctβ

S-Ctb735 rv	GGCTGATGCTTGAGAGAGCG	Ctβ
S-Ctb716-960_rv	GGATCTCTCGAGCAAGCTCAG	Ctβ
S-Ctb870_f	CTCTGCGCGAGTTCCTCGAC	Ctβ
S-Ctb807_rv	GACGACACCTTGATGGTGCA	Ctβ
S-Ctbp397 f	GTTAGGGTATTCGAGGGCAA	Ctβ´
S-Ctbp998 f	AGGACAACGAGCCCATCACT	Ctβ´
S-Ctbp1603 f	TACACGAACTCCACTAACCG	Ctβ´
S-Ctg347 f	ACCGACCAAATGCTATCCGC	Ctγ
S-Ctg995 f	GTTACCAAGTTCGCCGCGCT	Ctγ
S-Ctg1400 f	CGCATTCTCCACCTCCTTGG	Ctγ
S-Ctg1612 f	GACGTTGATGACGAAGTGAG	Ctγ
S-Ctg618 rv	CGCATGATACTGGGTCATGG	Ctγ
S-Ctg648-918 fw	GGCGCAGAAGTACGCCCAGG	Ctγ
S-Ctg841 f	GAGGCTACGGAGCAATTAGC	Ctγ
S-Ctg735 rv	CGACGAAAGCGTCCTCCAGC	Ctγ
S-Ctd530 f	GGAGGACCGGAGGCATGGGC	Ctδ
S-Cte	GCCTTGCTAGCCTTGTACTTG	Ctε
S-CtzCOP	CTATCGCGCAGCGCGAGCAG	Ctζ
pMA rev	ACGACAGGTTTCCCGACTGG	pMA-Vector
S-TN7R	GCCACCTCTGACTTGAGCGTCG	TN7 site
S-TN7L	CGCGACCGTTCACATCGCCAG	TN7 site
pETDuet-Up1	ATGCGTCCGGCGTAGA	pET-DUET MCSI
DUET-UP2	CTAATACGCCGGCACATGTT	pET-DUET MCSII
DuetDown1	GATTATGGCGGCCGTGTACAA	pET-DUET MCSI
T7 Terminator	GCTAGTTATTGCTCAGCGG	pET-DUET MCSII

Table 11: Sequencing primer

Hybridization oligonucleotides

Oligo name	Sequence 5´- 3´ restriction sites underlined	purpose
OS_fw NcoI	ATATCCATGGGCAGTGCTTGGAGCCATCCACAGTTTGAGAAAG GTGGAGGCTCTGGCGGGGGTAGCGGGGGCAGTGCCTGGTCTC ACCCACAATTCGAAAAGGGGGATCCATAT	OneStrep-TAG
OS_rv BamHI	ATATGGATCCCCCTTTTCGAATTGTGGGTGAGACCAGGCACTGC CCCCGCTACCCCCGCCAGAGCCTCCACCTTTCTCAAACTGTGGAT GGCTCCAAGCACTGCCCATGGATAT	OneStrep-TAG

Table 12: Hybridization oligonucleotides restriction sites ared depicted underlined

4.1.4 Plasmids

plasmid	insert	resistance	origin
pFBDM		Ampicillin, Gentamycin	PD Imre Berger
pET24d-GST-TEV	TEV-GST	Kanamycin	AG Hurt
pET-DUET		Ampicillin	Novagen
pETM11		Kanamycin	G. Stier
pCRBlunt-CtaCOP-NruI	CtaCOP-NruI	Kanamycin	J. Strating
pMaHOST2t-Cta-M	CtaCOP-NruI-M	Ampicillin	this thesis
pMaHOST2t-Cta825	CtaCOP 1-825	Ampicillin	this thesis
pFBDM1-CtaHOST	HOST-Cta-COP	Ampicillin, Gentamycin	this thesis
pFBDM1-Cta	CtaCOP	Ampicillin, Gentamycin	this thesis
pFBDM-HOST-Cta603	HOST-Cta603	Ampicillin, Gentamycin	this thesis
pMA-HOST2t-Cta825-F185KM189K	Cta825-F185KM189K	Ampicillin	this thesis
pMa-HOST2t-Cta825-F185KM189KN195KM199K	Cta825-F185KM189KN195KM199K	Ampicillin	this thesis
pMa-HOST2t-Cta825-F185KM189KN195KM199KF200K	Cta825-F185KM189KN195KM199KM200K	Ampicillin	this thesis
pMA-HOST2t-Cta650-825	Cta650-825	Ampicillin	this thesis
pFBDM1-aCOP-OS-D318	a-COPD318-OS	Ampicillin, Gentamycin	this thesis
pCRBlunt-CtbCOP	CtbCOP	Kanamycin	J. Strating
pCRBlunt-Ctb-NruI	Ctb-NruI	Kanamycin	this thesis
pMA-HOST2t-Ctb	Ctb-NruI	Ampicillin	this thesis
pMA-HOST2t-Ctb608	Ctb608	Ampicillin	this thesis
pMA-HOST2t-Ctb686	Ctb686	Ampicillin	this thesis
pMA-HOST2t-Ctb19-391	Ctb19-391	Ampicillin	this thesis
pMA-HOST2t-Ctb19-407	Ctb19-407	Ampicillin	this thesis
pETM11-Ctb716-959	Ctb716-959	Kanamycin	this thesis
pET-DUET-Ctb19-391	Ctb19-391	Ampicillin	this thesis
pET-DUET-Ctb19-407	Ctb19-407	Ampicillin	this thesis
pETM11-Ctb683-959	Ctb683-959	Kanamycin	this thesis
pFBDM-Ctb716-960	Ctb716-960	Ampicillin, Gentamycin	this thesis
pET-DUET-TEV-Ctb19-391	TEV-Ctb19-391	Ampicillin	this thesis
pET24d-GST-TEV-Ctb716-960	Ctb716-960	Kanamycin	this thesis
pCRBlunt-Ctbp COP	CtbpCOP	Kanamycin	J. Strating
pCRBlunt Ct bp COP -Nru	CtbpCOP	Kanamycin	this thesis
pFBDMCtbp793	Ctbp793	Ampicillin, Gentamycin	this thesis
pFBDMCtbp	CtbpCOP	Ampicillin, Gentamycin	this thesis
pFBDM-HOST-Ctbp585	HOST-Ctbp585	Ampicillin, Gentamycin	this thesis
pFBDM-HOST-Ctbp299	HOST-Ctbp299	Ampicillin,	this thesis

		Gentamycin	
pCRBlunt-Ctg	CtgCOP	Kanamycin	J. Strating
pFBDM-Ctg	Ctg	Ampicillin, Gentamycin	this thesis
pFBDM-Ctg586	Ctg586	Ampicillin, Gentamycin	this thesis
pFBDM-Ctg666	Ctg666	Ampicillin, Gentamycin	this thesis
pMA-HOST2t-Ctg372	Ctg372 1,121	Ampicillin	this thesis
pMA-HOST2t-Ctg	Ctg	Ampicillin	this thesis
pFBDM-Ctg648-918	Ctg648-918	Ampicillin, Gentamycin	this thesis
pET24d-GST-TEV-Ctg648-918	Ctg648-918	Kanamycin	this thesis
pCRBlunt-Ct d COP	CtdCOP	Kanamycin	J. Strating
pCRBlunt Ct d COP -Nru	Ctd-NruI	Kanamycin	this thesis
pFBDM-Ctd-NruI	Ctd-NruI	Ampicillin, Gentamycin	this thesis
pET24d-GST-TEV-Ctd124	Ctd124	Kanamycin	this thesis
pET24d-GST-TEV-Ctd137	Ctd137	Kanamycin	this thesis
pET24-GST-TEVd124COP	dCOP124	Kanamycin	this thesis
pET24d-GST-TEVd137COP	dCOP137	Kanamycin	this thesis
pET-DUET-Ctd137TEV	Ctd137TEV	Ampicillin	this thesis
pET-DUET-Ctd124TEV	Ctd124TEV	Ampicillin	this thesis
pCRBlunt-Cte COP	CteCOP	Kanamycin	J. Strating
pCRBlunt-Cte-AvrII	CteCOP-AvrII	Kanamycin	J. Strating
pCR-Blunt-Cte-AVRII-NheI wrong	CteCOP-AvrII-NheI wrong	Kanamycin	this thesis
pCRBlunt-Ctz COP	CtzCOP	Kanamycin	J. Strating
pFBDM-HOST-Cta825bp793	HOST-Cta825	Ampicillin, Gentamycin	this thesis
pFBDM-HOST-Cta825-F185KM189K-bp793	HOST-Cta825-F185KM189K	Ampicillin, Gentamycin	this thesis
pFDBM-HOST-Cta825-F185KM189KN195KM199KF200K-bp793	HOST-Cta825-F185KM189KN195KM199KF200K	Ampicillin, Gentamycin	this thesis
pFBDM-HOST-Cta650-825-bp793	HOST-Cta650-825	Ampicillin, Gentamycin	this thesis
pFBDM-HOST-Cta1-603-Ctb716-960	Ctb716-960	Ampicillin, Gentamycin	this thesis
pFBDM-HOST-Cta825M-bp793-b716-960	Ctb716-960	Ampicillin, Gentamycin	this thesis
pFBDM-Ctbpe	CteCOP	Ampicillin, Gentamycin	this thesis
pFBDM-HOST-CtCM3	HOST-CtaCOP	Ampicillin, Gentamycin	this thesis
pFBDM-CtCM3	CtaCOP	Ampicillin, Gentamycin	this thesis
pFBDM-CM3OS-bpD300	bp-COPD300	Ampicillin, Gentamycin	this thesis
pFBDM-CM3-aD318-OS	a-COPD318-OS	Ampicillin, Gentamycin	this thesis

pFBDM-CM3-aD318-OS-bpD300	bp-COPD300	Ampicillin, Gentamycin	This thesis
pFDBM-HOST-Ctbd	HOST-Ctb	Ampicillin, Gentamycin	this thesis
pFBDM-HOST-Ctb608d	HOST-Ctb608	Ampicillin, Gentamycin	this thesis
pFBDM-HOST-Ctb686d	HOST-Ctb686	Ampicillin, Gentamycin	this thesis
pFBDM-HOSTCtb19-391d	HOST-Cb19-391	Ampicillin, Gentamycin	this thesis
pFBDM-HOST-Ctb19-407d	HOST-Ctb19-407	Ampicillin, Gentamycin	this thesis
pFBDM-HOST-Ctb19-391d1-243	Ctd1-243	Ampicillin, Gentamycin	this thesis
pFBDM-HOST-Ctb19-391d1-175	Ctd1-175	Ampicillin, Gentamycin	this thesis
pFBDM-HOST-Ctb19-391d1-137	Ctd1-137	Ampicillin, Gentamycin	this thesis
pFBDM-HOST-Ctd19-391d1-124	Ctd1-124	Ampicillin, Gentamycin	this thesis
pFBDM-HOST-Ctbd1-137	Ctd1-137	Ampicillin, Gentamycin	this thesis
pFBDM-HOST-Ctbd243	Ctd1-243	Ampicillin, Gentamycin	this thesis
pET-DUET-Ctb19-407d1-137	Ctd1-137	Ampicillin	this thesis
pET-DUET-Ctb19-407d1-243	Ctd1-243	Ampicillin	this thesis
pET-DUET-Ctb19-391d1-137	Ctd1-137	Ampicillin	this thesis
pET-DUET-Ctb19-391d1-243	Ctd1-243	Ampicillin	this thesis
pET-DUET-Ctb19-407d	Ctd	Ampicillin	this thesis
pET-DUET-Ctb19-391d	Ctd	Ampicillin	this thesis
pET-DUET-HT-Ctb19-391-HT-Ctd1-137	HIS-TEV-Ctd1-137	Ampicillin	this thesis
pET-DUET-TEV-Ctb19-391d	Ctd	Ampicillin	this thesis
pET-DUET-OST-Ctb19-391-HT-Ctd1-137	OS-TAG	Ampicillin	this thesis
pET-DUET-TEV-Ctb19-319d1-137	TEV-Ctb19-391	Ampicillin	this thesis
pFBDM-Ctb716-960-Ctg648-918	Ctg648-918	Ampicillin, Gentamycin	this thesis
pFBDM-Ctgz	Ctz	Ampicillin, Gentamycin	this thesis
pFBDM-HOST-Ctgz	HOST-Ctg	Ampicillin, Gentamycin	this thesis
pFBDM-Ctg586z	Ctz	Ampicillin, Gentamycin	this thesis
pFBDM-Ctg666z	Ctz	Ampicillin, Gentamycin	this thesis
pFBDM-HOST-Cta825M-bp793-g648-918	Ctg648-918	Ampicillin, Gentamycin	this thesis
pFBDM-HOST-Ctbp1-585-Ctg648-918	Ctg648-918	Ampicillin, Gentamycin	this thesis

pFBDM-HOST-CtCM4	HOST-Ctbd	Ampicillin, Gentamycin	this thesis
pFBDM-HOST-CM4g586b608	HOSTCtb608d	Ampicillin, Gentamycin	this thesis
pFBDM-HOST-CM4g666b686	HOSTCtb686d	Ampicillin, Gentamycin	this thesis
pFBDM-HOST-CtCM4g586d243	Ctg586z	Ampicillin, Gentamycin	this thesis
pFBDM-HOST-CtCM4-g586	Ctg586z	Ampicillin, Gentamycin	this thesis
pFBDM-CM7-OS-g1z1-bpD300	CM3-OS-bpD300	Ampicillin, Gentamycin	this thesis
pFBDM-CM7-aD318-OS-bpD300	CM3-aD318-OS-bpD300	Ampicillin, Gentamycin	this thesis
pFBDM-CM7-aD318-OS	CM3-aD318-OS	Ampicillin, Gentamycin	this thesis
pETM11-ND20CtARF	ND20CtARF	Kanamycin	this thesis
pETM11-ND20CtARFT34N	ND20CtARF	Kanamycin	this thesis
pETM11-ND20CtARFQ74L	ND20CtARF	Kanamycin	this thesis
pET-DUET-ND20CtARF	HIS-TEV-ND20CtARF	Ampicillin	this thesis
pET-DUET-HTND20CtARF	TEVND20CtARF	Ampicillin	this thesis
pET-DUET-HTND20CtARFQ74L	TEVND20CtARF Q74L	Ampicillin	this thesis
pET-DUET-ND20CtARF-Ctd137M	TEV-Ctd137M	Ampicillin	this thesis
pET-DUET-ND20CtARF-CTd137MStop	TEV-Ctd137M	Ampicillin	This thesis

Table 13: Plasmids

4.1.5 Enzymes and Kits

Enzymes and Kits	Company
QIAprep Spin Miniprep Kit	Qiagen (Hilden)
QIAquick Gel Extraction Kit	Qiagen (Hilden)
Quick change site directed mutagenesis kit	Stratagene (La Jolla, USA)
T4-DNA Ligase	Thermo Fisher

Table 14: Enzymes and Kits

4.1.6 Equipment

Equipment	Company
Agarose gel electrophoresis	Peqlab (Erlangen)
Incubator *E.coli*	Infors (Bottmingen, Switzerland)
Incubator Sf9 insect cells	Infors (Bottmingen, Switzerland)
Ettan LC FPLC	GE Healthcare (Buckinghamshire, UK)

Gel Doc	Biorad (Munich)
Microfluidizer	Microfluidics (Newton, USA)
NanoDrop ND-1000 Spectrometer	Nanodrop Technologies (Wilmington,USA)
PCR thermo cycler	Thermo Hybaid (Ulm)
SDS gel-electrophoresis	Biorad (Munich)
Thermomixer comfort	Eppendorf (Wesseling-Berzdorf)
Table top centrifuge	Eppendorf (Wesseling-Berzdorf)
ultracentrifuge	Beckman Coulter (Brea, USA)
centrifuge	Sorvall/Thermo scientific (Waltham, USA)
HPLC	Waters (Eschborn)
Western-Blot	Biorad (Munich)

Table 15: General Equipment

4.1.7 DNA size standards

As standard for determination of the size of DNA fragments in agarose gels the *1kb DNA ladder* from the company New England Biolabs (New England, USA) was used. The sizes of the DNA fragments in the standard are listed in the following picture (picture 70).

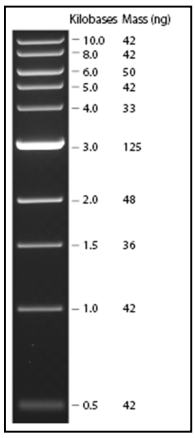

Figure 70: 1kb DNA size standart fragment sizes

4.1.8 DNA concentration determination

For the determination of the concentration of DNA in solution the absorption at 260 nm was measured. Therefor a ND-1000 spectrophotometer from the company NanoDrop (Wilminkton, USA) was used, which measures the DNA concentration in 1 µl of DNA solution and calculates the respective DNA concentration.

4.1.9 Ethanol precipitation of DNA

For precipitation of DNA 0.5 times the volume of 3M Sodium acetate was added to the DNA solution. After that 2.5 times the volume of ice cold 100% ethanol was added to the DNA solution. The mixture was incubated 30 minutes at -20 °C. After the incubation the mixture was centrifuged 10 minutes at 14000 rpm at 4°C in an Eppendorf table top centrifuge to pellet the precipitated DNA. The supernatant was discarded and 1 ml of 70% (v/v) ice cold Ethanol was added to the pellet followed by centrifugation for 5 minutes at 14000 rpm at 4 °C to remove residual salt. After the centrifugation the supernatant was discarded and the pellet was dried for 5 minutes at room temperature. After that the DNA pellet was resuspended in the desired volume of dH_2O water.

4.1.10 Analytical and preparative Agarose gel electrophoresis

The electrophoretic separation of DNA fragments was performed in 1 % to 0.5 % agarose gels, depending on the size of the DNA fragment. For preparation of the gels agarose was dissolved by heating in 1x TAE buffer. To stain the DNA the staining solution *Stain Clear G* (Serva, Heidelberg) was added to the gel in a dilution of 1:25000. The analyzed DNA samples were mixed with *5x DNA loading dye* (NEB, New England USA) before they were loaded in the wells of the gel. Depending on the analyzed sample the electrophoresis was performed at 16 V to 200 V. analytical gels were separated at higher voltage whereas preparative gels or gels with DNA fragments of similar sizes were separated at lower voltage. After electrophoresis the DNA fragments were visualized under UV at an excitation wavelength of 260 nm.

Buffer/Solution	Composition	
TAE electrophoresis buffer 1x	tris/HCl pH 8.0	40 mM
	acetic acid	20 mM
	EDTA	1 mM
Loading dye 5x	Tri/HCl pH 8.0	40 mM
	Urea	4 M
	Saccharose	25 % (w/v)
	Bromphenol Blue	0,1 % (w/v)
	EDTA	100 mM

Table 16: Buffers and Solutions for agarose gel electrophoresis

4.1.11 Polymerase-chain-reaction (PCR)

The selective amplification of DNA was performed by polymerase chain reaction (PCR) using a thermos cycler. The reaction was carried out using the thermostable *Phusion* polymerase (Thermo Fisher), which has a 3´- 5´ exonuclease activity for correction of falsely inserted nucleotides. For the reaction the following components were mixed in 0.2 ml PCR tubes.

component	volume
Template DNA 10 ng/µl	1 µl
Primer forward 10 µM	2.5 µl
Primer reverse 10 µM	2.5 µl
Desoxynucleotides 10 mM each	1 µl
5 x Phusion HF buffer	10 µl
Phusion polymerase	1 µl
H_2O	32 µl

Table 17: PCR reaction composition

PCR program

cycles	temperature	time
1	98 °C	30 sec
35	98 °C	10 sec
35	58 °C	10 sec
35	72 °C	depending on amplified fragment
1	72 °C	10 min
1	4 °C	hold

Table 18: PCR program

4.1.12 Site-specific mutagenesis

To introduce point mutations in a DNA sequence the *quick change site directed mutagenesis kit* was used. A sense and an antisense primer were generated, which contained the modified codon. The used sense and antisense primer had a length between 25 and 36 bps depending on the respective DNA sequence and the introduced mutations. For the mutagenesis reaction the following components were mixed.

component	volume
Template DNA 100 ng/µl	1 µl
Primer forward 10 µM	2.5 µl
Primer reverse 10 µM	2.5 µl
Desoxynucleotides 10 mM each	1 µl
5 x Phusion HF buffer	10 µl
Phusion polymerase	1 µl
H_2O	32 µl

Table 19: Mutagenesis PCR reaction composition

PCR program

cycles	temperature	time
1	98 °C	30 sec
35	98 °C	10 sec
35	58 °C	10 sec
35	72 °C	depending on amplified fragment
1	72 °C	10 min
1	4 °C	hold

Table 20: Mutagenesis PCR program

After the PCR reaction the reaction mix was purified using the Qiagen PCR purification Kit (Qiagen, Hilden). To the purified reaction 2 ml of the restriction enzyme *DpnI* (10U/ml) was added. *DpnI* specifically cuts methylated DNA thus eliminating the template DNA from the reaction mix. After the digest the reaction mix was again purified using the *Qiagen PCR purification kit*. The purified reaction mix was ligated overnight and transformed in *E. coli Dh10b* cells.

4.1.13 Hybridization of DNA oligonucleotides

To introduce Affinity Tags in a DNA sequence the DNA sequence of these Tags were synthesized as complementary DNA oligonucleotides with restriction sites to introduce them in the respective target plasmid. The complementary oligonucleotides were resuspended at the same molar concentration in *T4-DNA ligase buffer* (NEB, New England USA). Equal volumes of the oligonucleotides (at equimolar concentration) were mixed in a 1.5 ml Eppendorf tube. The mix was incubated at 95 °C for 5 minutes in a heating block. After the

incubation the heating block was switched of and the reaction mix was allowed to cool down to room temperature in approximately 45 minutes. After that the DNA mix was precipitated and resuspended in dH_2O. Then the purified DNA was digested and ligated in the respective target plasmid.

4.1.14 Isolation of plasmids

For the isolation of plasmid DNA in the range of 0.8 – 7 µg the *Qiagen plasmid mini prep kit* was used. An overnight culture of 5 to 10 ml LB (depending on the properties of the target plasmid (High copy or low copy)) with the respective selection antibiotic was inoculated with a single colony from a LB agar plate and incubated at 37 °C. The isolation was performed in accordance with the protocol of the kit. For the isolation of higher amounts of plasmid DNA the *Qiagen plasmid maxi prep kit* was used. The culture volume for the large scale isolation was 100 to 200 ml, depending on the target plasmid.

4.1.15 Restriction digests of DNA

The desired amount of DNA was mixed with the respective restriction enzymes and the necessary enzyme buffer in a way that the enzyme buffer was 1-fold concentrated in the final volume. All used restriction endonucleases were purchased from New England biolabs (New England, USA). The used amount of enzymes varied between 0.5 to 10 units per mg of DNA. The volume of the restriction digests was adjusted that way that the enzyme concentration did not exceed 10 % of the final digest volume in order to prevent star activity of the restriction enzymes. The digest reaction was performed at the optimal temperature for the respective enzymes for 30 minutes for analytical digests and for 2 hours for preparative digests. If two restriction enzymes did not have common buffer in which they were active, a sequential digest was performed. In between the two digest reaction the first enzyme was heat inactivated and the DNA was precipitated to exchange the enzyme buffer.

4.1.16 Dephosphorylation of DNA

In order to prevent re-ligation of vector DNA in a ligation reaction the digested vector DNA was dephosphorylated at its 5´-end. Therefor after the restriction digest the restriction enzymes were heat inactivated at 65 °C or 80°C for 20 minutes. If heat inactivation was not possible the digested vector DNA was precipitated. After that 1 µl of Calf intestine alkaline phosphatase was added to the vector DNA and incubated at 37 °C for 1 hour. Since the calf intestine alkaline phosphatase cannot be heat-inactivated the dephosphorylated vector was purified by preparative agarose gel electrophoresis.

4.1.17 Ligation of digested DNA

After the restriction digest of the DNA fragments the fragments were mixed with T4 DNA ligase buffer and the T4 DNA ligase. For sticky-end ligation the ligation reaction was incubated over night at 16 °C. For blunt-end ligation the ligation reaction was incubated for 1 hour at 25 °C. The ration of vector DNA to insert DNA was between 1:3 and 1:5. After the ligation reaction the ligation mix was transformed in *E. coli* Dh10b cells.

4.1.18 Sequencing of DNA

The sequencing of DNA was performed by the company GATC (Konstanz). Therefor 20 µl of plasmid DNA at a minimal concentration of 30 ng/µl was sent to the company.

4.1.19 Preparation of chemical competent cells

For preparation of chemical competent *E.coli* Dh10b and *E. coli* Bl21 (DE3) cells 800 ml of LB-medium supplemented with $MgCl_2$ and $MgSO_4$ was inoculated with 50 ml of an overnight culture of the respective strain to an OD_{600} of 0,1. The culture was incubated at 37 °C under shacking till an OD_{600} of 0.6 – 0.7 was reached. The cells were harvested by centrifugation in a Sorvall SLC-4000 rotor at 6000 rpm at 4°C for 10 minutes. The cell pellet was resuspended in 64 ml of ice-cold solution I and incubated for 30 minutes on ice. After that the cells were

harvested again by centrifugation with the same settings as before. The supernatant was discarded and the cell pellet was resuspended in 20 ml ice-cold solution II. The resuspended cells were incubated for 15 minutes on ice. 100 µl aliquots of the cells were flash frozen in liquid nitrogen and stored at -80 °C.

Solution I		**Solution II**	
RbCl	100 mM	MOPS	10 mM
$MnCl_2x4H_2O$	59 mM	RbCl	10 mM
$CaCl_2x2H_2O$	30 mM	$CaCl_2x2H_2O$	75 mM
Glycerol	15 % (w/v)	Glycerol	15%(w/v)
H_2O	add 1 l	H_2O	add 1 l
pH 5.8 adjusted with acetic acid		pH 5.8 adjusted with NaOH	
sterilized by passing through 0.2 µm pore filter		sterilized by passing through 0.2 µm pore filter	

Table 21: Solutions for chemical competent cells

4.1.20 Preparation of electro-competent cells

Electro-competent cells were prepared from *E. coli* Dh10b and *E.coli* Dh10b MultiBac cells. For electro-competent *E. coli* Dh10b MultiBac cells the cells were streaked on a LB low salt agar plate containing antibiotics kanamycin (50 mg/ml) and tetracyclin (10 mg/ml) as well as IPTG (40 mg/ml) and BlueGal (100 mg/ml). One blue colony was used to inoculate a 500 ml low salt LB culture with kanamycin and tetracyclin in the respective concentrations used before. The culture was incubated at 37 °C under shaking till OD_{600} 0.5 was reached. The culture was incubated and ice for 15 minutes and then harvested by centrifugation at 4000 rpm, 4°C for 15 minutes in a Sorvall SLC4000 rotor. The cells were resupended in 500 ml ice cold steril 10% glycerol. After that the cells were again harvested by centrifugation with the same settings as before. The cells were resupended in 250 ml ice cold steril 10% glycerol. The washing of the cell pellet was repeated two additional times. The volume of the ice cold steril 10% glycerol, in which the pellet was resuspended, was reduced to 10 ml in the third and to 1 ml in the fourth washing step. From the final volume of 1 ml 80 ml aliquots were prepared, flash frozen in liquid nitrogen and stored at -80°C. For *E. coli* Dh10b the preparation of electo-competent cells was performed the same way, but without the use of antibiotics.

4.1.21 Bacterial strains

Strain	genotype	origin
E. coli Dh10b	F^- endA1 recA1 galE15 galK16 nupG rpsL ΔlacX74 Φ80lacZΔM15 araD139 Δ(ara,leu)7697 mcrA Δ(mrr-hsdRMS-mcrBC) λ^-	Invitrogen (Karlsruhe)
E.coli Bl21 (DE3)	F^- ompT gal dcm lon $hsdS_B(r_B^- m_B^-)$ λ(DE3 [lacI lacUV5-T7 gene 1 ind1 sam7 nin5])	Stratagene (La Jolla, USA)
E. coli dam- dcm-	*ara-14 leuB6 fhuA31 lacY1 tsx78 glnV44 galK2 galT22 mcrA dcm-6 hisG4 rfbD1 R(zgb210::Tn10)* Tet^S *endA1 rspL136 (*Str^R*) dam13::Tn9 (*Cam^R*) xylA-5 mtl-1 thi-1 mcrB1 hsdR2*	
E. coli Dh10b MultiBac	F^- endA1 recA1 galE15 galK16 nupG rpsL ΔlacX74 Φ80lacZΔM15 araD139 Δ(ara,leu)7697 mcrA Δ(mrr-hsdRMS-mcrBC) λ^-	PD Imre Berger
E. coli rosetta(DE3)plysS	F^- ompT $hsdS_B(R_B^- m_B^-)$ gal dcm λ(DE3 [lacI lacUV5-T7 gene 1 ind1 sam7 nin5]) pLysSRARE (Cam^R)	

Table 22: Bacterial strains

4.1.22 Growth media for bacteria

medium	composition		purpose
Lauria-Bertani (LB) broth	Trypton NaCl Yeast extract	10 g/l 10 g/l 5 g/l	Propagation of *E. coli Dh10b*, *E.coli Bl21 (DE3)* and *E coli Dh10b* MultiBac strains
LB-Agar	LB-medium Agar	 15 g/l	Propagation of *E. coli Dh10b*, *E.coli Bl21 (DE3)* and *E coli Dh10b* MultiBac strains
Low salt LB	Trypton NaCl Yeast extract	10 g/l 5 g/l 5 g/l	Propagation of *E. coli Dh10b* MultiBac strain
Low salt LB-Agar	Low salt LB-medium Agar	 15 g/l	Propagation of *E. coli Dh10b* MultiBac strain
SOC-medium	Trypton Yeast extract NaCl KCl MgCl2 MgSO4 Glucose Note: glucose was filter sterilized and added separately to the autoclaved medium	2 % (w/v) 0,5 % (w/v) 10 mM 2,5 mM 10 mM 10 mM 20 mM	Propagation of transformed *E.coli Dh10b*, *E. coli Bl21 (DE3)* and *E. coli Dh10b* MultiBac strains

Table 23: Growth media for bacteria

4.1.23 Antibiotics

For preparation of selection media the following antibiotics were used:

antibiotic	concentration
ampicillin	100 µg/ml
kanamycin	50 µg/ml
tetracyclin	10 µg/ml
gentamycin	7 µg/ml
chloramphenicol	35 µg/ml

Table 24: Antibiotics

4.1.24 Additives

The following additives were used:

additive	concentration
IPTG	40 µg/ml
Bluo-Gal	100 µg/ml

Table 25: Additives

4.1.25 Transformation

The transformation of plasmid DNA in *E. coli* strains was done for the purpose of DNA amplification, plasmid construction and protein expression. In the case of *E. coli* Dh10b MultiBac cells the purpose was the recombination and transposition of the plasmid DNA into the Bacmid-DNA for the preparation of virus and the protein expression in SF9 insect cells. Depending on the plasmid properties, the replication origin and the methylation pattern different *E. coli* strains were used for the transformation.

4.1.26 Transformation of chemical compentent *E. coli* cells

100 µl of competent cells were thawed on ice and mixed with 10 ng of plasmid DNA or the complete ligation reaction. After incubation for 30 minutes on ice the mixture was subjected to a heat shock at 42 °C for 1 minute. After the heat shock the mixture was incubate for 2

minutes on ice again. 1 ml of SOC-medium was added to the cells and the mixture was incubated at 37 °C for 1 hour for regeneration and development of the plasmid encoded antibiotic resistance. In the last step the mixture was streaked on LB-agar plates containing the respective selection antibiotic.

4.1.27 Transformation of electro-competent *E. coli* cells

40 µl of electro-competent cells were thawed on ice and transferred to a precooled electroporation cuvette. 10 ng of plasmid DNA or a complete ligation reaction were mixed with the cells and incubated for 15 minutes on ice. For the electroporation 2 mm electroporation cuvettes (PeqLab, Erlangen) were used. The electroporation was carried out using a Gene Pulser Puls Controller (BioRad, Munich) at 2.0 kV, 200 Ω and 25 µF. After the electroporation 1 ml SOC-medium was added to the cells. The mixture was transferred to 15 ml Falcon tubes and incubated at 37 °C for 4 hours. In the last step the mixture was streaked on agar-plates containing selection antibiotics, IPTG and BluoGal.

4.1.28 The Baculovirus expression system

The Baculovirus expression system (Berger et al., 2004), (Fitzgerald et al., 2006) allows for the expression of multi protein complexes by the use of a recombinant Baculovirus, which contains all necessary encoding genes for the multi protein complex (Sahlmüller et al., 2011). This virus is used to infect SF9 insect cells, which are used for virus propagation and protein expression. The Baculoviruses are insect specific double stranded DNA viruses with a genome of 80 to 180 kbs. For recombinant protein expression most often the *Autographa california Nuclear Polyhedrosis* virus (AcNPV) with a genome size of 130 kbps is used. In the Baculo virus expression system the heterologous expressed gene is under the control of the strong *p10* or polyhedron (*polH*) promotors. The expression from these promotors is activated in the late phase of replication approximately 20 to 24 hours after infection.

The Baculo virus expression system is defined by two key components:

The first component are the transfer vectors pFBDM and pUCDM (pFBDM used in this thesis), which are designed for the generation of multigene- expression cassettes.

The second component is the engineered Baculovirus genome (MultiBAC) with improved protein production properties and the ability to introduce multigene-expression cassettes by recombination via *TN7* transposition or Cre/Lox recombination.

Both transfer vector contain an expression cassette with two multiple cloning sites, which is flanked by the p10 or the polyhedron (polH) promotor and HSVtk polyA- or the SV40 polyA terminator sequence. The multiplication module for the gene assembly is located between the two promotor sequences.

The pFBDM vector contains an ampicillin resistance gene (Ap^R) and two Tn7 transposition sites (Tn7L and Tn7R), which are flanking the expression cassette and a gentamycin (Gm^R) resistance gene. pFBDM is a high copy plasmid (> 20 copies per cell) with a ColEI replication origin, which is regulated by antisense RNA.

The pUCDM vector contains a *LoxP* sequence, which enables Cre/Lox recombination. Because of its *R6Ky* replication origins the pUCDM vector (15-250 copies per cell) can only be propagated in pir+-cells (Metcalf et al., 2004). The replication and copy number of pUCDM is regulated by the interaction of the γ-protein expressed by the pir+-cells with the interon of the g replication origin (Kuunimalaiyaan et al., 2005). The pUCDM vector contains the resistance gene chloramphenicol (Cm^R). The propagation of the Bacmid in pir-negative cells in the presence of chloramphenicol is dependent on a successful Cre/Loc recombination of the pUCDM vector.

In both transfer vectors enable the incorporation of as many genes in the expression cassette as necessary by the use of the multiplication module. The multiplication module is composed of four restriction sites. The sites *SpeI* and *NurI* are located between the two multiple cloning sites. The sites *PmeI* and *AvrII* are located downstream of the multiple cloning sites. The expression cassette, containing one or two heterologous genes, can be cut out from one transfer vector with the restriction sites *AvrII* and *PmeI*. The excised cassette can then be inserted in the Multiplication module of another transfer vector, which already contains one or two heterologous genes. The multiplication module can be opened with the

restriction sites S*peI* and *NurI* and the expression cassette is ligated in the second transfer vector. The restriction sites are eliminated in the process. *PmeI* and *NruI* are blunt end cutters, whose recognition sites are eliminated upon ligation. *SpeI* and AvrII are forming compatible sticky ends, but also the recognition sites of both enzymes are eliminated in the process. The resulting new transfer vector contains all heterologous genes (up to four after one use of the multiplication module) and a new multiplication module, which can be used again. The restriction sites *NruI* and *SpeI* in the new transfer vector are introduced by the ligated expression cassette. The restriction sites *PmeI* and *AvrII* in the new transfer vector were derived from the second transfer vector in which the expression cassette was ligated. The process can be repeated as often as necessary for the incorporation of all desired genes in the expression cassette.

After the generation of the transfer constructs these constructs are transformed into *E. coli* Dh10b MultiBac or *E. coli* Dh10b MultiBac^{Cre} cells. In the cells the recombination of the MultiBac-DNA takes place. Both bacterial strains contain the modified Baculoviral genome, which is replicated within the cells and a Tn7 helper plasmid, which contains a tetracyclin resistance (Tc^{R}). In the pFBDM constructs the expression cassette and a baculoviral promotor are flanked by by the left and right Tn7 sites. During Tn7 transposition the expression cassette is integrated in the MultiBac-Bacmid (selection blue/white screening, gentamycin). The Tn7 helper plasmid is delivering transposition proteins, which are involved in the recombination. *TnsA* and *TnsB* are forming together the Tn7-transposase. The Tn7-transposase cuts the transposon out of the donor DNA and integrates it into the target DNA. The regulatory protein *TnsC* activates the transposon and is interacting with the target DNA and the regulatory proteins *TnsD* or *TnsE*. In the presence of *TnsD* the transposon is integrated in the chromosomal *attTn7* recognition sequence.

The *E. coli* Dh10B^{Cre} cells contain an additional Cre helper plasmid (pBADZ), which encodes for the Cre-recombinase. The Cre-recombinase enables the integration of pUCDM constructs into the MultiBac-Bacmid (selection chloramphenicol). The Cre/Lox recombination system is derived from the bacteriophage P1 (Sauer, 1987) and promotes the divison of prophage P1. The Cre protein (38 kDa) is binding to the corresponding 34 bps LoxP sequence. It brings together the regions of recombination in the synapse process, cuts the DNA and ligates it to its new recombinated form (Shaikh and Sadowski, 1996).

To improve the quality of the expressed proteins two genes in the baculoviral DNA, Chitinase A and Chathepsin, were disrupted. This was done to reduce the virus dependent proteolysis and cell lysis, which reduces the contamination with proteases and metabolic products. Instead a LocP sequence was introduced as recipient for pUCDM constructs introduced by Cre-recombinase mediated katalysis. Within the *lacZ*α genes a *miniatt*-Tn7 sequence as recipient for Tn7-elements introduced by Tn7 transposition from pFBDM donor constructs is located. This enables a blue/white screening. In presence of the light sensitive substrate 5-brom-3-indolyl-b-D-galactopyranosid (BluoGal) and Isopropyl-β-D-galactopyranosid (IPTG) blue colonies are growing if the *lacZ* gene is intact. Upon Tn7 transposition the l*acZ* gene is disrupted, which results in the growth of white colonies. The MultiBac-Bacmid also contains a *mini-F replicon*, which enables a regulated replication and ensures that the Bacmid is present in a low copy number (1-2 copies per cell). Two antibiotic resistance genes kanamycin (Kn^R) and ampicillin (Ap^R) are encoded on the MultiBac-Bacmid, which are used for selection.

After the recombination of the MultiBac-Bacmid the resulting recombinant baculoviral DNA is purified and used for transfection of Sf9 insect cells. The produced virus is released in the supernatant of the insect cell medium. This viral stock is then used to infect fresh insect cells for propagation of the virus and subsequent expression of the encoded proteins.

Eukaryotic cell lines and growth media

Culturing of the insect cells was carried out at 27°C in Infors Incubators at 140 rpm for volumes between 100 ml and 500 ml in roller bottles and at 60 rpm for volumes between 25 ml and 100 ml in 250 ml flasks.

cell line	description	growth media	origin
Sf9	Ovary cells of *Spodopthera frugiperda*	SF900 II SFM	Invitrogen
Sf9	Ovary cells of *Spodopthera frugiperda*	921ΔSeries Methionine deficient	Expression systmes

Table 26: Eukaryotic cell lines and growth media

Cultivation of insect cells

For recombinant protein expression the insect cell line Sf9 (Summers and Smith, 1987) was used. The cell line is derived from a clone of the Sf21 cell line (Vaughn et al., 1977), of a ovary cell line of *Spodopthera frugiperda*. Sf9 cells can be cultivated adherent (monolayer culture) as well as in suspension culture. In both cases the cultivation was done at 27 °C and at ambient humidity. Under these conditions the doubling time of the culture is approximately 22 hours.

Monolayer culture

In the Monolayer culture the cells were grown adherent at the bottom of a 75 cm^2 cell culture flask (Greiner Bio One GmbH, Sollingen) with 20 ml of SF900 II SFM medium (Invitrogen, Karlsruhe). When the cells reached 100 % confluency they were detached from the bottom the flask by tapping the flask strongly on the bottom. The resulting cell suspension was split in three new flasks with equal volumes and the volume was adjusted to 20 ml with fresh medium. The Monolayer culture was used to take new cells in culture after thawing them and for the lipo-transfection of insect cells.

Suspension culture

Suspension cultures were grown in 250 ml Erlenmeyer flasks for volumes of 25 ml to 50 ml at 60 rpm and in 2 l roller bottles for volumes between 100 to 500 ml at 140 rpm in Infors HT Multitron incubators at 27 °C with SF900 II SFM medium. For culturing of SF9 cells in suspension Sf9 cells from 4 confluent Monolayer cultures were detached and transferred first to a 250 ml flask in 50 ml medium. The cell density of the culture was observed regularly (approximately every two to three days) and was kept between 1 $x10^6$ and 8 x 10^6 cells per milliliter. The cells density was determined using a *Neubauer cell counting chamber* (Roth, Karslruhe). Suspension cultures were used for culturing larger amount of cells, for virus propagation and for recombinant protein expression.

Freezing and Thawing of insect cells

For freezing 1 x 10^7 cells per milliliter were frozen in a mixture of 0.6 ml SF900 II SFM medium, 0.3 ml FCS and 0.2 ml Dimethyl sulfoxide (DMSO) in a cryo tube (Thermo Fisher). After 1 to 2 hours in the fridge the cryo tubes were transferred for 24 hours to -80°C for freezing and then stored in liquid nitrogen. For thawing the frozen insect cells were thawed at 37 °C in a water bath. The thawed cells were spun down in a centrifuge for 3 minutes at 1500 rpm at 4°C. The supernatant was discarded and the cell pellet was resuspended in Sf900 II SFM medium to remove DMSO and transferred to a cell culture flask.

Determination of cell viability

The cell viability was controlled using trypane blue staining. An aliquot was taken from a suspension culture and mixed with the equal volume of a 0.2 % trypane blue solution. After that the living (unstained) and the dead cells (blue stained) were counted in a Neubauer cell counting chamber. The cell number was calculated with the following equation:

z (cell number per milliliter)

Z (cell number in large square of Neubauer chamber)

V (Dilution factor)

$$z = Z * V * 10^4$$

Preparation of recombinant MultiBac Bacmids

The genome of the Baculovirus is too large to be used in cloning steps. To avoid this, the genes for heterologous protein expression were cloned in the transfer vector pFBDM. The resulting transfer vectors were than transformed into *E. coli* Dh10b MultiBac cells. In the cells the genes for heterologous protein expression where integrated into the MultiBac Bacmid by recombination.

Tn7 transposition between pFBDM Tn7 elements and MultiBac bacmid

10 ng DNA of the pFBDM construct was mixed with 40 µl of electro compentent *E. coli* Dh10b MultiBac cells and transformed by electroporation. After 5 hours of incubation at 37°C the transformation reaction was streaked on LB-agar plates containing the antibiotics as well as IPTG and Bluo-Gal. The agar plates were incubated at 37 °C for 24 to 48 hours. Colonies with successful recombination were selected by blue-white screening. White colonies were inoculated in 3 ml LB- medium containing antibiotics ampicillin, tetracyclin, kanamycin and gentamycin for Bacmid isolation. The culture was incubated at 37 °C and 180 rpm for 24 hours. The Bacmid DNA was isolated by the process of alkaline lysis using the buffers of the NucleoSpin Plasmid Kit (Macherey Nagel). 1.5 ml of the overnight culture was used for the Bacmid isolation. After the alkaline lysis the DNA in supernatant of the neutralized lysate (900 µl) was precipitated with isopropanol (700 µl). The resulting DNA pellet was washed with 1 ml of 70 % v/v Ethanol and dried at room temperature for 5 minutes. The dried Bacmid pellet was resupended in 20 µl steril H_2O.

Transfection of Sf9 insect cells

The preparation of recombinant infectious Baculovirus was done by transfection of the recombinant MultiBac Bacmid in Sf9 insect cells using the transfection reagent X-tremeGene HP (Roche, Basel). Insect cells at a density of 0.8 x 10^6 per 3 ml were sown in a six-well-plate with 3 ml of cell suspension per well. The recombinant Bacmid DNA resuspended in 20 µl steril H_2O was mixed with 200 µl of SF900 II SFM medium. In a separate 1.5 ml Eppendorf tube 100 µl SF900 II SFM medium was mixed with 15 µl X-treme Gene HP transfection reagent. After the cells had attached to the bottom of the six-well-plate the medium-tranfection reagent mix was mixed with the DNA. 167 µl of this final mixture was pipetted in two wells of the six-well-plate, harboring the insect cells. The plates were incubated for approximately 60 hours at 27 °C.

Amplification of virus

The primary virus was harvested after 60 hours. The supernatants of the two wells transfected with the same Bacmid were pooled and transferred to a 15 ml Falcon tube and stored at 4 °C in the dark. 2 ml of SF900 II SFM medium was added to the cells in the six-well-plate. The plate was incubated for 48 hours at 27 °C for a test expression. For virus amplification 25 ml insect cells at a density of 0.8 x 10^6 were put into 250 ml Erlenmeyer flasks. Replicates of these cells were infected with 300 µl, 600 µl, 1 ml and 3 ml of the primary virus stock. The infected cells were incubated at 27 °C and 80 rpm. The cells were counted the next day. If the cells had divided, they were diluted by adding 25 ml of SF9 II SFM to a total volume of 50 ml. If the cells had not divided, they were not diluted. The cells were incubated another 48 hours at 27 °C and 80 rpm. After 48 hours the secondary virus was harvested. The cell suspension was transferred to a 50 ml Falcon tube. The cells were spun down by centrifugation for 5 minutes at 2000 rpm and 4 °C. The supernatant was transferred to a new 50 ml falcon tube and stored at 4 °C in the dark. For expression control the cells of the primary virus are harvested after 48 hours. The cells of the two wells transfected with the same Bacmid are combined, spun down and resuspended in 150 µl H_2O and 50 µl 4 x SDS sample buffer. For expression control of the secondary virus a 1 ml sample of the cell suspension is taken before harvesting the virus, spun down and resuspended in 60 µl H_2O and 20 µl 4 x SDS sample buffer. Both expression controls are analyzed by SDS page and compared to uninfected SF9 cells.

In most cases the secondary virus is sufficient to infect large cultures for protein expression. If more virus is required a tertiary virus can be prepared. For the tertiary virus 200 ml insect cells at a density of 0.8 x 10^6 are placed in a 500 ml Erlenmeyer flask and infected with 5 ml of the secondary virus. The tertiary virus is incubated for 72 hours at 27°C and 140 rpm. After the incubation this virus is harvested and stored at 4 °C in the dark.

Preparation of Baculo infected insect cell stocks (BIIC stocks)

Since recombinant Baculo viruses are not stable for a prolonged time (more than 2 moths) virus infected insect cells can be prepared, which can be stored frozen for several years. To

prepare the stocks 200 ml insect cells at a density of 1.0 x 10^6 are infected with 4 to 10 ml of secondary or tertiary virus (depending on the virus titer) and incubated at 27 °C and 140 rpm for 24 hours. After the incubation the infected cells are harvested by centrifugation at 500 rpm and 4 °C for five minutes. The supernatant is discarded and the cells are resuspended in a mixture of 12 ml SF900 II SFM medium, 6 ml FCS and 2 ml DMSO. From the resulting suspension aliquots of 1 ml are prepared in cryo tubes. The stocks are stored for one to two hours at 3 °C and then transferred to -80 °C for freezing. After 24 hours the frozen stocks are transferred to liquid nitrogen for long term storage. The infected cells can used to infect a new expression culture.

Test expression with secondary or tertiary virus

To determine the optimal amount of virus to be used in expressions 25 ml insect cells at a density of 2 x 10^6 are transferred to 250 ml Erlenmeyer flasks. Replicates of these cells are infected with 0.25 ml, 0.5 ml, 1 ml and 2 ml of secondary or tertiary virus. The test expression is incubated at 27 °C at 80 rpm for 72 hours. After the incubation 1 ml samples from each flask are taken and spun down. The cells are resuspended in 150 µl H_2O and 50 µl 4x SDS sample buffer. The test expression is analyzed by SDS-page.

Test expression with BIIC-stocks

To determine the optimal amount of BIIC-stock to be used in expressions 25 ml insect cells at a density of 2 x 10^6 are transferred to 250 ml Erlenmeyer flasks. Replicates of these cells are infected with 25 µl, 50 µl, 75 µl, 100 µl and 125 µl of the thawed BIIC stock. The test expression is incubated at 27 °C at 80 rpm for 96 hours. After the incubation 1 ml samples from each flask are taken and spun down. The cells are resuspended in 150 µl H_2O and 50 µl 4x SDS sample buffer. The test expression is analyzed by SDS-page.

Overexpression of proteins in Sf9 insect cells

Overexpression was carried out in 500 ml cultures in rollerbottels at a cell density of 2 x 10^6 cells per milliliter. The cultures were infected with a suitable amount of secondary or tertiary virus. The amount was determined separately for each virus as described above. Infected cells were incubated at 27 °C for three days. After that the cells were harvested by centrifugation at 2000 rpm for five minutes at 4 °C. The cell pellet was washed with 50 ml of PBS and frozen in liquid nitrogen. The frozen pellet was stored at -80 °C until it was used. If the infection of expression cultures was carried out with BIIC-stocks the incubation time was prolonged to four days before the cells were harvested.

4.1.29 Selenomethionine labelling of coatomer subcomplexes in insect cells

To obtain additional phase information to solve crystal structures coatomer subcomplexes were labelled with selenomethionine. L-Selenomethionine is a natural occurring amino acid, which can be used as an anomalous scatterer if introduced in the amino acid sequence of proteins to solve the phase problem in crystallography using single- (SAD) or multi-wavelenght anomalous diffraction (MAD). In the Baculovirus expression system selenomethionine incorporations of up to 75 % can be achieved. The protein in yield in the overexpression is reduced because of selenomethionine toxicity dependend on the amount of selenemethionine that is used. The expression of recombinant proteins in the Baculovirus system starts between 16 to 20 hours post infection with the virus. For seleneomethionine labeling of proteins in the Baculovirus system two time windows have to be considered. The first window is determined by the time point, at which the medium of the culture is exchanged to methionine-free medium. The first time window determines the time the virus has for the infection of the culture and the production of more viruses. The second window is defined by the time point, at which selenomethionine is added to the culture. The second time window determines the time, in which the culture is depleted of residual methionine. Both time windows have two be determined experimentally for each virus. Also the amount of selenomethionine used is critically. Higher concentrations of selenomethionine improve the labeling efficiency but at the same time also reduce the protein yield. In general concentrations between 100 mg/l and 200 mg/l are used. However 200 mg/l

selenemethionine reduce the protein yield to approximately 35 % of an unlabeled expression. To label proteins with selenomethionine a 500 ml culture in SF99 II SFM medium (Invitrogen) was infected with the suitable amount of secondary virus and incubated at 27 °C and 140 rpm for the predetermined time of 6 to 10 hours. The cells were harvested by centrifugation at 1000 rpm at 25 °C for five minutes. The cell pellet was washed one time with 921ΔSeries Methionine deficient medium (Expression systems, USA) to remove residual methionine. The cell pellet was resuspended in 500 ml of pre-warmed 921ΔSeries Methionine deficient medium and incubated for the predetermined time of 6 to 10 hours at 27 °C and 140 rpm. After the incubation L-selenomethionine at a concentration of 150 mg/l dissolved in 921ΔSeries Methionine deficient medium was added to the culture. The expression was continued for 3 days at 27 °C and 140 rpm. After that the cells were harvested by centrifugation at 2000 rpm for five minutes at 4 °C. The cell pellet was washed with 50 ml of PBS and frozen in liquid nitrogen. The frozen pellet was stored at -80 °C until it was used.

4.1.30 Expression of recombinant *Chaetomium thermophilum* NΔ20CtArf

The soluble form of *Chaetomium thermophilum* Arf was expressed in *E. coli Bl21 (DE3)* cells. *E. coli Bl21 (DE3)* cells were transformed with the expression construct pETM11-NΔ20CtArf and selected for the kanamycin resistance encoded by the plasmid. A single colony from this transformation was used to inoculate on overnight culture of 200 ml LB-medium with 50 µg/ml kanamycin, which was incubated at 37 °C. This overnight culture was used the next day to inoculate two times 2 liters of LB-medium with 50 µg/ml kanamycin to an OD_{600} nm of 0.1 as expression cultures. The expression cultures were incubated at 37 °C and 80 rpm until an OD_{600} nm of 0.6 was reached. The expression of NΔ20CtArf was induced by addition of IPTG to a final concentration of 1 mM. After induction the expression culture was incubated for four hours at 37 °C and 80 rpm. The cells were harvested by centrifugation at 6000 rpm for ten minutes at 4 °C. The cell pellets were washed one time with 50 ml PBS and then frozen in liquid nitrogen until they were used. The mutant forms of soluble *Chaetomium thermophilum* Arf NΔ20CtArfQ74L and NΔ20CtArfT34N were expressed the same way as the wild type.

4.1.31 Expression of recombinant *Chaetomium thermophilum* coatomer subcomplexes in bacteria

Chemical competent *E.coli Bl21 (DE3)* or *E. coli rosetta(DE3)plysS* cells were transformed with the respective pET24d, pET-DUET or pETM11 expression constructs and selected for the antibiotic resistance encode by the expression plasmid. A single colony from this transformation was used to inoculate on overnight culture of 200 ml LB-medium with the respective antibiotic, which was incubated at 37 °C. This overnight culture was used the next day to inoculate the expression culture to an OD_{600} nm of 0.1. The expression cultures were incubated at 37 °C and 80 rpm until an OD_{600} nm of 0.6 was reached. The overexpression of the coatomer subcomplexes was induced by addition of IPTG to a final concentration of 1 mM. After induction the expression culture was incubated for four hours at 37 °C and 80 rpm. The cells were harvested by centrifugation at 6000 rpm for ten minutes at 4 °C. The cell pellets were washed one time with 50 ml PBS and then frozen in liquid nitrogen until they were used.

4.2 Biochemical methods

4.2.1 Sodium dodecyl sulfate polyacrylamide gel electrophoresis (SDS-PAGE)

Analytical separation of proteins was performed by discontinuous sodium dodecyl sulfate gel electrophoresis (SDS-PAGE) (Laemmli, 1970) or with commercially available gradient gels (Invitrogen, Karlsruhe). The protein samples were denatured and reduced by mixing with β-mercaptoethanol containing SDS sample buffer. Depending on the protein samples, which were to be separated, resolving gels between 7.5 % and 15% were used, which were overlaid with a 4 % stacking gel. Electrophoresis was carried out in Mini Protean III gel electrophoresis chambers (Biorad, Munich) at constant voltage of 100 V to 200 V. Polymerization of the acrylamide bisacrylamide mixture was started by addition of ammonium peroxy sulfate (APS) and N,N,N,N-tetramethylethylendiamine (TEMED). After the resolving gel was poured between the glass plates it was immediately overlaid with isopropanol. After polymerization the isopropanol was discarded and the gel surface was

dried. After that the stacking gel was poured on the resolving gel. Protein samples were mixed with 4 x SDS sample buffer and incubated for five minutes at 95 °C for denaturing before they were loaded on the gel.

Composition of gels

Stacking gel						
percentage gel	H_2O [ml]	Tris 0.5 M pH 6.8 [ml]	30 % acrylamide bisacrylamide (37.5:1) [ml]	APS 10 % [µl]	SDS 10 % [µl]	TEMED 10 % [µl]
4	1.5	0.625	0.325	25	25	5

Resolving gel						
percentage gel	H_2O [ml]	Tris 1.5 M pH 8.8 [ml]	30 % acrylamide bisacrylamide (37.5:1) [ml]	APS 10 % [µl]	SDS 10 % [µl]	TEMED 10 % [µl]
7.5	2.43	1.25	1.25	50	50	5
10	2.02	1.25	1.35	50	50	5
12	1.67	1.25	2.0	50	50	5
15	1.18	1.25	2.5	50	50	5

Table 27: SDS-PAGE gel composition

4.2.2 Western blot

For specific size dependent detection of proteins western blot was used. Proteins, which were separated in a SDS-PAGE, where transferred to a PVDF membrane (Immobilon-P Millipore, Eschborn) using the semi-dry protocol.

Six Whatman papers (Whatman 3MM) and one PVDF membrane were cut to the same size as the gel. The Whatman papers and the gel were equilibrated in transfer buffer and the PVDF membrane was activated in 100 % methanol. The blot sandwich was arranged as follows from bottom to top on the anode plate of the blotting chamber (Biorad, Munich): Three Whatman papers, the activated PVDF membrane, the gel and three Whatman papers. On top of the blot sandwich the cathode plate was placed. The transfer was performed at constant voltage of 24 V for 90 minutes.

Proteins transferred to the PVDF membrane were detected by protein antibodies, directed against specific epitopes of the target proteins. Initially the PVDF membrane was incubated for one hour in a solution of 5 % w/v milk powder dissolved in PBS-T to block unspecific binding sites. After that the PVDF membrane was washed three times in PBS-T for ten minutes. Then the membrane was incubated for one hour in 50 milliliter of PBS-T with 1 % BSA and the optimal concentration of the primary antibody. After this incubation the membrane was washed three additional times with PBS-T and then incubated for 30 minutes with the respective fluorescent secondary antibody diluted in PBS-T with 1 % BSA. The membrane was washed two additional times with PBS-T and one time with PBS. The membrane was scanned with the Li-Cor Odyssey Imaging system (Li-Cor Biosciences Newton, USA) to visualize the detected proteins.

Antibodies

antibody	antigen	epitop	species	dilution	origin
Cht Arf1 CT	Chaetomium Arf1	C-terminal peptide	rabbit	1:5000	AG Wieland
HIS antibody	Anti-his		mouse	1:2000	Qiagen
Strep-tagII	One Strep Tag		mouse	1:5000	IBA
GST	Vam3-GST		rabbit	1:2000	Ungerman

Table 28: Antibodies

As secondary antibodies goat-anti-rabbit Alexa Fluor 680 or goat-anti-mouse Alexa Fluor 680 from Invitrogen (Karlsruhe) were used. Antibodies were diluted 1:10000 in PBS-T with 1 % (w/v) BSA and stored at 4 °C.

4.2.3 Coomassie brilliant blue staining

For staining of proteins separated in SDS-PAGE the gel was placed in Coomassie staining solution and heated for 30 seconds in a microwave. After incubation for five to ten minutes on a shaker the staining solution was discarded and the gel was washed briefly in H_2O. The washed gel was placed in destaining solution, which was exchanged repeatedly until the gel was completely destained.

4.2.4 Bradford assay

Protein concentrations were determined with the Bradford assay (Bradford, 1976). Bradford reagent was diluted fivefold and 2 to 5 µl of protein solution were mixed with 1 ml of this solution. The mixture was incubated for ten minutes at room temperature. The absorption of the mixture at 595 nm was measured in a spectrum photometer. The protein concentration was calculated after a standard curve, which was prepared with BSA solutions of known concentrations.

4.2.5 Purification of recombinant Strep-tagged *Chaeomium thermophilum* coatomer and coatomer subcomplexes

A frozen cell pellet of a 500 ml insect cell expression culture was thawed for five minutes at 37 °C in a water bath. The thawed cells were resuspended in 25 ml lysis buffer. One tablet of complete Mini EDTA free protease inhibitor cocktail (Roche, Basel Switzerland) was added to prevent protein degradation. The resuspended cells were filtered through a syringe needle to prevent residual cell aggregates. After that the cells were lysed by passing them four times through a microfluidizer (Microfluidics, Newton USA) at 12 kPSI. The cell lysate was centrifuged at 100000 x g for one hour at 4 °C in a Beckman ultracentrifuge to pellet cell debris. After the centrifugation the supernatant was incubated with 2 ml Strep-Tactin Sepharose beads (IBA lifesciences, Göttingen), which had been equilibrated in lysis buffer, for one hour at 4 °C on a rotary wheel for binding. The beads were spun down at 3000 rpm for five minutes at 4°C. The supernatant was discarded and the beads were washed one time with 50 ml lysis buffer to remove unbound protein. After the washing step the beads were transferred to a gravity flow column (Biorad, Munich). The coatomer complex was eluted from the settled beads in 1 ml fractions by addition of elution buffer. The protein containing fractions were determined with Bradford solution and pooled. The protein concentration was determined by Bradford assay. *Chaetomium thermophilum* coatomer subcomplexes were purified using different buffers with higher salt concentration to optimize solubility.

Chaetomium thermophilum coatomer		
Buffer	**composition**	
Lysis buffer/wash buffer	HEPES/KOH pH 7.4 KCl DTT	25 mM 200 mM 1 mM
Elution buffer	HEPES/KOH pH 7.4 KCl Desthiobiotin DTT	25 mM 200 mM 2.5 mM 1 mM

Chaetomium thermophilum coatomer subcomplexes		
Buffer	**composition**	
Lysis buffer/wash buffer	Tris/HCl pH 8.0 NaCl DTT	25 mM 300 mM 1 mM
Elution buffer	Tris/HCl pH 8.0 NaCl Desthiobiotin DTT	25 mM 300 mM 2.5 mM 1 mM

Table 29: *Chaetomium* coatomer Strep tactin purification buffers

4.2.6 Purification of recombinant Strep-tagged *Chaeomium thermophilum* coatomer and coatomer subcomplexes by size exclusion cromytography

Affinity purified coatomer and coatomer subcomplexes were further purified using size exclusion chromytography to remove protein aggregates. The elution pool of the affinity purified proteins were concentrated to the appropriate volume using Amicon spin concentrators (Merck Millipore, Darmstadt) and subjected to size exclusion chromatography using an Ettan LC FPLC (GE Healthcare, Buckinghamshire UK) and the appropriate column for separation of the purified protein complex. The column was equilibrated in gelfiltration buffer. After equilibration the separation run was performed at the flow rate and pressure limits recommended for the respective column.

column	**flow rate [ml/min]**	**Protein complex**
Superose 6 10/300 GL	0.3 to 0.5	CM7 (heptamer) CM4 (tetramer) CM3 (trimer) CM4β686γ666 CM4β608γ586

		CM7Δe CM7δ243 β19-391δ1-124 β19-391δ1-137 β19-391δ1-175 β19-391δ1-243 β19-391δ β19-407δ βδ γζ α825β´793
Sephacryl S 300 16/60	0.3 to 0.5	CM4 CM4β686γ666 CM4β608γ586 α825β´793 β19-319δ β19-407δ
Superdex 75 16/60	0.5 to 0.8	β19-391δ1-137
Superdex 200 16/60	0.5 to 0.8	β19-391δ β19-407δ
Superdex 75 10/300 GL	0.3 to 0.5	β19-391δ1-137
Superdex 200 10/300 GL	0.3 to 0.5	β19-391δ β19-407δ

Table 30: Size exclusion chromatography columns

***Chaetomium thermophilum* coatomer**		
Buffer	**composition**	
Gelfiltration buffer	HEPES/KOH pH 7.4	25 mM
	KCl	200 mM
	DTT	1 mM
	Glycerol	10 % (v/v)

***Chaetomium thermophilum* coatomer subcomplexes**		
Buffer	**composition**	
Gelfiltration buffer	Tris/HCl pH 8.0	25 mM
	NaCl	300 mM
	DTT	1 mM
	Glycerol	10 % (v/v)

Table 31: *Chaetomium* coatomer size exclusion chromatography buffers

4.2.7 Purification of recombinant HIS_6-tagged *Chaetomium thermophilum* NΔ20CtARF

A frozen cell pellet of a 2 l expression culture was thawed for five minutes at 37 °C in a water bath. The thawed cells were resuspended in 25 ml lysis buffer. One tablet of complete Mini EDTA free protease inhibitor cocktail (Roche, Basel Switzerland) was added to prevent protein degradation. The resuspended cells were filtered through a syringe needle to prevent residual cell aggregates. After that the cells were lysed by passing them seven times through a microfluidizer (Microfluidics, Newton USA) at 12 kPSI. The cell lysate was centrifuged at 100000 x g for one hour and 20 minutes at 4 °C in a Beckman ultracentrifuge to pellet cell debris. After the centrifugation the supernatant was incubated with 4 ml Nickel Sepharose 6 fast flow beads (GE Healthcare, Buckinghamshire UK), which had been equilibrated in lysis buffer, for one hour at 4 °C on a rotary wheel for binding. The beads were spun down at 3000 rpm for five minutes at 4°C. The supernatant was discarded and the beads were washed one time with 50 ml washing buffer to remove unbound protein. After the washing step the beads were transferred to a gravity flow column (Biorad, Munich). NΔ20Arf was eluted from the settled beads in 1 ml fractions by addition of elution buffer. The protein containing fractions were determined with Bradford solution and pooled. The protein concentration was determined by Bradford assay. The buffer of the purified ND20Arf was exchanged to nucleotide exchange buffer using prepacked PD-10 desalting columns (GE Healthcare, Buckinghamshire UK). *Chaetomium thermophilum* soluble Arf mutants NΔ20ArfQ74L and NΔ20ArfT34N were purified the same way as the wild type.

***Chaetomium thermophilum* NΔ20CtArf**		
Buffer	**composition**	
Lysis buffer	HEPES/KOH pH 7.4 KCl imidazol β-mercapto ethanol	50 mM 300 mM 30 mM 2 mM
Washing buffer	HEPES/KOH pH 7.4 KCl imidazol β-mercapto ethanol	50 mM 300 mM 50 mM 2 mM
Elution buffer	HEPES/KOH pH 7.4 KCl imidazol β-mercapto ethanol	50 mM 300 mM 250 mM 2 mM
Nucelotide Exchange buffer	HEPES/KOH pH 7.0 KCl $MGCl_2$	20 mM 150 mM 2 mM

GF buffer	HEPES/KOH pH 7.5	20 mM
	KCl	150 mM
	$MgCl_2$	2 mM
	DTT	4 mM

Table 32: *Chaetomium* Arf purification buffers

4.2.8 Nucleotide exchange of *Chaetomium thermophilum* NΔ20CtArf

For nucleotide exchange to GTP or GMPPNP NΔ20Arf in nucleotide exchange buffer was mixed with 20 fold molar excess of GTP dissolved in 1 M HEPES pH 7.5, and a 1/50 molar ration of the guanine nucleotide exchange factor (GEF) ARNO. In case of an exchange to the non-hydrolysable analog GMPPNP also 2U/mg of the rAPid alkaline phosphatase (Roche, Basel Switzerland) were added to cleave residual GDP or GTP present in the GMPPNP. The complete mix was incubated at 4°C over night on a rotary wheel. The next day the mix was subjected to size exclusion chromatography to separate ARNO and free nucleotide. The size exclusion chromatography was performed using an Ettan LC FPLC (GE Healthcare, Buckinghamshire UK) and a HiLoad Superdex 75 16/60 column. The column was equilibrated in GF buffer. The peak fraction at the expected molecular weight of NΔ20Arf was collected. The protein concentration was determined by Bradford assay. 1 ml aliquots of GTP- or GMPPNP loaded NΔ20Arf were prepared, flash frozen in liquid nitrogen and stored at – 80°C until they were used.

4.2.9 Control of nucleotide state of NΔ20Arf by HPLC measurement

To control if the nucleotide exchange of NΔ20Arf was successful, an HPLC analysis was performed. A sample of the protein solution was diluted to 100 to 500 mM with GF buffer and incubated for one minute at 95 °C in order to denature NΔ20Arf and free the bound nucleotide. The denatured protein was pelleted by centrifugation for ten minutes at 14000 rpm at 4 °C. The supernatant was loaded on a HiChrom NT C18 column (MZ Analysetechnik, Mainz) equilibrated in HPLC buffer. The analytical run was performed on a model 1525 HPLC (Waters, Eschborn). Control measurements were performed for GDP, GTP and GMPPNP at

concentrations of 100 µM dissolved in 100 mM HEPES/KOH pH7.5. The detection of GDP, GTP and GMPPNP was performed at a flow rate of 1ml/min and at a wavelength of 254 nm.

Buffer	composition	
HPLC buffer	KH_2PO_4/K_2HPO_4	100 mM
	Tetra butyl ammonium bromide	10 mM
	Acetonitrile	7.5 % (v/v)

Table 33: HPLC buffer

4.2.10 Limited proteolysis

To determine the most stable domains of coatomer, which were suitable for crystallization limited proteolysis was performed with *Chaetomium thermophilum* coatomer and coatomer subcomplexes. For the limited proteolysis the protease subtilisin (Sigma Aldrich, St. Louis Missouri USA) was used. Subtilisin is a member of the serine S8 Endoproteinase family. It has a broad specificity, with a preference for large uncharged residues in the P1 position. Subtilisin is able to hydrolyze native and denatured proteins and is active under alkaline conditions. 25 µg of the respective complex were treated with a series of different molar rations of subtilisin dissolved in the same buffer as the complex. The complex was incubated with the subtilisin dilutions for 15 minutes on ice. The reaction was stopped by addition of PMSF to a final concentration of 1 mM and of 4 x SDS sample buffer and immediate heating of the sample to 95 °C for 10 minutes. The samples were separated by SDS-Page and the resulting fragments were analyzed by mass spectrometry.

Molar rations of complex and subtilisin for limited proteolysis	
complex	Subtilisin
1	1
1	0.3
1	0.1
1	0.03
1	0.01
1	0.003
1	0.001

Table 34: Limited proteolysis molar rations

4.2.11 Mass spectrometry

For mass spectrometric analysis of proteins the protein samples were separated on commercially available gradient gels (Invitrogen, Karlsruhe) and stained with colloidal Coomassie staining solution (Roti®Blue, Roth). The further treatment and analysis of the samples were done by Dr. Jürgen Reichert from the Lechner group at the BZH or by Dr. Bernd Hessling from the Mass Spectrometry facility at the ZMBH led by Dr. Thomas Ruppert.

4.2.12 Electron microscopy

Negative stain electron microscopy of coatomer and its subcomplexes was performed at the electron microscopy facility of the BZH led by Dr. Dirk Flemming. To prepare the grids for microscopy 5 µl of the protein solution at a suitable concentration (6 nM for coatomer) was placed on a glow-discharged carbon coated 400 mesh copper grid and incubated for 2 minutes. After the incubation excess liquid was removed from the grids with a piece of filter paper and the grids were washed with three drops of distilled water. The grids were stained with three drops of a 3 % (w/v) uranyl acetate solution. The last drop was left on the grid for seven minutes. After the staining residual uranyl acetate was removed with a piece of filter paper. The grids were left to dry for two minutes at room temperature. Stained grids were imaged in an EM-900 transmission electron microscop (Zeiss, Oberkochen) Acquisition of high quality images and processing of data for calculating 3D structures was done by Dr. Dirk Flemming at the Nicon Imaging Center.

4.2.13 Crystallization

Crystallization experiments were performed at the crystallization facility of the BZH led by Dr. Jürgen Kopp. *Chaetomium thermophilum* coatomer subcomplexes were tested in different concentration in crystallization screens. As initial screens JCSG I to IV screens were set up as sitting drop screens in 96 well plates. The volume ration of protein solution to crystallant solution was 1 : 1 in initial screens with a drop size of 0.5 µl. Initial screens were tested at 4 °C and at 18 °C. As additional screens a PEG-screen was used. For refinement of

conditions also an Additiv-Screen and an Optimizer-Screen were tested. All crystallization screens were done with subcomplexes of *Chaetomium thermophilum* coatomer.

4.2.14 Co-crystallization

For co-crystallization of coatomer subcomplexes with the soluble form of the small GTPase Arf in its GTP bound state both proteins were purified separately in a buffer of 25 mM Tris, 150 mM NaCl, 5 mM $MgCl_2$ and 1 mM DTT at pH 7.5. For the co-crystallization experiments the mutant NΔ20ArfQ74L was used, which is defective in GTP hydrolysis. After the purification the coatomer subcomplex and the small GTPase were mixed at a ratio of 1 to 1.2 or 1 to 2.4 depending on the number of the expected binding sites on the subcomplex. The co-crystallization was tested with different concentration of the mixed proteins. As initial screens JCSG I to IV screens were applied as sitting drop screens in 96 well plates. Crystallization was tested at 4 °C and at 18 °C.

4.2.15 Pull down assays

To test coatomer subcomplexes for binding of Arf 200 to 400 µg of the respective subcomplex was immobilized on 50 µl strep tactin sepharose beads by incubation for one hour at 4 °C on a rotary wheel. After immobilization of the subcomplex the beads were washed with washing buffer (25 mM Tris, 150 mM NaCl, 5 mM $MgCl_2$ 1 mM DTT, pH 7.5) to remove unbound protein. The beads were pelleted by centrifugation and samples of 20 µl beads (50 %) were taken for each subcomplex and mixed with 7 µl 4 x SDS sample buffer. The soluble form of the small GPase Arf in its GTP bound state was added to the immobilized subcomplexes and incubated at 4 °C for one hour on a rotary wheel. After the incubation the beads were washed extensively with washing buffer to remove unbound protein. Aftzer washing the beads were pelleted by centrifugation and samples of 20 µl beads (50 %) were taken for each subcomplex and mixed with 7 µl 4 x SDS sample buffer. The proteins bound to the beads were analyzed by SDS-PAGE and western blot.

4.2.16 Preparation of liposomes

To prepare unilamelar Golgi-like liposomes the lipids listed in table 35 were mixed in a glass vial with teflon cap. Chloroform was added to the mix to a final volume of 4 ml to achieve a lipid-mix concentration of 3 mM. Aliquots of the lipid mix were prepared in chloroform stable 2 ml Eppendorf tubes. The chloroform was evaporated under a gentle stream of nitrogen. After that the tubes were covered with parafilm that was punctured with a needle and the tubes were left for 2 hours to dry in a desiccator. The dried Golgi-like lipid-mix was overlaid with argon and stored at -80°C.

golgi-like lipidmix	
lipid	**mol %**
phosphatidlycholin (PC)	43
phosphatidylethanolamin (PE)	19
phosphatidylserin (PS)	5
phosphatidylinositol (PI)	10
sphingomyelin (SM)	7
cholesterol	16

Table 35: Golgi-like lipid mix composition

The dried lipid-mix was resuspended in the desired volume of chloroform and mixed with 1 mol % of PIP_2 and 15 nmol of P23 lipopeptide. After that the chloroform was evaporated under nitrogen as described above. The dried lipids were resuspended in the desired volume of HKM buffer to achieve the final liposome concentration (usually 2 mM). The dissolved lipids were mixed by vortexing and shock-frozen in liquid nitrogen. After that the liposome were thawed again at 37 °C in a water bath. The liposomes were subjected to 7 freeze-thaw cycles, frozen after the last cycle and stored at -80° C before they were used. Liposomes that were used for UV-crosslinks were resuspended in MKM buffer as HEPES can produce radicals upon UV-radiation.

Buffer	composition	
HKM	HEPES/KOH pH 7.2	20 mM
	K-acetate	150 mM
	Mg-acetate	2 mM
MKM	MOPS/KOH pH 7.2	20 mM
	K-acetate	150 mM
	Mg-acetate	2 mM

Table 36: Buffers liposome preparation

4.2.17 Binding of *Chaetomium* coatomer to golgi-like liposomes

Golgi-like liposomes with 1 mol % PI(4,5)P_2 and 3 mol % p23 lipopeptide at a final concentration of 300 µM were mixed with 50 µg *Chaetomium* coatomer, 5 µg *Chaetomium* Arf, 1 µg ARNO and 1 mM GTP in a final volume of 250 µl in HKM buffer and incubated at 37°C for 15 minutes. A 5 µl sample was taken as input control for SDS-PAGE and western-blot analysis. The sample was transferred in SW60 Ti tubes and underplayed with 50 µl 37 % (w/w) sucrose and 5 µl 50 % (w/w) sucrose both in HKM buffer. The density gradient was centrifuged for 50 minutes at 100000 x g and 4 °C in a SW60 Ti rotor with adaptors. The vesicle containing fraction of 16 µl was taken at the interface of both sucrose cushions and analysed by SDS-PAGE, western-blot and negative stain electron microscopy.

4.2.18 Site directed UV-Crosslink with ArfY167Bp

To investigate the binding of Arf to beta/delta-COP photo-crosslinking was employed. Therefore ArfY167Bp incorporating the photolabile amino acids p-benzoyl-phenylalanine in position 167 replacing the native tyrosine was used as crosslinking reagent. For generation of photolabile Arf the system developed by Schultz and co-workers was used (Chin et al., 2002). The plasmid for expression of ArfY167Bp was created by Dr. Simone Röhling (BZH, Heidelberg). Benzophenone the photoactive group of p-benzoyl-phenylalanine is forming a radical upon UV irradiation. The radical is forming a covalent bond with carbon-hydrogen bonds in the distance of 3 Å. For the crosslinking reaction 5 µg ArfY167Bp was mixed with 0.4 µg ARNO, 100 µM GTPγS and 500 µM golgi-like liposomes in a final volume of 100 µl in MKM buffer and incubated at 37 °C for 10 minutes. β19-391δ was added and incubation was

resumed at 37°C for 10 minutes. Membranes were pelleted by centrifugation at 16000 x g for 30 minutes at 4 °C. The pellet was resuspended in 10 µl MKM buffer and irradiated with 15 1 second UV_{366} pulses with 1 second pause between each pulse on ice. After irradiation the sample was mixed with 3.5 ml 4 x SDS sample buffer, heated for 10 minutes at 95 °C and separated on a BIS-Tris 4-12% gradient gel (ThermoFisher). The gel was analysed by western blot and massspectrometry.

5 Literature

Amlacher, S., P. Sarges, D. Flemming, V. van Noort, R. Kunze, D.P. Devos, M. Arumugam, P. Bork, and E. Hurt. 2011. Insight into structure and assembly of the nuclear pore complex by utilizing the genome of a eukaryotic thermophile. *Cell*. 146:277-289.

Amor, J.C., D.H. Harrison, R.A. Kahn, and D. Ringe. 1994. Structure of the human ADP-ribosylation factor1 complexed with GDP. *Nature*. 372:704-708.

Antonny, B., S. Beraud-Dufour, P. Chardin, and M. Chabre. 1997. N-Terminal Hydrophobic Residues of the G-Protein ADP-Ribosylation Factor-1 Insert into Membrane Phospholipids upon GDP to GTP Exchange. *Biochemistry*. 36:4675-4684.

Antonny, B., D. Madden, S. Hamamoto, L. Orci, and R. Schekman. 2001. Dynamics of the COPII coat with GTP and stable analogues. *Nature Cell Biology*. 3:531-537.

Arakel, E.C., K.P. Richter, A. Clancy, and B. Schwappach. 2016. δ-COP contains a helix C-terminal to its longin domain key to COPI dynamics and function. *Proceedings of the National Academy of Sciences (PNAS)*:1-6.

Bannykh, S.I., and W.E. Balch. 1997. Membrane dynamics at the endoplasmic reticulum-Golgi interface. *The Journal of Cell Biology*. 138:1-4.

Barlowe, C., C. d'Enfert, and R. Schekman. 1993. Purification and Characterization of SARlp, a Small GTP-binding Protein Required for Transport Vesicle Formation from the Endoplasmic Reticulum. *The Journal of Biological Chemistry*. 268:873-879.

Barlowe, C., L. Orci, T. Yeung, M. Hosobuchi, S. Hamamoto, N. Salama, M.F. Rexach, M. Ravazzola, M. Amherdt, and R. Schekman. 1994. COPII: A Membrane Coat Formed by Set Proteins That Drive Vesicle Budding from the Endoplasmic Reticulum. *Cell*. 77:895-907.

Barlowe, C., and R. Schekman. 1993. Sec12 encodes a guanin-nucleotide-exchange factor essential for transport vesicle budding from the ER. *Nature*. 365:347-349.

Beck, R., F. Adolf, C. Weimer, B. Brügger, and F.T. Wieland. 2009. ArfGAP1 Activity and COPI Vesicle Biogenesis. *Traffic*. 10:307-315.

Beck, R., S. Prinz, P. Diestelkötter-Bachert, S. Röhling, F. Adolf, K. Hoehner, S. Welsch, P. Ronchi, B. Brügger, J.A.G. Briggs, and F.T. Wieland. 2011. Coatomer and dimeric ADP ribosylation factor 1 promote distinct steps in membrane scission. *The Journal of Cell Biology*. 194:765-777.

Belden, W.J., and C. Barlowe. 2001. Role of Erv29p in collecting soluble secretory proteins into ER-derived transport vesicles. *Science*. 294:1528-1531.

Beraud-Dufour, S., S. Robineau, P. Chardin, S. Paris, M. Chabre, J. Cherfils, and B. Antonny. 1998. A glutamic finger in the guanine nucleotide exchange factor ARNO displaces Mg2 and the β-phosphate to destabilize GDP on ARF1. *The EMBO Journal*. 17:3651-3659.

Berger, I., D.J. Fitzgerald, and T.J. Richmond. 2004. Baculovirus expression system for heterologous multiprotein complexes. *Nature biotechnology*. 22:1583-1587.

Béthune, J., M. Kol, J. Hoffmann, I. Reckmann, B. Brügger, and F.T. Wieland. 2006a. Coatomer, the Coat Protein of COPI Transport Vesicles, Discriminates Endoplasmic Reticulum Residents from p24 Proteins. *Molecular and Cellular Biology*. 26:8011-8021.

Béthune, J., F.T. Wieland, and J. Moelleken. 2006b. COPI-mediated Transport. *The Journal of Membrane Biology*. 211:65-79.

Bhattacharya, N., J. O´Donnell, and S.M. Stagg. 2012. The Structure of the Sec13/31COPII Cage Bound to Sec23. *Journal of Molecular Biology*. 420:324-334.

Bigay, J., J.F. Casella, G. Drin, B. Mesmin, and B. Antonny. 2005. ArfGAP1 responds to membrane curvature through the folding of a lipid packing sensor motif. *The EMBO Journal*. 24:2244-2253.

Blagitko, N., U. Schulz, A.A. Schinzel, H.H. Ropers, and V.M. Kalscheuer. 1999. γ2-COP, a Novel Imprinted Gene on Chromosome 7q32, Defines a New Imprinting Cluster in the Human Genome. *Human Molecular Genetics*. 8:2387-2396.

Boehm, M., and J.S. Bonifacino. 2001. Adaptins The Final Recount. *Molecular Biology of the Cell*. 12:2907-2920.

Boguski, M.S., and F. McCormick. 1993. Proteins regulating Ras and its relatives. *Nature*. 366:643-654.

Bradford, M.M. 1976. A rapid and sensitive method for the quantitation of microgram quantities of protein utilizing the principle of protein-dye binding. *Analytical Biochemistry*. 72:248-254.

Chaudhuri, R., R. Mattera, O.W. Lindwasser, M.S. Robinson, and J.S. Bonifacino. 2009. A Basic Patch on -Adaptin Is Required for Binding of Human Immunodeficiency Virus Type 1 Nef and Cooperative Assembly of a CD4-Nef-AP-2 Complex. *Journal of virology*. 83:2518-2530.

Chin, J.W., A.B. Martin, D.S. King, L. Wang, and P.G. Schultz. 2002. Addition of a photocrosslinking amino acid to the genetic code of Escherichia coli. *Proceedings of the National Academy of Sciences (PNAS)*. 99:11020-11024.

Claude, A., B.P. Zhao, C.E. Kuziemsky, S. Dahan, S.J. Berger, J.P. Yan, A.D. Armold, E.M. Sullivan, and P. Melançon. 1999. GBF1: A Novel Golgi-associated BFA-resistant Guanine Nucleotide Exchange Factor That Displays Specificity for ADP-ribosylation Factor 5. *The Journal of Cell Biology*. 146:71-84.

Collins, B.M., A.J. McCoy, H.M. Kent, P.R. Evans, and D.J. Owen. 2002. Molecular Architecture and Functional Model of the Endocytic AP2 Complex. *Cell*. 109:523-535.

Cosson, P., and F. Letourneur. 1997. Coatomer (COPI)-coated vesicles: role in intracellular transport and protein sorting. *Current Opinion in Cell Biology*. 9:484-487.

Crowther, R.A., and B.M.F. Pearse. 1981. Assembly and Packing of Clathrin into Coats. *The Journal of Cell Biology*. 91:790-797.

Cukierman, E., I. Huber, M. Rotman, and D. Cassel. 1995. The ARF1 GTPase-Activating Protein: Zinc Finger Motif and Golgi Complex Localization. *Science*. 270:1999-2002.

DiNitto, J.P., A. Delprato, M.T. Gabe Lee, T.C. Cronin, S. Huang, A. Guilherme, M.P. Czech, and D.G. Lambright. 2007. Structural Basis and Mechanism of Autoregulation in 3-Phosphoinositide Dependent Grp1 Family Arf GTPase Exchange Factors. *Molecular Cell*. 28:569-583.

Dodonova, S.O., P. Diestelkoetter-Bachert, A. von Appen, W.J.H. Hagen, R. Beck, M. Beck, F.T. Wieland, and J.A.G. Briggs. 2015. A structure of the COPI coat and the role of coat proteins in membrane vesicle assembly. *Science*. 349:195-198.

Donaldson, J.G., and C.L. Jackson. 2011. Arf Family G Proteins and their regulators: roles in membrane transport, development and disease. *Nature Reviews Molecular Cell Biology*. 6:362-375.

Edeling, M.A., C. Smith, and D.J. Owen. 2006. Life of a clathrin coat: insights from clathrin and AP structures. *Nature Reviews*. 7:32-44.

Emery, G., M. Rojo, and J. Gruenberg. 2000. Coupled transport of p24 family members. *Journal of Cell Science*. 113:2507-2516.

Eugster, A., G. Frigerio, M. Dale, and R. Duden. 2000. COPI domains requeired for coatomer integrity and novel interactions with ARF and ARFGAP. *The EMBO Journal*. 19:3905-3917.

Eugster, A., G. Frigerio, M. Dale, and R. Duden. 2004. Thea- and bp-COP WD40 Domains Mediate Cargoselective Interactions with Distinct Di-lysine Motifs. *Molecular Biology of the Cell*. 15:1011-1023.

Faini, M., S. Prinz, R. Beck, M. Schorb, J.D. Riches, K. Bacia, B. Brügger, F.T. Wieland, and J.A.G. Briggs. 2012. The Structures of COPI-Coated Vesicles Reveal Alternate Coatomer Conformations and Interactions. *Science*.

Farquhar, M.G., and G.E. Palade. 1981. The Golgi apparatus (complex)—(1954–1981)—from artifact to center stage. *The Journal of Cell Biology*. 91:77s-103s.

Fath, S., J.D. Mancias, X. Bi, and J. Goldberg. 2007. Structure and Organization of Coat Proteins in the COPII Cage. *Cell*. 129:1325-1336.

Fiedler, K., M. Veit, M.A. Stamnes, and J.E. Rothman. 1996. Bimodal Interaction of Coatomer with the p24 Family of Putative Cargo Receptors. *Science*. 273:1396-1399.

Field, M.C., A. Sali, and M.P. Rout. 2011. On a bender—BARs, ESCRTs, COPs, and finally getting your coat. *The Journal of Cell Biology*. 193:963-972.

Fitzgerald, D.J., P. Berger, C. Schaffitzel, K. Yamada, T.J. Richmond, and I. Berger. 2006. Protein complex expression by using multigene baculoviral vectors. *Nature Methods*. 3:1021-1032.

Fotin, A., Y. Cheng, P. Sliz, N. Grigorieff, S.C. Harrison, T. Kirchhausen, and T. Walz. 2004. Molecular model for a complete clathrin lattice from electron cryomicroscopy. *Nature*. 432:573-579.

Fotin, A., T. Kirchhausen, N. Grigorieff, S.C. Harrison, T. Walz, and Y. Cheng. 2006. Structure determination of clathrin coats to subnanometer resolution by single particle cryo-electron microscopy. *Journal of Structural Biology*. 156:453-460.

Franco, M., P. Chardin, M. Chabre, and S. Paris. 1996. Myristoylation-facilitated Binding of the G Protein ARF1GDP to Membrane Phospholipids Is Required for Its Activation by a Soluble Nucleotide Exchange Factor. *The Journal of Biological Chemistry*. 271:1573-1578.

Frigerio, G., N. Grimsey, M. Dale, I. Majoul, and R. Duden. 2007. Two Human ARFGAPs Associated with COP-I-Coated Vesicles. *Traffic*. 8:1644-1655.

Füllekrug, J., T. Suganuma, B.L. Tang, W. Hong, B. Storrie, and T. Nilsson. 1999. Localization and Recycling of gp27 (hp24g3): Complex Formation with Other p24 Family Members. *Molecular Biology of the Cell*. 10:1939-1955.

Gaidarov, I., Q. Chen, J.R. Falck, K.K. Reddy, and J.H. Keen. 1996. A Functional Phosphatidylinositol 3,4,5-Trisphosphate/Phosphoinositide Binding Domain in the Clathrin Adaptor AP-2 a Subunit. *The Journal of Biological Chemistry*. 271:20922-20929.

Glick, B.S., T. Elston, and G. Oster. 1997. A cisternal maturation mechanism can explain the asymmetry of the Golgi stack. *FEBS Letters*. 414:177-181.

Glick, B.S., and A. Luini. 2011. Models for Golgi Traffic: A Critical Assessment. *Cold Spring Harbor Perspectives in Biology*:1-15.

Glick, B.S., and V. Malhotra. 1998. The curious status of the Golgi apparatus. *Cell*. 95:883-889.

Goldberg, J. 1998. Structural Basis for Activation of ARF GTPase: Mechanisms of Guanine Nucleotide Exchange and GTP–Myristoyl Switching. *Cell*. 95:237-248.

Goldberg, J. 1999. Structural and functional analysis of the ARF1-ARFGAP complex reveals a role for coatomer in GTP hydrolysis. *Cell*. 96:893-902.

Gommel, D.U., A.R. Memon, A. Heiss, F. Lottspeich, J. Pfannstiel, J. Lechner, C. Reinhardt, J.B. Helms, W. Nickel, and F.T. Wieland. 2001. Recruitment to Golgi membranes of ADP-Ribosylation factor 1 is mediated by the cytoplasmic domain of p23. *The EMBO Journal*. 20:6751-6760.

Griffiths, G. 2000. Gut thoughts on the Golgi complex. *Traffic*. 1:738-745.

Hakulinen, N., O. Turunen, J. Jänis, M. Leisola, and J. Rouvinen. 2003. Three-dimensional structures of thermophilic beta-1,4-xylanases from Chaetomium thermophilum and Nonomuraea flexuosa. Comparison of twelve xylanases in relation to their thermal stability. *FEBS Letters*. 270:1399-1412.

Heldwein, E.E., E. Macia, J. Wang, H.L. Yin, T. Kirchhausen, and S.C. Harrison. 2004. Crystal structure of the clathrin adaptor protein 1 core. *Proceedings of the National Academy of Sciences (PNAS)*. 101:14108-14113.

Hirst, J., L.D. Barlow, G.C. Francisco, D.A. Sahlender, M.N.J. Seaman, J.B. Dacks, and M.S. Robinso. 2011. The Fifth Adaptor Protein Complex. *PLoS Biology*. 9:1-17.

Hoffman, G.R., P.B. Rahl, R.N. Collins, and R.A. Cerione. 2003. Conserved Structural Motifs in Intracellular Trafficking Pathways: Structure of the gCOP Appendage Domain. *Molecular Cell*. 12:615-625.

Honda, A., O.S. Al-Awar, J.C. Hay, and J.G. Donaldson. 2005. Targeting of Arf-1 to the early Golgi by membrin, an ER-Golgi SNARE. *The Journal of Cell Biology*. 168:1039-1051.

Höning, S., D. Ricotta, M. Krauss, K. Späte, B. Spolaore, A. Motley, M. Robinson, C. Robinson, V. Haucke, and D.J. Owen. 2005. Phosphatidylinositol-(4,5)-Bisphosphate Regulates Sorting Signal Recognition by the Clathrin-Associated Adaptor Complex AP2. *Molecular Cell*. 18:519-531.

Hsia, K.C., and A. Hoelz. 2010. Crystal structure of α-COP in complex with ϵ-COP provides insight into the architecture of the COPI vesicular coat. *Proceedings of the National Academy of Sciences (PNAS)*. 107:11271-11276.

Jackson, C.L., and J.E. Casanova. 2000. Turning on ARF: the Sec7 family of guanine-nucleotide-exchange factors. *Trends in Cell Biology*. 10:67-67.

Jackson, L.P., B.T. Kelly, A.J. McCoy, T. Gaffry, L.C. James, B.M. Collins, S. Höning, P.R. Evans, and D.J. Owen. 2010. A Large-Scale Conformational Change Couples Membrane Recruitment to Cargo Binding in the AP2 Clathrin Adaptor Complex. *Cell*. 141:1220-1229.

Jackson, L.P., M. Lewis, H.M. Kent, M.A. Edeling, P.R. Evans, R. Duden, and D.J. Owen. 2012. Molecular Basis for Recognition of Dilysine Trafficking Motifs by COPI. *Developmental Cell*. 23:1-8.

Kawamoto, K., Y. Yoshida, H. Tamaki, S. Torii, C. Shinotsuka, S. Yamashina, and K. Nakayama. 2002. GBF1, a Guanine Nucleotide Exchange Factor for ADPRibosylation Factors, is Localized to the cis-Golgi and Involved in Membrane Association of the COPI Coat. *Traffic*. 3:483-495.

Kelly, B.T., A.J. McCoy, K. Späte, S.E. Miller, P.R. Evans, S. Höning, and D.J. Owen. 2008. A structural explanation for the binding of endocytic dileucine motifs by the AP2 complex. *Nature Letters*. 458:976-979.

Kirchhausen, T. 2000. CLATHRIN. *Annual Review of Biochemistry*. 69:699-727.

Kleene, R., and E.G. Berger. 1993. The molecular and cell biology of glycosyltransferases. *Biochimica et Biophysica Acta*. 1154:283-325.

Kuunimalaiyaan, S., R.B. Inman, S.A. Rakowski, and M. Filutowicz. 2005. Role of pi dimers in coupling ("handcuffing") of plasmid R6K's gamma ori iterons. *Journal of Bacteriology*. 187:3779-3785.

La Touche, C.J. 1948. A Chaetomium-like thermophilic fungus. *Nature*. 161:320.

Laemmli, U.K. 1970. Cleavage of structural proteins during the assembly of the head of bacteriophage T4. *Nature*. 227:650-685.

Lahav, A., H. Rozenberg, A. Parnis, D. Cassel, and N. Adir. 2015. Structure of the bovine COPI d subunit l homology domain at 2.15 A° resolution. *Acta Crystallographica*:1328-1334.

Langer, J.D., C.M. Roth, J. Béthune, E.H. Stoops, B. Brügger, D.P. Herten, and F.T. Wieland. 2008. A Conformational Change in the a-subunit of Coatomer Induced by Ligand Binding to g-COP Revealed by Single-pair FRET. *Traffic*. 9:597-607.

Langer, J.D., E.H. Stoops, J. Béthune, and F.T. Wieland. 2007. Conformational changes of coat proteins during vesicle formation. *FEBS Letters*. 581:2083-2088.

Lee, C., and J. Goldberg. 2010. Structure of Coatomer Cage Proteins and the Relationship among COPI, COPII, and Clathrin Vesicle Coats. *Cell*. 142:123-132.

Lee, I., B. Doray, J. Govero, and S. Kornfeld. 2008. Binding of cargo sorting signals to AP-1 enhances its association with ADP ribosylation factor 1 – GTP *The Journal of Cell Biology*. 180:476-472.

Lee, M.C.S., L. Orci, S. Hamamoto, E. Futai, M. Ravazzola, and R. Schekman. 2005. Sar1p N-Terminal Helix Initiates Membrane Curvature and Completes the Fission of a COPII Vesicle. *Cell*. 122:605-617.

Leidig, C., G. Bange, J. Kopp, S. Amlacher, A. Aravind, S. Wickles, G. Witte, E. Hurt, R. Beckmann, and I. Sinning. 2013. Structural characterization of a eukaryotic chaperone--the ribosome-associated complex. *Natur Structural & Molecular Biology*. 20:23-28.

Letourneur, F., E.C. Gaynor, S. Hennecke, C. Démollière, R. Duden, S.D. Emr, H. Riezman, and P. Cosson. 1994. Coatomer is essential for retrieval of dilysine-tagged proteins to the endoplasmic reticulum. *Cell*. 79:1199-1207.

Liu, Y., R.A. Kahn, and J.H. Prestegard. 2010. Dynamic structure of membrane-anchored Arf•GTP. *Nature structural & molecular biology*. 17:876-881.

Lowe, M., and T.E. Kreis. 1995. In Vitro Assembly and Disassembly of Coatomer. *The Journal of Biological Chemistry*. 270:31364-31371.

Ma, W., and J. Goldberg. 2013. Rules for the recognition of dilysine retrieval motifs by coatomer. *EMBO Journal*.

Majoul, I., M. Straub, S.W. Hell, R. Duden, and H.D. Söling. 2001. KDEL-Cargo Regulates Interactions between Proteins Involved in COPI Vesicle Traffic: Measurements in Living Cells Using FRET. *Developmental Cell*. 1:139-153.

Malsam, J., D. Gommel, F.T. Wieland, and W. Nickel. 1999. A role for ADP ribosylation factor in the control of cargo uptake during COPI-coated vesicle biogenesis. *FEBS Letters*. 462:267-272.

Matsuoka, K., L. Orci, M. Amherdt, S.Y. Bednarek, S. Hamamoto, R. Schekman, and T. Yeung. 1998. COPII-Coated Vesicle Formation Reconstituted with Purified Coat Proteins and Chemically Defined Liposomes. *Cell*. 93:263-275.

Metcalf, W.W., W. Jiang, and B.L. Wanner. 2004. Use of the rep technique for allele replacement to construct new Escherichia coli hosts for maintenance of R6K gamma origin plasmids at different copy numbers. *Gene*. 138:1-7.

Mironov, A.A., G.V. Beznoussenko, E.V. Polishchuk, and A. Trucco. 2005. Intra-Golgi transport: A way to a new paradigm? *Biochimica et Biophysica Acta*. 1744:340-350.

Mironov, A.A., A.A.J. Mironov, G.V. Beznoussenko, A. Trucco, P. Lupetti, J.D. Smith, W.J.C. Geerts, A.J. Koster, K.N. Burger, and M.E. Martone. 2003. ER-to-Golgi carriers arise through direct en bloc protrusion and multistage maturation of specialized ER exit domains. *Developmental Cell*. 5:583-594.

Moelleken, J., J. Malsam, M.J. Betts, A. Movafeghi, I. Reckmann, I. Meissner, A. Hellwig, R.B. Russell, T. Söllner, B. Brügger, and F.T. Wieland. 2007. Differential localization of coatomer complex isoforms within the Golgi apparatus. *Proceedings of the National Academy of Sciences (PNAS)*. 104:4425-4430.

Monetta, P., I. Slavin, N. Romero, and C. Cecilia Alvarez. 2007. Rab1b Interacts with GBF1 and Modulates both ARF1 Dynamics and COPI Association. *Molecular Biology of the Cell*. 18:2400-2410.

Nickel, W., J. Malsam, K. Gorgas, M. Ravazzola, N. Jenne, J.B. Helms, and F.T. Wieland. 1998. Uptake by COPI-coated vesicles of both anterograde and retrograde cargo is inhibited by GTPγS in vitro. *Journal of Cell Science*. 111:3081-3090.

Nickel, W., K. Sohn, C. Bunning, and F.T. Wieland. 1997. p23, a major COPI-vesicle membrane protein, constitutively cycles through the early secretory pathway. *Proceedings of the National Academy of Sciences (PNAS)*. 94:11393-11398.

Nilsson, T., C.E. Au, and J.J. Bergeron. 2009. Sorting out glycosylation enzymes in the Golgi apparatus. *FEBS Letters*. 583:3764-3769.

Noble, A.J., Q. Zhang, J. O´Donell, H. Hariki, N. Bhattacharya, A.G. Marshall, and S.M. Stagg. 2013. A pseudoatomic model of the COPII cage obtained from cryo-electron microscopy and mass spectrometry. *Nature structural & molecular biology*. 20:167-173.

Ohno, H., S. Stewart, M.C. Fournier, H. Bosshart, I. Rhee, S. Miyatake, T. Saito, A. Gallusser, T. Kirchhausen, and J.S. Bonifacino. 1995. Interaction of tyrosine-based sorting signals with clathrin-associated proteins. *Science*. 269:1872-1875.

Orci, L., M. Ravazzola, A. Volchuk, T. Engel, M. Gmachl, M. Amherdt, A. Perrelet, T.H. Söllner, and J.E. Rothman. 2000. Anterograde flow of cargo across the Golgi stack potentially mediated via bidirectional ‘‘percolating’’ COPI vesicles. *Proceedings of the National Academy of Sciences (PNAS)*. 97:10400-10405.

Owen, D.J., B.M. Collins, and P.R. Evans. 2004. ADAPTORS FOR CLATHRIN COATS: Structure and Function. *Annual Review of Cell and Developmental Biology*. 20:153-191.

Owen, D.J., and P.R. Evans. 1998. A structural explanation for the recognition of tyrosine-based endocytotic signals. *Science*. 282:1327-1332.

Owen, D.J., Y. Vallis, M.E. Noble, J.B. Hunter, T.R. Dafforn, P.R. Evans, and H.T. McMahon. 1999. A structural explanation for the binding of multiple ligands by the alpha-adaptin appendage domain. *Cell*. 97:805-815.

Owen, D.J., Y. Vallis, B.M.F. Pearse, H.T. McMahon, and P.R. Evans. 2000. The structure and function of the beta 2-adaptin appendage domain. *The EMBO Journal*. 19:4216-4227.

Paris, S., S. Béraud-Dufou, S. Robineau, J. Bigay, B. Antonny, M. Chabre, and P. Chardin. 1997. Role of protein-phospholipid interactions in the activation of ARF1 by the guanine nucleotide exchange factor Arno. *The Journal of Biological Chemistry*. 272:22221-22226.

Pasqualato, S., L. Renault, and J. Cherfils. 2002. Arf, Arl, Arp and Sar proteins: a family of GTP-binding proteins with a structural device for 'front–back' communication. *The EMBO Journal*. 3:1035-1041.

Pavel, J., C. Harter, and F.T. Wieland. 1998. Reversible dissociation of coatomer: Functional characterization of a byd-coat protein subcomplex. *Proceedings of the National Academy of Sciences (PNAS)*. 95:2140-2145.

Pelham, H.R., and J.E. Rothman. 2000. The debate about transport in the Golgi–two sides of the same coin. *Cell*. 102:713-719.

Pevzner, I., J.R.P.M. Strating, L. Lifshitz, A. Parnis, F. Glaser, A. Herrmann, B. Brügger, F.T. Wieland, and D. Cassel. 2012. Distinct Role of Subcomplexes of the COPI Coat in the Regulation of ArfGAP2 Activity. *Traffic*. 13:849-856.

Pfeffer, S.R. 2010. How the Golgi works: A cisternal progenitor model. *Proceedings of the National Academy of Sciences (PNAS)*. 107:19614-19618.

Popoff, V., F. Adolf, B. Brügger, and F.T. Wieland. 2011. COPI Budding within the Golgi Stack. *Cold Spring Harbor Perspectives in Biology*:1-19.

Rabouille, C., N. Hui, F. Hunte, R. Kieckbusch, E.G. Berger, G. Warren, and T. Nilsson. 1995. Mapping the distribution of Golgi enzymes involved in the construction of complex oligosaccharides. *Journal of Cell Science*. 108:1617-1627.

Rabouille, C., and J. Klumperman. 2005. Opinion: The maturing role of COPI vesicles in intra-Golgi transport. *Nature Reviews Molecular Cell Biology*. 6:812-817.

Rawet, M., S. Levi-Tal, E. Szafer-Glusman, A. Parnis, and D. Cassel. 2010. ArfGAP1 interacts with coat proteins through tryptophan-based motifs. *Biochemical and Biophysical Research Communications*. 394:553-557.

Reinhardt, C., C. Harter, M. Bremser, B. Brügger, K. Sohn, J.B. Helms, and F.T. Wieland. 1999. Receptor-induced polymerization of coatomer. *Proceedings of the National Academy of Sciences (PNAS)*. 96:1224-1228.

Reinhardt, C., M. Schweikert, F.T. Wieland, and W. Nickel. 2003. Functional reconstitution of COPI coat assembly and disassembly using chemically defined components. *Proceedings of the National Academy of Sciences (PNAS)*. 100:8253-8257.

Ren, X., G.G. Farias, B.J. Canagarajah, J.S. Bonifacino, and J.H. Hurley. 2012. Structural Basis for Recruitment and Activation of the AP-1 Clathrin Adaptor Complex by Arf1. *Cell*. 152:755-762.

Rohde, G., D. Wenzel, and V. Haucke. 2002. A phosphatidylinositol (4,5)-bisphosphate binding site within mu2-adaptin regulates clathrin-mediated endocytosis. *The Journal of Cell Biology*. 158:209-214.

Rothman, J.E. 1981. The golgi apparatus: Two organelles in tandem. *Science*. 213:1212-1219.

Rothman, J.E., and G. Warren. 1994. Implications of the SNARE hypothesis for intracellular membrane topology and dynamics. *Current Biology*. 4:220-233.

Rothman, J.E., and F.T. Wieland. 1996. Protein sorting by transport vesicles. *Science*. 272:227-234.

Sahlmüller, M.C., J.R.P.M. Strating, R. Beck, P. Eckert, V. Popoff, M. Haag, A. Hellwig, I. Berger, B. Brügger, and F.T. Wieland. 2011. Recombinant Heptameric Coatomer Complexes: Novel Tools to Study Isoform-Specific Functions. *Traffic*. 12:682-692.

Sauer, B. 1987. Functional expression of the cre-lox site-specific recombination system in the yeast Saccharomyces cerevisiae. *Molecular and Cellular Biology*. 7:2087-2096.

Schledzewski, K., H. Brinkmann, and R.R. Mendel. 1999. Phylogenetic analysis of components of the eukaryotic vesicle transport system reveals a common origin of adaptor protein complexes 1, 2, and 3 and the F subcomplex of the coatomer COPI. *Journal of molecular Evolution*. 48:770-778.

Schröder-Köhne, S., F. Letourneur, and H. Riezman. 1998. α-COP can discriminate between distinct, functional di-lysine signals in vitro and regulates access into retrograde transport. *Journal of Cell Science*. 111:2459-3470.

Schröder, S., and E. Ungewickell. 1991. Subunit Interaction and Function of Clathrin-coated Vesicle Adaptors from the Golgi and the Plasma Membran. *The Journal of Biological Chemistry*. 266:7910-7918.

Seaman, M.N.J., P.J. Sowerby, and M.S. Robinson. 1996. Cytosolic and Membrane-associated Proteins Involved in the Recruitment of AP-1 Adaptors onto the Trans-Golgi Network. *The Journal of Biological Chemistry*. 271:25466-25451.

Serafini, T., L. Orci, M. Amherdt, M. Brunner, R.A. Kahn, and J.E. Rothman. 1991. ADP-Ribosylation Factor Is a Subunit of the Coat of Golgi-Derived COP-Coated Vesicles: A Novel Role for a GTP-Binding Protein. *Cell*. 67:239-253.

Shaikh, A.C., and P.D. Sadowski. 1996. The Cre Recombinase Cleaves the lox Site in trans*. *The Journal of Biological Chemistry*. 272:5695-5702.

Simmen, T., S. Höning, A. Icking, R. Tikkanen, and W. Hunziker. 2002. AP-4 binds basolateral signals and participates in basolateral sorting in epithelial MDCK cells. *Nature* 4:154-159.

Sohn, K., L. Orci, M. Ravazzola, M. Amherdt, M. Bremser, F. Lottspeich, K. Fiedler, B.J. Helms, and F.T. Wieland. 1996. A Major Transmembrane Protein of Golgi-derived COPI-coated Vesicles Involved in Coatomer Binding. *The Journal of Cell Biology*. 135:1239-1248.

Söllner, T., M.K. Bennett, S.W. Whiteheart, R.H. Scheller, and J.E. Rothman. 1993. A Protein Assembly-Disassembly Pathway In Vitro That May Correspond to Sequential Steps of Synaptic Vesicle Docking, Activation, and Fusion. *Cell*. 75:409-418.

Spang, A. 2008. The life cycle of a transport vesicle. *Cellular and Molecular Life Sciences*. 65:2781-2789.

Spang, A., J.M. Herrmann, S. Hamamoto, and R. Schekman. 2001. The ADP Ribosylation Factor-Nucleotide Exchange Factors Gea1p and Gea2p Have Overlapping, but Not Redundant Functions in Retrograde Transport from the Golgi to the Endoplasmic Reticu. *Molecular Biology of the Cell*. 12:1035-1045.

Stagg, S.M., C. Gürkan, D.M. Fowler, P. LaPointe, T.R. Foss, C.S. Potter, B. Carragher, and W.E. Balch. 2006. Structure of the Sec13/31 COPII coat cage. *Nature Letters*. 439:234-238.

Stagg, S.M., P. LaPointe, A. Razvi, C. Gürkan, C.S. Potter, B. Carragher, and W.E. Balch. 2008. Structural Basis for Cargo Regulation of COPII Coat Assembly. *Cell*. 134:474-484.

Stalder, D., H. Barelli, R. Gautier, E. Macia, C.L. Jackson, and B. Antonny. 2011. Kinetic Studies of the Arf Activator Arno on Model Membranes in the Presence of Arf Effectors Suggest Control by a Positive Feedback Loop. *The Journal of Biological Chemistry*. 286:3873-3883.

Stamnes, M.A., M.W. Craighead, M.H. Hoe, N. Lampen, S. Geromanos, P. Tempest, and J.E. Rothman. 1995. An integral membrane component of coatomer-coated transport vesicles defines a family of proteins involved in budding. *Proceedings of the National Academy of Sciences (PNAS)*. 92:8011-8015.

Stamnes, M.A., and J.E. Rothman. 1993. The Binding of AP-1 Clathrin Adaptor Particles to Golgi Membranes Requires ADP-Ribosylation Factor, a Small GTP-Binding Protein. *Cell*. 73:999-1005.

Suckling, R.J., P.P. Poon, S.M. Travis, I.V. Majoul, F.M. Hughson, P.R. Evans, R. Duden, and D.J. Owen. 2015. Structural basis for the binding of tryptophan-based motifs by δ-COP. *Proceedings of the National Academy of Sciences (PNAS)*.

Summers, M.D., and G.E. Smith. 1987. A manual of methods for baculovirus vectors and insect cell culture procedures. *Texas Agricultural Experimental Station Bulletin*. 1555.

Sun, Z., F. Anderl, K. Föhlich, L. Zhao, S. Hanke, B. Brügger, F.T. Wieland, and J. Béthune. 2007. Multiple and Stepwise Interactions Between Coatomer and ADP-Ribosylation Factor-1 (Arf1)-GTP. *Traffic*. 8:582-593.

Szul, T., R. Garcia-Mata, E. Brandon, S. Shestopal, C. Alvarez, and E. Elizabeth Sztul. 2005. Dissection of Membrane Dynamics of the ARF-Guanine Nucleotide Exchange Factor GBF1. *Traffic*. 6:374-385.

Szul, T., and E. Sztul. 2011. COPII and COPI Traffic at the ER-Golgi Interface. *Physiology*. 26:348-364.

ter Haar, E., A. Musacchio, S.C. Harrison, and T. Kirchhausen. 1998. Atomic Structure of Clathrin: A b Propeller Terminal Domain Joins an a Zigzag Linker. *Cell*. 95:563-573.

Traub, L.M., M.A. Downs, J.L. Westrich, and D.H. Fremont. 1999. Crystal structure of the a appendage of AP-2 reveals a recruitment platform for clathrin-coat assembly. *Proceedings of the National Academy of Sciences (PNAS)*. 96:8907-8912.

Vaughn, J.L., R.H. Goodwin, G.J. Tompkins, and P. McCawley. 1977. The establishment of two cell lines from the insect Spodoptera frugiperda (Lepidoptera; Noctuidae). *In vitro*. 13:213-217.

Vetter, I.R., and A. Wittinghofer. 2001. The Guanine Nucleotide–Binding Switch in Three Dimensions. *Science*. 294:1299-1304.

Volpicelli-Daley, L.A., Y. Li, C.J. Zhang, and R.A. Kahn. 2005. Isoform-selective effects of the depletion of ADP-ribosylation factors 1-5 on membrane traffic. *Molecular Biology of the Cell*. 16:4495-4508.

Watson, P.J., G. Frigerio, B.M. Collins, R. Duden, and D.J. Owen. 2004. g-COP Appendage Domain – Structure and Function. *Traffic*. 5:79-88.

Wegmann, D., P. Hess, C. Baier, F.T. Wieland, and C. Reinhardt. 2004. Novel Isotypicg/z Subunits Reveal Three Coatomer Complexes in Mammals. *Molecular and Cellular Biology*. 24:1070-1080.

Weimer, C., R. Beck, P. Eckert, I. Reckmann, J. Moelleken, B. Brügger, and F.T. Wieland. 2008. Differential roles of ArfGAP1, ArfGAP2, and ArfGAP3 in COPI traffi cking. *The Journal of Cell Biology*. 183:725-735.

Weiss, M., and T. Nilsson. 2000. Protein sorting in the Golgi apparatus: A consequence of maturation and triggered sorting. *FEBS Letters*. 486:2-9.

Wilbur, J.D., P.K. Hwang, J.A. Ybe, M. Lane, B.D. Sellers, M.P. Jacobson, R.J. Fletterick, and F.M. Brodsky. 2010. Conformation Switching of Clathrin Light Chain Regulates Clathrin Lattice Assembly. *Developmental Cell*. 18:854-861.

Wilson, D.W., M.J. Lewis, and H.R.B. Pelham. 1993. pH-dependent binding of KDEL to its receptor in vitro. *The Journal of Biological Chemistry*. 268:7465-7468.

Wittinghofer, A., S.M. Franken, A.J. Scheidig, H. Rensland, A. Lautwein, E.F. Pai, and R.S. Goody. 1993. Three-dimensional structure and properties of wild-type and mutant H-ras-encoded p21. *Ciba foundation symposium*. 176:21-27.

Ybe, J.A., F.M. Brodsky, K. Hofmann, K. Lin, S.H. Liu, L. Chen, T.N. Earnestk, R.J. Fletterick, and P.K. Hwang. 1999. Clathrin self-assembly is mediated by a tandemly repeated superhelix. *Nature*. 399:371-375.

Yip, C.K., and T. Walz. 2011. Molecular structure and flexibility of the yeast coatomer as revealed by electron microscopy. *Journal Molecular Biology*. 408:825-831.

Yu, W., J. Lin, C. Kin, and B. Xia. 2009. Solution Structure of Human ζ-COP: Direct Evidences for Structural Similarity between COP I and Clathrin-Adaptor Coats. *Journal Molecular Biology*. 386:903-912.

Yu, X., M. Breitman, and J. Goldberg. 2012. A Structure-Based Mechanism for Arf1-Dependent Recruitment of Coatomer to Membranes. *Cell*. 148:530-542.

Zanetti, G., S. Prinz, S. Daum, A. Meister, R. Schekman, K. Bacia, and J.A.G. Briggs. 2013. The structure of the COPII transport-vesicle coat assembled on membranes. *eLIFE*.

Zaremba, S., and J.H. Keen. 1985. Limited proteolytic digestion of coated vesicle assembly polypeptides abolishes reassembly activity. *Journal of Cellular Biochemistry*. 28:47-58.

Zhao, L., B.J. Helms, B. Brügger, C. Harter, B. Martoglio, R. Graf, J. Brunner, and F.T. Wieland. 1997. Direct and GTP-dependent interaction of ADP ribosylation factor 1 with coatomer subunit b. *Proceedings of the National Academy of Sciences (PNAS)*. 94:4418-4423.

Zhao, L., J.B. Helms, J. Brunner, and F.T. Wieland. 1999. GTP-dependent Binding of ADP-ribosylation Factor to Coatomer in Close Proximity to the Binding Site for Dilysine Retrieval Motifs and p23. *The Journal of Biological Chemistry*. 274:14198-14203.

Zhao, X., T.K.R. Lasell, and P. Melancon. 2002. Localization of Large ADP-Ribosylation Factor-Guanine Nucleotide Exchange Factors to Different Golgi Compartments: Evidence for Distinct Functions in Protein Traffic. *Molecular Biology of the Cell*. 13:119-133.

6 Abbreviations

ALPS	Amphipatic lipid packing sensor
AP	Adaptor protein complex
APS	Ammonium peroxy sulfate
Arf	ADP ribosylation Factor
BIIC	Baculo infected inscet cells
CCV	Clathrin coated vesicle
CGN	Cis-Golgi network
CHC	Clathrin heavy chain
CLC	Clathrin light chain
COP	coat protein complex
Coatomer	coat protomer
DNA	Desoxyribonucleic acid
DMSO	Dimethyl sulfoxid
DTT	Dithiothreitol
EDTA	Ethylenediaminetetraacetic acid
EM	Electron mircroscopy
ER	Endoplasmic reticulum
ERAD	ER-associated degradation
ERES	ER-exit sites
ERGIC	ER-Golgi intermediate compartment
FPLC	Fast protein liquid chromatography
GAP	GTPase-activating protein
GDP	Guanosin diphosphate
GEF	Guanine nucleotide exchange factor
GMPPNP	5'-Guanylyl imidodiphosphate

GNBP	Guanin nucleotide binding protein
GPCR	G protein coupled receptor
GTP	Guanosin triphosphate
GTPγS	Guanosine 5'-O-[gamma-thio] triphosphate
HPLC	High pressure liquid chromatography
IPTG	Isopropyl-β-D-thiogalactopyranosid
LC	Liquid chromatography
MHD	μ-homology domain
MAD	Multi-wavelenght anomalous diffraction
NTA	Nitrilotriacetic acid
OD	Optical density
PAGE	Polyacrylamide gel electrophoresis
PCR	Polymerase chain reaction
PEG	Polyethylene glycol
PVDF	Polyvinylidene fluoride
Rpm	rounds per minute
SDS	Sodium dodecyl sulfate
SNARE	Soluble NSF Attachment Protein Receptor
SRP	Signal recognition particle
TGN	Trans-Golgi network
TEV	Tobacco etch virus
UPR	Unfolded protein response
UV	Ultraviolet

7 Publications

Rose, I., G. Biukovic, P. Aderhold, V. Müller, G. Grüber and B. Averhoff. 2011. Identification and characterization of a unique, zinc-containing transport ATPase essential for natural transformation in Thermus thermophiles HB27. *Extremophiles*. 15:191-202.

8 Acknowledgement

Foremost I would like to thank Prof. Dr. Felix Wieland for the opportunity to do my thesis in his group and for the interesting and challenging topic I could work on. Also I would like to thank Prof. Dr. Felix Wieland and Prof. Dr. Irmgard Sinning for the supervison of my thesis. Both of them provided invaluable scientific advice and support, without which this thesis would haven been impossible.

Prof. Dr. Britta Brügger I would like to thank for being part of my TAC comitee and for the advice and support she provided during my thesis.

I would like to thank Dr. Jürgen Kopp for his great help regarding all question of crystallization and of course for the solving of the protein structure. Dr. Andrea Gumiero and Dr. Fabilola Rodriguez Calviño I would like to thank for their help in fishing crystals and for the help in seleno-methionine labelling. Also I would like to thank Dr. Bernd Hessling and Dr. Dirk Flemming for their help with mass spectrometry and with electron microscopy.

All members of the Wieland group I would like to thank for the great atmosphere in the lab and for all the discussions, the help they provided and the fun we had together. I was a great time, which I will always remember.

At the end of this challenging and interesting time I would like to thank my family, which enabled me to do this thesis and was there to support me all the time.

My special thanks go to my girlfriend for her support and her love, which was invaluable for me during the whole time of my thesis.

8 Acknowledgement

Vornehmlich möchte ich Prof. Dr. Felix Wieland für die Gelegenheit danken meine Doktorarbeit in seiner Gruppe anzufertigen, sowie für das interresante und herausfordernde Thema an dem ich arbeiten konnte. Ebenso möchte ich Prof. Dr. Felix Wieland und Prof. Dr. Irmgard Sinning für die Betreuung meiner Arbeit danken, sowie die wertvolle Unterstützung und die wissenschaftlichen Anregungen, ohne die diese Arbeit nicht möglich gewesen wäre.

Ich danke Prof. Dr Britta Brügger dafür Mitglied meines TAC-Komittees gewesen zu sein und für den Rat und die Unterstützung die sie mir während dieser Arbeit zu Teil werden ließ.

Herrn Dr. Jürgen Kopp danke ich für seine große Hilfe alle Fragen der Kristallisation betreffend und natürlich für das Lösen der Proteinstruktur. Bei Herrn Dr. Andrea Gumiero und Frau Dr. Fabiola Rodriguez Calviño möchte ich für ihre Hilfe beim Fischen der Kristalle, sowie dem Seleno-Methionin Labeln bedanken. Ebenso möchte ich Herrn Dr. Bernd Hessling und Herrn Dr. Dirk Flemming für ihre Hilfe bei der Massenspektrometrie und der Elektronenmikroskopie danken.

Allen Mitgliedern der Arbeitsgruppe Wieland danke ich für einen spannende und lustige Zeit, die tolle Atmosphäre im Labor, die Diskussionen und den Spaß den wir zusammen hatten. Es war eine tolle Zeit, die ich nie vergessen werde.

Am Ende dieser spannenden und herausfordernden Arbeit möchte ich meiner Familie danken, die es mir ermöglicht hat diese Arbeit anzufertigen und die immer für mich da gewesen ist.

Mein besonderer Dank gilt meiner Freundin für ihre Unterstützung und ihre Liebe, die mir während der ganzen Zeit unendlich viel bedeutet hat und ohne die diese ganze Arbeit nicht möglich gewesen wäre.

9 Appendix I

Size exclusion chromatography on a Superose 6 10/300 Gl column of the tetrameric subcomplex β686γ666δζ is depicted in figure 71. The subcomplex eluted at the expected size of 234.25 kDa and showed a symmetric peak. Fractions of the peak were analysed by SDS-PAGE. As depicted in figure 71 the subcomplex shows high purity with no residual visible contaminations.

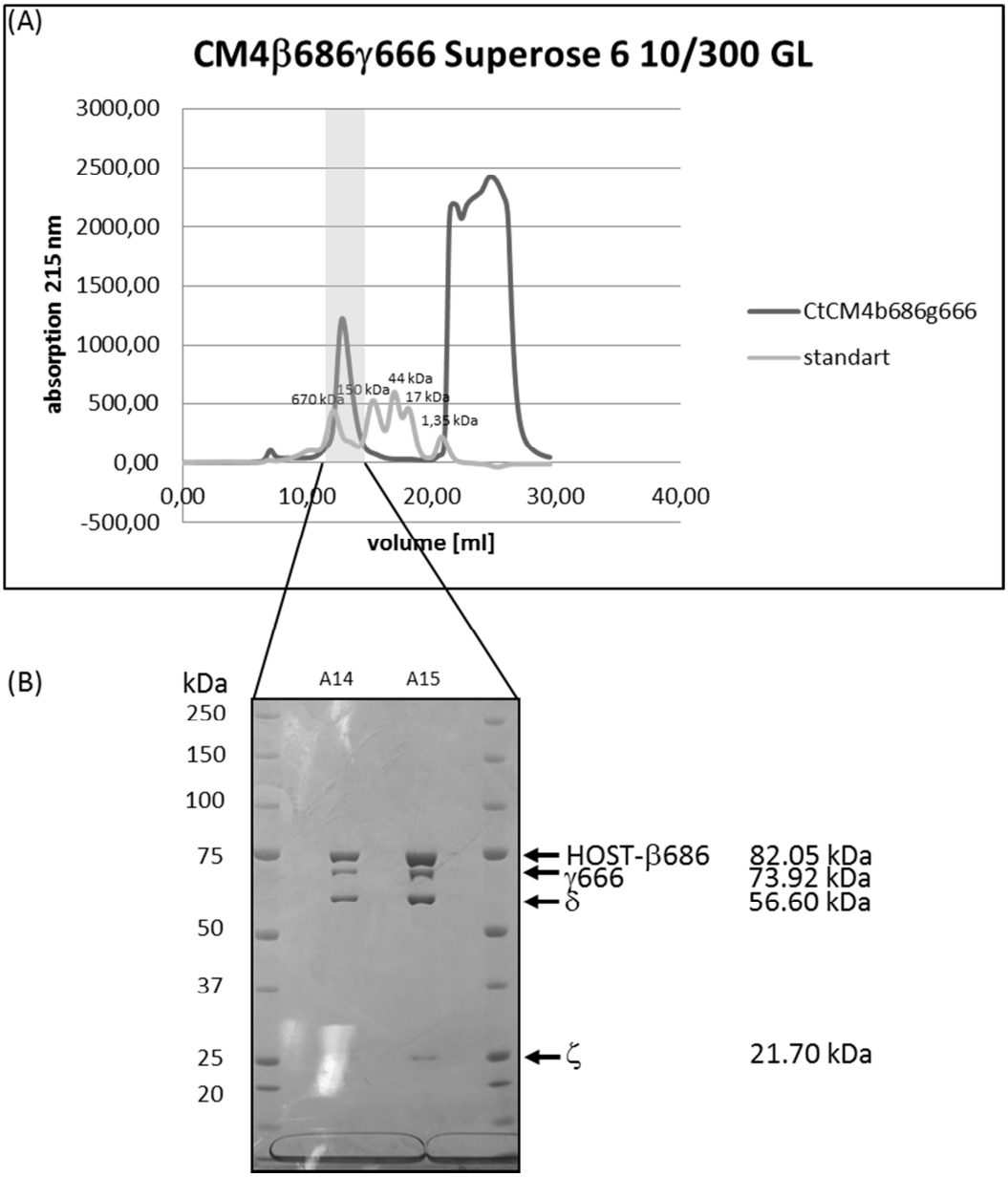

Figure 71: Chromatographic profile of the size exclusion chromatography of the tetrameric subcomplex β686γ666δζ

(A): The elution profile of the tetrameric coatomer subcomplex (dark grey) is overlayed with the elution profile of a protein size standard (light grey). The UV absorption at 215 nm is blotted against the elution volume in ml.

(B): 15 % SDS-PAGE stained with Coomassie. 5 µl of each truncated coatomer β´-subunit Superose 6 10/300 GL elution fraction mixed with 3.5 µl 4 x SDS sample buffer was loaded on the gel.

Profile of the size exclusion chromatography of the truncated β´-subunit β´585 on a Superdex 200 10/300 GL column is depicted in figure 72. The truncated subunit eluted at the expected size of 70.75 kDa and showed a symmetric peak. Fractions of the peak were analysed by SDS-PAGE. As depicted in figure 72 the subunit contains some visible

contaminations of higher molecular weight, which are most probably aggregates of the subcomplex.

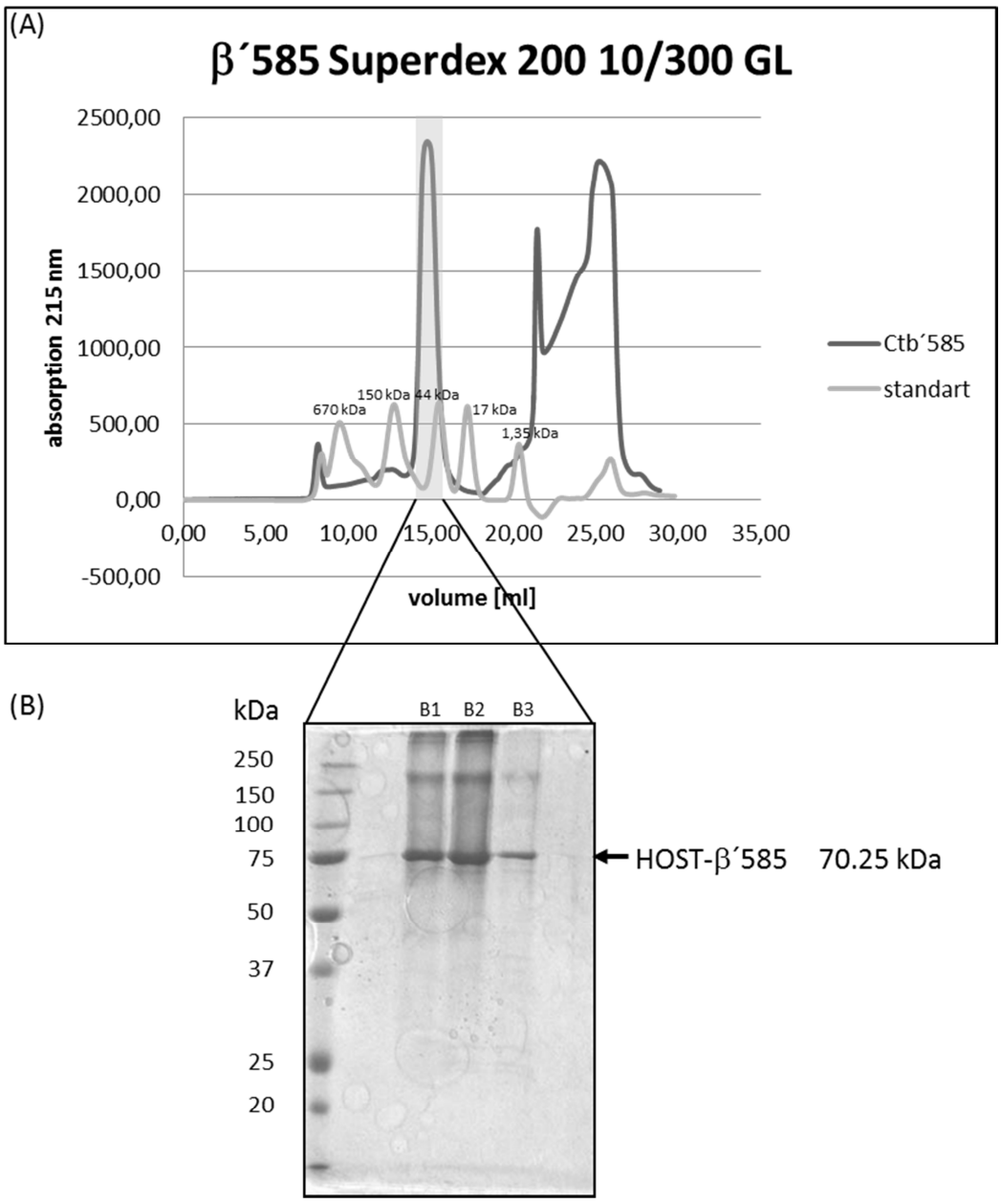

Figure 72: Chromatographic profile of the size exclusion chromatography of β´585

(A): The elution profile of the truncated coatomer β´-subunit (dark grey) is overlayed with the elution profile of a protein size standard (light grey). The UV absorption at 215 nm is blotted against the elution volume in ml.

(B): 15 % SDS-PAGE stained with Coomassie. 5 µl of each truncated coatomer β´-subunit Superose 6 10/300 GL elution fraction mixed with 3.5 µl 4 x SDS sample buffer was loaded on the gel.

The chromatographic profile of the size exclusion chromatography of the truncated βδ subcomplex β19-391δ1-243 on a Superose 6 10/300 GL column is depicted in figure 73. The coatomer subcomplex eluted at the expected size of 75.15 kDa and showed a symmetric peak. Fractions of the peak were analyzed by SDS-PAGE, as depicted in figure 73.

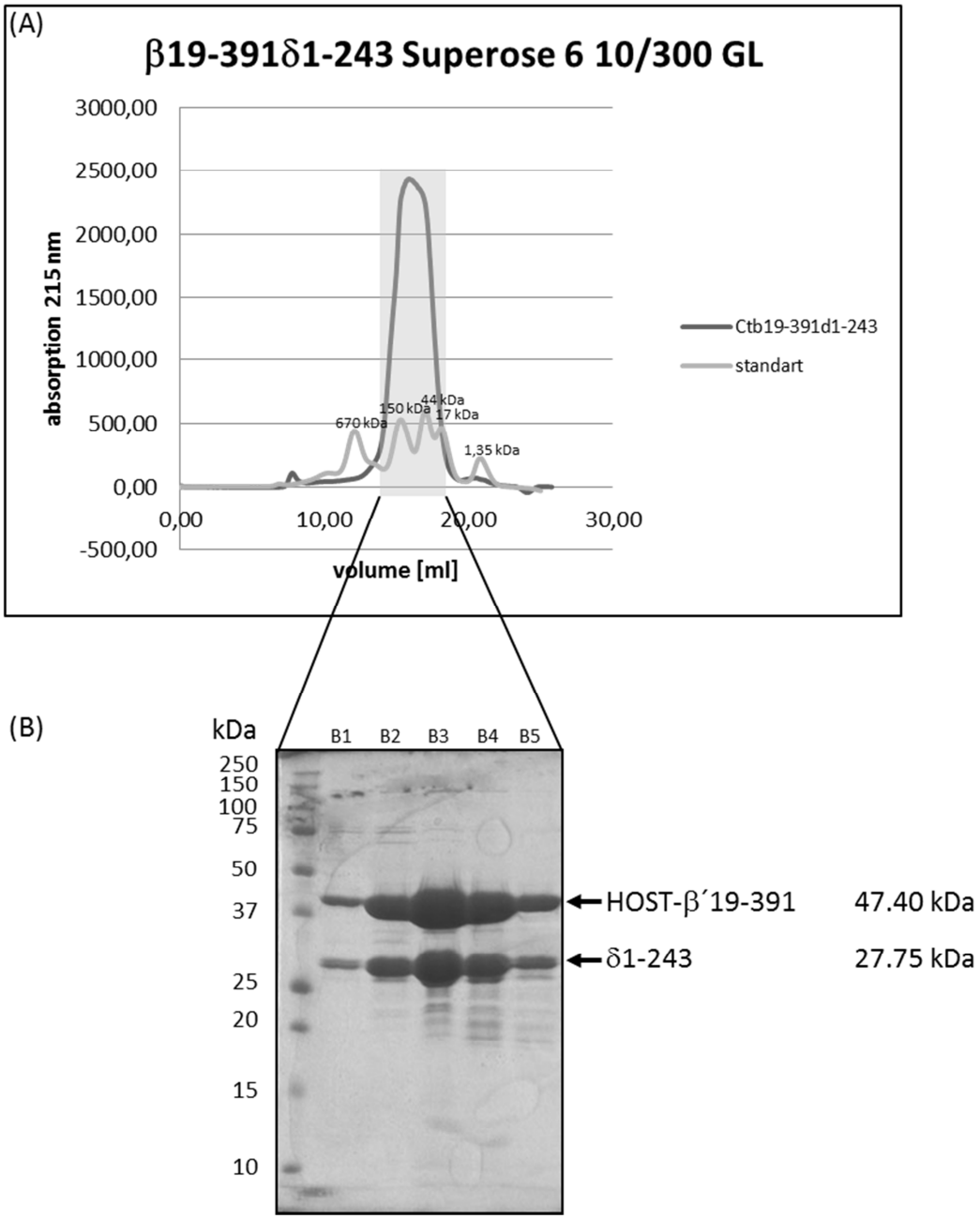

Figure 73: Chromatographic profile of the size exclusion chromatography of the dimeric subcomplex β19-391δ1-243

(A): The elution profile of the truncated coatomer βδ-subcomplex (dark grey) is overlayed with the elution profile of a protein size standard (light grey). The UV absorption at 215 nm is blotted against the elution volume in ml.

(B): 15 % SDS-PAGE stained with Coomassie. 5 µl of each coatomer dimer Superose 6 10/300 GL elution fraction mixed with 3.5 µl 4 x SDS sample buffer was loaded on the gel.

The chromatographic profile of the size exclusion chromatography of the truncated coatomer βδ subcomplex β19-391δ1-124 on a Superose 6 10/300 GL column is depicted in figure 74. The subcomplex eluted at the expected size of 61.56 kDa and showed a symmetric

peak. Fractions of the peak were analyzed by SDS-PAGE. As depicted in figure 74 the δ1-124 subunit seems to be partially degraded, indicating a reduced stability of this truncation.

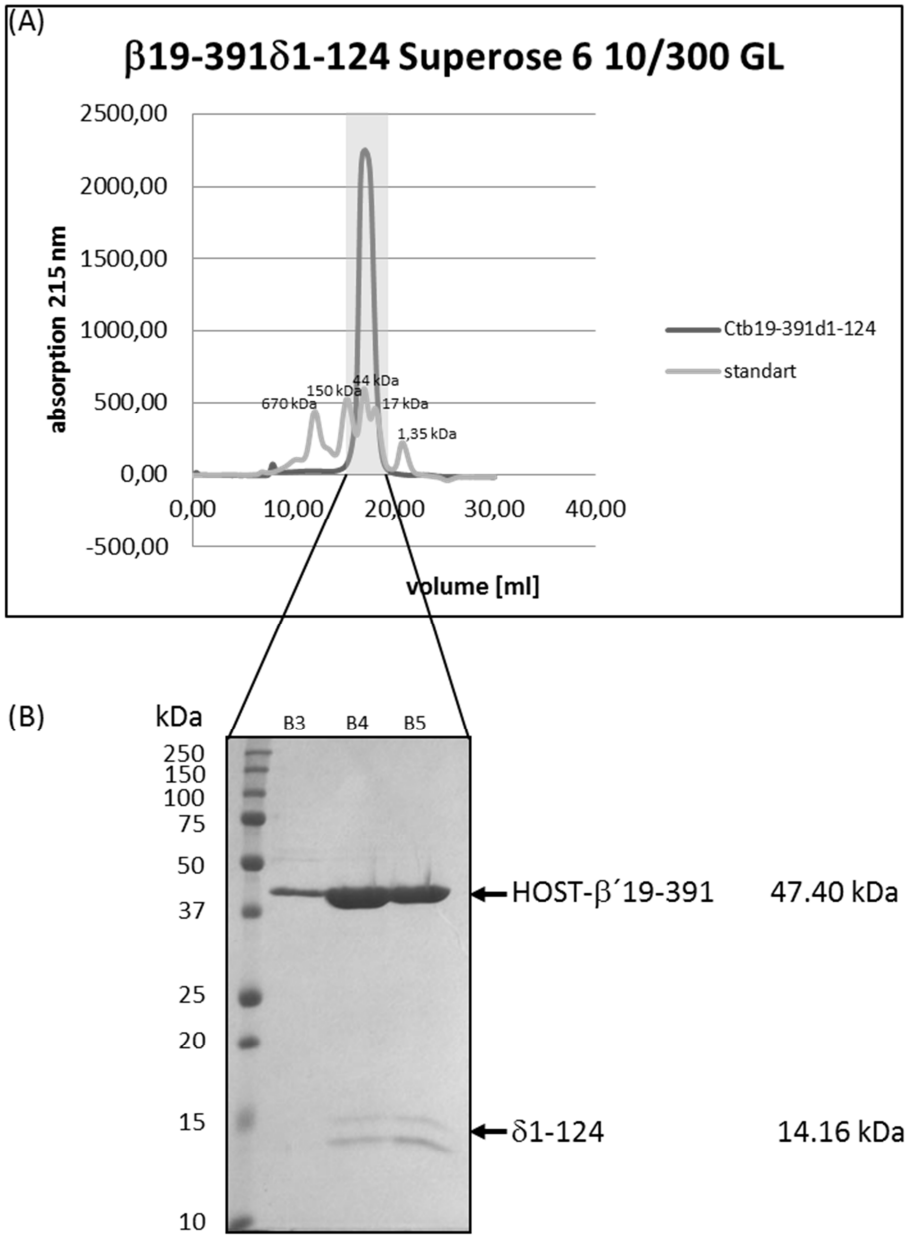

Figure 74: Chromatographic profile of the size exclusion chromatography of the dimeric subcomplex β19-391δ1-124

(A): The elution profile of the truncated coatomer βδ-subcomplex (dark grey) is overlayed with the elution profile of a protein size standard (light grey). The UV absorption at 215 nm is blotted against the elution volume in ml.

(B): 15 % SDS-PAGE stained with Coomassie. 5 µl of each coatomer dimer Superose 6 10/300 GL elution fraction mixed with 3.5 µl 4 x SDS sample buffer was loaded on the gel.